Development of mass spectrometric methods to understand the mechanism of action of transition metal-based anticancer compounds

THÈSE N^{O} 7234 (2016)

PRÉSENTÉE LE 4 NOVEMBRE 2016

À LA FACULTÉ DES SCIENCES DE BASE
LABORATOIRE DE CHIMIE ORGANOMÉTALLIQUE ET MÉDICINALE
PROGRAMME DOCTORAL EN CHIMIE ET GÉNIE CHIMIQUE

ÉCOLE POLYTECHNIQUE FÉDÉRALE DE LAUSANNE

POUR L'OBTENTION DU GRADE DE DOCTEUR ÈS SCIENCES

PAR

Fook Seng Ronald LEE

acceptée sur proposition du jury:

Prof. L. Helm, président du jury
Prof. P. J. Dyson, Prof. K. Johnsson, directeurs de thèse
Dr B. Murray, rapporteur
Dr M. Grössl, rapporteur
Prof. A. Meibom, rapporteur

ÉCOLE POLYTECHNIQUE
FÉDÉRALE DE LAUSANNE

Suisse
2016

Acknowledgements

I would first like to thank my thesis directors Paul Dyson and Kai Johnsson for providing me with the amazing opportunity to work in both the Laboratory of Organometallic and Medicinal Chemistry (LCOM) and Laboratory of Protein Engineering (LIP) which they head respectively. They have both been extremely supportive during these four years, providing much wisdom and guidance whenever I needed it. I would also like to thank Prof. Lothar Helm for presiding over the jury, and Prof. Anders Meibom, Prof Benjamin Murray, and Dr. Michael Grössl for kindly agreeing to evaluate my dissertation.

I am extremely grateful to the present and past members of both LCOM and LIP, for friendship, moral and scientific support. With a combined total of more than 50 members from both labs, many of whom I have formed great friendships with, and have touched my life in a special way, such a brief acknowledgement section does not do sufficient justice to express my gratitude to these wonderful group of friends, whom I hope we will continue to work and hang out with for a long time to come. Work in this thesis was greatly supported by a wide variety of collaborations. These include members of the lab of Professor Roman Zubarev in Karolinska Institute, Sweeden especially Alexey and Dorothea who helped perform proteomics experiments and guided me through the workflow. Thanks also goes to Dr. David Hacker of the protein expression core facility for protein expression. Not to forget, ISIC's mass spectrometry team especially Laure, Daniel and Luc whose help and advice was invaluable for the MS protein-metallodrug binding studies and whose positivity made working with them a pure joy. Work on NanoSIMS was greatly aided by the help of the labs of Professor Anders Meibom, and EPFL's BioEM team, amongst whom I want to mention Stéphane, Julia, Catherine, Mary, Stephanie and Graham who helped a ton. Finally, work on metallodrug binding to BRCA1 was done in collaboration with the group of Prof. Adisorn Ratanaphan and his student Dr. Pornvichai Temboot from Prince Songkla University, Thailand.

Besides work colleagues, I also like to thank my parents and sibling for supporting me through this journey, as well as friends from back home in Malaysia/Singapore. A big thanks also to my Catholic friends in Centre Culturel Florimont and Our Lady of Faith Lausanne, for the camaraderie and spiritual guidance. Finally I thank the good Lord for these wonderful 4 years in Switzerland.

“The more you know, the more you know you don’t know.”

-Aristotle-

Abstract

Metal based anti-cancer drugs (metallodrugs) such as cisplatin are a cornerstone of cancer chemotherapy. However, development of this class of compound has been hindered by our lack of understanding of how they function. This is mainly because existing method to study the mechanism of action of metallodrugs are lacking as they were either directly adapted from methods to study organic drugs which have very different chemical properties or current limits in technology and knowledge were a bottleneck to the development of suitable methods.

Mass spectrometry (MS) has emerged as a powerful tool which can be applied to study the mechanism of action of metallodrugs. Many different MS methods exist which can be adapted to study different aspects of drug action while accounting for the unique chemical nature of metallodrugs. In this dissertation, we develop MS strategies to study how platinum and ruthenium metallodrugs work and study a few important aspects of their function. Firstly, the *in vitro* distribution of and ligand state of metallodrugs were studied by imaging mass spectrometry. Next, we attempted to find novel protein targets of metallodrugs using a novel protein expression profiling approach. Promising metallodrug protein targets obtained from this study were then validated via biochemical methods. To facilitate the application of MS based protein-metallodrug fragmentation experiments for finding binding sites of metallodrugs on proteins, we developed and optimized web-based tools for automatic processing of complex spectra from these experiment. We then applied these tools to study the interaction of metallodrugs on relevant proteins, which provided insight into the specific binding properties of metallodrugs on proteins.

Keywords
Platinum, ruthenium, metallodrugs, mass spectrometry, anti-cancer, imaging, proteomics, fragmentation.

Résumé

Les médicaments anti-cancéreux composés d'un centre métallique (métallodrogues) comme le cisplatin sont des médicaments incontournables dans le traitement du cancer par chimiothérapie. Cependant, le développement de nouvelles métallodrogues est lent dû à la faible compréhension du mode d'action de ces derniers. Ce manque de compréhension est essentiellement dû au fait que les méthodes pour étudier les mécanismes des métallodrogues ne sont pas adaptées. En effet, ces méthodes sont souvent issues directement de méthodes utilisées pour comprendre le fonctionnement de drogues organiques (qui ont des propriétés chimiques très différentes). De plus, les limites techniques ont freinés le développement de méthodes appropriées pour ces analyses.

La spectrométrie de masse (MS) a émergé comme un outil puissant pour l'étude des mécanismes des métallodrogues. De nombreuses méthodologies MS existent, et celles-ci peuvent être ajustées, ce qui permettrait d'étudier les différents modes d'actions de la métallodrogue, tout en prenant en compte les propriétés uniques de celles-ci. Dans cette thèse, nous proposons des stratégies MS pour étudier le fonctionnement de médicaments contenant des centres Platine ou Ruthénium. Tout d'abord, la distribution et l'environnement (ligands) des métallodrogues a été étudié par imagerie MS *in vitro*. Ensuite, nous avons utilisé une nouvelle méthode de profilage de protéines afin de tenter d'identifier des cibles des métallodrogues. Ces cibles potentielles ont ensuite été confirmées par le biais de méthodes biochimiques. Afin de faciliter l'identification de sites de fixation de la métallodrogue par le biais de méthodes MS basé sur la fragmentation de complexes protéine-métallodrogues, un outil web pour le traitement automatique de données a été développé. Ces outils ont ensuite été utilisés pour étudier l'interaction des métallodrogues avec des protéines d'intérêt, ce qui a apporté des données sur le mode d'action et les modes de fixation des métallodrogues sur les protéines.

Mots-clés
Platine, ruthénium, métallodrogues, La spectrométrie de masse, anti-cancéreux, imagerie, profilage de protéines, fragmentation.

Contents

List of figures

List of tables

List of abbreviations

PTA	1,3,5-triaza-7-phosphatricyclo[3.3.1.1]decane
RAPTA	Ruthenium-arene PTA
RAPTA-T	RAPTA -Toluene
RAPTA-EA	RAPTA - Ethacrynic acid
SIMS	Secondary ion mass spectrometry
MALDI	Matrix assisted laser desorption ionization
LA-ICP-IMS	Laser ablation inductively coupled plasma imaging mass spectrometry
TOF	Time of flight
TEM	Transmission electron microscopy
EFTEM	Energy filtered transmission electron microscopy
FITExP	Functional identification of targets by expression profiling
MS/MS	Tandem mass spectrometry
CID	Collision induced dissociation
HCD	Higher-energy C-trap dissociation
ETD	Electron transfer dissociation
IRMPD	Infrared multiphoton dissociation
SR-XRF	Energy-filtered transmission electron microscopy
HPF	High pressure freezing
FS	Freeze substitution
GST	Glutathione S-transferase
LC-MS	Liquid chromatography - mass spectrometry
GSH	Glutathione
ERBB2	Receptor tyrosine-protein kinase erbB-2
DDB2	DNA damage-binding protein2
HSPA 1A/1B	Heat shock 70 kDa protein 1A/1B
HMOX1	Heme oxygenase 1
TRAFD1	TRAF-type zinc finger domain-containing protein 1
SRXN1	Sulfiredoxin-1
TXNRD1	Thioredoxin reductase 1, cytoplasmic
DNAJB4	DnaJ homolog subfamily B member 4
BLVRB	Flavin/bilverdin reductase

G6PD	Glucose-6-phosphate 1-dehydrogenase
PLD3	Phospholipase D3
MAT2A	S-adenosylmethionine synthase isoform type-2
MT2A	Metallothionein-2
ZNHIT2	Zinc finger HIT domain-containing protein 2
RBM47	RNA-binding protein 47
PDP1	Pyruvate dehydrogenase phosphatase catalytic subunit 1, mitochondrial
CHTOP	Chromatin target of PRMT1 protein
CHTF8	Chromosome transmission fidelity protein 8 homolog isoform 2
HEK	Human embryonic kidney
CHO	Chinese hamster ovary
VPA	Valproic acid
SAMe/AdoMet	S-adenosylmethionine
DTT	Dithiothreitol
EDTA	Ethylenediaminetetraacetic acid
SDS-PAGE	Sodium dodecyl sulphate polyacrylamide gel electrophoresis
FIDAS	Fluorinated N,-N-dialkylaminostilbene
MSAPM	Mass spectra analysis of protein modifications
PI	Isoelectric point
BRCA1	Breast cancer susceptibility gene 1
ZF	Zinc finger
RING	Really interesting new gene
BRCT	BRCA1 C-terminal
BARD1	BRCA1-associated RING domain 1
NLS	Nuclear localization signal
DSB	Double strand breaks
CD	Circular dichroism
Tm	Melting temperature

Chapter 1
General Introduction

1.1 Cancer and the history of cancer therapy

Cancer is a general term used to describe a group of diseases that can affect any organs in our body and is characterized by abnormal cells that divide and grow beyond their usual boundaries and can potentially invade adjoining parts of the body and spread to other organs.[1] Cancer is a major cause of morbidity and mortality worldwide (ranking second behind heart disease) with 14.1 million new cases reported and 8.2 million deaths (13% of deaths) in 2012[2] with this number projected to rise to 21.4 million new cases and 13.1 million deaths by the year 2030. Considering the costs of prevention and treatment of cancer and the economic value of lost lives and disability, cancer carries an annual financial burden of 1.16 trillion US dollars worldwide.[3] The first suspected documentation of cancer was by an ancient Egyptian physician Imhotep, who lived around 2625 BC.[4] For more than three millennia since its discovery, cancer has been regarded as an almost incurable disease. However, in the past 200 years, medical sciences have made great strides in the understanding and treatment of cancer.

In the mid-19th century, with major developments in surgery, such as the discovery of anesthesia, surgery became a widespread option for cancer treatment.[5] The understanding of cancer at the time was that it was a localized disease, thus "radical surgeries", where large parts of an organ was removed with its underlying lymph nodes were often performed.[6] However, upon the discovery of the metastatic character of tumors by Stephen Paget[7], such radical surgeries fell out of favor and were replaced by precise procedures, where cancerous tissue is carefully removed with minimal removal of normal tissue; a practice still the mainstay of cancer surgery today.[6]

The next step forward in cancer treatment came with the discovery of the link between hormones and cancer by Thomas Beatson in 1896[8] which eventually led to the development of hormonal therapy based drugs such as aromatase inhibitors and luteinizing hormone-releasing hormone analogues and inhibitors. Subsequently, the discovery and subsequent use or radiation therapy for cancer by Conrad Roentgen[9] led to the development of techniques such as conformal radiation therapy, proton beam radiation therapy and intraoperative radiation therapy.

During the Second World War, the use of mustard gas led to the discovery of nitrogen mustard in 1942 (a DNA alkylating agent), the first chemotherapeutic agent ever used.[10] Subsequently, findings that aminopterin, a folic acid analogue, caused remissions of acute leukemia in children led to the development of methotrexate in 1950[11], a drug still commonly used in clinics nearly 60 years later. Modern chemotherapy has evolved tremendously from its early days with the development of new drugs and chemotherapeutic combinations, usage of more efficient and targeted drug delivery systems[12] (e.g. liposomal therapy and monoclonal antibodies) and the use of drugs to mitigate side effects (blood cell stimulating agents, chemoprotective agents and anti-emetics). With our increased understanding of cancer biology, modern therapies have evolved with the introduction of immunotherapies and targeted therapies.[13] Immunotherapy attempts to either directly utilize our immune system to directly alter cancer cell growth[14] (e.g. monoclonal antibodies against specific cancer cell types like rituximab against lymphomas and trastuzumab against breast cancers), or augment our own immune system in fighting cancers[15] (e.g. sipuleucel-T therapy, where a patients white blood cells extracted are trained to recognize and attack prostate cancer cells before being reintroduced into the patient). Targeted therapies on the other hand, seek to utilize specific cancer pathways as targets against cancers [16] such as the tyrosine kinase inhibitor imatinib (Gleevec) against chronic myelogenous leukemia.[17] With these advancements in cancer therapy, the prognosis of cancer when has improved significantly, where in developed countries such as the United States, two thirds of cancer patients survive for more than 5 years upon diagnosis.[18]

1.2 Cancer chemotherapy, the end of non-targeted therapies?

Classical cancer chemotherapy which originated in the 1940's relied mostly on drugs which interfered with replicating cancer cells. Examples of these therapeutic agents are alkylating agents, topoisomerase inhibitors, antimetabolites and platinum drugs. However, these therapies were notorious for being non-specific, where any rapidly dividing cells (hair follicles, intestinal cells, blood cells), would also be targeted by these anti-cancer agents leading to side effects commonly associated with classical cancer chemotherapy such as hair loss, nausea, vomiting and immune suppression.[19]

With modern developments in cancer biology, we now have a much better fundamental understanding of the molecular basis of cancer. For example it has become apparent that

cancers, though all characterized by uncontrolled cell proliferation, is not a single disease but a group of them with more than 100 different types.[1] Furthermore, a myriad of molecular pathways are involved in cancer implicating hundreds of possible drug targets.[20] With this knowledge, modern chemotherapy aims to target these cancer targets specifically to have a more controlled anti-cancer effect whilst having less side effects.

However, the paradox of specific targeting against cancer, is that cancers are capable of mutation, thus targeted strategies against cancer invariably fail once the cancer target mutates.[21] Thus, in clinical practice, targeted therapies are never given as monotherapies but in combination with one or more non-targeted agents.[22] Non-targeted agents are also a lot more cost effective, as generic versions of many of these agents are available at a fraction of the cost of targeted therapies. However, looking to the future, it raises a question, should development of non-targeted therapies continue? One could consider an ideal scenario, where targeted compounds for every cancer pathway are available and cancer genotyping be used to identify susceptible targets for each patient followed by tailored therapies for them. However, in reality such a strategy may not be viable for the foreseeable decade due to the high cost and relatively scarce availability of genotyping especially in non-developed countries. There also remains a large gap in our understanding of cancer targets, and considering the hundreds of potential cancer targets the burden of time and cost for drugging these targets would be prohibitive. As it stands, the current cost of development of a new drug is 2.6 billion dollars[23] and it takes an average of 12 years to complete all stages of clinical testing before approval.[24] On the other hand, non-targeted compound development remains an attractive strategy as these compounds are amenable to different cancers, and the ability of cancers to gain resistance to them is mitigated by their more general mode of action. In addition, these compounds could be used as tools to further increase our knowledge of cancer biology, since they are mostly discovered via phenotypic screening based strategies and their exact mechanism of action could involve a plethora of pathways, which if elucidated could allow us to discover new cancer pathways. Thus, it becomes apparent, that non-targeted therapies still have a role to play in cancer therapy, and that the continuous development and study of these compounds is desirable.

1.3 Metal based anti-cancer drugs (metallodrugs)

In 1965, an American chemist named Barnett Rosenberg, chanced upon an observation that electrolysis products from a platinum electrode inhibited cell division in *Escherichia coli*.[25] This anti-proliferative activity was subsequently ascribed to a soluble platinum product called cisplatin formed during electrolysis. Further experiments eventually lead to the discovery of the anti-cancer activity of cisplatin and, following clinical development, it was approved for use by the U.S. Food and Drug Administration in 1978.[26] The discovery of cisplatin revolutionized the treatment of cancers such as testicular cancer (with cure rates rising from 10% to almost 80%).[27] Now it is still the first line therapy for testicular, ovarian, bladder, cervical and non-small cell lung cancers[28] and is used in approximately 50-70% of all anti-cancer regimens.[29] However, in the past 50 years since the discovery of cisplatin, only two other metallodrugs have been FDA approved (i.e. carboplatin and oxaliplatin).[30] This as opposed to the 88 clinically approved anti-cancer compounds currently on the market,[31] highlights the slow development of metallodrugs. The sluggish development could be due to a lack of understanding of how these metallodrugs work. For example, though it is generally accepted that cisplatin exerts its action through forming adducts with DNA, only 1% of intracellular cisplatin is found attached to DNA.[32] Furthermore, the three platinum compounds used clinically (Figure 1.1), have selectivity towards different cancer types and strikingly different side effect profiles which cannot be explained by DNA binding alone.

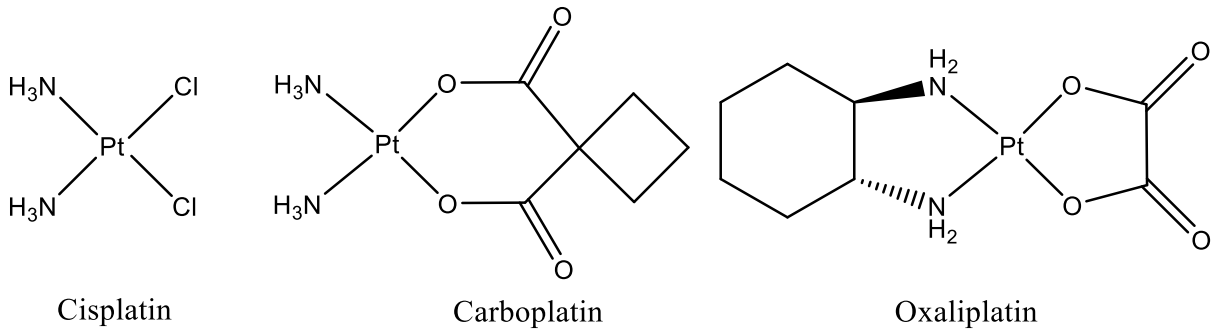

Figure 1.1 Structures of the three FDA approved platinum anti-cancer compounds currently in clinical use

There has also been an interest in the development of non-platinum based metallodrugs for cancer due to problems commonly associated with platinum therapy such as resistance and severe side effects.[33] Metallodrugs based on iron, ruthenium, osmium, iridium, rhodium, rhenium have been explored as potential anti-cancer agents.[33] Amongst these new agents, the

ruthenium metallodrugs NAMI-A and RAPTA-T (Figure 1.2) have been shown to possess anti-metastatic and anti-angiogenic properties not seen in platinum compounds. However, there is limited data on the biological targets of these upcoming compounds.[33]

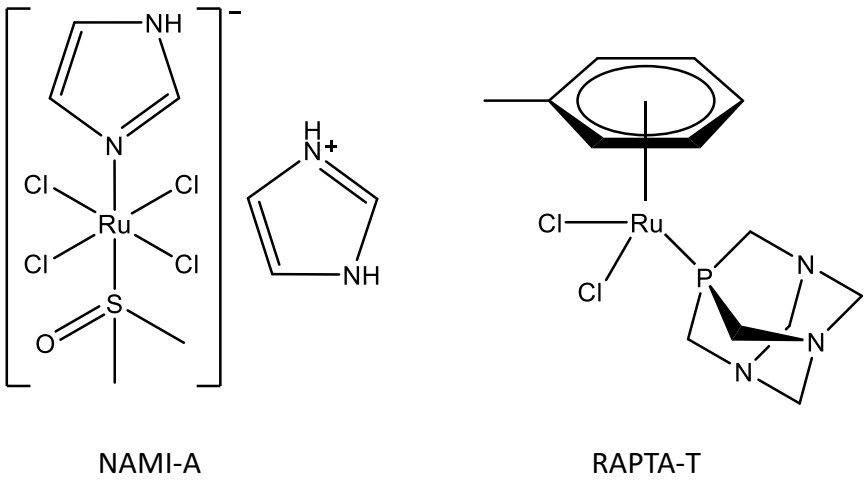

NAMI-A RAPTA-T

Figure 1.2 Structures of the ruthenium complexes NAMI-A and RAPTA-T

1.4 Mass Spectrometric Methods for Studying Metal Drugs

Mass spectrometry (MS) is an analytical technique that measures the distribution of mass-to-charge of ionized gaseous atoms/molecules in a sample. The first mass spectrometer was created by J.J. Thomson in 1897 to measure the mass-to-charge ratio of electrons.[34] Ever since, MS technologies have evolved tremendously, and the technique is applied in various settings such as environmental research, security checks, sports doping tests, clinical tests, and geological research.[35]

In the field of drug research, MS has emerged as a powerful tool for studying the mechanism of action of drugs. Various aspects of drug action can be studied via MS such as a) distribution of drugs in biological systems b) the protein targets of a drug and c) effects of a drug on a protein in terms of conformation, binding sites, or thermodynamic properties. In this section we discuss MS methods specifically for the study of metallodrugs and highlight their advantages and disadvantages including the recent literature surrounding them.

1.4.1 Cellular distribution of metallodrugs

Imaging mass spectrometry (IMS) for metallodrugs is mainly performed with four different techniques, namely matrix assisted laser desorption ionization-mass spectrometry imaging (MALDI-IMS), laser ablation-inductively coupled plasma mass spectrometry imaging (LA-ICP-IMS) and the secondary ion mass spectrometry (SIMS) techniques nanoscale SIMS (NanoSIMS) and time-of-flight SIMS (TOF-SIMS). An overview and comparison of the features, advantages and limitations of these mass spectrometry-based imaging techniques is shown in Figure 1.3 and Table 1.1, respectively.

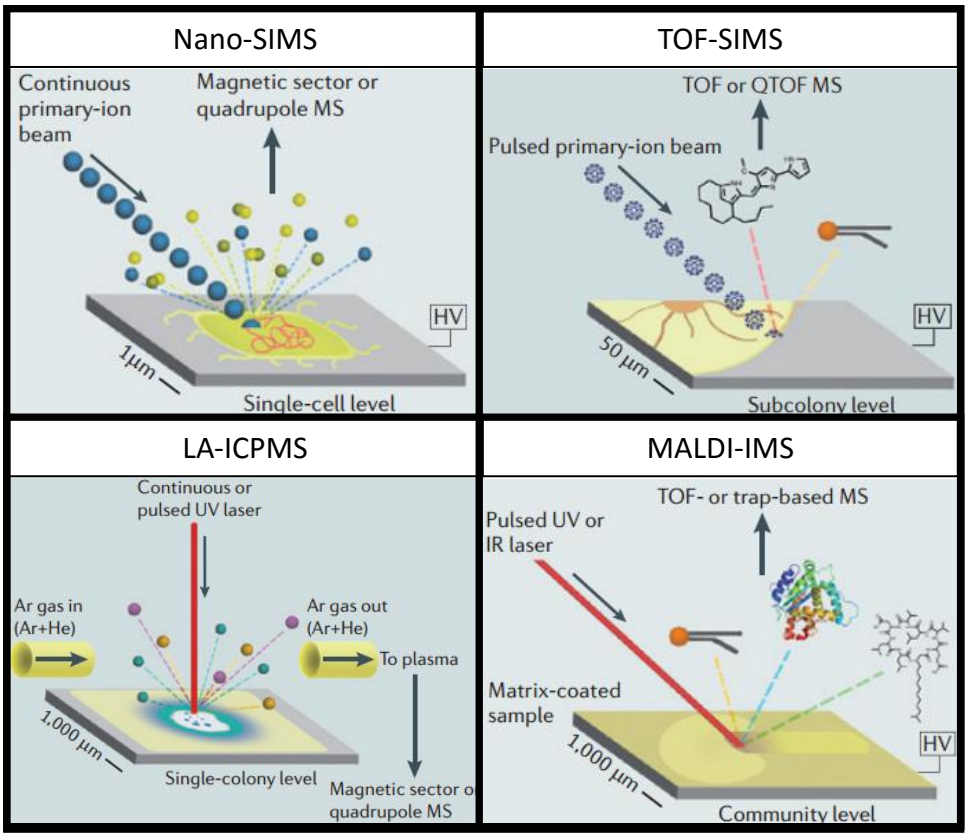

Figure 1.3 Illustration of the ionization sources of the different MS imaging techniques for metal drugs (adapted from Dorrestein et. al. *Nature Rev. Microbiol* 2011[36]).

In general, all IMS methods involve the rastering of a primary laser or ion beam onto a sample surface generating ions which are detected with a mass spectrometer. Images of single m/z ions are then generated where relative abundance is displayed as a false color image (in which colors represent signal intensity of each signal). In general, IMS requires no modifications of the parent compound for detection. However, isotopic labeling can be applied

in certain cases either to increase signal of endogenously ubiquitous elements or for quantitation.

Modality	Ion source	Ionization strength	Spatial resolution	Analyte type	Advantages	Disadvantages	Metal drugs elements imaged
Nano-SIMS	Ion gun	Hard	Up to 50nm	Atoms	High spatial resolution High sensitivity for smaller elements	Low sensitivity for transition metals Small sampling area Sample preparation must resist high vacuum Samples must be flat	Pt, Ru, Au
LA-ICP-MS	UV laser beam	Hard	Up to 1-10µm	Atoms	High sensitivity for transition metals Operates at atmospheric pressures	Low spatial resolution	Pt, Ru,
MALDI-MS	UV laser beam	Soft	Up to 20µm	Molecules	Analyses a full range of m/z Can operate at atmospheric pressures Non destructive	Samples must be covered in an organic matrix Low spatial resolution	Pt
TOF-SIMS	Ion gun	Hard	Up to 100nm	Molecules	Can analyse molecules Analyses a full range of m/z	Low sensitivity for transition metals Small sampling area Sample preparation must resist high vacuum Samples must be flat	Pt

Table 1.1 Comparison of different imaging MS techniques used in metal-based anti-cancer drug research.

For metallodrug imaging at the cellular level, an essential requirement is a high lateral resolution to resolve cellular structures and organelles. Amongst the IMS techniques used to probe the cellular distribution of metallodrugs, NanoSIMS is the most used in current practice, as it can achieve spatial resolutions of ca. 50 nm for metals and it can be used in conjunction with fluorescence microscopy[36] or electron microscopy[37], to further resolve cellular structures. SIMS methods has been used to characterize the subcellular distribution of several metallodrugs based on gold, platinum and ruthenium to elucidate their cellular targets and possible mode of action.

Platinum complexes act largely in the nucleus of cells, forming adducts with DNA leading to cell apoptosis.[38] The first reported use of NanoSIMS was to study cisplatin-induced intracellular alterations to the composition of kidney (LLC-PK_1) cells treated with 6 µM

cisplatin for 4 hours.[39] Although intracellular Pt was detected no subcellular distribution could be prescribed due to the low lateral resolution (500 nm) of the experiment. Nevertheless, this study showed the potential of NanoSIMS to study the distribution of metallodrugs at a cellular level and highlighted the major challenge of low sensitivity for the detection of certain transition metals.[39] Subsequently, the cellular distribution of the two ^{15}N labelled platinum(II) complexes, cisplatin and TriplatinNC, was determined in MCF7 human breast adenocarcinoma cells dosed at 20 μM with the compounds. The images showed that the polynuclear Pt compound, TriplatinNC, accumulated in the nucleolus and in cytoplasmic vesicle-like structures. Interestingly, an increased non-correlation between ^{15}N and Pt signals was observed from 1 to 2 hours incubations, showing the dissociation of the NH_3 ligands from the Pt complex, indicating metabolism of TriplatinNC. However, with cisplatin Pt or ^{15}N signals were not detected in the cells further exemplifying the sensitivity issues associated with NanoSIMS.[40]

A more recent study combined fluorescence microscopy with NanoSIMS analysis to map the distribution of cisplatin in SW480 colorectal cancer cells.[36] Cells were treated with ^{15}N labelled cisplatin (at different concentrations ranging from 0-150μM for 24 hours) and Pt was found to accumulate in small cytoplasmic sulfur-rich aggregates, acidic organelles and the nuclei. From plots of ^{15}N vs. Pt accumulation in different cellular organelles, they observed a partial dissociation of the Pt-N bonds in cisplatin, particularly within the nucleolus at high cisplatin concentrations (ca. 150 μM). With correlative fluorescence microscopy using lysotracker red to label acidic organelles, Pt and florescence images overlapped showing accumulation of cisplatin in these organelles.[36]

The distribution of cisplatin in U87MG human glioblastoma cells has been determined using TOF-SIMS in cells dosed with 30 μM of the compound for 48 hours.[41] Platinum concentrations were found to be up to 1.5 times higher in the nucleus compared to the cytoplasm. In addition, up to 40 different phospholipids were identified on the cell membrane, highlighting a key strength of TOF-SIMS where besides localization of the metallodrug, information on the surrounding cellular environment is also mapped simultaneously. However, current limitations in the spatial resolution for Pt detection in TOF-SIMS precluded subcellular differentiation other than between the nucleus and cytoplasm .[41]

Platinum drug loaded nanoparticle formulations help to target the drug to tumors potentially reducing side effects.[42] Probing the intracellular distribution of such nanomedicines

is important to understand release characteristics of the metallodrug from the nanocarrier and, in a recent study, the fate of oxaliplatin loaded in polymeric nanoparticles was studied in HeLa cells following treatment with 3 µM for 4 and 24 hours. Fluorescence structured illumination microscopy and NanoSIMS were combined to image the cellular distribution of the ^{15}N & florescent labelled nanoparticle polymer and the oxaliplatin.[43] Figure 1.4 shows time dependent NanoSIMS maps of nanoparticle treated cells. It can be seen that from 4 to 24 hour incubations, there is an increased uptake of the nanoparticles and a dissociation of ^{15}N from Pt signals showing the release of free Pt from the nanoparticle which correlates well with the observed cytotoxicity of the formulation.

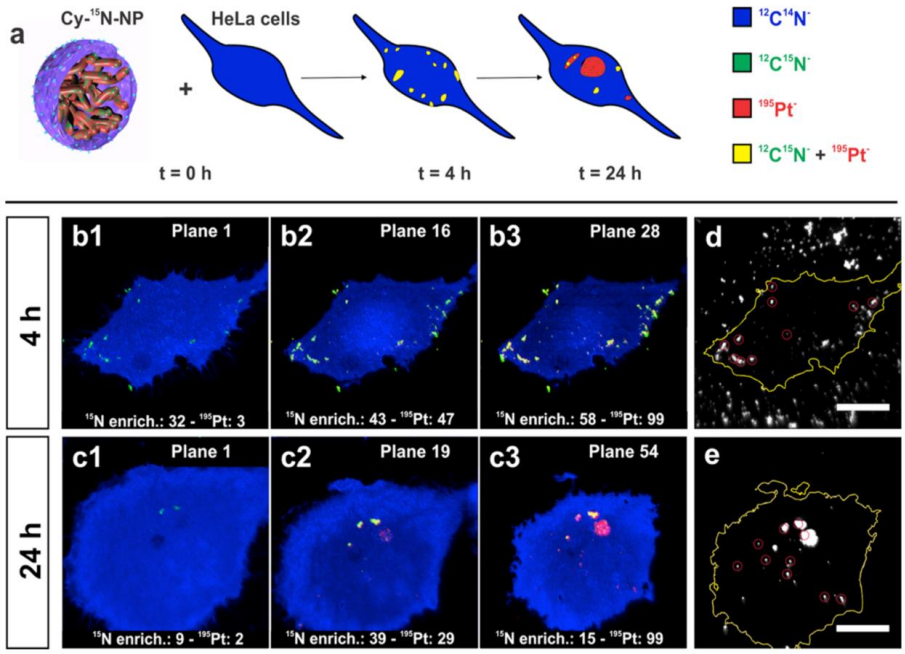

Figure 1.4 (a) Scheme summarizing the time-dependent NanoSIMS experiments carried out in HeLa cells treated with Cy-^{15}N-NP. (b and c) HeLa cells incubated with Cy-^{15}N-NP for 4 h (top three panels, b1−3) or 24 h (bottom three panels, c1−3) and imaged by NanoSIMS. Removal of layers of organic matter from the cell surface followed by imaging shows colocalization (yellow) of the ^{195}Pt (red) and ^{15}N (green) of the NP inside the cell. The cell surface is represented by the $^{12}C^{14}N^-$ ion map (blue). Summed observed ^{195}Pt signals (white pixels) in HeLa cells incubated for 4 h (d) and 24 h (e). Red circles are the ROIs selected for $^{15}N/^{14}N$ quantification where ^{195}Pt counts are observed. Cell boundaries (yellow line) were delimited from the corresponding $^{12}C^{14}N^-$ ion images. The averaged ^{15}N and ^{195}Pt signals per selected ROIs at each of the selected planes are shown for panels b and c. The scale bars represent 10 µm. (Adapted from Proetto et. al *ACS Nano* 2016).

The distribution of two investigational platinum (IV) complexes in tissue and cells extracted from an *in vivo* murine CT-26 colon cancer model was probed using LA-ICP-MS and NanoSIMS.[44] LA-ICP-MS was used to study the platinum accumulation on tissue level in the kidneys and tumor to select areas with highest Pt levels for further cellular distribution investigations using NanoSIMS. In the renal cortical cells Pt was found to accumulate in cells

of the glomerulus relative to the tubules, with Pt accumulating in sulfur rich organelles in the podocytes of the glomerulus. In the tumor cells similar amounts of platinum were detected in the nucleus and cytoplasm. However, local Pt levels in the nucleolus were elevated and cytoplasmic Pt accumulation was also concentrated in sulfur-rich organelles, namely in lysosomes (identified by electron microscopy).

Gold complexes are currently used in clinics as anti-arthritic medications and their potential as anticancer agents has also been investigated. [45,46] Gold has a high affinity towards organosulfur (S) and selenium (Se) moieties and it has been assumed that a subcellular target of certain gold complexes includes the thioredoxin system, a family of proteins responsible for redox homeostasis in the cytoplasm, mitochondria and nucleus of cells.[47] Gold(I) complexes with bidentate phosphine ligands have been shown to be selectively toxic to cancer cells thus studying the cellular distribution of these complexes could help to confirm their mechanism of action.[45] In a combined study using NanoSIMS and energy filtered transmission electron microscopy (EFTEM) the subcellular distribution of the Au(I) phosphine complex, $[Au(d2pype)_2]Cl$, was investigated in MDA-MB-231 human breast adenocarcinoma cells.[37] Gold was observed to accumulate in aggregates, mostly in non-DNA containing nuclear areas and inside the nuclear membrane. Figure 1.5 shows the elemental images of $^{31}P^-$, $^{197}Au^-$ and ^{34}S, with overlaid images mapping Au and S regions. Images (c) and (d) in Figure 1.5 show a clear co-localisation of Au and S which is in accordance with the hypothesis that gold complexes bind to S rich regions in the thioredoxin system.[37]

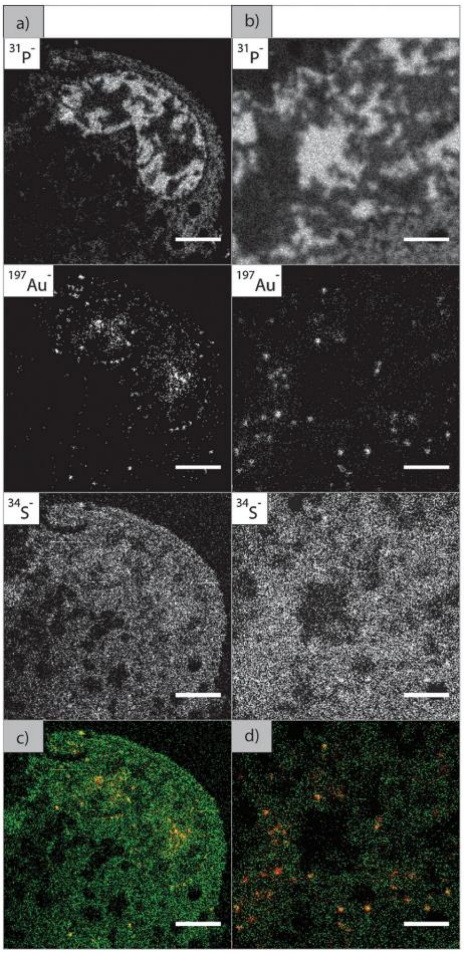

Figure 1.5 (a) and (b) NanoSIMS ion maps showing ^{31}P and ^{197}Au and ^{34}S secondary ions in MDA-MB-231 cells after 2 h incubation with 1 (100 mM). (c) and (d) are overlays of the ^{34}S and ^{197}Au ion maps shown in (a) and (b), respectively, where ^{34}S and ^{197}Au are falsely coloured in green and red, respectively. Yellow pixels indicate colocalisation of ^{34}S and ^{197}Au, which can be observed in the cytoplasmic, perinuclear and nuclear regions. Scale bars: (a) and (c) = 2 mm, (b) and (d) = 1 mm. (Reproduced from Wedlock et. al *Metallomics* 2011).

The lateral resolution in LA-ICP-IMS is mainly influenced by the laser spot diameter and the wash out times of the cell. Depending on the laser parameters used and the nature of the experiment the typical lateral resolution for bioimaging studies in tissue samples by LA-ICP-MS lies in the low µm to the tenths of µm range.[48] In recent years, advances in cell design as well as strategies in sample preparation (such as antibody or elemental labelling) have enabled the detection of elements with LA-ICP-MS at the cellular level.[49] Thus far the technique has been used to study the distribution of biomarkers in breast cancer tissue[49] and to study Ag and Au nanoparticles in cellular substructures of individual cells.[50]

A recent study adapted a LA-ICP-MS setup to determine the uptake of platinum(IV) complexes in multicellular tumor spheroids as possible screening and selection tool for novel metallodrugs.[51] Three dimensional multicellular tumor models are increasingly used as bridge

between conventional monolayer cell culture systems and animal models in preclinical metal-based anticancer drug development. Depending on their size they are able to mimic the complex tumor microenvironment in terms of oxygen, pH gradients, the development of a necrotic core and hypoxic regions.[52] The lateral resolution of approximately 10 µm allowed the accumulation of platinum in the different compartments of the tumor spheroid to be visualized, showing that platinum(IV) complexes are not only taken up by the tumor spheroids, but are also able to penetrate into the different layers reaching the necrotic pseudo-tumor core.[51] A subsequent study was able to correlate the platinum distribution, determined by LA-ICP-IMS, in HCT116 tumor spheroids with the total platinum uptake determined by ICP-MS and the spatially-resolved platinum accumulation in tumor tissue.[53]

1.4.2 Protein target screening

Mass spectrometric approaches for target screening of small molecules can be broadly divided into three types, namely expression profiling based, affinity purification based, and proteome stability based approaches. The principles, advantages and disadvantages of each are summarized in the following table.

Method	Principal	Advantages	Disadvantages
Expression profiling	Protein expression between a biological system (cell/tissues/animal) treated and untreated with small molecule are quantified via MS and correlated to its target.	No modification of parent drug required Done in intact systems (cells or tissue) Can obtain information regarding pathways affected by the drug	Does not measure binding directly, thus usually statistical methods are used to correlate small molecule target
Affinity purification	Immobilized small molecule is incubated with cell/tissue lysate and washed. The captured proteins are then identified via MS and correlated to the small molecule target.	Only method that measures a direct binding event	Requires modification of parent compound Requires lysis of cells; i.e. doesn't account for distribution of small molecule into cells
Proteome stability	Proteome of a biological system (whole cells or lysate) is destabilized (by heat or enzymatically), and under the assumption that small molecule binding stabilizes its target, protein quantities measured by MS are correlated to the small molecule target.	Correlates better with actual drug target (versus just measuring expression) Optimized experimental setup would also allow expression profiling data to be acquired simultaneously	Assumption of increased stability may not always hold true generating false negatives Experimentally more complex as destabilization method requires optimization

Table 1.2 Comparison of the different mass spectrometry techniques for small molecule target identification.

Ideally a method for screening small molecules protein targets would function on an intact cellular/tissue/animal system, involve no or little modification of the small molecule and able to measure direct binding of a drug to proteins. As seen in table 1.2, no method

encompasses all these characteristics, however for organic molecules, affinity purification based proteomics approaches are widely used and have been successful in identifying the targets of kinase inhibitors and natural products.[54] However, for metal drugs affinity based methods are challenging. To immobilize a drug for affinity purification, appropriate chemical strategies must be selected such that the resulting molecule is stable with activity similar to that of the parent compound. For organic molecules, this is achieved by introducing long linkers located far from the drugs binding site. For metal drugs however, this is less straightforward as a) most metal drugs are prodrugs, b) ligands surrounding the metal center can be labile and might play an important role in the drugs mechanism. Furthermore, metal drugs tend to be promiscuous in protein binding, thus strategies that expose these compounds to a mixture of proteins (e.g. cell lysate), may yield many unspecific targets.

A study using affinity purification of a ruthenium(II) based RAPTA-type complex was described for lysate of ovarian cancer CH1 cells, where RAPTA was chemically bound via the arene to biotin.[55] Initial pull-down experiments detected 184 protein targets, which were narrowed down to 29 via competition experiments with free compound. Amongst these they identified several classes of cancer related proteins which were suspected to be the targets or RAPTA, ranging from extracellular growth factors, cell cycle regulators, histone related, and ribosomal proteins which are listed in Table 1.3.

Protein type	Gene	Name	Drug pull-down (data set 1)[a]	Competition experiment (data set 2)[a]
Extracellular growth factor	MK_HUMAN	Midkine	6	2
	PTN_HUMAN	Pleiotrophin	5	3[b]
	FGFP3_HUMAN	Fibroblast growth factor-binding protein 3	2	0
Cell cycle-regulating	GNL3_HUMAN	Guanine nucleotide-binding protein-like 3	2	0
	FA32A_HUMAN	Protein FAM32A	4	0
	VIR_HUMAN	Protein virilizer homolog	3	0
	CGBP1_HUMAN	CGG triplet repeat-binding protein 1	2	0
Histone-related	H31_HUMAN	Histone H3.1	4	1
	FBRL_HUMAN	rRNA 2′-*O*-methyltransferase fibrillarin	2	0
	CGBP1_HUMAN	CGG triplet repeat-binding protein 1	2	0
Ribosomal	RS20_HUMAN	40S ribosomal protein S20	2	0
	RRP1B_HUMAN	Ribosomal RNA processing protein 1 homolog B	4	1

[a] The numbers indicate the spectral counts. [b] Decrease of spectral counts by a factor of 1.5.

Table 1.3 List of cancer-related proteins identified by chemical proteomics (adapted from Babak et. al *Chem Sci* 2015).

The mentioned work, while proving the applicability of affinity purification based proteomics approaches to metal complexes, also highlights issues with metal drug promiscuity where only 15 of the 29 proteins obtained were cancer related. Other studies on RAPTA

complexes utilized expression profiling for protein target identification which allowed the use of unmodified compound and takes into account the distribution of metal drugs into the biological system of choice. A profiling study on protein expression in A2780 ovarian cancer cells upon treatment with 300 µM of RAPTA-T for 3 hours followed by 2D liquid chromatography separation before mass spectrometry analysis was done revealing expression changes in 74 different proteins.[56] Of these, nearly 40% were histone related, and the remaining were mitochondrial related (11%), cytosolic proteins (7%), ribonuclearproteins (4%), plasma membrane proteins (4%), and endoplasmic reticulum related proteins (1%). In a related study, protein expression profiles of the same A2780 cell line treated with the antimetastatic ruthenium metal drugs RAPTA-T and NAMI-A at 50 µM for 24 hours was performed applying a 2D gel separation methodology.[57] The study discovered a very similar profile of expression changes induced by both compounds and was significantly different from that of the platinum compound cisplatin. Tables 1.4 and 1.5 summarize the targets found by the study.

Table 1
Mass spectrometry identified proteins.

Spot no.	AC[a]	Protein name	MASCOT search results			Fold change[e]	
			No. of matched peptide[b]	Sequence coverage%[c]	Score[d]	NAMI-A/control	RAPTA-T/control
1	Q969Q6	Serine/threonine-protein phosphatase 2A regulatory subunit B	7	19	94	1.39	
2	Q08752	Peptidyl-prolyl cis-trans isomerase D	6	24	99	1.31	
3	P29692	Elongation factor 1-delta	9	31	102	1.67	
4	P07339	Cathepsin D	5	14	72	1.31	
5	P26447	Protein S100-A4	2	RTDEAAFQK	54/34	1.42	
6	Q06830	Peroxiredoxin-1	7	45	127	1.47	
7	Q9BWD1	Acetyl-CoA acetyltransferase, cytosolic	7	34	108		1.42
8	P33316	Deoxyuridine 5′-triphosphate nucleotidohydrolase, mitoch.	6	32	107		1.45
9	P62253	Ubiquitin-conjugating enzyme E2 G1	2	YGYEKPEER	35/32		1.40

[a] Swiss-Prot/TrEMBL accession number.
[b] Number of peptide masses matching the top hit from Ms-Fit PMF.
[c] Percentage of amino acid sequence coverage of matched peptides in the identified proteins.
[d] MASCOT score (Matrix Science, London, UK; http://www.matrixscience.com).
[e] Fold change (NAMI-A *vs* control and RAPTA-T *vs* control) was calculated dividing %V from NAMI-A or RAPTA-T by the %V from control.

Table 1.4 Mass spectrometry identified proteins (adapted from Guidi et.al. *J Inorg Biochem* 2013).

Table 2
Mass spectrometry identified proteins in common between the two compounds.

Spot no.	AC[a]	Protein name	MASCOT search results				
			No. of matched peptide[b]	Sequence coverage%[c]	Score[d]	Fold change[e]	1-Way-ANOVA
10	Q9NQR4	Omega-amidase NIT2	11	41	176	1.37	0.022
11	P23919	Thymidylate kinase	10	44	122	1.52	0.035
12	P49773	Histidine triad nucleotide-binding protein 1	7	64	114	1.54	0.031
13	Q9NRF9	DNA polymerase epsilon subunit 3	2	EALPDGVNISK	50/33	−1.62	0.035
14	P61758	Prefoldin subunit 3	4	LKGQIPEIK	48/33	1.36	0.015

[a] Swiss-Prot/TrEMBL or NCBInr accession number.
[b] Number of peptide masses matching the top hit from Ms-Fit PMF.
[c] Percentage of amino acid sequence coverage of matched peptides in the identified proteins. Reported sequence peptide correspond to one of those resulted from MS/MS analysis after ambiguous identifications by MALDI-ToF in that spot.
[d] MASCOTscore (Matrix Science, London, UK; http://www.matrixscience.com).
[e] Fold change [NAMI-A + RAPTA-T] vs [Control] was calculated dividing %V from NAMI-A and RAPTA-T by the %V from control.

Table 1.5 Mass spectrometry identified proteins in common between both compounds (adapted from Guidi et.al. *J Inorg Biochem* 2013).

For cisplatin, various expression profiling studies have also been performed.[58–62] Simple expression profiling studies provide a general idea of the possible classes of protein targets perturbed by drug exposure, but do not pinpoint the actual proteins targeted by these drugs. There are, however, new expression profiling approaches which utilize modified experimental conditions combined with biostatistics calculations to deduce drug targets from induced changes in protein expression profiles. One such approach deemed functional identification of targets by expression profiling (FITExP)[63] will be discussed later in chapter 3.

Methods that identify targets based on protein stability could be very useful for finding the targets of metal drugs. These methods infer the protein target of a drug by its effect on stabilizing its bound target to either enzymatic degradation[64] or thermal denaturation.[65] Thus, protein targets can be identified by comparison with untreated controls. Though not yet applied to metallodrugs, these methods have been used successfully to validate known targets and identify new targets of drugs such as rapamycin, FK506, dasatinib, staurosporine and FSK3182571. Experimentally, these are more complex than simple expression profiling, however protein stability methods provide information on both the drug targets, and expression profiles of the compound on the biological system of choice. Furthermore, since no modifications to the parent compound are required and such systems can be adapted for use in intact cells, they show great potential for the discovery of metal-drug targets.

1.4.3 Specific metallodrug-protein interactions

Mass spectrometry has emerged as a powerful tool to study interactions of metallodrugs with proteins, and properties such as bound amino acid residues, changes in protein conformation, and binding constants can be determined. The main MS techniques that can be used to study metallodrug-protein interactions are bottom up or top down MS/MS proteomics, ion mobility MS, and hydrogen/deuterium exchange, and are detailed in Table 1.6.

Method	Principal	Instrumentation required	Information obtained	Advantages	Challenges
Bottom up MS/MS	Metallodrug-protein incubations are enzymatically digested and fragments are analysed by MS to correlate metallodrug binding sites on proteins	Mass spectrometers coupled with LC separation would work	Amino acid residues in a protein where metallodrugs are bound	Does not require high end mass spectrometers Analysis of peptide spectra simpler	More sample treatment required Enzymatic digestion/column separation may alter binding sites
Top down MS/MS	Metallodrug-protein incubations are directly analysed by fragmentation MS to correlate metallodrug binding sites on proteins	Usually an orbtitrap or FT-ICR mass spectrometers for proteins above 10kDa, though lower resolution machines can be used for smaller proteins.	Amino acid residues in a protein where metallodrugs are bound	Retains modifications to proteins more readily due to minimal sample pre-processing	Efficiency varies based on fragmentation method chosen Data interpretation difficult Requires expensive mass spectrometers Difficult for proteins > 30kDa
Ion mobility MS	Metallodrug-protein incubations are separated by ion mobility based on mass, charge, shape and size, subsequent MS analysis allows identification of separated species	Ion mobility mass spectrometer or modules allowing ion mobility like separations to be injected into existing mass spectrometers	Number of different conformers of metallodrug-protein adducts	Allows separation of different conformers for subsequent analysis	High cost
Hydrogen deuterium exchange (HDX)	Metallodrug-protein incubations are incubated with deuterated solvents and the rate of amide hydrogen/deuterium exchange rates in the presence and absence of ligand are correlated to conformational changes	HPLC modified for online pepsin digestion and column separation coupled with a mass spectrometer for peptide analysis	Protein conformation and changes, when bound to metal drug, binding constants.	Informative	Extensive method development required Need for expensive machinery or modifications of existing equipment for use

Table 1.6 Comparison of the different mass spectrometry techniques for specific metallodrug-protein interaction studies.

A bottom up workflow refers to one involving enzymatic digestion of large proteins into smaller peptide fragments before MS analysis.[66] Data obtained from these small fragments are then linked back to their parent proteins hence the term “bottom up”. This workflow was extensively developed for proteomic studies due to its amenability to measure complex protein mixtures and large proteins as well as being less reliant on high resolution mass spectrometers. Top down methodologies on the other hand, involve direct analysis of proteins via MS and

application of fragmentation to trapped gas phase ions to obtain structural information.[67] A comparison of both methods is shown in Figure 1.6. Currently, bottom up approaches provide more useful information on metallodrug-protein binding due to not being limited by protein size, where in top down analysis of proteins > 30 kDa[68] is difficult due to the high MS resolving power required for large proteins. Furthermore, analysis of different digested fragments obtained from bottom up experiments provides valuable information on non-terminal metallodrug binding sites on proteins. These are typically not seen in top down MS/MS experiments because the obtained spectra are complex and challenging to interpret and there is a lack of automated tools for such analysis. On the other hand, data obtained from bottom up approaches are thought to be less reliable due to the many processing steps involved prior to MS analysis, which could introduce artefacts such as ligand dissociation or shifts. Thus, with continual advancement of MS technology and software for automated analysis, top down methods may become the mainstay of metallodrug protein binding studies.

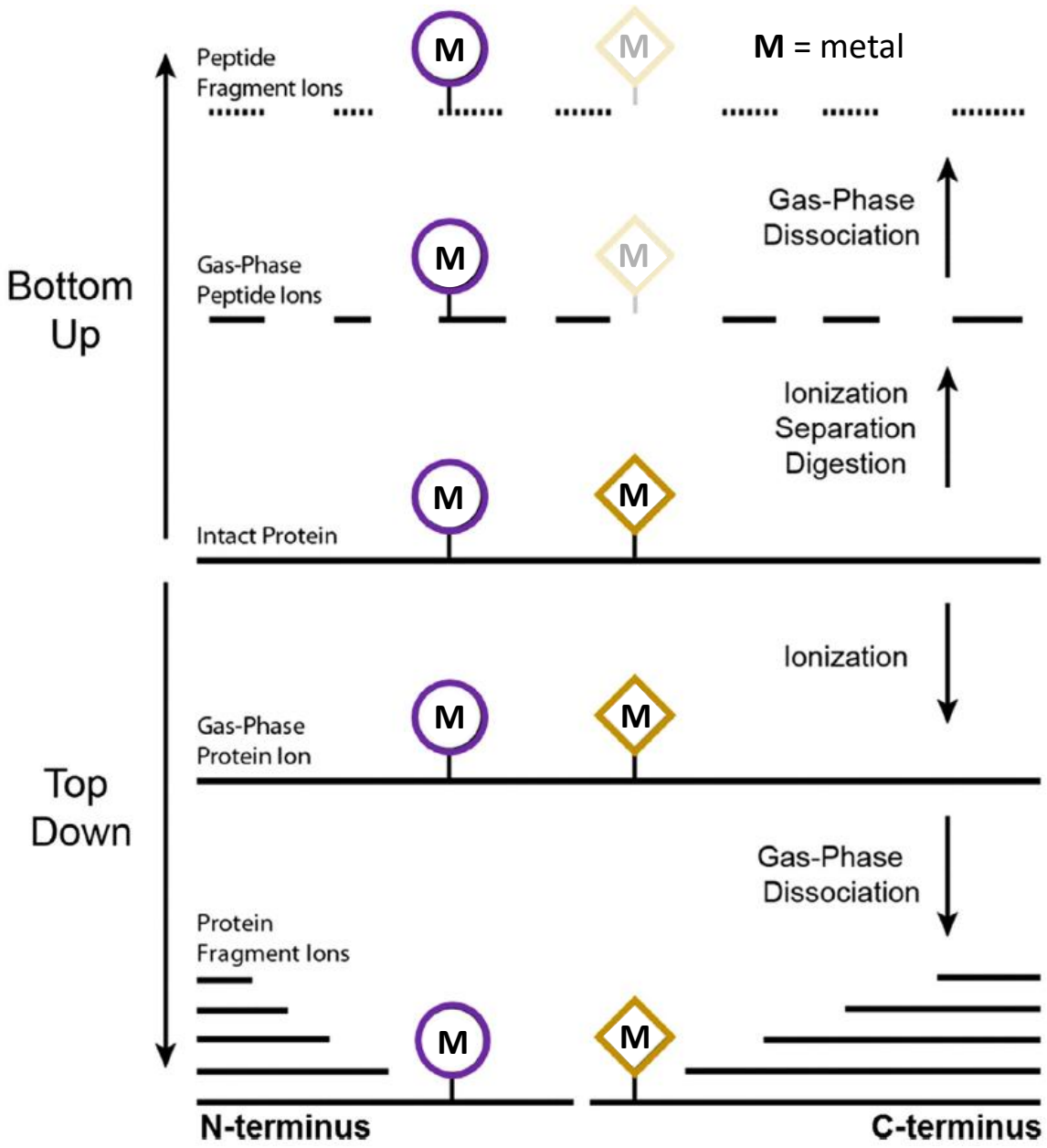

Figure 1.6 Comparison of Top Down and Bottom up mass spectrometry (Adapted and modified from Catherman et.al. *Biochem. Biophys. Res. Commun*., 2014).

Ion mobility spectrometry allows separation of ions in the gas phase based on their size and shape.[69] When combined with MS detection, it becomes a powerful technique that provides structural information on different conformers of ligands bound to macromolecules. This is especially useful for metallodrug-protein interactions, which can occur at different sites in a protein leading to various protein confirmations. Hydrogen/deuterium exchange coupled to MS allow the study of conformational dynamics of proteins following ligand binding. Structural

information on binding is obtained by measurement of the rate of hydrogen/deuterium exchange rates on the amide in the presence and absence of ligand which can be mathematically linked to induced conformational changes.[70]

For platinum based drugs various MS studies have been carried out. The binding sites of cisplatin on the calcium binding protein calmodulin was elucidated via a combinatorial bottom up and top down approach. The approach revealed binding of up to 8 atoms of Pt to Met, Glu and Asp residues in calmodulin resulting in the displacement of calcium.[71] With the undecapeptide substance P, cisplatin was bound to Arg and Lys residues and three different confirmers of this binding were revealed with ion mobility measurements.[72] Utilizing a bottom up approach to elucidate cisplatin binding sites to the 80 kDa iron binding glycoprotein transferrin,[73] Pt was seen at the hydroxyl group of Thr457 which is located in its iron(III) binding site. Furthermore, a study of cisplatin with the copper metallochaperone protein[74], Atox1 revealed the copper binding site Cys12GlyGlyCys15 as the primary binding site of cisplatin.

For the analysis of cisplatin-insulin adducts, both bottom up[75] and top down[76] approaches have been attempted. Platinum was found bound to the N terminal B chain His5, His10, Cys7, Cys19 residues and A chain Cys6, Cys7 Cys20 residues. It was also observed that the bottom up approach was more informative with 7 binding sites identified versus only 3 via top down. Another study confirmed the His10 binding site on the B chain of insulin[72], and also found additional binding sites, Glu13 and Glu31 as well as the cross-linking of residues Lys29 and E21.

A comparison of the fragmentation methods collision induced dissociation (CID), higher-energy C-trap dissociation (HCD), and electron transfer dissociation (ETD) for determining binding sites of oxaliplatin on ubiquitin was performed via top down MS. The study found Met1, Glu64 and His68 as the binding sites of the drug and showed that ETD was more useful than CID or HCD fragmentation for adduct site determination. Subsequently, binding of ubiquitin with three platinum drugs; cisplatin, transplatin and oxaliplatin was studied via top down MS with CID and infrared multiphoton dissociation (IRMPD).[77] It revealed binding of oxaliplatin and cisplatin to Met1 and transplatin to a short oligopeptide section of 19Pro-Ser-Asp-Thr-Ile-Glu24.

A comparative study of RAPTA-C, cisplatin and transplatin incubated with ubiquitin, cytochrome c and superoxide dismutase was performed using high resolution MS.[78] Through competitive experiments incubations of all 3 proteins in excess of metallodrug, it was found that platinum compounds were less selective than RAPTA-C, which was more reactive towards ubiquitin and cytochrome c than superoxide dismutase. Furthermore, both cisplatin and RAPTA-C have affinities towards similar amino acid residues upon binding. Bimetallic RAPTA complexes were incubated with a model peptide (amino acid sequence DAEFRHDSGYEVHHQK) and binding properties were studied via top down MS and IM-MS.[79] ETD fragmentation revealed binding and cross linking of the complex at His residues, and additional IM-MS studies revealed two isomeric adduct species leading the authors to propose crosslinking between His6-His13 and His6-His14.

1.5 Research objective and thesis layout

The study of how metallodrugs function is important for two reasons. Most metallodrug design approaches involve synthesizing libraries of these compounds and performing phenotypic screens against cancer models which has had limited success in generating new clinically approved drugs. Thus, an increased understanding of metallodrug action could allow tailoring of its ligands to achieve desired drug properties such as specific targeting and release or in choosing different metallodrugs for different cancer types, which could increase the success rate of metallodrug development. Also, metallodrugs which posess unique properties such as anti-metastic or anti-angiogenic action can be useful as tools to understand the molecular mechanisms of cancer. This knowledge could then be used to develop more effective cancer therapies.

As seen before, MS based approaches for studying the mechanism of action of metallodrugs has shed much light on the distribution, protein targets and specific interactions of these compounds. However, there are also various drawbacks associated with current MS methods, and some potentially useful MS based methodologies have been left unexplored. In this work, we develop and utilize MS approaches to study the mechanism of action of metallodrugs with a focus on cisplatin and RAPTA-type complexes. Specifically, the IMS method Nano-SIMS was developed and used to answer relevant biological problems related to cisplatin and RAPTA-T distribution in cells (chapter 2). Functional Identification of Target by Expression Proteomics (FITExP), was utilized to screen for potential protein targets of cisplatin,

RAPTA-T and RAPTA-EA (chapter 3), and we validated promising protein targets of RAPTA-T via enzymatic and binding assays (chapter 4). Finally, an automated tool for matching of complex mass spectra from high resolution top down and bottom up tandem MS was developed using ubiquitin-cisplatin/RAPTA-T as a model system (chapter 5) and then applied to study the binding of RAPTA-C and RAPTA-EA on the zinc finger region of the breast cancer susceptibility protein type 1 (chapter 6).

Chapter 2
NanoSIMS analysis of an isotopically labelled metallodrugs to probe their distribution and ligand state in cells.

2.1 Introduction

Mapping the distribution of drugs in cells is essential as it gives valuable insight into its site preference and mechanism of action and is therefore a useful tool for tuning the desired distribution properties of a drug. For metallodrugs, various strategies for mapping cellular distribution have been attempted such as florescence microscopy, radiation induced X-ray florescence (SR-XRF), energy-filtered transmission electron microscopy (EFTEM), and imaging mass spectrometry (IMS) which have been summarized well in the following review.[80] A unique property of metallodrugs is that they are usually prodrugs which undergo activation, either via ligand exchange or changes in oxidation state, before interacting with their desired target. This makes it difficult to apply methods that require external labels as used in florescence microscopy, as judicious selection of a non-labile site for attachment would be necessary in addition to selecting a suitable label which does not affect the physicochemical properties of the parent metallodrug.

An ideal technique for studying metallodrug distribution in cells, would involve minimal to no modification to the original compound, whilst possessing the ability to visualize the metal centre and all ligands simultaneously, with a good sensitivity and spatial resolution. In this respect the IMS technique nano-scale secondary ion mass spectrometry (NanoSIMS) provides a good balance of desirable properties such as a spatial resolution of up to 50 nm, often no requirement of labelling, and the ability to visualize both the metal centre and the ligands if isotope labels are applied or the ligands have elements rarely found in biological systems.

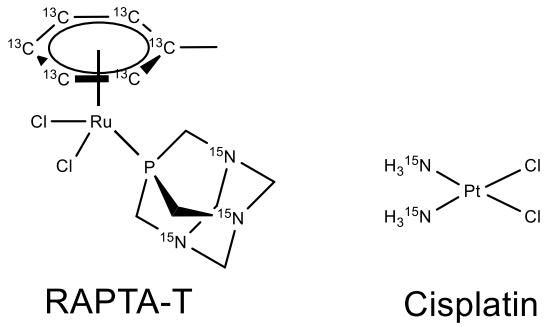

Figure 2.1 Structures of isotopically labelled metal complexes.

NanoSIMS mapping of metallodrugs has been carried out for both gold and platinum compounds in cells.[37,81] However, for ruthenium, an important metal where certain ruthenium metallodrugs are in clinical trials,[82] no NanoSIMS methods have been applied to probe the cellular distribution of these compounds. Here we developed a NanoSIMS method to study the distribution of ruthenium and platinum based metallodrugs in cells. We then apply this methodology to explore important biological problems related to the distribution of ruthenium and platinum based metallodrugs utilizing isotopically labelled RAPTA-T and cisplatin (Figure 2.1).

2.2 Results and discussion

2.2.1 Cell fixation

Samples prepared for NanoSIMS must meet several requirements for analysis. They must be topographically flat, conducting and able to resist high vacuum.[83] Thus cell sample preparation for NanoSIMS usually involves dehydration of the sample followed by resin embedding and sectioning for NanoSIMS and other complementary analysis. Fixing can be achieved via either chemical or cryo fixation methods, and with, cryo fixation achieved via high pressure freezing (HPF) and freeze substitution (FS) considered as the best method for preserving sample integrity.[84]

In this study, both chemically fixed and HPF-FS methodologies were used for NanoSIMS sample preparation. Figure 2.2 shows counts per layer of $^{102}Ru^-$ as $^{194}Pt^-$ for all NanoSIMS runs carried out. Although not directly comparable, as different cell lines and dosing regiments and fixation methods were used, the data gives a general idea of the sensitivity of NanoSIMS for these metals. On average, the sensitivity of NanoSIMS for ruthenium is lower than for platinum regardless of the sample preparation method. A 5-fold loss in sensitivity was observed when HPF-FS fixation was used instead of chemical fixation. This estimate takes into account that cisplatin was dosed for twice as long in chemically fixed cells and that previous reports show negligible difference in cisplatin concentration in A2780CR cells dosed for 3 or 24 hours at 10 μM.[85] For ruthenium a loss of sensitivity of about 2.5 fold was observed in HPF-FS fixed cells.

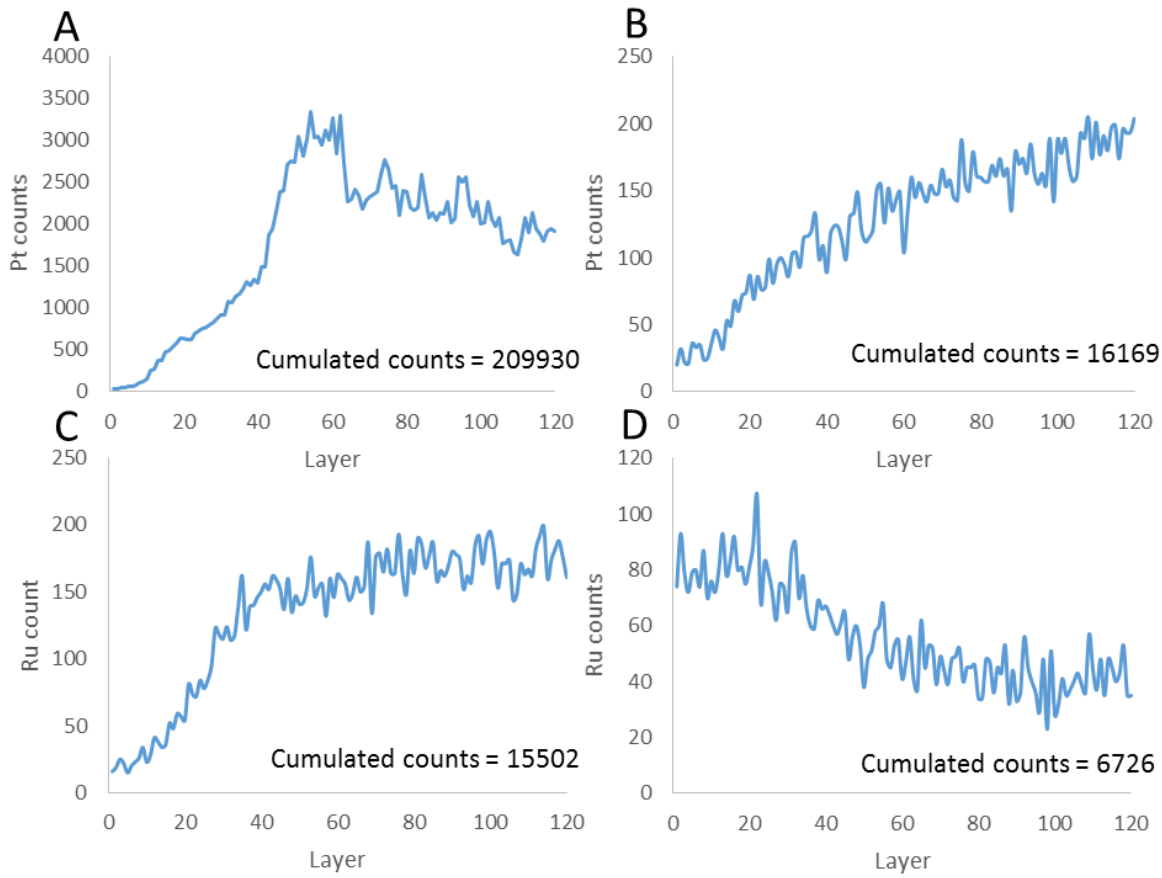

Figure 2.2 Graphs of mean counts $^{102}Ru^-$ and $^{194}Pt^-$ per layer. **A:** $^{194}Pt^-$ counts of chemically fixed A2780CR cells treated with cisplatin (30 µM, 24 hours). **B:** $^{194}Pt^-$ counts of high pressure freeze fixed A2780CR cells treated with cisplatin (30 µM, 12 hours). **C:** $^{102}Ru^-$ counts of chemically fixed A2780CR cells treated with RAPTA-T (500 µM, 24 hours). **D:** $^{102}Ru^-$ counts of chemically fixed MDA-MB-231 cells treated with RAPTA-T (500 µM, 24 hours).

The overall loss in sensitivity between conditions can be mostly attributed to the matrix difference due to sample preparation. Samples treated by HPF-FS have to be mixed with cryoprotectants (fetal bovine serum in our case). This could have reduced the sensitivity of NanoSIMS for ruthenium or platinum, thus judicious selection of cryoprotectants for HPF-FS should be taken to avoid such losses in sensitivity.

2.2.2 Sample cutting and considerations for TEM imaging

A challenging aspect of metallodrug analysis in NanoSIMS is the inherent low sensitivity for certain transition metal elements such at Pt and Ru due to: 1) Low quantity in the sample due to low uptake/dose or sample loss during sample preparation, 2) Low secondary ion yields of these elements, 3) matrix effects leading to lowered sensitivity.

For platinum and ruthenium based metallodrugs, the low sensitivity necessitates the use of long scan times of ~20 hours per image to obtain sufficient signals. Since NanoSIMS is a destructive technique, firing an ion beam for such long periods necessitates a sample surface thickness of 200-1000nm to avoid puncturing the sample during analysis and minimize signal drift during long analysis times. However, due to the limits of electron transmission, thick samples are difficult to analyze via transmission electron microscopy (TEM), a useful method providing ultrastructural details of cellular organelles which cannot be seen using NanoSIMS alone.

In our work, we attempted to circumvent this issue by consecutive sectioning of thin sections (~50 nm) for TEM followed by semi-thin sections (~500 nm) for NanoSIMS. As a result of the overlay of the TEM and NanoSIMS images, though not perfectly correlating, was considered sufficiently accurate, considering that the size of most cellular organelles are above 1 µm in diameter and that ion beam rastoring during analysis would only remove < 100 nm of the sample surface.

2.2.3 NanoSIMS imaging of isotopically labelled RAPTA-T in A2780CR cells.

To develop a NanoSIMS method for ruthenium imaging, we dosed a cisplatin resistant ovarian cancer cell line (A2780CR) with 500µM of isotopically labelled RAPTA-T (enriched with six ^{13}C atoms on η^6-toluene, and three ^{15}N atoms on PTA) for 24 hours. Subsequently the cells were chemically fixed, dehydrated, resin embedded and cut into semi thin sections for NanoSIMS imaging.

NanoSIMS was used to image the distribution of ^{13}C, ^{15}N, and Ru and in order to visualize where in cells the RAPTA-T molecules located, and if they remain intact, using the NanoSIMS we sputtered semi-thin sections with a primary Cs^+-beam current of 4 pA and a probe size of ~150 µm (see experimental section for details) for a scanning .time of ca. 22 hours, corresponding to 120 consecutive images with 256*256 pixels over an area of 30x30 μm^2. $^{102}Ru^-$ counts steadily increased with time, plateauing at around 8 hours (~40 planes) into the analysis (Figure 2.2, C), demonstrating that a large dose of Cs^+ implantation is required before efficient ionization of $^{102}Ru^-$ is achieved. Such long analysis times represent a severe challenge

with respect to machine stability. For example, even small thermal perturbations can cause the instrument, and hence the images, to drift. By minimizing any thermal perturbation to the instrument for over one week (including not entering the lab-space around the instrument), we obtained an image drift totaling only 6 pixels during the 22 hour acquisition period, corresponding to 0.7 microns. Such stable instrument conditions make it possible to add all images together with minimal drift correction, and thus obtain clear total images of even very weak signals.

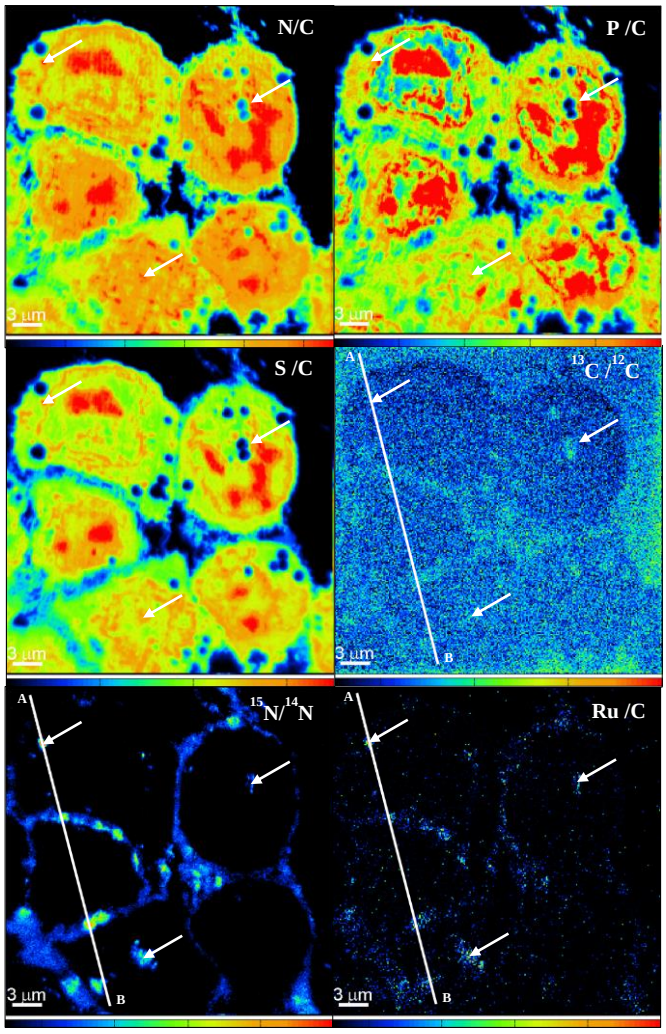

Figure 2.3 Secondary ion maps of $^{31}P^-/^{12}C_2^-$, $^{32}S^-/^{12}C_2^-$, $^{14}N^{12}C^-/^{12}C_2^-$, $^{15}N^{12}C^-/^{14}N^{12}C^-$, $^{102}Ru^-/^{12}C_2^-$ and $^{13}C^{12}C^-/^{12}C_2^-$ (Figure labels have been simplified) in A2780CR cells treated with ^{15}N and ^{13}C-labelled RAPTA-T (500 µM, 24 hours). White line (AB) represents the line profile shown in Figure 2.6.

Figure 2.3 shows the elemental distribution maps obtained from a resin-embedded section of A2780CR cells after 24 hours exposure to 500 µM of isotopically labelled RAPTA-T. Highly resolved images of $^{14}N^{12}C^-$, $^{32}S^-$, and $^{31}P^-$ allow clear visualization of the cellular

compartments of the cell (labelled in Figure 2.5, B). The $^{13}C/^{12}C$ map (Figure 2.3) shows faint variations in the $^{13}C/^{12}C$ between cell interiors and the adjacent epoxy resin (also observed in untreated controls, Figure 2.4), but no clear enrichments that can be ascribed to the presence of isotopically labeled RAPTA-T molecules, or its subcomponents. This absence of discernable ^{13}C enrichment in regions clearly enriched in ^{15}N and Ru (Figure 2.3 and 2.6) could indicate that sample preparation (which includes epoxy embedding) dilutes the ^{13}C-isotopic enrichment from the ^{13}C-enriched η^6-toluene ligands to below the detection limit of the NanoSIMS.[86] However, given the strength of the ^{15}N enrichment observed, the presence of the corresponding ^{13}C-enriched η^6-toluene ligands should be visible in these NanoSIMS $^{13}C/^{12}C$ images, which would reveal ^{13}C-enrichment anomalies down to about 30‰. Thus, it is not unreasonable to hypothesize that the ^{13}C-enriched η^6-toluene ligands have partially detached from the complex and have been diluted over the sample. Indeed, dissociation of the arene has been previously observed in binding studies to isolated oligonucleotides.[87] In humans, this detached toluene would undergo detoxifaction in the liver to hippuric acid which would then be excreted in the kidneys.[88]

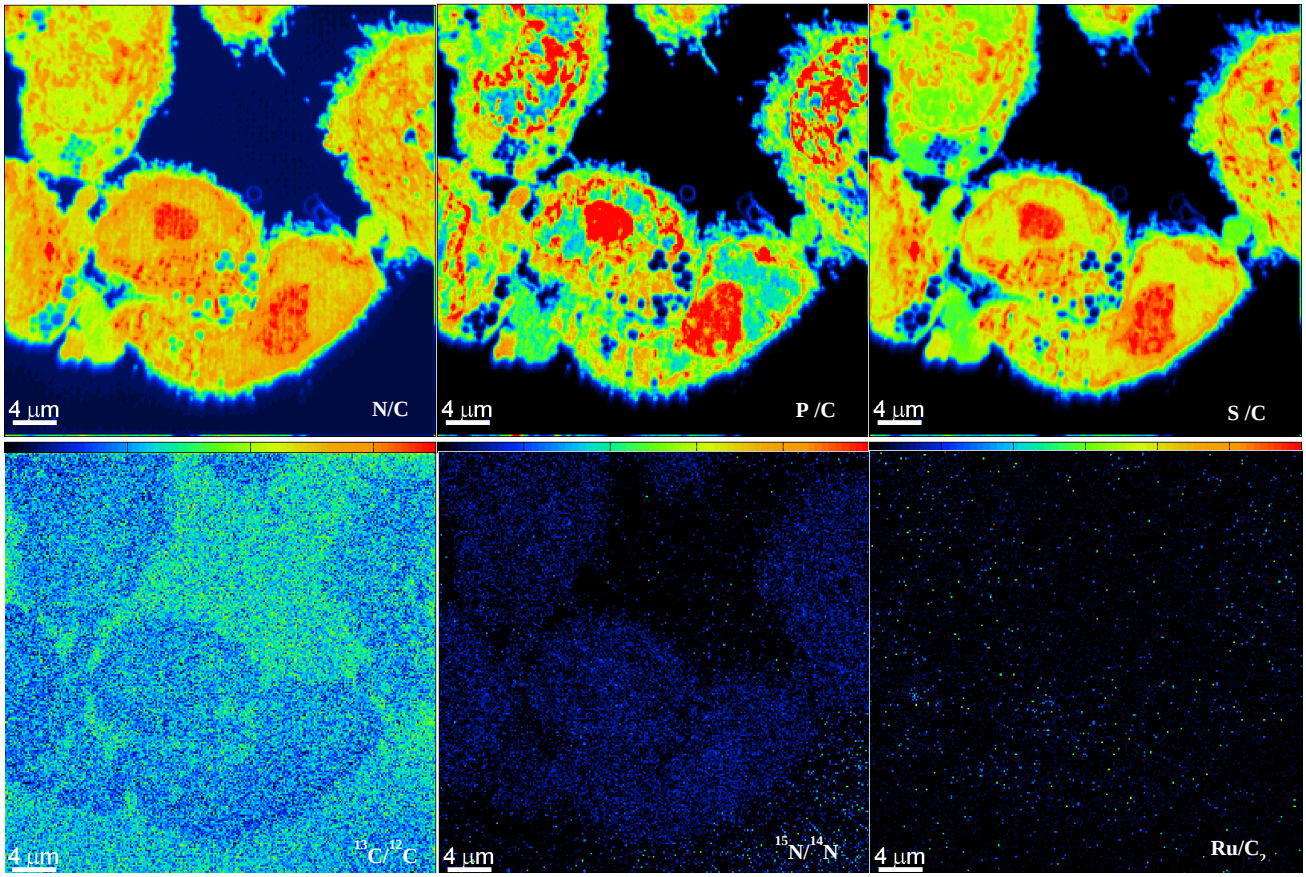

Figure 2.4 Secondary ion maps of $^{31}P^-/^{12}C_2^-$, $^{32}S^-/^{12}C_2^-$, $^{14}N^{12}C^-/^{12}C_2^-$, $^{15}N^{12}C^-/^{14}N^{12}C^-$, $^{102}Ru^-/^{12}C_2^-$ and $^{13}C^{12}C^-/^{12}C_2^-$ in untreated A2780CR cells. (Figure labels have been simplified).

On the other hand, overlaid images of $^{15}N/^{14}N$, Ru/C (Figure 2.5, D) and line profiles (Figure 2.6, B) reveal co-accumulation of ^{15}N and Ru indicating that the PTA ligand remains coordinated to the metal center after 24 hours. Enrichment via ^{15}N (hereby used as a marker for RAPTA-T enrichment) is mainly seen on the cell membrane or interphase between cells (Figure 2.5 A, B & C). The observed localization of RAPTA-T indicates that interactions with membrane receptors or extracellular proteins are likely to be critical to its mode of action. In this respect, it has been previously shown that RAPTA-T interacts with cell adhesion proteins such as fibronectin and collagen IV, preventing detachment and re-adhesion of highly metastatic breast cancer cells.[89,90]

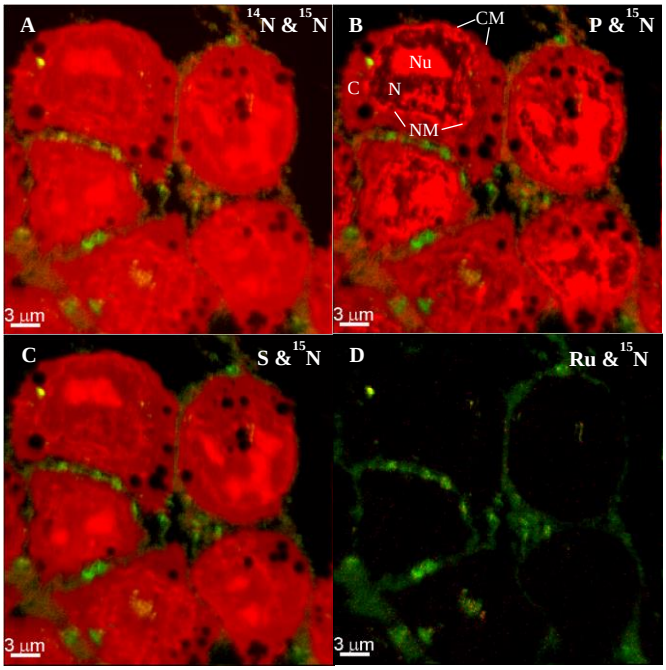

Figure 2.5 Composite RBG images of semi thin sections of A2780CR cells treated with ^{15}N and ^{13}C labelled RAPTA-T (500 µM, 24 hours). $^{15}N^{12}C^-/\,^{14}N^{12}C^-$ is coloured green and $^{31}P^-/\,^{12}C_2^-$, $^{32}S^-/\,^{12}C_2^-$, $^{14}N^{12}C^-/\,^{12}C_2^-$ and $^{102}Ru^-/\,^{12}C_2^-$ is coloured red (figure labels have been simplified). Subcellular compartments N (nucleus), Nu (nucleolus), C (cytoplasm), NM (nuclear membrane) and CM (cell membrane) have been labelled in image B.

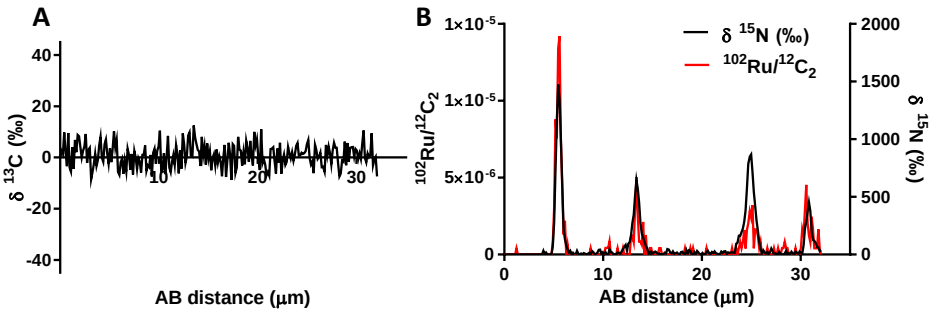

Figure 2.6 Line profiles of $^{13}C^{12}C^{-}/^{12}C_2^{-}$ (A) and overlaid line profile of $^{15}N^{12}C^{-}/^{14}N^{12}C^{-}$ and $^{102}Ru^{-}/^{12}C_2^{-}$ (B) across line AB (shown in Figure 2.3).

Only small pockets of Ru were observed inside the cells, (Figure 2.3, arrows). From the cellular compartments identified (Figure 2.5, B), these pockets seem to lie generally within the nuclear region of the cells which is likely as RAPTA complexes have been shown to bind to histones.[91,92] However, the exact subcellular localization cannot be determined accurately without correlated electron microscope imaging. The lack of correlation between these $^{102}Ru^{-}$ hotspots and $^{32}S^{-}$ shows that RAPTA-T distributes differently to cisplatin, which was found to accumulate in the nucleolus and S-rich regions of the cells.[81] This difference is not unexpected considering the contrasting *in vitro* and *in vivo* anti-tumor effects of cisplatin and RAPTA-T, respectively. The observed distribution pattern is in reasonable agreement with cell uptake studies of RAPTA-T in A2780 CR cells,[93] where ruthenium was found in the membrane as well as the particulate, cytoskeletal and nuclear fractions under similar treatment conditions.

From our data, the observed co-accumulation of ^{15}N and Ru shows that the PTA ligand remains coordinated to the ruthenium ion. This result highlights one of the key strengths of NanoSIMS for the detection of metal-based drugs, i.e. that the stability/lability of the ligands coordinated to the metal center can be probed via isotopic labelling. The ability to differentiate between the accumulation of a compound on the membrane versus intracellular accumulation in specific organelles illustrates the utility of the NanoSIMS relative to other techniques used to probe metallodrug distribution, other such techniques include inductively coupled plasma mass spectrometry and atomic absorption spectroscopy,[93,85,94,95] where such a spatial distinction cannot be made without cell fractionation, a process likely to introduce other distribution artifacts.

In the case of RAPTA-T, the liability of the η^6-toluene ligand presumably acts, in addition to aquation, as an activation mechanism of the compound, although the extent of

detachment is difficult to assess from the data. Moreover, the observed accumulation of Ru on the membrane or at the interface between cells is in agreement with a number of *in vitro* and *in vivo* properties of RAPTA-T[93,96] and provides further insight into the drugs mechanism of action.

2.2.4 NanoSIMS imaging of isotopically labelled cisplatin in ovarian cancer cells.

The method used to image RAPTA-T was adapted for imaging platinum via NanoSIMS. As a proof of principle, A2780CR cells were exposed to 30 μM of isotopically labelled cisplatin (enriched with two atoms of ^{15}N) for 24 hours. Subsequently the cells were chemically fixed and prepared for NanoSIMS imaging as semi-thin sections.

From secondary ion maps of Pt (Figure 2.7) there is no enrichment observed in the nucleus of A2780CR cells. This is not surprising considering cisplatin acts by forming adducts with DNA and thus its site of action is the nucleolus.[38] Therefore the resistance of this cell line could be due to reduced net Pt accumulation in the nucleus caused by mechanisms such as reduced uptake, increased efflux or increased detoxification of the drug.[38] Pt enrichment is generally well correlated with sulfur rich hotspots which could be associated with sulfur containing molecules such as glutathione, metallothioneines and thioredoxins which detoxify metals in cells. This was similarly observed in other reports of NanoSIMS for studying Pt distribution in cells.[81]

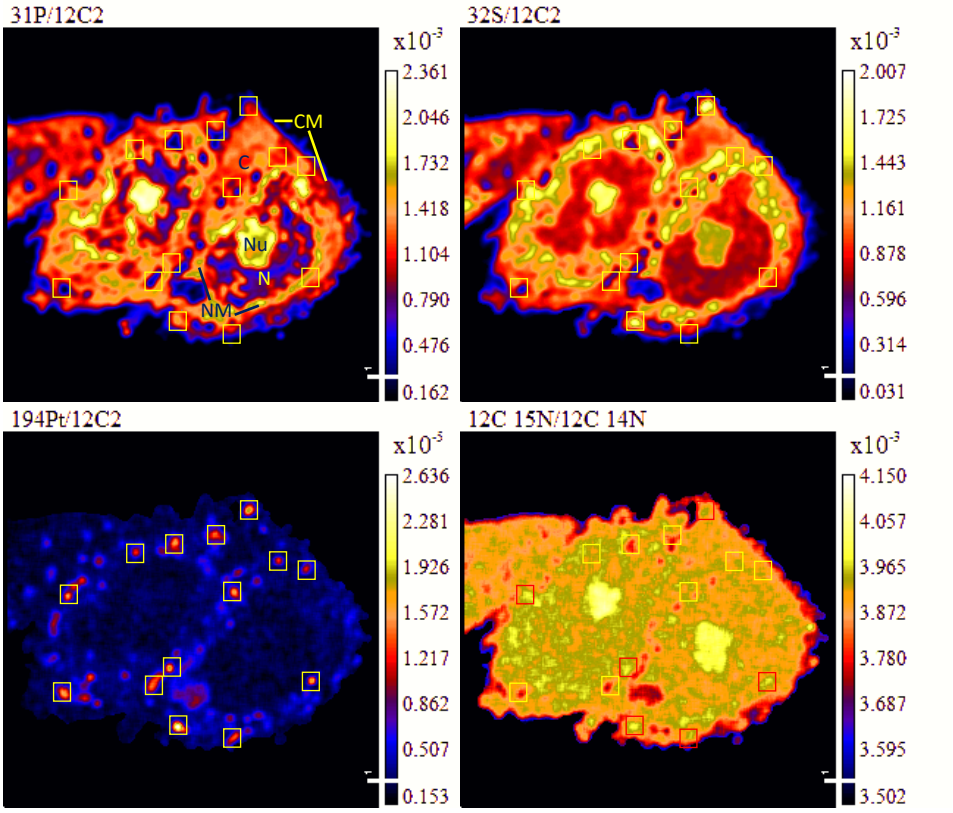

Figure 2.7 Secondary ion maps of $^{31}P^-/^{12}C_2^-$, $^{32}S^-/^{12}C_2^-$, $^{15}N^{12}C^-/^{14}N^{12}C^-$ and $^{194}Pt^-/^{12}C_2^-$ of two A2780CR cells treated with cisplatin (30 µM, 24 hours). Yellow boxes are platinum enriched hotspots. Subcellular compartments N (nucleus), Nu (nucleolus), C (cytoplasm), NM (nuclear membrane) and CM (cell membrane) have been labelled in the $^{31}P^-/^{12}C_2$ map.

There was a co-enrichment of ^{15}N and Pt observed at various Pt hotspots (red boxes in the $^{15}N/^{14}N$ maps in Figure 2.7). This shows that there is at least some detachment of the NH_3 ligand from cisplatin correlating to what was previously reported.[81] Surprisingly, we also observed an enrichment of ^{15}N in the nucleolus of the cells. Though we cannot explain this observation with our current experimental data, presumably over the course of the 24 hour incubation, cisplatin entered the nucleolus and subsequently the Pt moiety could be detoxified or effluxed leaving only the NH_3.

Having developed a Pt imaging method via NanoSIMS, we proceeded to apply this to study cellular resistance to cisplatin. Though cisplatin is used as first line treatment for a wide range of malignancies including testicular, ovarian and lung cancers, a major challenge with its use is the development of resistance to the drug which results in the recurrence of cancers insensitive to platinum therapy.[97] This resistance is thought to be mediated by a plethora of factors including under expression of membrane transporters, overexpression of drug efflux pumps, expression of proteins related to stress response such as heat shock and ribosomal

proteins, epigenetic changes in DNA methylation, chromatin and histones, changes in transcription factors and signalling pathways and involvement of microRNAs.[97]

Due to the complexity of cisplatin resistance, developing strategies for overcoming resistance to these drugs is challenging due to the many facets of resistance development. Thus it is important to understand which factors contribute most to resistance in order to find solutions to this issue. Imaging of the distribution of cisplatin in cells could shed light on resistance to cisplatin, as certain aspects of resistance can be localized to particular cellular organelles or seen as shifts in distribution or concentrations of the drug in cellular systems. Here, we studied the distribution of A2780 cisplatin sensitive and resistant cells exposed to 30 µM of isotopically labelled cisplatin for 12 hours. We applied HPF-FS as a fixation method as it is reported to be superior to chemical fixation in terms of retaining cellular morphology and distribution of diffusible ions.[98] The selection of a shorter incubation period of 12 hours and different fixation method was mainly due to our previous unexplained observation where ^{15}N was enriched in the nucleus in the absence of Pt. This could potentially be caused by distributional effects which occur over long incubation times or distributional defects caused by organic solvent dehydration during cell preparation for NanoSIMS thus we modified these parameters accordingly to resolve this.

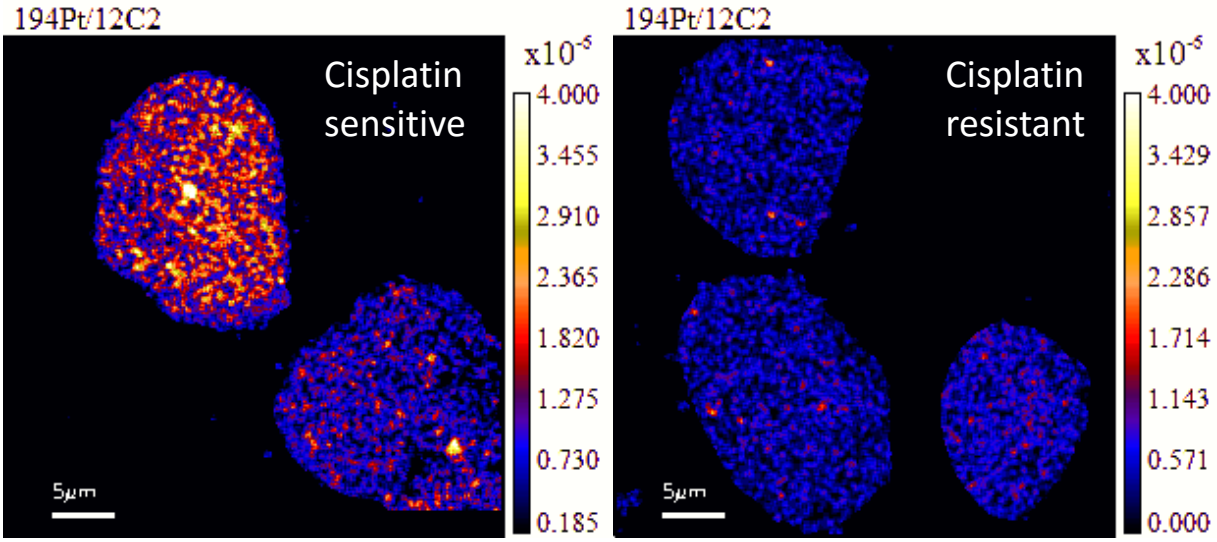

Figure 2.8 Secondary ion maps of $^{194}Pt^-/\ ^{12}C_2^-$ of A2780 sensitive and cisplatin resistant cells treated with cisplatin (30 µM, 12 hours).

NanoSIMS elemental maps of $^{31}P^-/^{12}C_2^-$, provide clear visualization of the major cellular compartments, including the nucleus, nucleolus, cytoplasm and nuclear/cellular membranes (Figure 2.9). The TEM images provided extra structural details of smaller organelles such as autophagosomes, mitochondria, and lysosomes. From the $^{194}Pt^-$ maps of A2780 and A2780CR cells (Figure 2.8), we observed much lower amounts of platinum in the cisplatin resistant cell. This difference in accumulation is in accordance with various studies comparing cisplatin resistant and sensitive cell lines[85,99,100], and agrees well with resistance being mediated by mechanisms of increased efflux or impaired uptake.[97]

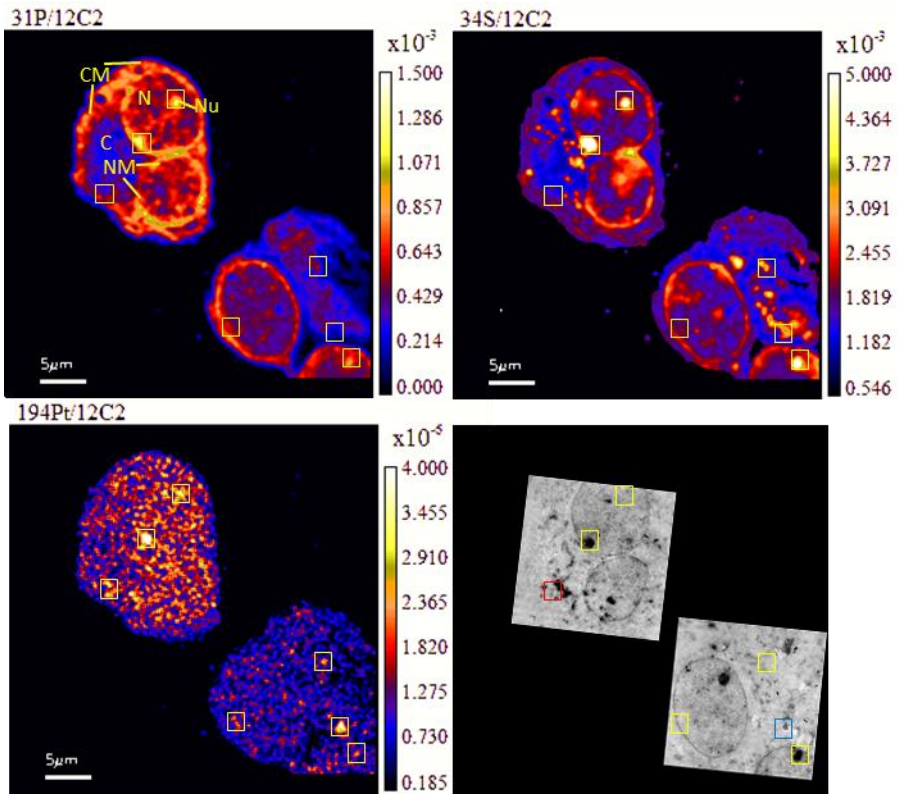

Figure 2.9 Secondary ion maps of $^{31}P^-/^{12}C_2^-$, $^{32}S^-/^{12}C_2^-$, $^{194}Pt^-/^{12}C_2^-$ and TEM of A2780 cells treated with cisplatin (30 µM, 12 hours). Boxes represent platinum enriched hotspots which were overlaid in other elemental maps and the TEM images. Mitochondria and autophagosome are labelled in red and blue boxes respectively in the TEM image. Subcellular compartments N (nucleus), Nu (nucleolus), C (cytoplasm), NM (nuclear membrane) and CM (cell membrane) have been labelled in the $^{31}P^-/^{12}C_2$ map.

We next scrutinized the distribution of platinum in the two cell lines to compare if resistance may be brought about by distributional differences between the cells. Significantly, combining NanoSIMS images with ~100 nm spatial resolution with excellent low nm spatial resolution of TEM images, allowed unparalleled comparison for determination of distribution of Pt in the cells. In A2780 cells (Figure 2.9), platinum was seen to distribute diffusely throughout the cell with some areas having larger agglomerations of Pt signal. These Pt hotspots

seem to co-accumulate at nucleolus of the cell as seen in both $^{31}P^-/^{12}C_2^-$ and TEM images. This is in agreement with cisplatins mechanism of action of entering the nucleolus and forming crosslinked adducts with DNA.[101] The distribution pattern however, also shows that only a small fraction of Pt is in the nucleolus and the remaining is thus largely available to interact with other cellular organelles and proteins as confirmed by various proteomic studies.

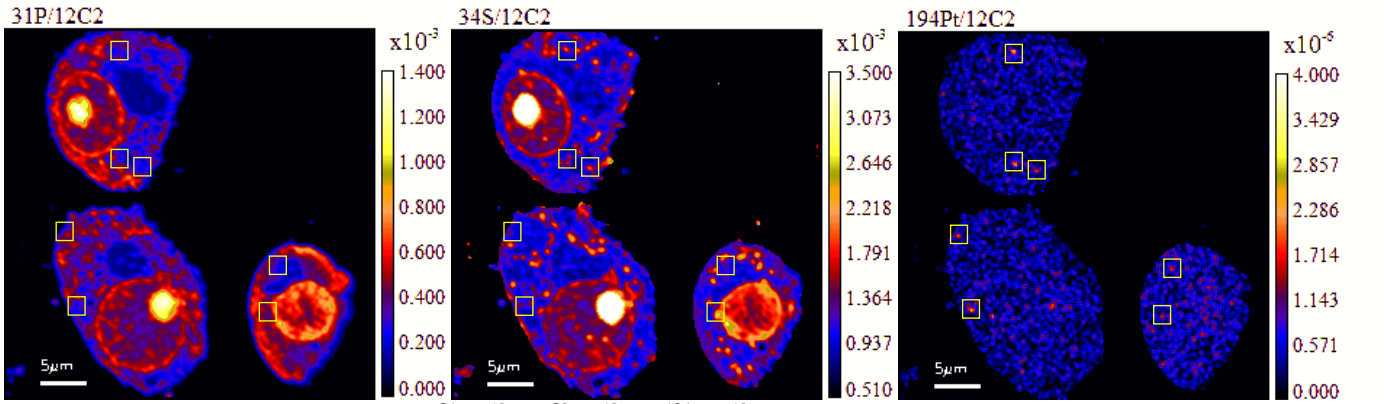

Figure 2.10 Secondary ion maps of $^{31}P^-/^{12}C_2^-$, $^{32}S^-/^{12}C_2^-$, $^{194}Pt^-/^{12}C_2^-$ of A2780CR cells treated with cisplatin (30 µM, 12 hours). Boxes represent Pt enriched spots in cells.

From TEM images, we found platinum hotspots accumulating in both an autophagosome and in the mitochondria of A2780 (Figure 2.9). The formation of autophagosomes is important for removing damaged organelles and molecules, which are then degraded by lysosomes.[102] A previous study has shown that the formation of autophagosomes is involved in the detoxification of cisplatin,[103] which correlates well with our findings. Cisplatin has been also shown to act in the mitochondria either by binding mitochondrial DNA[104,105] or inducing a mitochondrial-reactive oxygen species response,[106] which contributes to its cytotoxicity. In A2780CR cells however (Figure 2.10), little nuclear accumulation was observed and the small pockets of Pt seen were mostly co-accumulated with sulfur in the cell, which correspond to areas associated with sulfur containing molecules involved in metal detoxification as seen previously in section 2.2.3.

The switch in fixation method and dosing duration however resulted in no enrichment of ^{15}N in the samples (Figure 2.11). Considering that only very weak ^{15}N enrichment in cells dosed with isotopically labelled platinum complexes has been observed before,[40,81] and the weak ^{15}N enrichment observed previously in chemically fixed samples dosed with cisplatin (Figure 2.7), presumably the change in fixation methods resulted in a lowered ionization yield of ^{15}N resulted in no observable enrichment.

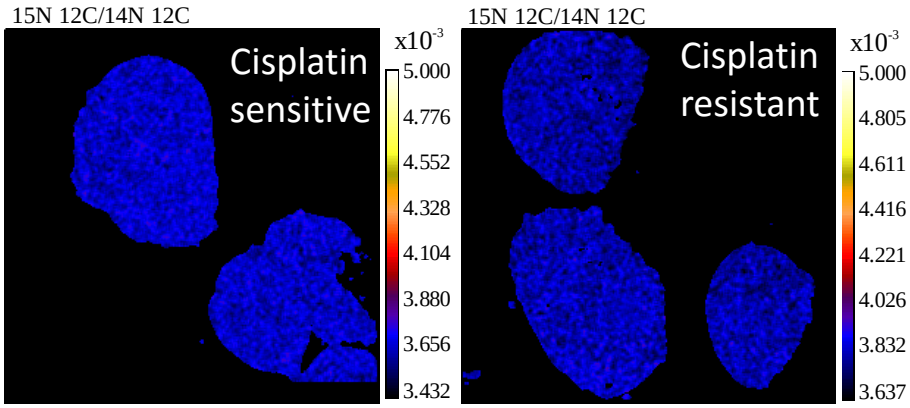

Figure 2.11 Secondary ion maps of $^{15}N^{12}C^{-}$/ $^{14}N^{12}C^{-}$ of A2780 sensitive and cisplatin resistant cells treated with cisplatin (30 µM, 12 hours).

Overall, we used NanoSIMS combined with TEM for studying the distribution of cisplatin in ovarian cancer cells sensitive and resistant to the drug. NanoSIMS elemental maps allowed us to semi-quantitatively determine cellular accumulation and distribution of Pt in cells. We observed a reduced accumulation of Pt in cisplatin resistant cells as compared to its cisplatin sensitive counterpart. We also visualized for the first time Pt accumulation in mitochondria and autophagosomes, which was previously shown indirectly with methods such as cell fractionation followed by ICP-MS[32] or inferred from phenotypic studies.[103] Our findings demonstrate the potential of using NanoSIMS to shed light on complex biological problems related to the clinical use of Pt metallodrugs.

2.2.5 NanoSIMS imaging to study the distribution of RAPTA-T in non-invasive and invasive breast cancer cells.

The ruthenium(II) metallodrug RAPTA-T has been shown to possess *in vitro* anti-metastatic properties, where the drug prevented migration, detachment and reattachment of invasive MDA-MB-231 breast cancer cells significantly more effectively than non-invasive MCF-7 breast cancer cells.[96] In addition, studies in an *in vivo* mammary carcinoma murine model showed RAPTA-T treatment was effective in preventing the lung metastasis of these tumors.[96] Thus, having shown the applicability of NanoSIMS for imaging RAPTA-T in A2780CR cells, we extended this work to study its distribution in MDA-MB-231 and MCF-7 cells to probe whether there is a difference in distribution in cells possessing different metastatic phenotypes. Both MCF-7 and MDA-MB-231 breast cancer adenocarcinomas isolated from pleural effusions.[107] Genetically, MDA-MB-231 are a triple negative cell line lacking estrogen and progesterone receptors in addition to having no HER2/Neu amplification leading to it being resistant to most chemotherapeutic agents versus MCF-7 cells which are positive for both

estrogen and progesterone receptors and thus sensitive to hormonal based therapies.[108] For this work, cells were dosed with 500 µM of isotopically labelled RAPTA-T for 24 hours and applied HPF-FS for cell fixation in lieu of chemical fixation used in the previous study with RAPTA-T in 2.2.3.

As seen in A2780CR cells treated with RAPTA-T, ^{13}C enrichment was not observed in RAPTA-T treated MDA-MB-231 and MCF-7 cells showing that there is at least partial detachment of the η^6-toluene in RAPTA-T during the 24 hour incubation period. In MDA-MB-231 cells, all Ru hotspots found were co-enriched with ^{15}N (Figure 2.12, green boxes) showing that part of the phosphine ligand in RAPTA-T stays intact. However, there were several ^{15}N enriched hotspots which did contain Ru. This could be attributed to either detachment of PTA from Ru or the loss of sensitivity for Ru detection due to matrix changes induced by HPF-FS fixation (Figure 2.2). Having, previously shown a strong correlation between ^{15}N and Ru signal (section 2.2.3) we used ^{15}N maps as a marker for the presence of RAPTA-T.

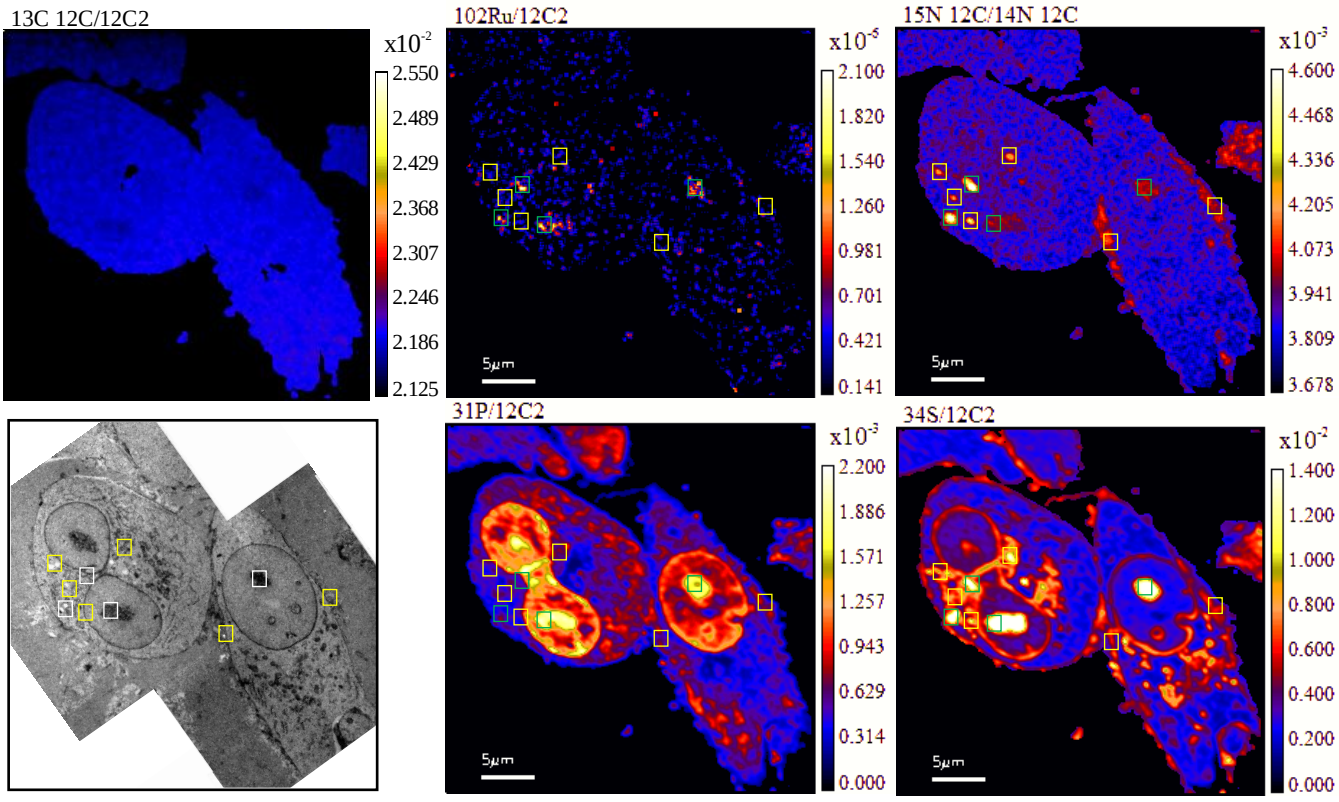

Figure 2.12 Secondary ion maps of $^{31}P^-/^{12}C_2^-$, $^{32}S^-/^{12}C_2^-$, $^{14}N^{12}C^-/^{12}C_2^-$, $^{15}N^{12}C^-/^{14}N^{12}C^-$, $^{102}Ru^-/^{12}C_2^-$ and $^{13}C^{12}C^-/^{12}C_2^-$ and TEM of MDA-MB-231 cells treated with ^{15}N and ^{13}C-labelled RAPTA-T (500µM, 24 hours). Blue boxes show Ru enriched hotspots, yellow boxes show ^{15}N enriched hotspots and green boxes show hotspots co-enrichment with ^{15}N and Ru.

RAPTA-T was seen to distribute into the nucleolus of MDA-MB-231 cells (Figure 2.12). This is highly likely considering RAPTA-T has been shown to interact with the histone proteins which package and order DNA into nucleosomes.[91] We also observed accumulation of RAPTA-T on the cell membrane of MDA-MB-231 cells where it could interact with extracellular cell adhesion proteins implicated in its anti-metastatic activity.[96] When Ru/^{15}N maps are overlaid with TEM images, we observed RAPTA-T accumulation in autophagic vacuoles as well as mitochondria. Since autophagy is involved in detoxification of harmful substances in cells,[102] presumably RAPTA-T is also removed by this mechanism. The distribution and action of RAPTA-T in mitochondria has been shown previously, where treatment with the drug resulted in an appreciable accumulation in mitochondrial fractions of cells[85] and results in perturbation of the expression of several mitochondrial proteins.[93] We observed a general co-accumulation of sulfur in RAPTA-T enriched hotspots which is unsurprising considering most organelles in which RAPTA-T is distributed to contain sulfur rich molecules such as iron sulfur clusters in mitochondria and the nucleus[109] as well as sulfur containing molecules such as glutathione, metallothioneines and thioredoxins which detoxify metals in cells.

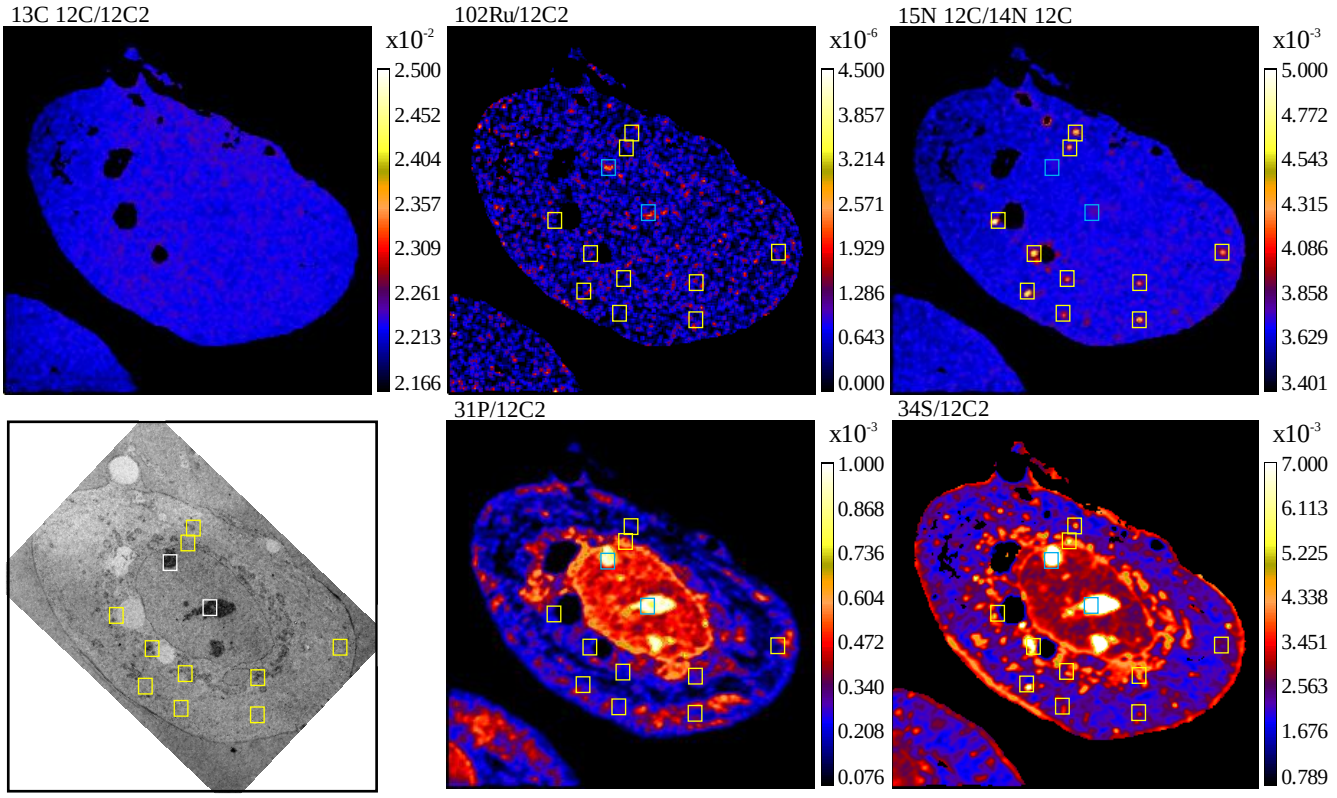

Figure 2.13 Secondary ion maps of $^{31}P^-/^{12}C_2^-$, $^{32}S^-/^{12}C_2^-$, $^{14}N^{12}C^-/^{12}C_2^-$, $^{15}N^{12}C^-/^{14}N^{12}C^-$, $^{102}Ru^-/^{12}C_2^-$ and $^{13}C^{12}C^-/^{12}C_2^-$ and TEM of MCF-7 cells treated with ^{15}N and ^{13}C-labelled RAPTA-T (500µM, 24 hours). Blue boxes show Ru enriched hotspots, yellow boxes show ^{15}N enriched hotspots and green boxes show hotspots co-enrichment with ^{15}N and Ru.

In MCF-7 cells, we found accumulation of RAPTA-T in the nucleolus and a general co-accumulation of the drug at sulfur rich hotspots, which was similarly observed in MDA-MB-231 cells (Figure 2.13). We did not see any accumulation of RAPTA-T in the nucleus or cell membrane. However, from overlaid TEM images RAPTA-T was seen to accumulate in mitochondria and lysosomal structures. The lack of distribution in the nucleus and membrane of MCF-7 cells could partially explain the weaker activity of RAPTA-T in preventing migration, detachment and reattachment of these cells compared to MDA-MB-231 cells. Similar to MDA-MB-231 cells, mitochondrial accumulation was expected and lysosomal accumulation could be attributed to cellular processes related to detoxification of heavy metals.

When compared to our earlier study on A2780CR cells, we see a marked decreased in accumulation of RAPTA-T in the membrane of both MDA-MB-231 and MCF-7 cells. These could be caused by various factors. Firstly, the cells were derived from two different cell lines where A2780CR is an ovarian cancer cell, and MDA-MB-231 and MCF-7 are breast cancer cells. Thus the difference in RAPTA-T distribution is partially caused by the heterogeneity both in terms of cell type and phenotype. It has been shown previously that A2780CR cells unlike their cisplatin sensitive counterparts undergo metastasis and shorten survival rates of mice xenografted with these cells.[110] Considering the fact that both A2780CR and MDA-MB-231 are both highly invasive, this strengthens the tenet that membrane association of RAPTA-T could be correlated with its anti-metastatic properties. This is further exemplified by the lack of membrane accumulation of RAPTA-T in noninvasive MCF-7 cells.

Overall, we successfully applied NanoSIMS to differentiate between the distribution of RAPTA-T in invasive and non-invasive breast cancer cell lines. The distributional differences observed provide some insight into how RAPTA-T distribution correlates with the phenotypic changes induced by its activity on cancer cells.

2.3 Conclusion

We have successfully developed methods for visualizing Pt and Ru metallodrugs in cells using NanoSIMS. We applied this method to study distribution of the metallodrugs cisplatin and RAPTA-T in biologically relevant cell lines to investigate the differences and whether they correlate well with the mechanisms of action and resistance to these drugs. For cisplatin, ovarian cancer cells resistant to cisplatin exhibit markedly reduced accumulation of the drug and in the

sensitive variant we observed accumulation of cisplatin in the mitochondria and authophagosome. For RAPTA-T, we observed partial loss of the arene and possibly the phosphine ligand which could be important for drug activation. RAPTA-T's distribution pattern was markedly different between ovarian and breast cancer cells, and we observed a larger extent of membrane association of the drug in invasive cancer cell lines, which could partly explain how RAPTA-T exerts its anti-metastatic activity. These findings showcase the applicability of NanoSIMS to study complex biological problems involving cellular metallodrug distribution. With further developments in speed, sensitivity, and spatial resolution of NanoSIMS instrumentation, it could potentially be applied for metallodrug development, where tuning of ligands to achieve specific subcellular distribution of metallodrugs could be facilitated by this technique.

2.4 Experimental

Cell preparation for NanoSIMS (fixation, resin embedding and cutting) and TEM imaging was performed by the biological electron microscopy centre in the EPFL. Sample gold coating and NanoSIMS data acquisition was performed in the Laboratory for Geological Biochemistry, EPFL.

2.4.1 Synthesis of ^{15}N labelled cisplatin and ^{13}C, ^{15}N labelled RAPTA-T.

^{15}N labelled cisplatin was synthesized according to literature method[111] by replacing $^{14}NH_4OH$ with $^{15}NH_4OH$. ^{15}N enriched 1,3,5,7-tetraazatricyclo[3.3.1.1 (3,7)] decane was synthesized using a literature method[112] by replacing $^{14}NH_4OH$ with $^{15}NH_4OH$ and used to prepare ^{15}N labelled 1,2,5-triaza-7-phosphatricyclo[3.3.1.1.] decane (PTA).[113] ^{13}C labelled metyl-cyclohexadiene was synthesized from a birch reduction of Toluene-(phenyl-$^{13}C6$) and used to prepare RAPTA-T.[114]

^{15}N, ^{13}C Enriched RAPTA-T

^{1}H NMR (400 MHz, Methanol-d_4) = δ 5.95 – 5.22 (m, 5H), 4.60 (s, 6H), 4.35 (s, 6H), 2.17 (s, 3H).

^{13}C NMR (101 MHz, Methanol-d_4) only enriched ^{13}C = δ 108.33, 88.64 – 85.31 (m), 77.87 – 75.73 (m).

^{31}P NMR (162 MHz, Methanol-d_4) = δ -33.43.

HRMS (ESI+) m/z calculated for $C_7{}^{13}C_6H_{20}Cl{}^{15}N_3PRu$ $[M\text{-}Cl+H]^+$: 395.0239; found: 395.0242

2.4.2 Cell culture

A2780 cisplatin sensitive and resistant (human ovarian carcinoma) [A2780 and A2780CR] cells (ATCC) were cultured in RPMI 1640 Glutamax medium supplemented with 10% fetal calf serum, penicillin 100 units/mL streptomycin 100 µg/mL (Invitrogen). MDA-MB-231 and MCF-7 (human breast adenocarcinoma) were cultured in DMEM medium supplemented with 10% fetal calf serum, penicillin 100 units/mL streptomycin 100 µg/mL (Invitrogen). Cells were incubated at 37^0C in a moist environment containing 5% CO_2.

2.4.3 Cell preparation

Cells were seeded 50000 cells/well in 24-well or 500000cells/well in 6-well clear bottom plates fitted with 13mm thermanox slips or sapphire disks. After 24 hours, cell media was aspirated and fresh media containing ^{15}N cisplatin 30 µM or ^{15}N, ^{13}C, RAPTA-T 500 µM was added.

Chemical fixation

Upon incubation, media was aspirated, and cells were washed twice with PBS. Subsequently cells were fixed with buffered aldehydes (2% PAF, 2.5% Gluteraldehyde in PBO 1M, pH 7.4) for one hour and then washed in cacodylate buffer (0.1M, pH 7.4). Then cells were postfixed for 40 minutes in a solution of 1% osmium tetraoxide and 1.5% potassium ferrocyanide in cacodylate buffer. This was followed by a further staining of 1% osmium tetraoxide in cacodylate buffer, for 40 minutes, and then 1% aqueous solution of uranyl acetate for 40 minutes. The samples were then dehydrated in an ascending alcohol series (1 X 50%, 1 X 70%, 2 X 96%, 2 X 100%, 3 minutes each) and resin embedded with Durcupan resin which was then hardened overnight at 65 ^{0}C. The resin embedded cells were semi-thin sectioned onto glass coverslips ready for analysis in the nanoSIMS.

HPF-FS fixation

Upon incubation, sapphire disks were removed from media and then high pressure frozen (Leica HPM100, Leica Microsystems), with excess 20% BSA solution in 0.01M PBS (phosphate buffer solution) to avoid any air bubbles becoming trapped and the formation of ice crystals. The frozen cells were then embedded in resin at low temperature.[115] Sapphire discs were placed on a frozen solution of 1% osmium, 0.5% uranyl acetate, 5% water in pure acetone. The samples where then warmed to room temperature in an ice bucket containing solid carbon dioxide blocks that was allowed to sublime over a period of 2 hours until room temperature was reached. At

this point the solution was removed and replaced with dry acetone. After washing a further 2 times with acetone the samples were embedded in increasing concentrations of epon resin in acetone. At 100% concentration of resin the samples were then left overnight to fully infiltrate and then polymerised in a 60°C oven for at least 12 hours. Samples where then glued to empty resin blocks, trimmed, and sections of alternating thickness of 500nm and 50 nm cut sequentially from the face. The thicker sections were collected onto a glass coverslip stained with 1% touldine blue and imaged with light microscopy, and nanoSIMS, and the 50 nm thick sections collected on to an electron microscopy slot grid ready for imaging with transmission electron microscopy at a final magnification of around 1400 times (Tecnai Spirit, FEI Company, Netherlands).

2.4.4 Nano-SIMS analysis

NanoSIMS measurements were performed at the Laboratory of Biological Geochemistry, EPFL and the Universtiy of Lausanne. Prior to NanoSIMS imaging, the samples were gold-coated in order to avoid charging effects. Before acquiring an image, Cs ions were implanted into the surface of the sample in order to enhance the ionization of the element of interests. In our study, the electron multiplier detectors were set up to measure $^{12}C_2^-$, $^{13}C^{12}C^-$, $^{12}C^{14}N^-$, $^{12}C^{15}N^-$, $^{31}P^-$, $^{32}S^-$, $^{102}Ru^-$ and $^{194}Pt^-$ secondary ions, generated by bombarding the sample with a ~4 pA Cs^+ primary beam focused to a spot size of approximately 160 nm. In order to resolve the possible isobaric interferences, the instrument was operated at a mass-resolving power (MRP) of about 10.000. For$^{102}Ru^-$ and $^{194}Pt^-$ due to the very low signal obtained on cells, peak-shape and mass resolving power was checked using a Ru and Ptmetal standard. Data acquisition was performed by scanning the Cs^+ primary beam over areas of 34x34µm with a 256x256 pixel image resolution. The per pixel dwell time of the primary ion beam was 10 ms. The final images are the accumulation of 120 layers obtained by sequential scanning and correspond to a cumulated acquisition time per pixel of 1.2 seconds. Between every layer, the focusing of the secondary ion beam was optimized and automatic peak centering was performed for $^{12}C_2^-$, $^{13}C^{12}C^-$, $^{12}C^{14}N^-$, $^{12}C^{15}N^-$. The Ru and Pt peak could not be centered due to the low count rates. However, post-analysis check revealed that there was no significant change in the peaks position during the entire acquisition time. The total acquisition time including the centering procedure was 22 h per image.

2.4.5 Data extraction and image processing

All Nano-SIMS image processing was performed using MatLab with the look@NanoSIMS program (http://nanosims.geo.uu.nl/nanosims-wiki/doku.php/nanosims:lans) and with L'image (L. Nittler, Carnegie Institution of Washington). Over the 22 hours of image acquisition, the image drift of a 34x34 µm image was less than 7 pixels (i.e. less than 1µm). The data reduction software can easily correct for such a drift by aligning the position of identified structures.

Regions of interest (ROI's) were defined manually based on identifiable cell features on $^{12}C^{14}N^-$, $^{31}P^-$ and $^{32}S^-$ elemental maps. Images were accumulated from planes where accumulated counts per ROI were stable with $^{12}C^{14}N^-$ used as the alignment mass. Natural abundance ratios of $^{13}C/^{12}C$ and $^{15}N/^{14}N$ were obtained from elemental maps of untreated cells. Ratios for isotopically enriched elements were calculated using the delta-notation:

$$\boldsymbol{\delta = \left[\left(\frac{\text{ratio measured}}{\text{standard ratio measured}}\right) - 1\right] * 1000}$$

All other elements were normalized against $^{12}C_2$, the images of which are essentially flat, to normalize out small ionization variations across the sample surface.

For comparative red, green, blue (RGB) images, $^{15}N^{12}C^-/^{14}N^{12}C^-$ is colored green and $^{102}Ru^-/^{12}C_2^-$, $^{14}N^{12}C^-/^{12}C_2^-$, $^{31}P^-/^{12}C_2^-$, and $^{32}S^-/^{12}C_2^-$ are colored red.

Data for line profiles and mean counts/region of interest graphs were extracted using L'image and replotted using GraphPad Prism version 6.00 for Windows.

Chapter 3
Functional identification of targets by expression proteomics (FITExP) for identification of cisplatin, RAPTA-T and RAPTA-EA protein targets.

3.1 Introduction

Simple RAPTA complexes (with benzene, toluene or p-cymene arenes) are not known to be as toxic to primary tumors as classical metallodrugs such as cisplatin.[116] However, these complexes possess interesting anti-metastatic[96] and antiangiogenic[117] properties, and various functionalities can be introduced via the arene or PTA moiety to augment their anti-cancer activity. Due to their very different activity from cisplatin, the biological target of RAPTA complexes are thought to be proteins and not DNA.[33] Furthermore cellular fractionation of cancer cells exposed to RAPTA complexes have also revealed that an appreciable amount distributes to cytosolic and mitochondrial fractions containing proteins.[32]

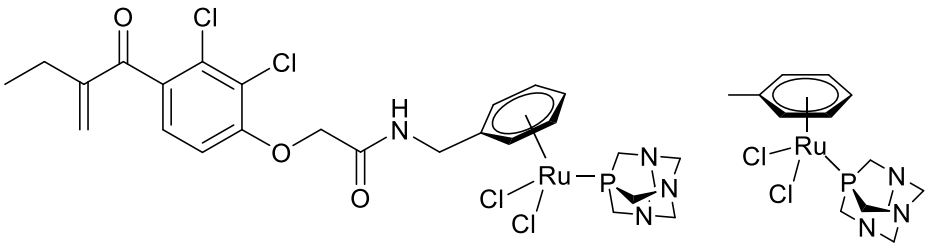

RAPTA-EA RAPTA-T

Figure 3.1 RAPTA complexes used in the FITExP study

Identifying the protein targets of metallodrugs presents unique challenge as these drugs exhibit promiscuity in protein binding, where any exposed labile amino acid residues such as cysteine, methionine, glutamic acid and histidine can potentially coordinate to these compounds.[118] Thus, affinity purification based methods for protein target screening, which are extremely useful for organic molecules, are less useful for metallodrugs due to the amount of unspecific interactions which can occur.[55] To be useful for metallodrug target identification methodologies must also take into account the pharmacokinetics of absorption and distribution of compounds into their cellular compartments. Thus, methods such as proteome expression profiling which rely on probing targets in whole cells,[119] are more informative for metallodrugs. Standard proteome expression profiling experiments provide a general profile of regulated proteins in the presence and absence of drug treatment and this information is then linked to the mechanism of the drug. Two such approaches were performed on RAPTA-type complexes.[57,119] However, these studies do not directly reveal the primary protein target of the drugs as changes in protein regulation can be brought about by a plethora of mechanisms besides ligand binding to proteins.

Recently, a protein expression profiling method for direct identification of the protein target of small molecules called Functional Identification of Target by Expression Proteomics (FITExP) was reported.[63] FITExP operates based on the observation that for the protein target of small molecules, the abundance change in late apoptosis is exceptionally large compared to other proteins that are normally co-regulated with the drug-target.[63] Experimentally, two to three different cancer cell lines are treated with apoptosis inducing concentrations of the compound of interest and several control anti-cancer drugs which proteins targets are known. For every cell line, protein and drug treatment three characteristics namely regulation, specificity and exceptionality are calculated. Regulation denotes the change in protein expression from untreated controls. Specificity was defined as regulation for a given treatment normalized by the average regulation in other treatments and controls. Exceptionality is a quantitative assessment of unexpected character of a proteins regulation in a given treatment. These three characteristics were then subjected to rank product analysis that calculated final ranks and p-values for protein candidates. For drug target identification, using exceptionality and regulation provided a short list of statistically significant candidates (hereby called the "main target list"), while for mechanism of action using regulation and specificity provided a longer list of implicated proteins (hereby called the "associated protein list") to be mapped on protein-protein networks (Figure 3.2). This approach overcomes the limitations associated with standard proteome expression profiling methods in identification of protein targets of anti-cancer compounds.

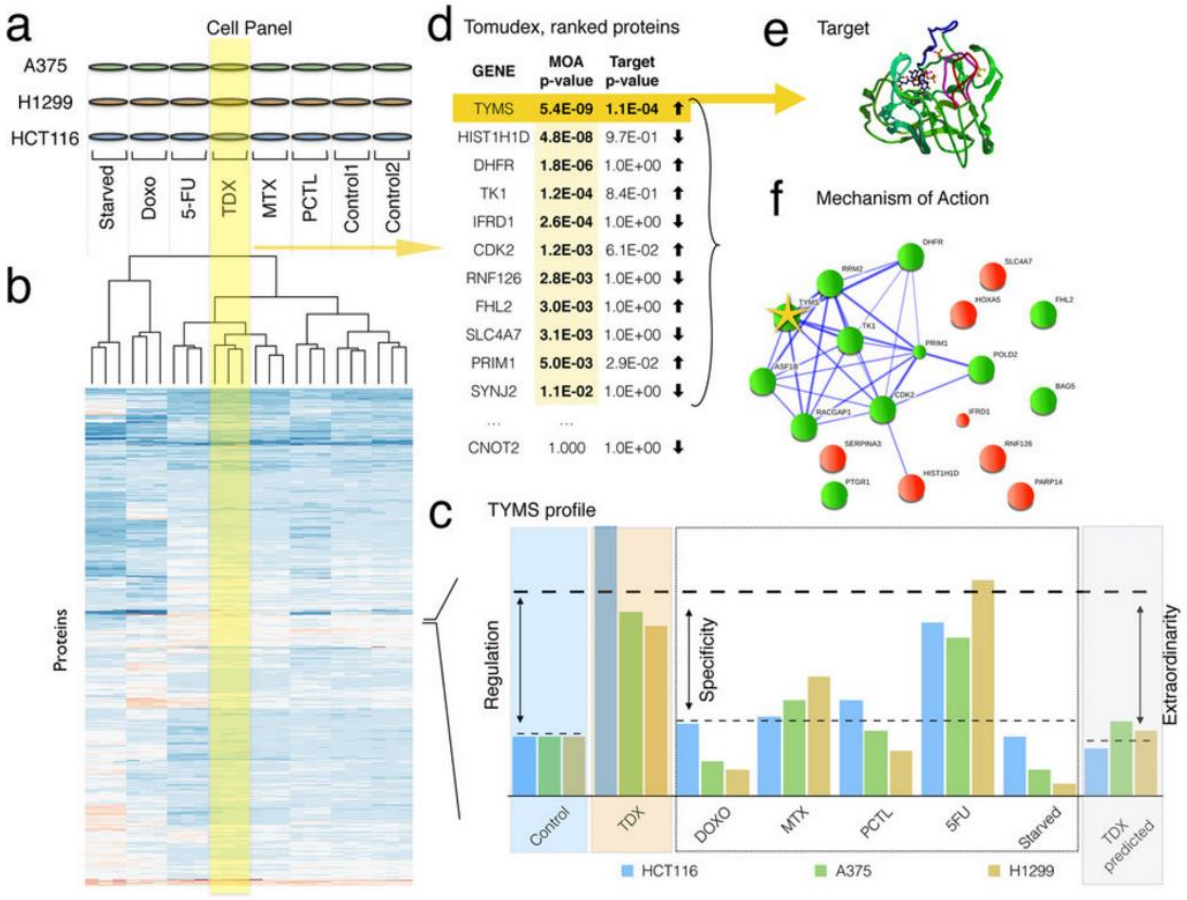

Figure 3.2 General workflow of the FITExP method for drug target identification. (**a**) a panel of cell lines is treated by a panel of drugs; (**b**) LC-MS/MS based proteomics identifies and quantifies ≥3,500 proteins, proteomic profiles are shown in a schematic heatmap with color-coded normalized abundances; the dendrogram shows hierarchical clustering of proteomic profiles with correlation-based distances; (**c**) for each protein, cell line and treatment, regulation (*Reg)*, specificity (*Spec)* and exceptionality *Exc* are calculated; (**d**) for each treatment, final protein ranks based on *Reg* and *Exc* are established and the p-values are calculated using the Bonferroni correction; the protein list is sorted in ascending order of p-values; (**e**) proteins with $p \leq 0.05$ (threshold p-value) represent the most likely drug targets; (**f)** top *n* proteins with $p \leq 0.05$ according to *Reg* and *Spec* rankings are mapped on protein networks to identify the drug target mechanism. (Figure adapted from Chernobrovkin et. al. Sci. Rep. 2015).

In this work, we used FITExP to study the protein targets of RAPTA-T, a GSH inhibiting RAPTA complex RAPTA-EA[120] and cisplatin. We performed analysis in two breast cancer cell lines, highly invasive MDA-MB-231 cells and non-invasive MCF-7. Paclitaxel served as controls of known biological targets.

3.2 Results and discussion

3.2.1 Experimental validation

To validate the reliability of the experimental data generated, FITExP analysis was carried out to find protein targets of paclitaxel. Paclitaxel is a cytoskeletal drug that is known to bind to tubulin promoting polymerization of microtubules leading to mitotic arrest in cells.[121] From the main drug target list generated based on protein regulation and exceptionality characteristic, tubulin beta-6 chain as the only statistically significant target. This is in agreement with the actual biological target of paclitaxel.[121] We then mapped associated protein lists generated based on regulation and specificity (Appendix A, Table A.1) onto a STRING network.

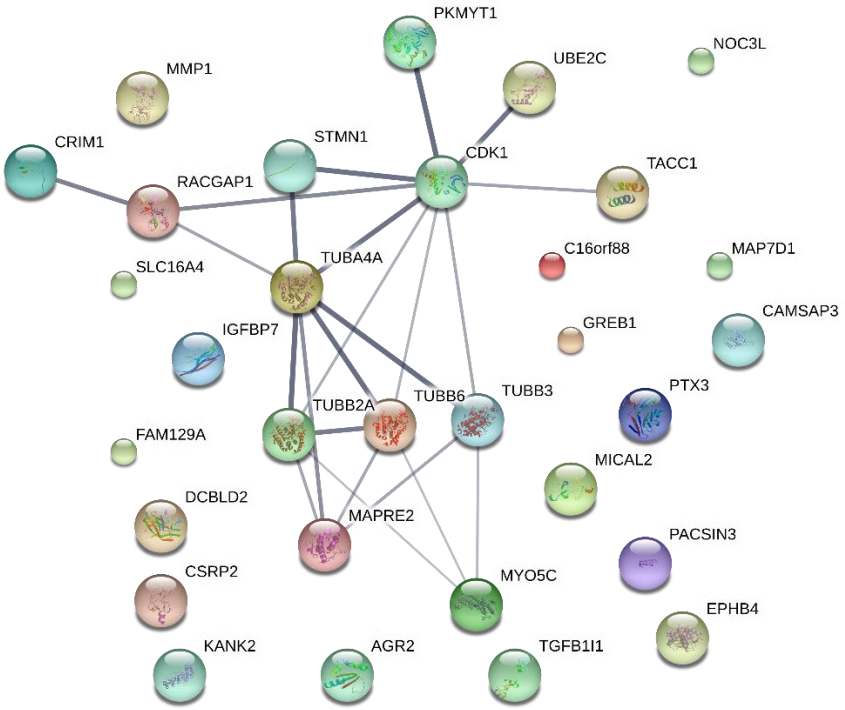

Figure 3.3 STRING protein-protein interaction network associated protein list of Paclitaxel generated using protein lists from specificity and regulation criteria.

STRING is an open web-based biological database of known and predicted protein-protein interactions (http://www.string-db.org/).[122] The database aggregates most of the available information on protein-protein interactions, scores and weighs it and augments with predicted interactions and results of automatic literature-mining searches. In our case, mapping the FITExP obtained targets on a STRING network allowed observe the interactions between the protein targets obtained to better understand the mechanism of our compounds. In STRING,

individual proteins are represented in different coloured bubbles and lines linking these bubbles represent the interactions between these proteins with increasing line thickness representing the increased confidence of these interactions based on available data. From the STRING network generated (Figure 3.3), we observed a network of closely linked proteins implicated in the mechanism of action of Paclitaxel. From the protein network, we identified 4 different tubulins and various proteins involved in microtubule regulation and function such as cyclin-dependent kinase, Rac GTPase activation protein 1 and microtubule associated protein, RP/EB family. Overall, our results agree with the proposed protein target and mechanism of action of Paclitaxel and with this validation we proceeded to analyse targets obtained from metallodrugs.

3.2.2 Targets of Cisplatin

The main mechanism of cisplatin is thought to be binding to nucleophilic N-7 sites of purine based in DNA forming DNA-DNA interstrand and intrastrand adducts which inhibit DNA replication and cause cell death.[101] However, cisplatin is also known to bind to proteins.[38] From our main target list, two significant cisplatin targets were identified, receptor tyrosine-protein kinase erbB-2 (ERBB2) and DNA damage-binding protein2 (DDB2). ERBB2 or HER2/Neu is the protein product of an oncogene and plays an important role in the development of aggressive forms of breast cancer.[123] Breast cancer chemotherapy regiments which combine the anti-HER2/neu antibody trastuzumab with cisplatin has been shown to be clinically efficacious.[124] Thus cisplatins effect on this protein could explain its synergistic activity when combined with trastuzumab. DDB2 is a required protein in the nucleotide excision repair (NER) pathway to initiate DNA repair.[125] DNA repair pathways have been implicated in the efficacy of cisplatin treatment where reduced levels of DNA repair proteins in testicular cancers account for the effectiveness of cisplatin treatment for this malignancy.[126,127] On the other hand, alternations in DNA repair processes are important in mediating resistance of cancers to cisplatin therapy.[128] Considering that NER is the main DNA repair pathway involved in detoxifying cisplatin-DNA adducts[129] binding to DDB2 could be implicated in its mechanism of action.

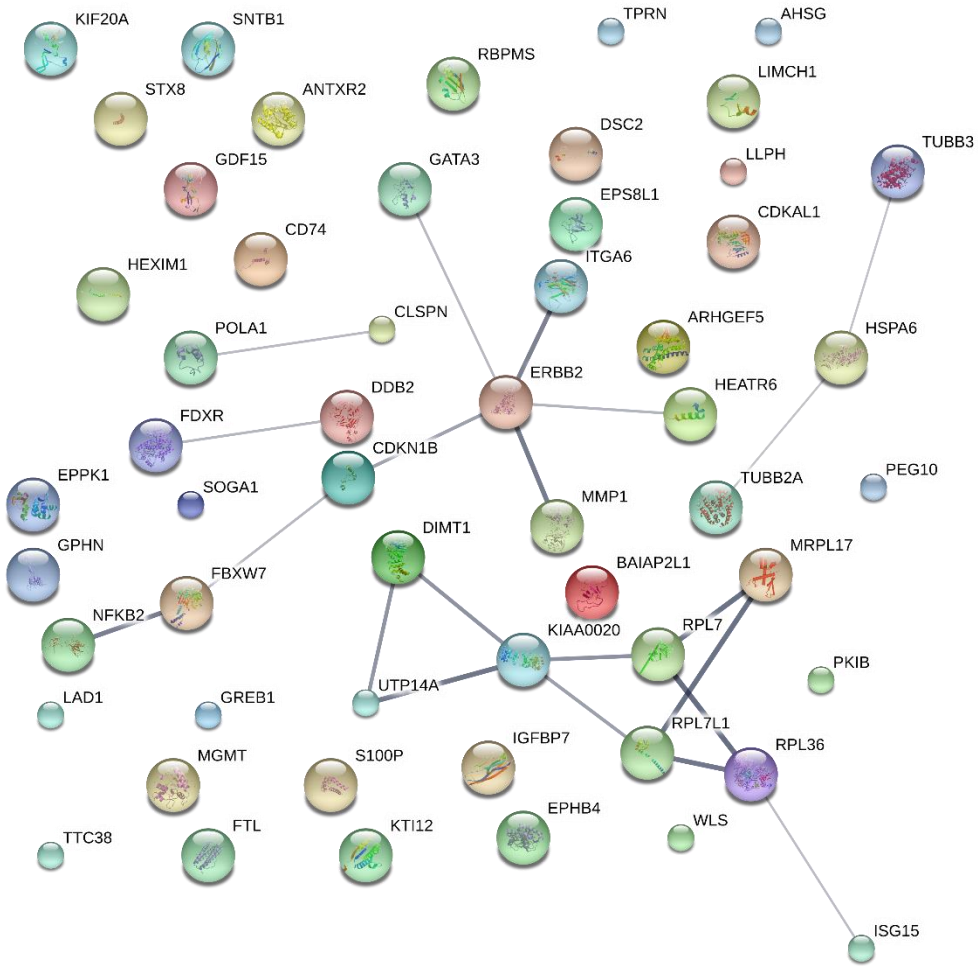

Figure 3.4 STRING protein-protein interaction network associated protein list of Cisplatin generated using protein lists from specificity and regulation criteria.

From a STRING network generated from the associated protein lists of cisplatin (Figure 3.4 and Table S 3.2), we found a few networks of associated proteins. In general, there was a significant downregulation of various ribosomal proteins upon cisplatin treatment (Appendix A, Table A.2). Ribosomal proteins are implicated in the function of ribosomes for protein translation[130] and cisplatin induced reduction of ribosomal protein expression has been observed in breast cancer cells.[131] Cisplatin was also seen to perturb the regulation of another network of proteins consisting of oncogenes and tumor suppressor genes such as ERBB2, cyclin dependent kinase inhibitor 1B, HEAT repeat containing 6 along with proteins involved in tumor metastasis and proliferation such as matrix metallopeptidase 1 and integrin alpha 6 and GATA binding protein 3. Considering that ERBB2 was one of the two cisplatin targets identified in the main target list its effect on regulation of associated proteins is thus not surprising. Finally, we observed an overexpression of tubulin subunits 2A and B3 from cisplatin treatment, which

is possible considering cisplatin is known to bind to tubulin causing aberrant microtubule protein polymerization.[132] However, we could not draw any conclusions on a main mechanistic pathway of cisplatin from the STRING network as multiple different protein associations were observed. This could also be indicative of the fact that the main target of cisplatin is DNA and its secondary effects on proteins are not very specific.

3.2.3 Targets of RAPTA-EA

Glutathione transferases (GST) are involved in the removal of exogenous substances such as cancer chemotherapeutic agents.[133] GST is often overexpressed in solid tumors upon exposure to anti-cancer drugs,[134] thus inspiring the development of RAPTA-EA, a RAPTA-type compound tethered to the GST inhibitor ethacrynic acid (EA) to enhance its anti-tumor activity (Figure 1). RAPTA-EA shows *in vitro* GST inhibition levels superior to that of EA alone[120] and has a much higher cytotoxicity than simple RAPTA-type complexes. However, an unbiased analysis of its protein target in cells was never performed leading us to apply the FITExP methodology to find its most important protein targets.

Protein	Acronym	P-value	Regulation
Heat shock 70 kDa protein 1A/1B	HSPA 1A/1B	2.46E-05	Up
Heme oxygenase 1	HMOX1	7.44E-05	Up
TRAF-type zinc finger domain-containing protein 1	TRAFD1	5.94E-04	Up
Sulfiredoxin-1	SRXN1	2.17E-03	Up
Thioredoxin reductase 1, cytoplasmic	TXNRD1	2.21E-02	Up
DnaJ homolog subfamily B member 4	DNAJB4	3.52E-02	Up
Flavin/bilverdin reductase (NADPH)	BLVRB	4.47E-02	Up
Glucose-6-phosphate 1-dehydrogenase	G6PD	4.48E-02	Up

Table 3.1 Main target list for RAPTA-EA obtained from FITExP analysis

Table 3.1 lists the main target list obtained from FITExP analysis of RAPTA-EA. We obtained a total of 8 RAPTA-EA protein targets. The top hit, heat shock 70 kDa protein 1A/1B (HSPA 1A/1B), comes from the class of heat shock proteins (HSPs), a class of proteins produced by cells in response to environmental or metabolic stress such as heat, anoxia,

ischemia or heavy metals.[135] Most HSPs also function as chaperones which stabilise pre-existing proteins against aggregation and facilitates proper folding of newly translated and misfolded proteins.[136] Another HSP protein in the main target list DnaJ homolog subfamily B member 4, functions as both a chaperone and tumor repressor protein mainly involved in the targeting and degradation of the cell adhesion protein E-cadherin.[137] A previous proteome profiling revealed HSPs are possibly implicated in the mechanism of RAPTA-type compounds.[119] Furthermore HSPA 1A/1B, overexpression has been similarly demonstrated in MCF-7 cells treated with RAPTA-EA for 48 hours.[138]

Heme oxygenase 1 (HMOX 1) is an enzyme which cleaves heme at the alpha methane bridge forming bilverdin and is involved in hematopoesis (Figure 3.5). It is also a marker of oxidative stress, and deficiency in this protein results in impaired stress hematopoiesis resulting in marked erythrocyte fragmentation, coagulation abnormalities, and iron deposition in renal and hepatic tissues.[139] Exposure to EA has been previously shown to result in elevated expression of this protein[140], leading us to believe that the observed hit is due to the EA moiety in RAPTA-EA. Flavin/bilverdin reductase is an oxidoreductase that catalyzes the NADPH-dependent reduction of bilverdin to bilirubin (Figure 3.5),[136] the next step in heme catabolism thus it was not surprising to find co-regulation of this related protein in RAPTA-EA

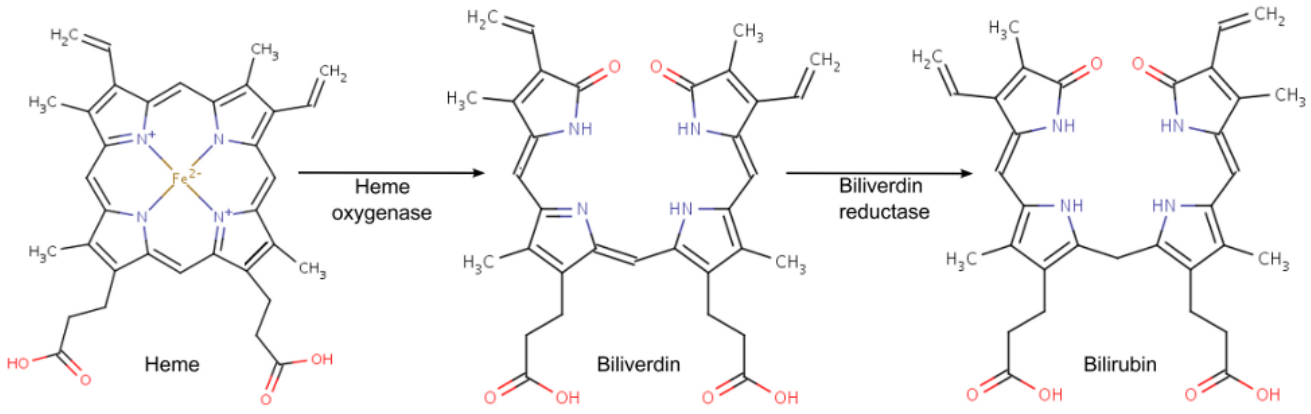

Figure 3.5 Enzymatic reaction of heme catabolism to bilirubin.

Sulfiredoxin-1 (SRXN1) contributes to oxidative stress resistance by reducing cysteine-sulfinic acid formed by exposure to oxidants into peroxiredoxins. As both HMOX1 and SRXN1 play a role in oxidative stress and have been shown to be co-regulated in cells exposed to anti-cancer compounds[141], we predict that the regulation of both were due to EA. Glucose-6-

phosphate 1-dehydrogenase, is a cytosolic protein whose main role is the production of NADPH an electron donor in the defense against oxidising agents and in reductive biosynthetic reactions.[137] Deficiency in this protein in humans can cause neonatal jaundice and haemolysis upon exposure to oxidative stress. Thioredoxin reductase 1 reduces thioredoxins and other substrates and plays a role in selenium metabolism and protection against oxidative stress[137]. Since depletion of GST is correlated to increased levels of oxidative stress response[142], regulation of this protein upon exposure to RAPTA-EA is unsurprising.

TRAF-type zinc finger domain-containing protein 1 is a negative feedback regulator that controls excessive immune response in vertebrates.[143] Though not expected to be a target of RAPTA-EA, it was shown in previous studies that RAPTA-type complexes can bind to proteins containing zinc-finger domains possibly perturbing the regulation of this protein.[55]

We subsequently mapped the associated target list obtained from RAPTA-EA into a STRING network (Figure 3.6 and Appendix A, Table A.3). From the STRING map, we saw a very strong network of oxidative stress related proteins perturbed by RAPTA-EA treatment. A large family of heat shock proteins and proteins involved in cellular respiration along with all the protein candidates from the main target list of RAPTA-EA were implicated in the association network, strongly suggesting that the mechanism of action of the drug was related oxidative stress response.

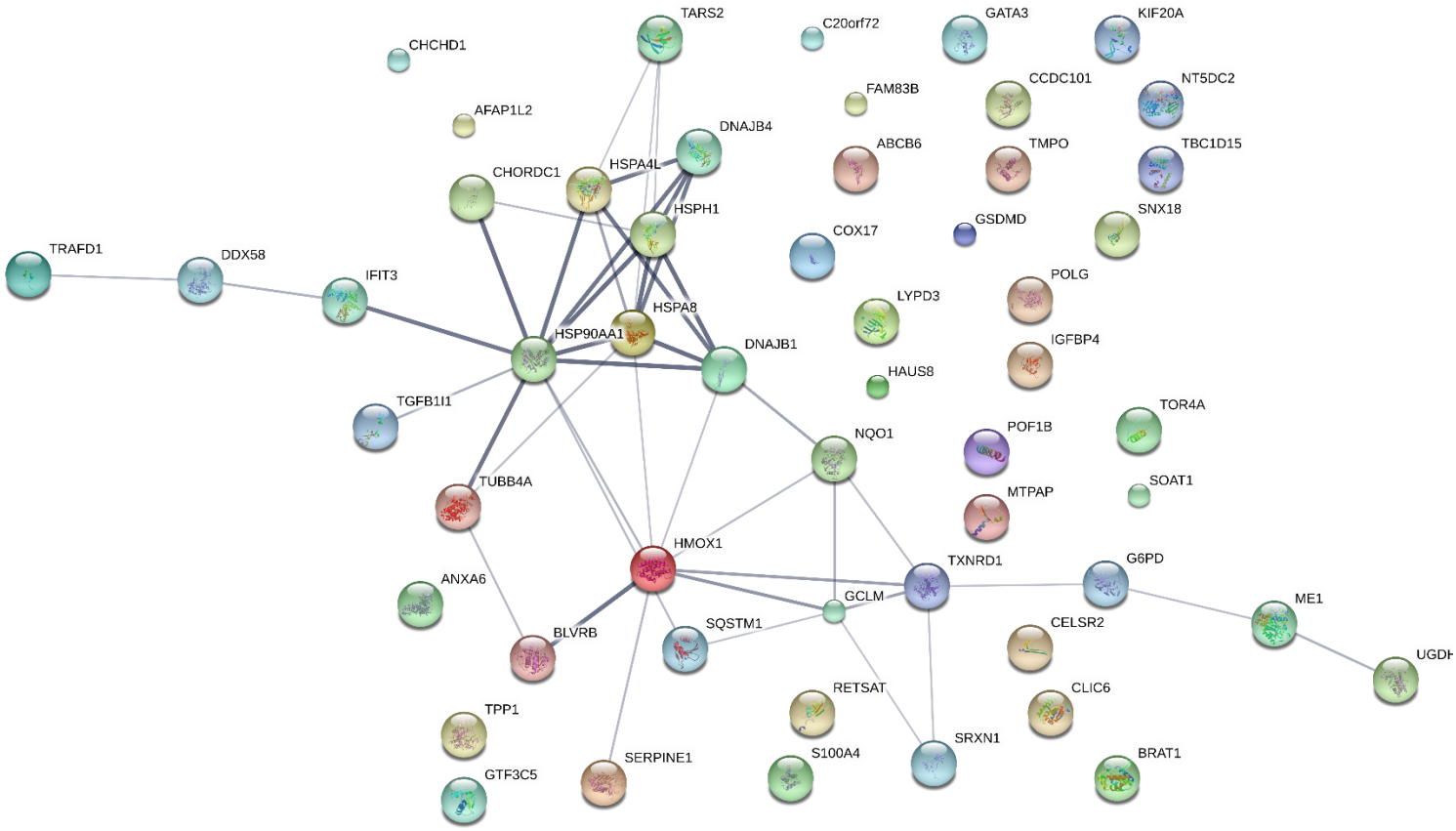

Figure 3.6 STRING protein-protein interaction network associated protein list of RAPTA-EA generated using protein lists from specificity and regulation criteria.

Overall, the RAPTA-EA protein targets found via FITExP were mostly related to oxidative stress response, which is possibly to the GST inhibition activity of this compound. Surprisingly the suspected main target of the protein, GST was not found as one of the significant hits of the screen. Possibly tethering of EA to a RAPTA-type compound, though potentiating GST inhibition, could switch its dominant action to the binding to other oxidative stress response proteins. We attributed most of the targets of RAPTA-EA to the EA moiety and not the RAPTA fragment.

3.2.4 Targets of RAPTA-T

The organometallic ruthenium(II) complex, RAPTA-T has been previously shown to possess both *in vitro* and *in vivo* anti-metastatic properties. Specifically in RAPTA-T treated breast cancer cells, highly metastatic MDA-MB-231 showed a greater reduction to the extent of detachment, readhesion, migration and invasion compared with less metastatic MCF-7 cells[96]. This motivated our choice of MDA-MB-231 cells and MCF-7 cells for our FITExP

analysis.

Protein	Acronym	P-value	Regulation
Phospholipase D3	PLD3	9.11E-04	Up
S-adenosylmethionine synthase isoform type-2	MAT2A	1.11E-03	Up
Metallothionein-2	MT2A	2.33E-03	Up
Zinc finger HIT domain-containing protein 2	ZNHIT2	1.39E-02	Up
RNA-binding protein 47	RBM47	1.86E-02	Up
Pyruvate dehydrogenase phosphatase catalytic subunit 1, mitochondrial	PDP1	3.56E-02	Up
Chromatin target of PRMT1 protein	CHTOP	4.01E-02	Up
Chromosome transmission fidelity protein 8 homolog isoform 2	CHTF8	4.37E-02	Up

Table 3.2 Main target list for RAPTA-T obtained from FITExP analysis.

Table 3.2 shows the main target list obtained from FITExP analysis of RAPTA-T, a total of eight protein targets. The top ranked protein target obtained PLD3, is from the phospholipase D (PLD) family of enzymes which catalyse the hydrolysis of membrane phospholipids.[137] PLD3 is the least well studied phospholipase D subtype and current data does not implicate it in cancer progression. However, its transcript variants phospholipases D1 and D2 have been shown to be involved in the progression of metastatic breast cancers,[144] and isoform-selective inhibitors of PLD were shown to modulate invasiveness in metastatic breast cancer models.[145] Thus, we selected this target for further validation (See Chapter 4).

The second ranked protein hit MAT2A, is a protein that catalyses the production of S-adenosylmethionine from methionine and ATP. S-adenosylmethionine is a key methyl donor in cellular processes. MAT2A has been shown to be overexpressed in gastric cancers.[146] Furthermore, inhibition of expression of MAT2A has been shown to significantly supress growth of hepatocellular carcinomas.[147] In addition, specific inhibitors of MAT2A have also been shown to be effective agents against colorectal cancers.[148] Since this was a well-established protein implicated in cancer progression, we selected MAT2A as a target for further validation (See Chapter 4).

Metallotheinins (MTs) are a class of proteins with high content of cysteine residues that are responsible for detoxifying heavy metals, and high levels of MT expression has been associated with poor clinical outcomes of cancer patients undergoing therapy with platinum based metallodrugs.[149] MT2 has been previously shown to bind to a RAPTA-C, an analogue of RAPTA-T with p-cymene instead of toluene as the arene, and shows very similar phenotype in terms of anti-cancer activity.[150] RAPTA binding to MT2 caused a displacement of zinc suggesting binding occurred in Cys residues in MT2.

Zing finger HIT (zf-HIT) are sequence motifs found in various proteins which contain conserved cysteine and histidine residues that can coordinate zinc atoms.[151] These motifs are suggested to play important roles in gene regulation and chromatin remodelling. It was shown previously that RAPTA complexes bind proteins with zinc finger domains[55] and these complexes can also displace zinc.[150] Furthermore top down MS/MS results also show binding of these complexes to zinc finger domains in the breast cancer type 1 susceptibility protein (BRCA1) (Chapter 6).

RNA binding proteins (RBMs), are proteins that bind to single or double stranded RNA and play a role in post-transcriptional control of RNAs such as splicing, mRNA stabilization, mRNA localization and translation.[152] RBM47 has been shown to play an important role in metastatic breast cancers, where low expression of this protein is associated with highly metastatic phenotype.[153] Furthermore RMB47 knockout mice xenografted with lung adenocarcinomas were found to show enhanced tumor formation and metastasis.[154] It is possible that treatment with RAPTA-T activates compensatory pathways causing increased expression of RMB47 which could link to its anti-metastatic activity.

The pyruvate dehydrogenase complex converts pyruvate into acetyl-CoA a substrate used in the citric acid cycle for cellular respiration. Pyruvate dehydrogenase phosphatases (PDPs) in the mitochondria catalyze the dephosphorylation and reactivation of the alpha subunit of the E1 component of the pyruvate dehydrogenase complex[136]. PDP1 has been implicated in promoting the Warburg effect and growth in tumors and has been suggested to be a promising anti-cancer target.[155] *In vitro* studies of the cellular effects of RAPTA-T has shown that the compound accumulates appreciably in the mitochondria and perturbs the expression of a large number of mitochondrial proteins including causing an overexpression of ATP synthetase[119] an enzyme heavily involved in cellular respiration.

Protein arginine methyltransferases (PRMTs) catalyze the process of arginine methylation a widespread post translational modification in eukaryotic cells. PRMTs use S-adenosyl-L-methionine as the methyl donor a product of another RAPTA-T obtained target MAT2A. The chromatin target of PRMT1 protein (CHTOP) is a chromatin associated protein which has been shown to be critical for estrogen-dependent gene activation[156] and is also implicated in the tumorgenicity of glioblastoma cells[157]. Considering that RAPTA complexes are known to bind to histones (Figure 3.7)[92] a component of chromatin, and could be a binding partner to MAT2A, it is possible that its activity also perturbs expression of CHTOP.

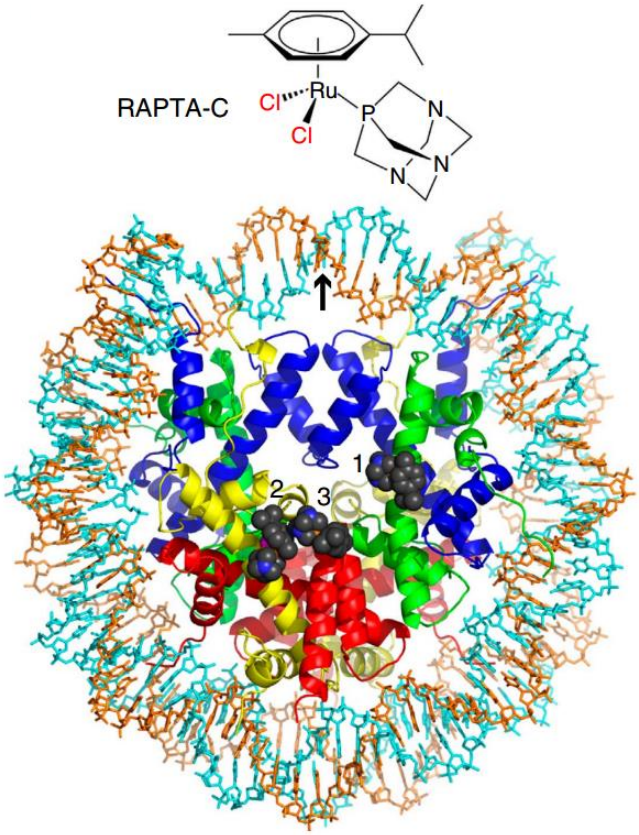

Figure 3.7 Chemical structures and nucleosomal adducts of RAPTA-C. X-ray structures of adducted nucleosome core particles are shown looking down the DNA superhelical axis, with the nucleosome pseudo-twofold axis running vertically (arrow). Histone proteins are shown in blue (H3), green (H4), yellow (H2A) and red (H2B), and the two 145-nucleotide DNA strands are cyan and orange. RAPTA-C adducts appear with space-filling representation (sites 1–3, histone associated). (Adapted from Adhireksan et. al *Nat Commun*. 2014).

The chromosome transmission fidelity factor 8 (CTF8) is a chromosome cohesion protein involved in sister chromatid cohesion and fidelity of chromosome transmission.[2.9] It has been implicated in the DNA replication and repair pathway and has been shown to have reduced expression in renal and prostate tumours.[137] Since it is a nuclear protein associated with

chromatin, RAPTA-T could possibly bind to this target too.

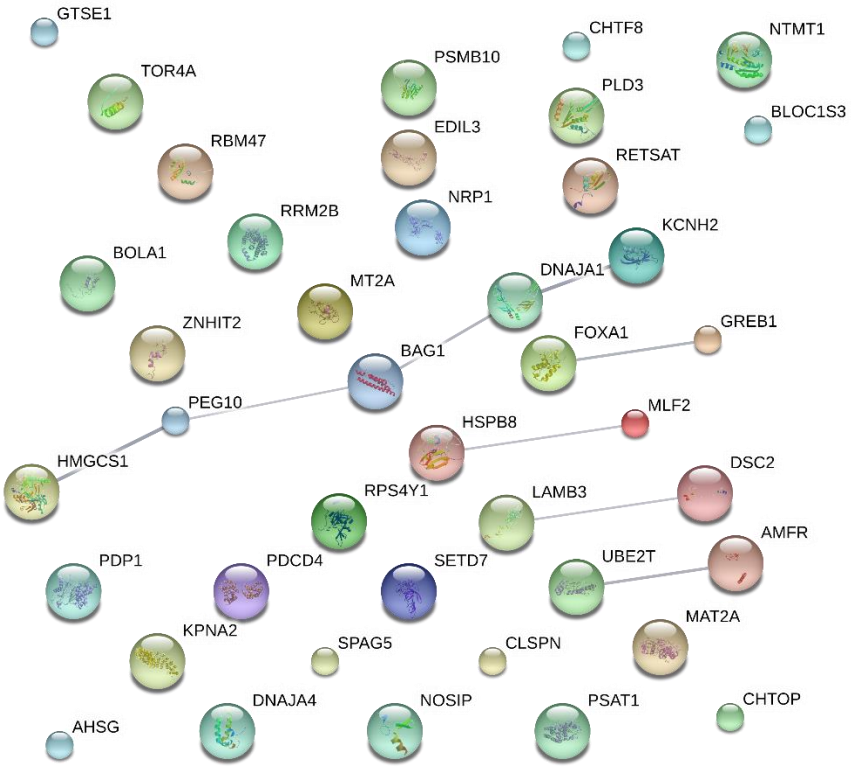

Figure 3.8 STRING protein-protein interaction network associated protein list of RAPTA-T generated using protein lists from specificity and regulation criteria.

Figure 3.8 shows a STRING network of proteins from the associated protein list of RAPTA-T (Appendix A, Table A.4). As seen, there is generally little association between the different proteins in the network. Thus, the effects of RAPTA-T may be brought about by binding to distinct proteins. Indeed, the different phenotype changes of primary toxicity, anti-angiogenesis and anti-metastasis which can be induced by RAPTA-T are not thought to originate from binding to a single class of proteins.

Overall, of the eight potential RAPTA-T protein targets obtained from this study, two of them were previously validated. The remaining six targets were physiologically viable based on what is known on the phenotypic effects or RAPTA-T and affinity proteomics/expression profiling based studies. We selected two targets PLD3 and MAT2A for further evaluation.

3.3 Conclusion

A proteomics profiling approach, FITExP was used to probe potential protein targets of cisplatin, RAPTA-T and RAPTA-EA. Validation experiments with paclitaxel showed the reliability of the method, and main protein target lists for all three compounds gave physiologically viable anti-cancer protein targets. The main targets obtained for cisplatin were DNA repair related, which were in line with the main mechanism of cisplatin on nuclear DNA. RAPTA-EA's mechanism of action is mainly on regulation of oxidative stress response and is thought to be conferred by the ethacrynic acid moiety in the drug. This is in great contrast to the simple RAPTA-type complex RAPTA-T, which seemed to have a broad mechanism of action targeting proteins involved in both metastasis and tumorigenicity. From a therapeutic standpoint, RAPTA-EA could be explored in cancers where EA alone has shown potency such as chronic lymphocytic leukemias[158] or where EA combined with another agent shows synergy, such as the combination of EA with afatinib, an irreversible epidermal growth factor receptor tyrosine kinase inhibitors for breast cancers[159]. On the other hand, due to its broad mechanism of action, RAPTA-T could potentially be more useful if used concomitantly with drugs that target specific cancer pathways and could also play a role in therapies for later stage cancers due to its anti-metastatic properties. From this study, we selected two targets of RAPTA-T for binding confirmation.

3.4 Experimental

All cell culture experiments and interpretation of protein lists obtained were performed in the EPFL. Preparation of samples for LC-/MS/MS, data acquisition, and biostatistical analysis was performed at the lab of Professor Roman Zubarev, Karolinska Institute, Sweeden.

3.4.1 Cell maintenance, treatment and preparation for expression profiling

MDA-MB-231 (human mammary gland adenocarcinoma) and MCF-7 (human mammary gland adenocarcinoma cells), were cultured in DMEM Glutamax medium supplemented with 10% fetal calf serum, penicillin 100 units/mL Streptomycin 100 µg/mL (Invitrogen). Cells were incubated at 37^0C in a moist environment containing 5% CO_2. For proteomic expression experiments, cells were seeded at a density of $5x10^5$ cells in a 6-well plate for 24 hours. Media was aspirated and cells were rinsed with 1 X PBS before addition of fresh media containing solutions of compound (Paclitaxel, Cisplatin, RAPTA-EA and RAPTA-T, dosed at a concentration to achieve a cell kill of approximately 50% after 48 hours). After 48 hours, cells were detached with enzyme free cell dissociation solution and centrifuged at 200G for 5 minutes. Cell pellets were snap frozen in liquid N_2 and stored at -80 ^{0}C before sample preparation for mass spectrometry.

3.4.2 Protein digestion

Breast cancer cell pellets were thawed on ice and depending on the number of cells/pellet reconstituted in 100-200µl 8M Urea with 100 mM NaCl. Cells were disrupted by probe sonication (Vibra-Cell™ CV18, Sonics & Materials, Newtown, USA) two times for 5/5 seconds cycles over 20 seconds followed by centrifugation at 12,000 rpm for 10 minutes at 4°C. Solubilized proteins were transferred into fresh vials and the protein concentrations were determined using microBCA from Pierce (Thermo Fisher Scientific Inc). From each sample 10 µg extracted protein were dissolved in a final concentration of 0.1% ProteaseMax (Thermo Fisher Scientific Inc), 50 mM ammonium bicarbonate and 10% acetonitrile in a total volume of 80 µl. The resulting protein solutions were incubated for 45 minutes at 37 °C while shaking followed by an additional bath soncication of 10 minutes at room temperature. Samples were centrifuged and directly subjected to a tryptic digestion protocol carried out by a liquid handling robot (MultiProbe II, Perkin Elmer). This included protein reduction in 5 mM DTT at 56 °C and alkylation in 15 mM iodacetamide for 30 minutes at room temperature in the dark. Trypsin was added in an enzyme to protein ratio of 1:30 and digestion was carried out over night at

37°C. Samples were acidified by adding 6 µl concentrated formic acid, incubated for 30 minutes at room temperature and centrifuged for 20 minutes at 3000 rpm in order to remove undigested material.

3.4.3 LC-MS/MS experiment

Tryptic peptides were cleaned with C18 StageTips (Thermo Fisher Scientific Inc) and the resulting peptide mixture was injected into a nano-Ultimate system (Thermo Scientific, Bremen, Germany) in-line coupled to a QExactive mass spectrometer (Thermo Scientific, Bremen, Germany). The chromatographic separation of the peptides was achieved using an 28 cm long in-house packed column (C18-AQ ReproSil-Pur®, Dr. Maisch GmbH, Germany) with the following gradient: 4−26% acetonitrile in 120 minutes, 26−95% ACN for 5 minutes and 95% ACN for 5 minutes all at a flow rate of 300 nl/ minutes.

The MS acquisition method was comprised of one survey full scan ranging from m/z 300 to m/z 1650 acquired with a resolution of R= 140,000 at m/z 200 and a target value of 5e6, followed by data-dependent higher-energy collisional dissociation fragmentation scans from maximum sixteen most intense precursor ions with a charge state ≥ 2. Sequencing was done with a target value of 2e5 ions determined with predictive automatic gain control, for which the isolation of precursors was performed with a window of 4 m/z. Scans were acquired with a resolution of R=17,500 and normalized collision energy was set to 26.

3.4.4 Data processing

Fragmentation spectra were extracted using Raw2MGF (in-house developed software), and the resulting mascot generic files were searched against a SwissProt protein database (reversed protein sequences had been added to database for decoy search) using the Mascot 2.3.0 (Matrix Science Ltd.). Mascot was set up to search a concatenated SwissProt protein database (selected for Homo sapiens) with enzyme specificity set as C-terminal to arginine and lysine, allowing cleavage before proline and a maximum of and two missed cleavage sites. The allowed peptide mass deviation was set to 10 ppm and 0.02 Da for the fragment ions. Carbamidomethylation of cysteine was specified as a fixed modification, whereas oxidation of methionine, N-termianl protein acetylation and deamidation of asparagine and glutamine were defined as variable modifications.

Quantitative information was extracted using in-house developed label-free software Quanti v.2.5.3.122. Only reliably identified (FDR<0.01), unmodified peptides with unique sequences were considered and only proteins discovered with at least two such peptides were quantified. For each protein, one database identifier (ID) was selected, covering all the peptide sequences identified for this specific protein. If two proteins belonging to different protein groups had a partial sequence overlap, then all the peptides belonging to this overlap were ignored. The results were reported as a set of relative protein abundances ***A*** scaled such that the geometric mean of the abundance of each protein over all samples was 1.0.

3.4.5 Scoring system

For combining the data from replicate analysis, "medians of ratios" are used instead of "ratios of medians", as has previously been suggested.[160] If relative protein abundance of *i*-th quantified protein in *c*-th cell line under *j*-th treatment is denoted as $A_{i,j}^{c}$, then regulation ***Reg*** is calculated as:

$$\boldsymbol{Re}\ \boldsymbol{g}_{i,j}^{c} = Median\left(\left|log\frac{A_{i,j}^{c}}{A_{i,0}^{c}}\right|\right), \qquad (1)$$

and specificity ***Spec*** is defined as:

$$\boldsymbol{Spec}_{i,j}^{c} = Median_{k\neq j}\left(\left|log\frac{A_{i,j}^{c}}{A_{i,k}^{c}}\right|\right), \qquad (2)$$

where j = 0 corresponds to untreated cells for ***Reg*** calculation, and $j\neq k$ for ***Spec*** calculations.

3.4.6 Exeptional behavior measure

For each *I*-th protein and each *J*-th drug treatment, two vectors were calculated:

$$\boldsymbol{C}_{\boldsymbol{i}}^{\boldsymbol{I},*} = Corr\,(\boldsymbol{Re}\ \boldsymbol{g}_{i,j}^{c}, \boldsymbol{Re}\ \boldsymbol{g}_{I,j}^{c}), \qquad (3)$$

$$\boldsymbol{C}_{\boldsymbol{i}}^{\boldsymbol{I},\boldsymbol{J}} = Corr\,(\boldsymbol{Re}\ \boldsymbol{g}_{i,j\neq J}^{c}, \boldsymbol{Re}\ \boldsymbol{g}_{I,j\neq J}^{c}), \qquad (4)$$

where $\boldsymbol{C}_{\boldsymbol{i}}^{\boldsymbol{I},*}$ are the Pearson's correlation coefficients of expression profiles over all treatments of *i*-th and *I*-th proteins, while $\boldsymbol{C}_{\boldsymbol{i}}^{\boldsymbol{I},\boldsymbol{J}}$ are correlation coefficients of the expression profiles of *i*-th and *I*-th proteins excluding treatment J. Then, the linear

model $C_i^{I,*} \sim C_i^{I,J}$ was created and the coefficient of determination of the model was used to calculate the measure of exceptional behavior $Exc^{I,J}$ of *I*-th protein under *J*-th treatment:

$$Exc^{I,J} = \frac{1}{\bar{R}^2_{I,J}} \qquad (5)$$

3.4.7 p-value calculation

In estimation of the p-value of a protein with a certain rank, we used the rank product method, which has previously been found to be robust and tolerant to missing values in detection differentially regulated genes in replicated experiments.[161] The method has also been successfully applied to proteomics datasets for detection of significantly regulated proteins.[162] In adaptation of the method by Schwämmle et al., we treated ***Reg, Spec*** and ***Exc*** ranks as independent variables, and their values for different cell lines as well as at different incubation times were considered as independent replicate measurements. The rank product was considered to have a gamma distribution under null hypothesis, from which we calculated the p-values for the set of ranks of every protein. Adjusted p-values were calculated using standard Bonferroni correction, using the total number of proteins as a multiplication factor.

3.4.8 Network mapping

STRING v9.116[163] was used to map drug-specific, significantly regulated proteins onto protein-protein interaction networks. Gene names corresponding to up- and down-regulated proteins were submitted into STRING web-site (http://string-db.org). Medium confidence threshold (0.4) was used to define protein-protein interactions. Gene set enrichment analysis built in STRING with the whole genome background was used to identify enriched gene ontology terms and KEGG pathways. A 0.05% threshold was applied to the p-values after Benjamini-Hochberg correction.

Chapter 4
Validation of potential RAPTA-T protein targets Phospholipase D3, and S-adenosylmethionine synthase isoform type-2 obtained from FITExP analysis

4.1 Introduction

In general, targets obtained via protein target screening methodologies have to be externally validated as false positives can occur when such strategies are applied. Furthermore, since the approach FITExP deduces the most likely protein target of a small compounds via the exceptional regulation of its protein target during late apoptosis and not through a physical binding event, evidence of binding or inhibition was necessary. Validation of ligand-protein binding can be carried out via binding assays or in the case of enzymes, inhibitory constants can be obtained if activity assays can be developed. Ligand-binding assays can be broadly classed into labelled, label-free, structural and thermodynamic assays. Table 4.1 lists the different binding assays used and their operating principle.

Group of assays	Assay	Principle
Labeled ligand-binding assays	Fluorescent ligand binding assays	Fluorescent labeled ligand is used to detect its binding to a target.
	Radioligand binding assays	Radioactively labeled ligand is used to detect its binding to a target.
Label-free ligand binding assays	Surface plasmon resonance	Light-excited surface plasmon polaritons are applied to track the binding of ligands to proteins bound to a gold surface.
	Plasmon-waveguide resonance	Polarized continuous wave lasers are applied to excite electromagnetic waves in a resonator made of a thin silver film with a layer of SiO_2 and a glass prism. Ligand binding changes amplitude, position and width of reflected lights.
	SPR imaging for affinity-based biosensors	Binding kinetics are measured and related to intensity modulation and the reflectivity of monochromatic incident p-polarized light detected at a fixed angle.
	Whispering gallery microresonator	Binding of molecules to the surface of the cavity induces changes of the resonant wavelength changes. The resonant changes of light permit multiple analyses of molecules.
	Resonant waveguide grating	A nanograting is used to couple light into the waveguide via diffraction. The light illuminates the biosensors in microplate at a nominally normal incident angle. The drug binding of the immobilized receptors results in a shift in the resonant wavelength.
	Biolayer Interferometry Biosensor	A spectrometer is used to detect interference patterns formed by light reflected from an optical layer and a biolayer containing proteins of interest.
Structure-based ligand binding assays	Nuclear magnetic resonance	Magnetic characteristics of certain atomic nuclei, which absorb electromagnetic radiation in the magnetic field are related to ligand binding characteristics
	X-ray crystallography	The diffracted X-ray beams of ligand bound protein crystals are resolved to produce a three-dimentional image

		of electron density. 3D structure obtained gives knowledge of binding sites of ligand on protein.
Thermodynamic binding assays	Thermal denaturation assays	Thermal denaturation of proteins is measured by differential scanning fluorimetry, which applies a probe fluorophore to monitor thermal denaturation process of proteins in the presence of ligands.
	Isothermal titration calorimetry	Measures the enthalpy variation of ligand-protein binding which is mathematically related to its binding properties.

Table 4.1 Ligand-protein binding assays and their principles (Adapted from Konstantin Y. *Mater Methods* 2011).

In our study, the two targets we obtained, phospholipase D3 (PLD3) and methionine adenosyltransferase II, alpha (MAT2A) are both enzymes, thus our initial validation strategy involved expressing both proteins and developing activity assays to assay the inhibition of RAPTA-T towards these enzymes.

4.2 Results and discussion

4.2.1 Expression and purification of proteins

PLD3 is a 55 kDa transmembrane glycoprotein thought to be localized in the endoplasmic reticulum membrane.[164] Phospholipase D enzymes catalyse the hydrolysis of the phosphodiester bond in phospholipids into phosphatidic acid[165] and choline as seen in Figure 4.1.

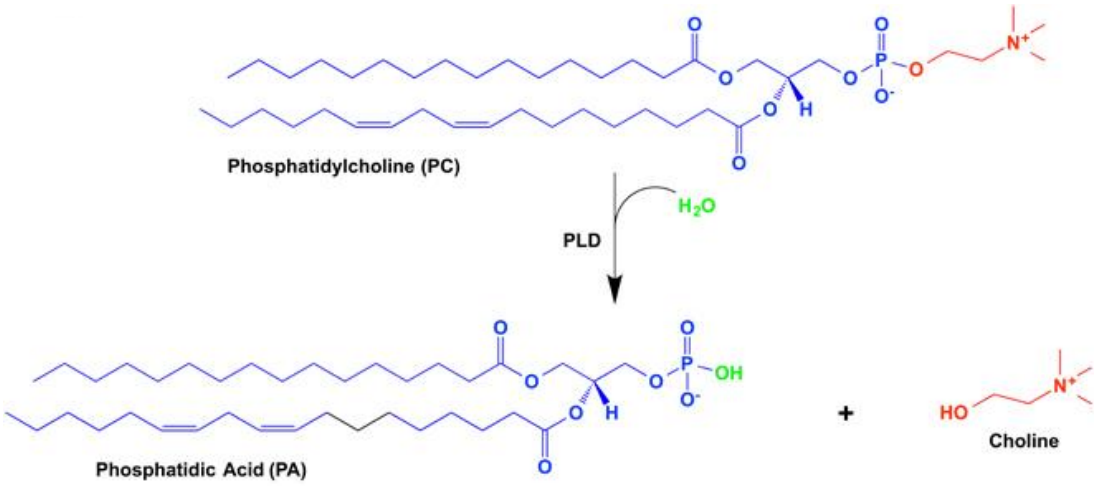

Figure 4.1 Enzymatic reaction catalysed by phospholipase D.

Being a glycosylated membrane protein we opted for a mammalian expression system for PLD3. Its gene sequence was synthesized commercially with an N-terminal IgG kappa secretory sequence and a C-terminal His-tag for purification. The gene of interest was cloned into the mammalian pXLG-eGFP plasmid vector for expression. Tests cultures were first carried out in both human embryonic kidney 293 (HEK293) cells, and chinese hamster ovary (CHO) cells with and without inducers DMSO and valproic acid (VPA), respectively.

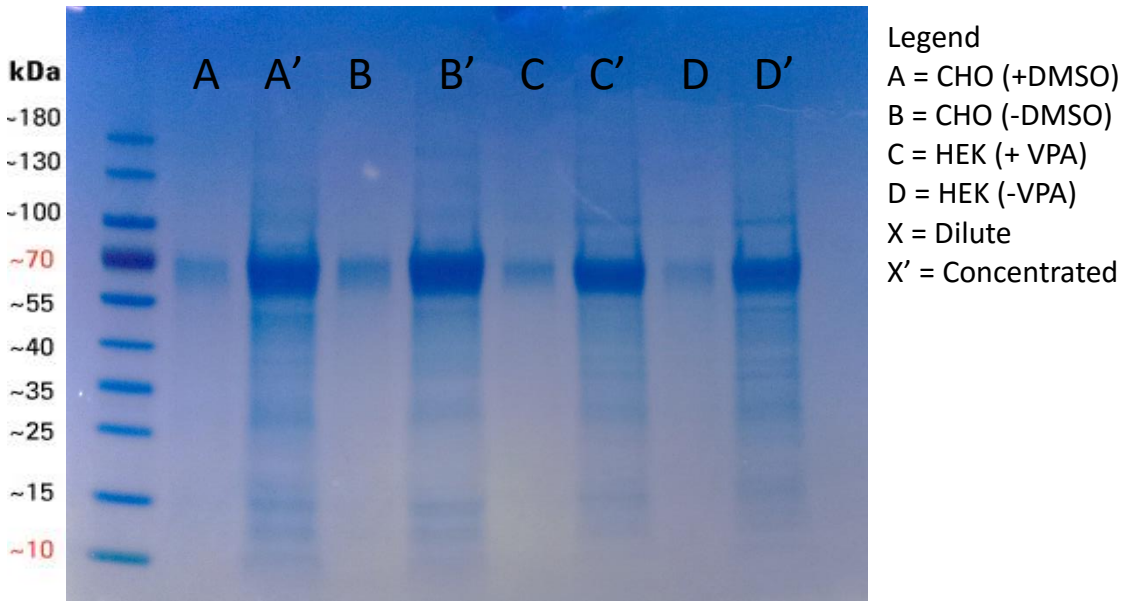

Figure 4.2 Sodium dodecyl sulfate polyacrylamide gel electrophoresis (SDS-PAGE) of test cultures of PLD3 expression.

Negligible difference was observed in the expression yields between all expression conditions tested (Figure 4.2). Thus, we selected HEK293 for cost savings, as transfection in these cells requires half the DNA load of an equivalent batch of CHO cells. Though PLD3 has a molecular weight of 55 kDa its appearance as a relatively thick band near 70 kDa is probably caused by the effects of glycosylation on SDS-PAGE, where the heterogeneity of glycosylation can dramatically increase the mass of the protein, and interactions of SDS with sugars and amino acids are different leading to the observed band shift and thickening.

MAT2A is a 44 kDa cytosolic enzyme which catalyses the formation of S-adenosylmethionine (SAMe or AdoMet), from the reaction of methionine and adenosine triphosphate (ATP) as seen in Figure 4.3. SAMe is the principle methyl donor in cells and plays a central role in cellular biochemistry as a precursor to methlation, aminopropylation and transulfuration pathways.[166] Expression of MAT2A was relatively simple as the protein has no post translational modifications and its plasmid vector for bacterial expression was available in the AddGene[167] database. Both MAT2A and PLD3 were expressed with good yields of 25mg/L and 4.5mg/L and purities of ~90% which were deemed suitable for enzyme assays. (Figure 4.4)

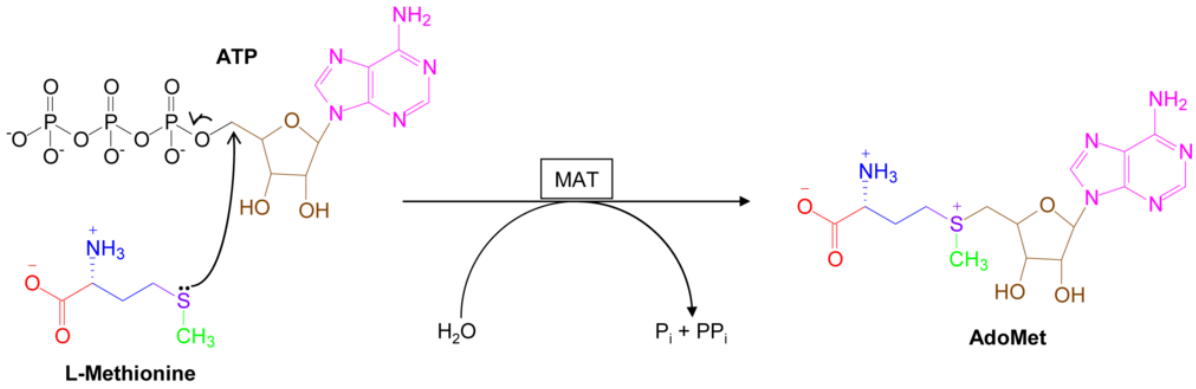

Figure 4.3 Enzymatic reaction catalysed by MAT2A.

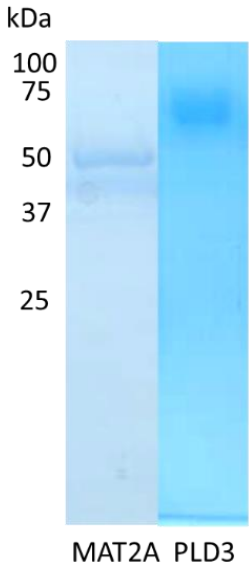

Figure 4.4 SDS-PAGE of MAT2A and PLD3 proteins after immobilized ion affinity chromatography.

4.2.2 MAT2A assay development and RAPTA-T IC_{50} measurements

A MAT2A assay was developed based on a similar assay reported previously[148] with modifications. Briefly, the activity of the MAT2A enzyme is quantified as the concentration of free phosphate liberated from ATP during conversion to SAMe (Figure 4.3), which occurs at a 1:1 stoichiometric ratio to the product formed. Free phosphate is measured by the malachite green phosphate colorimetric assay, based on formation of a complex between malachite green, ammonium molybdate and free orthophosphate under acidic conditions, which is then measured at a λ_{max} 640nm (Figure 4.5). In our assays, buffer conditions were selected carefully to avoid the inclusion of chelating agents (e.g. EDTA) of reducing agents (e.g. DTT) which could coordinate with RAPTA-T. Since the substrate L-methionine contained a sulphur group which could potentially coordinate to ruthenium(II) complexes[168] we tried to minimize the

concentration of substrate added. In enzymatic reactions, reaction rates can be described using the Michaelis-Menten model:

$$v = \frac{V_{max}[S]}{K_m}$$

Where [S] is substrate concentration, v is reaction rate, V_{max} is the maximum rate achieved by the system, and K_M is the substrate concentration at which reaction rate is half of V_{max}. From a Michaelis-Menten saturation curve of absorbance vs. L-methionine concentration (figure 4.6), we found the K_M of MAT2A to be 35 µM and selected a non-saturating L-methionine concentration of 50 µM, which provided a good signal-to-noise ratio in the calorimetric phosphate assay used as activity readout.

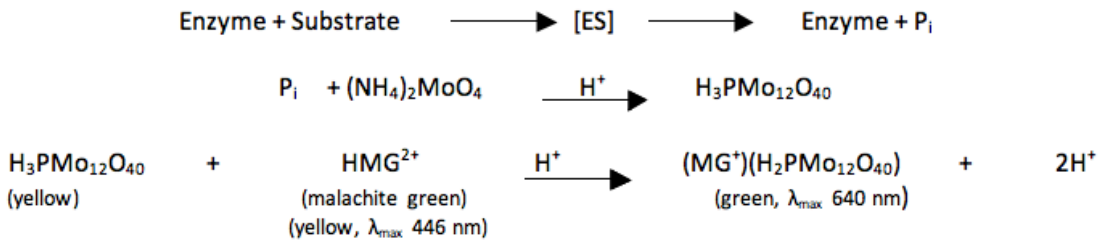

Figure 4.5 Principle of malachite green phosphate assay.

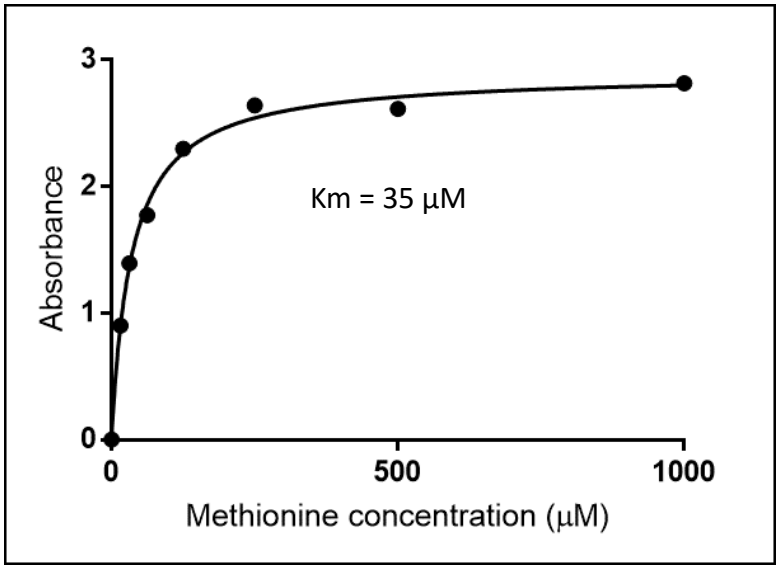

Figure 4.6 Michaelis-menten curve of MAT2A activity vs. L-methionine concentration.

Since RAPTA-T is a prodrug which undergoes aquation of its chloride ligands before binding[169], we attempted to study the effect of RAPTA-T and MAT2A pre-incubation time on the IC_{50} of RAPTA-T to determine if this greatly influenced its inhibition. There was a reduction of the IC_{50} of RAPTA-T from 121 µM to 75 µM upon increasing the pre-incubation time from 30-90 minutes which did not change further upon longer pre-incubations, indicating an equilibrium state of binding is achieved after 90 minutes (Figure 4.7).

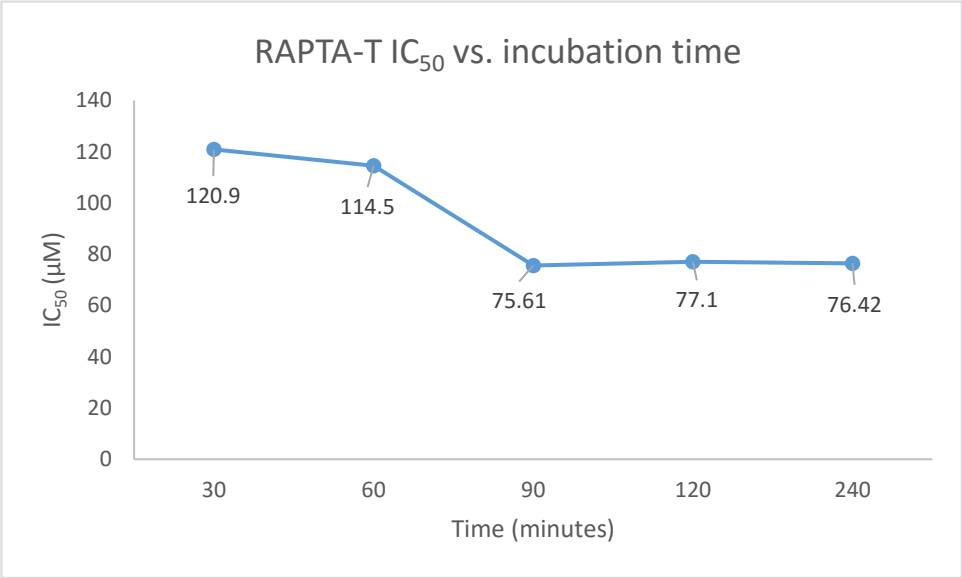

Figure 4.7 IC_{50} value of RAPTA-T on MAT2A as a function of different ligand-protein pre-incubation times.

Since the inhibition type of RAPTA-T on MAT2A was unknown, we made initial attempts to determine if its inhibitory activity was competitive, non-competitive or uncompetitive. Differentiation of these inhibition-types can be done via observing the shifts in K_M and V_{max} from Michaelis-Menten curves plotted with different concentrations of inhibitor.[170] Competitive inhibition is characterized by reversible binding of inhibitor to free enzyme and is characterized by an increase in K_M with no change in V_{max}. Non-competitive inhibitors bind equally well to the free enzyme and enzyme-substrate complex resulting in a lowered V_{max} but with an unchanged K_M values. Uncompetitive inhibition occurs when the inhibitor binds exclusively to the enzyme-substrate complex, inactivating it and is characterized by a drop in both K_M and V_{max}. Michaelis menten curves of MAT2A in the presence of 100µM and 300µM of RAPTA-T showed a clear reduction of both K_M and V_{max} of MAT2A, showing RAPTA-T has properties of uncompetitive inhibition (Figure 4.8).

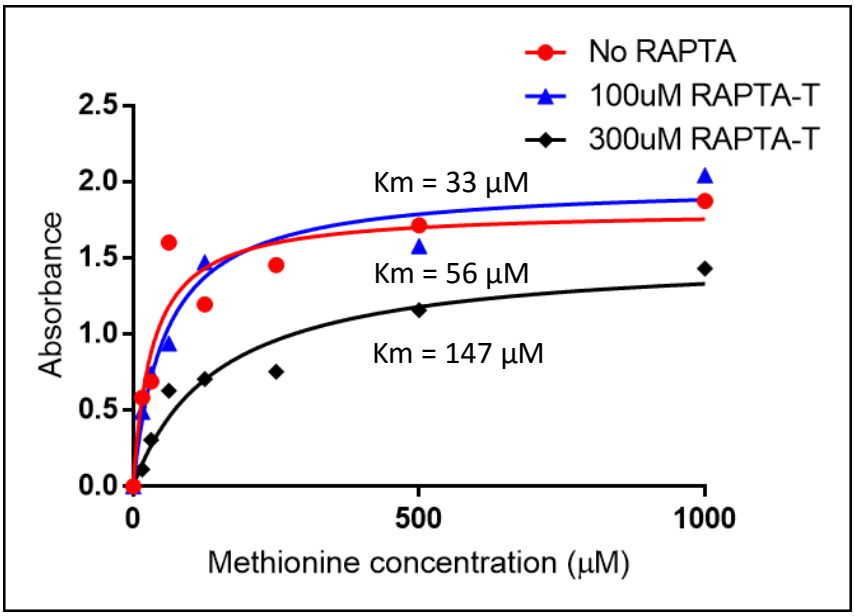

Figure 4.8 Michaelis-menten curve of MAT2A with different concentrations of of RAPTA-T.

Overall, RAPTA-T appears to be an uncompetitive inhibitor of MAT2A with an IC_{50} of ~75 µM. This indicates a rather weak inhibition as compared to specific inhibitors of MAT2A such as the fluorinated N,-N-dialkylaminostilbene agents (FIDAS) agent FIDAS-3 which has an MAT2A inhibition IC_{50} of 5µM (Figure 4.9).[148] Considering MAT2A is one of several potential RAPTA-T binding targets, perhaps inhibition of this enzyme though weak, still contributes partially to the overall anti-cancer activity of the compound. These results should also be interpreted with caution, as inhibition measurements done on purified proteins are markedly different than conditions in cells or tissues. Thus, these results should be followed up by measurement of MAT2A inhibition by RAPTA-T directly in cells and performing other binding assays.

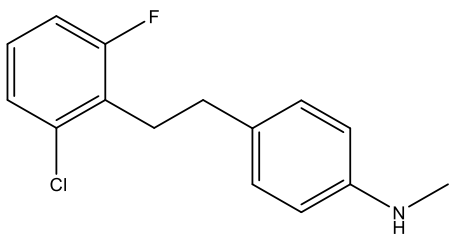

Figure 4.9 FIDAS-3 a specific inhibitor of MAT2A.

4.2.3 PLD3 activity assay

PLD3 activity was assayed with the commercial Amplex Red Phospholipase D (PLD) assay kit. Briefly, PLD activity was measured from a series of three stoichiometric reactions, firstly the conversion of phosphotidylcholine to choline by PLD (Figure 4.1), followed by oxidation of choline to betaine liberating H_2O_2 which then reduces the Amplex red reagent into a florescent substrate resorufin (Figure 4.10). Floresence intensity of resorufin is then measured at absorption and emission of 540 and 590 nm respectively and correlated with PLD activity. PLD from *Streptomyces chromofuscus* was used as a positive control for PLD activity, H_2O_2 was used as a positive control for assay function and PLD3 buffer functioned as a negative control.

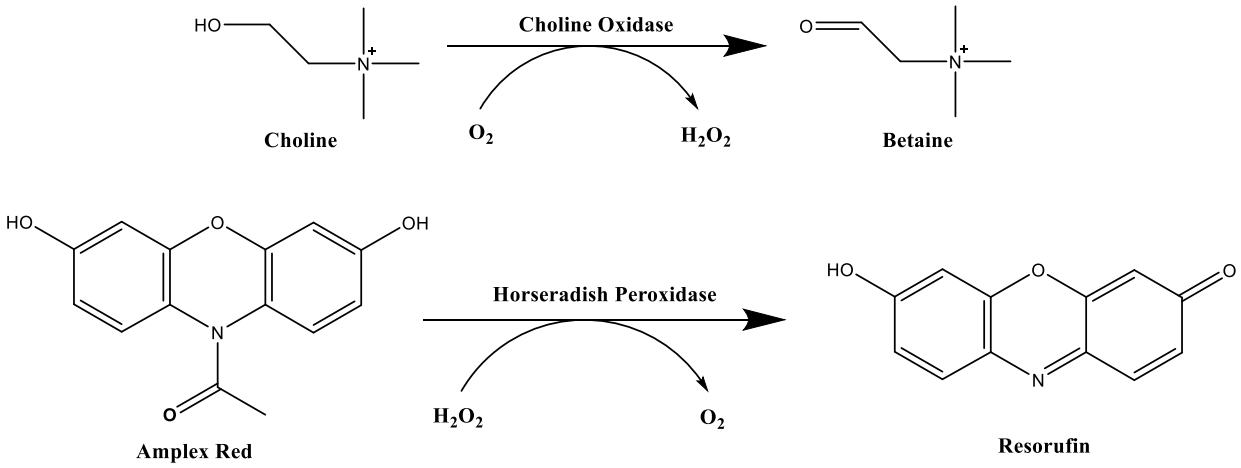

Figure 4.10 Principle of AmplexRed phospholipase D assay kit.

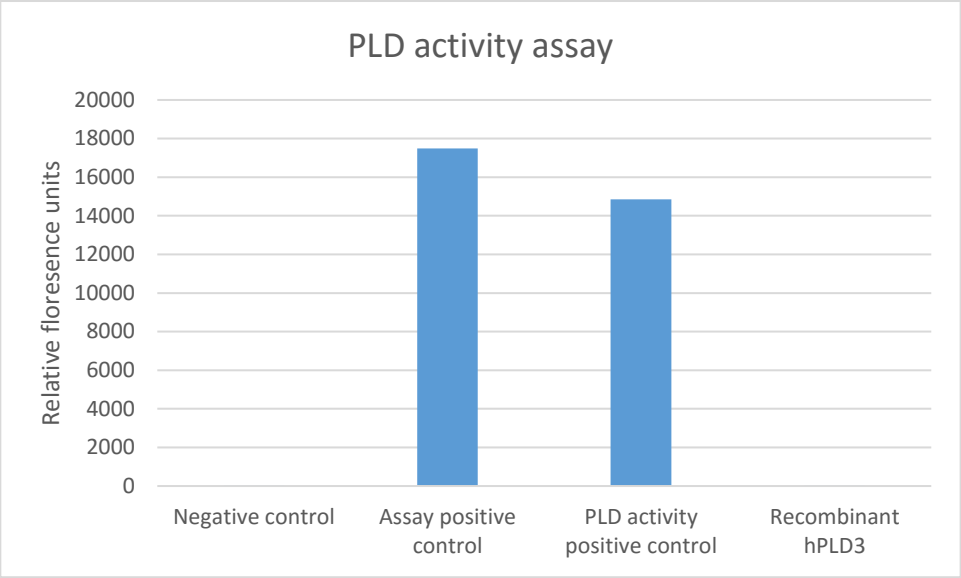

Figure 4.11 PLD activity measurement for recombinant human PLD3 and PLD from *Streptomyces chromofuscus.*

We observed no activity from the expressed recombinant human PLD3 (Figure 4.11). This was similarly observed by the group who first identified the protein.[164] We expressed only the lumenal portion of the topological domain of PLD3 thought to be in charge of catalytic activity.[136] However, it is possible that its association with the membrane structure is critical for enzymatic activity, or expression in our organism of choice led to misfolding or an incorrect glycosylation pattern on PLD3 leading to loss of function. Thus, an alternative option would be to assay PLD3 activity in intact cell assays, which should be explored subsequently.

4.3 Conclusions

We successfully expressed recombinant human MAT2A and PLD3. We show that RAPTA-T is potentially an uncompetitive inhibitor of MAT2A with an IC_{50} of ~75 µM. From this, RAPTA-T could be useful for cancers where MAT2A is upregulated such as liver and colorectal cancer.[148] Recombinant PLD3 shows no enzymatic activity as previously reported, thus other validation strategies have to be considered.

4.4 Experimental

All protein expression was performed by Dr. David Hacker at the protein expression core facility Ecole Polytechnique Fédérale de Lausanne.

4.4.1 Materials

Amplex red phospholipase D assay kit was purchased from ThermoFisher Scientific and used based on manufacturer's instructions. Phosphate colorimetric kit was purchased from Sigma Aldrich and used based on manufacturer's instructions. Phospholipase D (PLD) from *Streptomyces chromofuscus* was purchased from Sigma Aldrich. All other reagents were commercially purchased and used without further purification.

4.4.2 Recombinant protein expression

MAT2A/2B

hMAT2A and hMAT2B plasmid was obtained from Addgene (www.addgene.org, plasmid #53648 & *34795 respectively) as a bacterial stab. Plasmid DNA was amplified in antibiotic media and extracted with a plasmid miniprep kit (Qiagen) according to manufacturer's instructions and sequenced by GATC biotech for validation. The plasmid was transformed into competent E. coli strain BL21 (DE3) Rosetta and selected with ampicillin. One colony was picked from the LB agar plate and used to inoculate a 10-mL culture of LB with ampicillin. The culture was grown overnight at 37°C with agitation at 150 rpm in an incubator shaker. The next day, 10-mL culture was used to inoculate a 1-L culture of LB and ampicillin. The culture was incubated at 37°C with agitation as before until an OD600 of 0.6 was reached. The temperature of the incubator shaker was then reduced to 16°C, and IPTG was added to the culture to a final concentration of 1 mM. The culture was allowed to incubate overnight at 16°C. In the morning, the culture was centrifuged at 3,500 rpm for 20 minutes, and the cell pellets were maintained frozen at -80°C. The frozen cell pellet was allowed to thaw and was resuspened in 60 mL of binding buffer (150 mM NaCl and 25 mM sodium phosphate (pH 7.3)) containing the Roche protease cocktail. The resuspended cells were sonicated 8 x 20 seconds. The solution was then centrifuged at 11'000 rpm for 30 minutes. The supernatant was retained and imidazole was added to 10 mM. Then 2 ml of FastFlow IMAC beads (GE Healthcare) were added. The solution was mixed by rotation for 1 hour at 4°C. The resin was transferred to a column and the washed with 10 column volumes (CV) of binding buffer with 10 mM imidazole. Then washed sequentially with 10

CVs of binding buffer with 25 mM imidazole, 5 CVs of binding buffer with 50 mM imidazole, and 5 CVs of binding buffer with 100 mM imidazole. The protein was then eluted with 4 x 2Cvs of binding buffer with 250 mM imidazole. The washes and elutions were analyzed by reducing SDS-PAGE. The fractions with the recombinant protein were pooled and dialyzed twice against 2 L of PBS. After dialysis the concentration of the protein was determined by absorbance at 280 nm.

PLD3

PLD3 plasmid with N-terminal IgG kappa secretory sequence and a C-terminal His-tag was obtained commercially from GeneArt gene synthesis (ThermoFisher Scientific). Gene of interest was extracted and cloned into the mammalian pXLG-eGFP plasmid vector for expression using Gibson assembly.[171] Plasmid was amplified in E.coli and extracted with a plasmid miniprep kit for mammalian expression. Final plasmid obtained was sequenced before use. Suspension-adapted HEK-293E cells were routinely maintained in serum-free ExCell 293 medium (SAFC Biosciences, St. Louis, MO) with 4 mM glutamine with inoculation at 0.3 x 10^6 cells/mL as described.[172] On the day before transfection, cells were inoculated into fresh medium at a density of 1 x 10^6 cells/ml. The next day, 2 x 10^8 cells were harvested by centrifugation at 1,200 rpm for 5 min and resuspended at a density of 20 x 10^6 cells in 10 ml of RPMI 1640 medium with 0.1% pluronic F68 (SAFC Biosciences) in a TubeSpin® bioreactor 50 tube (TPP, Trasadingen, Switzerland).[173]Plasmid DNA (0.3 mg) and linear 25 kDa polyethylenimine (0.6 mg; 1 mg/ml in H_2O; Polysciences, Eppenheim, Germany) were sequentially added and mixed. The culture was agitated by orbital shaking at 180 rpm in an ISF-4-W incubator (Kühner AG, Birsfelden, Switzerland) at 37°C in the presence of 5% CO_2. After 60 min, the transfected culture was transferred to a 500-mL glass bottle containing 190 ml of Excell293e medium (Invitrogen) with 4 mM glutamine and 3.75 mM valproic acid (500 mM in H_2O) (SAFC Biosciences).[174] The culture was transferred to an incubator shaker at 37°C with 5% CO_2 with agitation at 110 rpm. At 7 d post-transfection, the cell culture medium was recovered by centrifugation at 2,500 rpm for 20 min and filtered through a 0.22 µm membrane. Imidazole was added to the medium to 10 mM, then 2 ml of FastFlow IMAC beads (GE Healthcare) were added. The solution was mixed by rotation for 1 hour at 4°C. The resin was transferred to a column and the washed with 10 column volumes (CV) of binding buffer with 10 mM imidazole. Then washed sequentially with 10 CVs of binding buffer with 25 mM imidazole, 5 CVs of binding buffer with 50 mM imidazole, and 5 CVs of binding buffer with 100 mM imidazole. The protein was then eluted

with 4 x 2Cvs of binding buffer with 250 mM imidazole. The washes and elutions were analyzed by reducing SDS-PAGE. The fractions with the recombinant protein were pooled and dialyzed twice against 2 L of PBS. After dialysis the concentration of the protein was determined by absorbance at 280 nm.

4.4.3 MAT2A Enzymatic assays

Recombinant human MAT2A stored in 50% glycerol was dialysed into MAT2A buffer containing 50mM MOPS at pH 7.4, 50mM potassium acetate, 20mM magnesium acetate. All substrates and compounds used were dissolved in MAT2A buffer. Final reaction volumes were fixed at 150 µL.

Michaelis menten curves

MAT2A was pre-incubated in the presence/absence of RAPTA-T for 30 minutes at 37°C. L-methionine in different concentrations (1000, 500, 250, 125, 62.5, 31.3, 15.6, 7.8 and 0 µM) and subsequently 1mM ATP was added to start the reaction. After 30 minutes, reactions were quenched with 5uL acetic and cooled on an ice pellet. 25uL of sample is used for a phosphate colorimetric assay and Km values are calculated in Graphpad Prism.

IC_{50} value determination

MAT2A was pre-incubated with different concentrations of RAPTA-T (1000, 500, 250, 125, 62.5, 31.3, 15.6, 7.8 and 0 µM) at various time-points at 37°C. 50 µM L-methionine and 1 mM ATP was added to start the reaction. After 30 minutes, reactions were quenched with 5 µL acetic and cooled on an ice pellet. 25 µL of sample is used for a phosphate colorimetric assay and IC_{50} values are calculated in Graphpad Prism.

4.4.4 PLD3 Enzymatic assays

Recombinant human PLD3 stored in 50% glycerol was buffer exchanged were performed with amicon 10 kDa cutoff centrifugal filters according to manufactueres instructions, into PLD3 reaction buffer containing 250 mM TrisHCl, 25 mM $CaCl_2$, pH 8.0. All substrates and compounds used were dissolved in PLD3 buffer except commercially available reagents from the assay.

Determination of recombinant PLD3 activity

A sample of 5 µg in 100 µL of PLD3 and 100 units in 100µL of PLD from *Streptomyces chromofuscus* was used for the Amplex Red Phospholipase D assay according to manufacturer's instructions.

Chapter 5
Development of an automated approach to determine metallodrug-protein binding sites

5.1 Introduction

An important aspect of the clinical development of new metallodrugs is studying the interaction of these compounds with proteins, as these interactions could account for the pharmacokinetic and pharmacodynamics properties of these compounds including their mechanism and side effects. In this respect, the development of high resolution mass spectrometers and fragmentation methods such as collision induced dissociation (CID), higher energy collisional dissociation (HCD) and electron capture dissociation (ETD) has made fragmentation mass spectrometry a valuable tool for studying metallodrug-protein binding. Such methods have in recent years, been applied to the study of metallodrug binding to proteins such as insulin, metallothionein-2, carbonic anhydrase, calmodulins and ubiquitin.[1–6] However, data processing for such applications still remains a significant challenge owing to the complexity of the mass spectra obtained from such experiments, in terms of a) quantity of peaks to assign b) isotopic complexity of the drug-protein adducts associated with metals c) the numerous ligand bound states which could adduct with proteins.

Here we developed the mass spectra analysis of protein modifications (MSAPM) tool, which calculates theoretical MS and MS/MS spectra based on a given protein/peptide sequence, and user defined modifications to this sequence, and automatically matches these to experimental MS spectra. The tool was developed based on chemcalc,[180] a web based architecture developed in the EPFL to create tools to solve chemistry related problems. In chemcalc, a series of web accessible applications known as web services are combined in a modular fashion to create web based tools. Using chemcalc, tools for isotopic distribution simulation, protein mass fragmentation and generation of molecular formulas for a given mass were previously developed, and this architecture was then adapted for creating MSAPM tool. The MSAPM tool was originally developed for the study of binding of a homo-bimetallic ruthenium complex on a polypeptide chain.[79] We subsequently realized the potential of this approach to study other protein-metallodrug related problems, and decided on further developing the MSAPM tool. For this purpose, we studied the binding of metallodrugs based on platinum (cisplatin) and ruthenium (RAPTA-T) with the 8.5 kDa protein ubiquitin. Ubiquitin was considered a suitable test protein as it is a relatively small full protein with no disulfide bridges or complex post translational modifications, thus posing less of a challenge instrumentally for resolving. Moreover, the binding of cisplatin to ubiquitin has been well

described in literature,[77,175,177,181,182] providing us a wealth of data for comparison and validation of the tool.

The initial version of the MSAPM tool allowed matching of MS/MS spectra of modified proteins by specifying separately the protein sequence, protein modification (metallodrug adduct in this case), and the type of expected fragments (a, b, c, x, y, z type fragments) based on the fragmentation type. The tool then generates theoretical spectra based on the specified parameters and automatically matches these to imported experimental spectra producing a list of possible fragments (Figure 5.1 and 5.20). The tool generates theoretical isotopic patterns for each possible protein-adduct fragment with peak areas defined as trapezoids with fixed bottom and top widths. However, an initial problem we encountered was the variation of peak widths across the m/z range in MS spectra. Since for any MS spectra recorded a fixed resolving power, the relationship between mass, peak widths and resolving power is given by;

$$\text{Mass resolving power} = \frac{mass}{peak\ width}$$

thus, the peak widths of individual isotopic peaks increasingly broaden from low to high m/z. This posed a problem because with fixed peak widths, similarity scores were inaccurate for m/z of fragment adducts far from the isotope width specified. We thus implemented the option of specifying a variable peak width based on mathematical functions to resolve this feature. Subsequently, we implemented the option of handling digested fragments from 6 different enzymes (trypsin, chymotrypsin, LysylC, GlucylC, thermolysin and cyanogen bromide) for bottom up experiments.

Recent literature on metallodrug-protein top down experiments do not take into account internal fragmentation. Taking into account the analytical burden of calculating the myriad of possible internal fragments, and the fact that currently no automated means of matching internal fragment spectra of proteins with modifications exists, it was not surprising that this had not been explored. For metallodrug-protein interactions, analysis of internal fragments is important, as they provide important information regarding the binding of metallodrugs to residues far from the termini. Thus, we implemented this function into the MSAPM tool to calculate a-y and b-y type fragments of CID and HCD based MS/MS spectra. Currently implementation of c-y, c-z fragments from ETD fragmentation is also underway. Subsequently, we also implemented neutral loss calculations which was especially important for higher energy MS/MS fragmentation such as HCD. Specifically the tool considers loss of H_2O on Ser, Thr,

Glu, Asp residues, NH_3 on Arg, Lys, Gln, Asn, H_3PO_4 on phosphorylated Ser, Thr, and Tyr residues and $SOCH_4$ for oxidized Met residues.

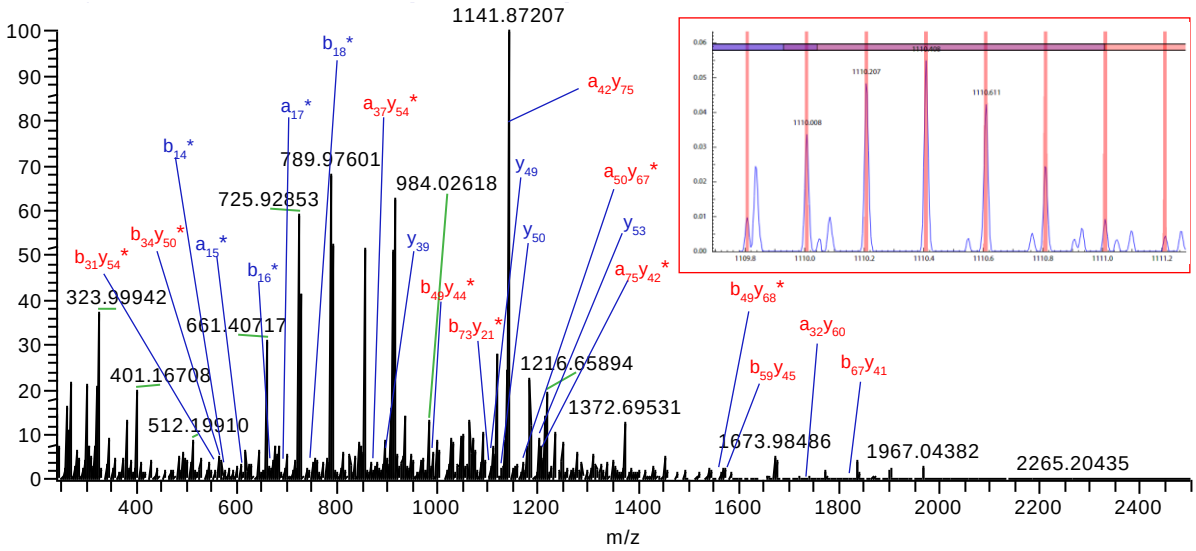

Figure 5.1 Example of matching performed by MSAPM tool. Top down MS/MS spectra from HCD fragmentation of $[RuC_7H_8 + Ub]^{9+}$, where the tool detected various terminal fragments (in blue) and internal fragments (in red) from the experimental spectra. Inset shows second zone matching of experimental peaks (blue) to theoretical peaks (red).

One problem encountered in tandem mass spectrometry experiments is the loss of peak signal-to-noise ratio during subsequent rounds of fragmentation and the generation of very complex spectra with a large number of overlapping peaks. In the initial matching algorithm, the tool considered a user defined zone before and after the monoisotopic mass of the adduct peak of interest for calculation of matching similarities. However, this posed a problem when in spectra where there were many overlapping peaks and signal-to-noise ratio of the peak of interest was low. We thus modified the tool to consider each individual isotope peak within an isotopic pattern as a separate entity, eliminating the influence of surrounding peaks on the matching similarity score (Figure 5.1, inset). With these developments, the tool became a powerful tool that for matching complex MS/MS spectra of proteins and its modifications.

5.2 Results and discussion

5.2.1 Analysis of full scans of metallodrug-ubiquitin incubations

To validate the applicability of the tool to detect different metal-adduct species and to find suitable adducts for fragmentation, we performed full scans of 5:1 (metallodrug: ubiquitin) incubations from 0.5 to 18 hours. In cisplatin samples, as the incubation time was increased, we observed a general shift towards species which were either hydrolysed or had lost chloride ligands and also an increasing number of platinated adducts (up to 5) on the protein over the 18 hour incubation period (Figure 5.2). Surprisingly, we observed a ubiquitin adduct with $Pt(NH_3)_2Cl_2$ corresponding to full cisplatin across all incubation times tested. This is probably due to non-covalent type interactions such as Van der Waals forces, hydrogen and halogen bonding.

Upon an 18 hour incubation, RAPTA-T also showed multiple adduct species with ubiquitin, but a lesser extent of ruthenation of up to 2 adducts (Figure 5.3). Multiple charge states of each adduct species were also detected via the tool. Similar to the case with cisplatin, we saw ubiquitin adduct of full RAPTA-T, which could be explained by similar non-covalent inreactions. Overall, this showed the ability of the tool for assigning different types and amounts metal-protein adduct species with multiple charge states.

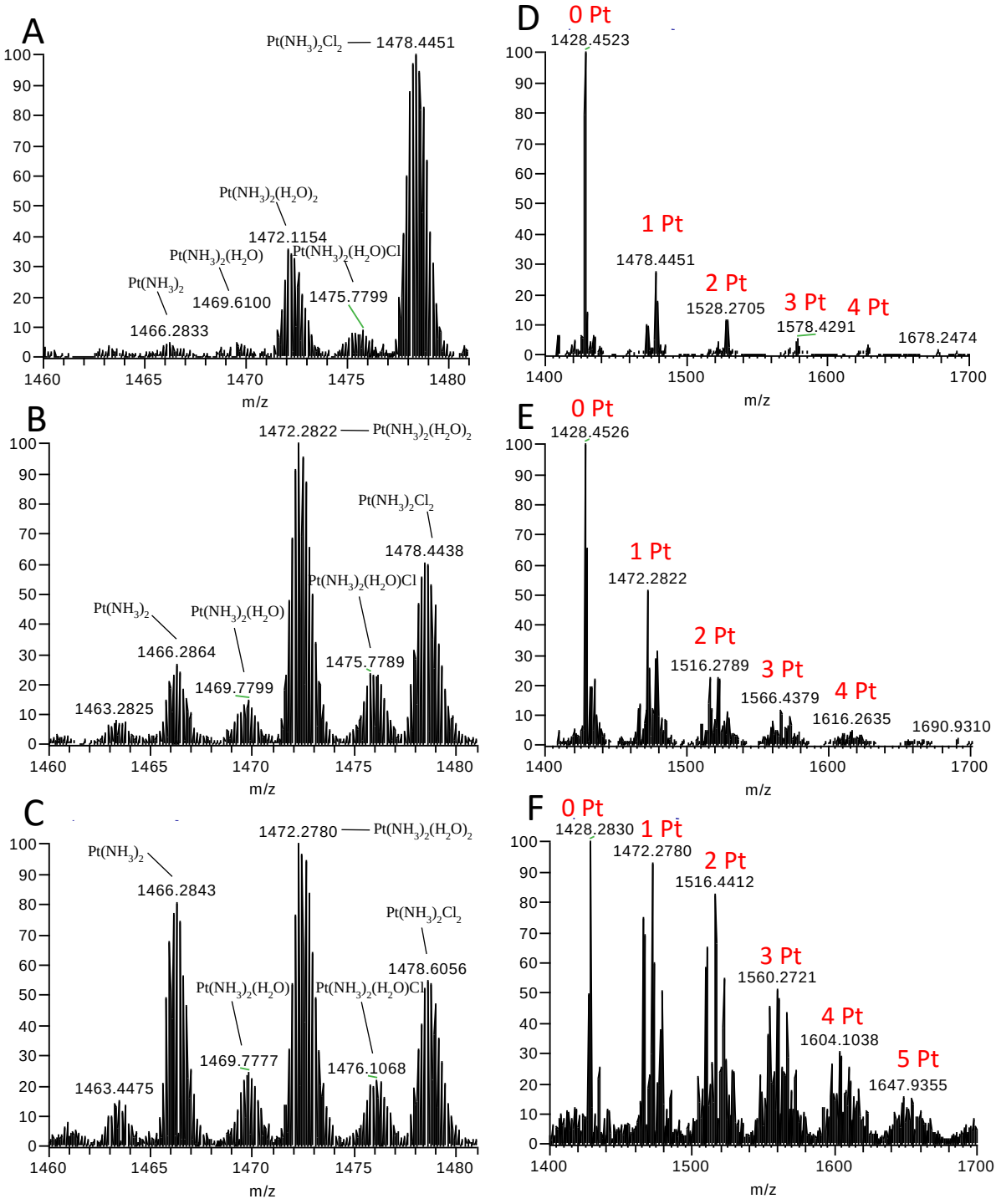

Figure 5.2 Changes of adduct types (A,B and C) and number of platinated adducts (D, E and F) of 1:5 (ubituitin:cisplatin) incubated for 0.5 hours (A & D) , 4 hours (C & E) and 18 hours (C & F) at 37 °C. There is a general shift towards increased adduct species with hydrated or displaced ligands as well as increase in platination of the protein as the incubation time increases.

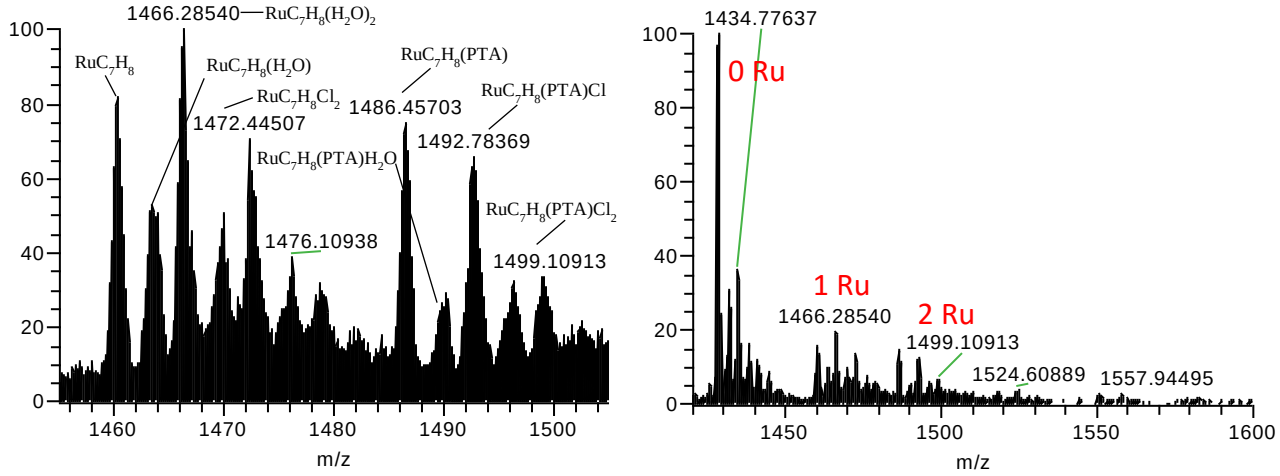

Figure 5.3 Adduct types (left panel) and number of platinated adducts (right panel) of 1:5 (ubituitin:RAPTA-T) incubated for 18 hours at 37 °C. Different adduct species of RAPTA-T were matched by the tool and up to 2 ruthenation sites was observed.

5.2.2 Analysis of top down MS/MS of metallodrug-ubiquitin incubation

To investigate the suitability of the tool for interpretation of high resolution fragmentation mass spectrometry data, we performed CID, HCD and ETD fragmentation experiments on the metal-drug ubiquitin incubated samples, selecting two high charge states (> +8) for each adduct species examined. The tool provided an extensive coverage of both terminal and internal adduct fragments from MS/MS experiments, discriminating well the different adduct types (terminal a, b, c, x, y, z, and internal a-y and b-y ions) with high similarities.

As proof of principle to show the tool could find binding sites of a well-known metallodrug-protein system,[77,175,177,181] we attempted to validate the tool by identify binding sites of cisplatin on ubiquitin. Upon 1:1 incubations of cisplatin:ubiquitin for 18 hours in water, fragmented two metallated cisplatin adducts [7H+ Ubiquitin + PtN_2H_6]$^{9+}$ and [8H+ Ubiquitin + PtN_2H_8O]$^{10+}$ were subjected to HCD, CID and ETD fragmentation. Importantly, none of the prepared solutions were diluted in organic solvents or acid before electrospray ionization, but were directly sprayed in water. When compared against spraying in a 1:1 water:ACN mixture with 0.1% formic acid, directly spraying from water showed much better retention of metallated fragments. For interpretation of Pt binding sites we considered all metallated fragments with similarity scores of over 65% (Figure 5.4).

A MQIFVKTLTGKTITLEVEPSDTIENVKAKIQDKEGIPPDQQRLIFAGKQLEDGRTLSDYNIQKESTLHLVLRLRGG

B

[7H+ Ubiquitin + PtN_2H_6]$^{9+}$

CID

MQIFVKTLTGKTITLEVEPSDTIENVKAKIQDKEGIPPDQQRLIFAGKQLEDGRTLSDYNIQKESTLHLVLRLRGG (a11, 73%)
MQIFVKTLTGKTITLEVEPSDTIENVKAKIQDKEGIPPDQQRLIFAGKQLEDGRTLSDYNIQKESTLHLVLRLRGG (y18, 94%)
MQIFVKTLTGKTITLEVEPSDTIENVKAKIQDKEGIPPDQQRLIFAGKQLEDGRTLSDYNIQKESTLHLVLRLRGG (b74y19, 96%)
MQIFVKTLTGKTITLEVEPSDTIENVKAKIQDKEGIPPDQQRLIFAGKQLEDGRTLSDYNIQKESTLHLVLRLRGG (b62y24, 94%)
MQIFVKTLTGKTITLEVEPSDTIENVKAKIQDKEGIPPDQQRLIFAGKQLEDGRTLSDYNIQKESTLHLVLRLRGG (a36y53, 93%)
MQIFVKTLTGKTITLEVEPSDTIENVKAKIQDKEGIPPDQQRLIFAGKQLEDGRTLSDYNIQKESTLHLVLRLRGG (b16y73, 90%)
MQIFVKTLTGKTITLEVEPSDTIENVKAKIQDKEGIPPDQQRLIFAGKQLEDGRTLSDYNIQKESTLHLVLRLRGG (a28y67, 90%)
MQIFVKTLTGKTITLEVEPSDTIENVKAKIQDKEGIPPDQQRLIFAGKQLEDGRTLSDYNIQKESTLHLVLRLRGG (b57y35 89%)
MQIFVKTLTGKTITLEVEPSDTIENVKAKIQDKEGIPPDQQRLIFAGKQLEDGRTLSDYNIQKESTLHLVLRLRGG (b48y51, 83%)
MQIFVKTLTGKTITLEVEPSDTIENVKAKIQDKEGIPPDQQRLIFAGKQLEDGRTLSDYNIQKESTLHLVLRLRGG (a32y65, 83%)
MQIFVKTLTGKTITLEVEPSDTIENVKAKIQDKEGIPPDQQRLIFAGKQLEDGRTLSDYNIQKESTLHLVLRLRGG (a47y52, 81%)
MQIFVKTLTGKTITLEVEPSDTIENVKAKIQDKEGIPPDQQRLIFAGKQLEDGRTLSDYNIQKESTLHLVLRLRGG (a20y70, 70%)

HCD

MQIFVKTLTGKTITLEVEPSDTIENVKAKIQDKEGIPPDQQRLIFAGKQLEDGRTLSDYNIQKESTLHLVLRLRGG (y13, 66%)
MQIFVKTLTGKTITLEVEPSDTIENVKAKIQDKEGIPPDQQRLIFAGKQLEDGRTLSDYNIQKESTLHLVLRLRGG (b57y35, 88%)
MQIFVKTLTGKTITLEVEPSDTIENVKAKIQDKEGIPPDQQRLIFAGKQLEDGRTLSDYNIQKESTLHLVLRLRGG (b62y24, 90%)
MQIFVKTLTGKTITLEVEPSDTIENVKAKIQDKEGIPPDQQRLIFAGKQLEDGRTLSDYNIQKESTLHLVLRLRGG (a24y75, 84%)
MQIFVKTLTGKTITLEVEPSDTIENVKAKIQDKEGIPPDQQRLIFAGKQLEDGRTLSDYNIQKESTLHLVLRLRGG (b54y31, 84%)
MQIFVKTLTGKTITLEVEPSDTIENVKAKIQDKEGIPPDQQRLIFAGKQLEDGRTLSDYNIQKESTLHLVLRLRGG (b74y19, 84%)
MQIFVKTLTGKTITLEVEPSDTIENVKAKIQDKEGIPPDQQRLIFAGKQLEDGRTLSDYNIQKESTLHLVLRLRGG (b32y58, 84%)
MQIFVKTLTGKTITLEVEPSDTIENVKAKIQDKEGIPPDQQRLIFAGKQLEDGRTLSDYNIQKESTLHLVLRLRGG (a22y72 83%)
MQIFVKTLTGKTITLEVEPSDTIENVKAKIQDKEGIPPDQQRLIFAGKQLEDGRTLSDYNIQKESTLHLVLRLRGG (b62y30, 80%)
MQIFVKTLTGKTITLEVEPSDTIENVKAKIQDKEGIPPDQQRLIFAGKQLEDGRTLSDYNIQKESTLHLVLRLRGG (a35y55, 75%)
MQIFVKTLTGKTITLEVEPSDTIENVKAKIQDKEGIPPDQQRLIFAGKQLEDGRTLSDYNIQKESTLHLVLRLRGG (b31y58, 75%)
MQIFVKTLTGKTITLEVEPSDTIENVKAKIQDKEGIPPDQQRLIFAGKQLEDGRTLSDYNIQKESTLHLVLRLRGG (a30y67, 74%)
MQIFVKTLTGKTITLEVEPSDTIENVKAKIQDKEGIPPDQQRLIFAGKQLEDGRTLSDYNIQKESTLHLVLRLRGG (a74y17, 70%)

ETD

MQIFVKTLTGKTITLEVEPSDTIENVKAKIQDKEGIPPDQQRLIFAGKQLEDGRTLSDYNIQKESTLHLVLRLRGG (c17, 71%)
MQIFVKTLTGKTITLEVEPSDTIENVKAKIQDKEGIPPDQQRLIFAGKQLEDGRTLSDYNIQKESTLHLVLRLRGG (z17, 75%)

[8H+ Ubiquitin + PtN_2H_8O]$^{10+}$

CID

MQIFVKTLTGKTITLEVEPSDTIENVKAKIQDKEGIPPDQQRLIFAGKQLEDGRTLSDYNIQKESTLHLVLRLRGG (b16, 93%)
MQIFVKTLTGKTITLEVEPSDTIENVKAKIQDKEGIPPDQQRLIFAGKQLEDGRTLSDYNIQKESTLHLVLRLRGG (a28y67, 92%)
MQIFVKTLTGKTITLEVEPSDTIENVKAKIQDKEGIPPDQQRLIFAGKQLEDGRTLSDYNIQKESTLHLVLRLRGG (a22y71, 90%)
MQIFVKTLTGKTITLEVEPSDTIENVKAKIQDKEGIPPDQQRLIFAGKQLEDGRTLSDYNIQKESTLHLVLRLRGG (b33y58, 89%)
MQIFVKTLTGKTITLEVEPSDTIENVKAKIQDKEGIPPDQQRLIFAGKQLEDGRTLSDYNIQKESTLHLVLRLRGG (a23, y70 83%)
MQIFVKTLTGKTITLEVEPSDTIENVKAKIQDKEGIPPDQQRLIFAGKQLEDGRTLSDYNIQKESTLHLVLRLRGG (b74y25, 82%)
MQIFVKTLTGKTITLEVEPSDTIENVKAKIQDKEGIPPDQQRLIFAGKQLEDGRTLSDYNIQKESTLHLVLRLRGG (a39y53, 81%)
MQIFVKTLTGKTITLEVEPSDTIENVKAKIQDKEGIPPDQQRLIFAGKQLEDGRTLSDYNIQKESTLHLVLRLRGG (b56y44, 78%)
MQIFVKTLTGKTITLEVEPSDTIENVKAKIQDKEGIPPDQQRLIFAGKQLEDGRTLSDYNIQKESTLHLVLRLRGG (a17y75, 76%)
MQIFVKTLTGKTITLEVEPSDTIENVKAKIQDKEGIPPDQQRLIFAGKQLEDGRTLSDYNIQKESTLHLVLRLRGG (b29y65, 75%)
MQIFVKTLTGKTITLEVEPSDTIENVKAKIQDKEGIPPDQQRLIFAGKQLEDGRTLSDYNIQKESTLHLVLRLRGG (a29y65, 72%)
MQIFVKTLTGKTITLEVEPSDTIENVKAKIQDKEGIPPDQQRLIFAGKQLEDGRTLSDYNIQKESTLHLVLRLRGG (a74y17 69%)
MQIFVKTLTGKTITLEVEPSDTIENVKAKIQDKEGIPPDQQRLIFAGKQLEDGRTLSDYNIQKESTLHLVLRLRGG (a70y23 68%)

HCD

MQIFVKTLTGKTITLEVEPSDTIENVKAKIQDKEGIPPDQQRLIFAGKQLEDGRTLSDYNIQKESTLHLVLRLRGG (b50y52, 85%)
MQIFVKTLTGKTITLEVEPSDTIENVKAKIQDKEGIPPDQQRLIFAGKQLEDGRTLSDYNIQKESTLHLVLRLRGG (b36y64, 79%)
MQIFVKTLTGKTITLEVEPSDTIENVKAKIQDKEGIPPDQQRLIFAGKQLEDGRTLSDYNIQKESTLHLVLRLRGG (b50y50, 72%)
MQIFVKTLTGKTITLEVEPSDTIENVKAKIQDKEGIPPDQQRLIFAGKQLEDGRTLSDYNIQKESTLHLVLRLRGG (b30y69, 71%)
MQIFVKTLTGKTITLEVEPSDTIENVKAKIQDKEGIPPDQQRLIFAGKQLEDGRTLSDYNIQKESTLHLVLRLRGG (a48y51, 67%)
MQIFVKTLTGKTITLEVEPSDTIENVKAKIQDKEGIPPDQQRLIFAGKQLEDGRTLSDYNIQKESTLHLVLRLRGG (b45y52, 66%)

ETD

MQIFVKTLTGKTITLEVEPSDTIENVKAKIQDKEGIPPDQQRLIFAGKQLEDGRTLSDYNIQKESTLHLVLRLRGG (c18, 92%)
MQIFVKTLTGKTITLEVEPSDTIENVKAKIQDKEGIPPDQQRLIFAGKQLEDGRTLSDYNIQKESTLHLVLRLRGG (y17, 88%)

Figure 5.4 Top down MS/MS from CID fragmentation of [7H+ Ubiquitin + PtN_2H_6]$^{9+}$ and [8H+ Ubiquitin + PtN_2H_8O]$^{10+}$ **A**: Full length ubiquitin sequence with most accessible metal binding sites in red and inaccessible binding sites in blue **B**: full length ubiquitin sequence with detected metallated fragments highlighted in red.

In CID and HCD fragmentation considering internal fragments, we obtained a large coverage of metallated fragments covering nearly the whole ubiquitin sequence. From literature reports of cisplatin binding to ubiquitin, cisplatin has been shown to bind to Met1, His68, Thr12, Thr14, and Asp32 residues.[175,181] In general, our data validated these findings. From the N-terminal [a11+Pt] $^{2+}$ fragment of CID fragmentation of [7H+ Ubiquitin + $PtN_2H_6]^{9+}$ we validated the Met1 binding site. From the C-terminal [y17+$PtNH_3]^{+}$ & [y17+$PtN_2H_6]^{2+}$ fragments from ETD fragmentation of adducts [7H+ Ubiquitin + $PtN_2H_6]^{9+}$ & [8H+ Ubiquitin + $PtN_2H_8O]^{10+}$ respectively, His68 was the most likely binding residue. For the reported binding sites of Thr12, Thr14 and Asp32, multiple platinated internal fragments obtained covered sequences containing these residues (Figure 5.4). This highlights an important strength of the MSAPM tool which calculated internal fragmentation, where these internal binding sites were previously identified through a bottom up approach,[175] whereas here we managed to reproduce these for the first time via top down MS.

However, from the extensive coverage of metallated fragments we obtained due to automated tool matching, it became apparent that cisplatin binding to ubiquitin is more complex than that reported so far. From combined information of the crystal structure of ubiquitin, and coordination chemistry of transition metal complexes along with our incubation and spray conditions, we predicted the most likely metal binding sites on ubiquitin. Since incubations and electrospray ionization was done in water (~pH 6), the most likely metal binding sites are acidic Asp and Glu residues, sulphur containing Met and nucleophilic His residues. All basic residue side chains were expected to be charged at this pH and thus unable to coordinate to the metal centre. Further scrutiny of the crystal showed some of these sites were sterically inaccessible leading us to a total of 12 possible metal binding sites in the metal (Figure 5.5.). In general, all internal and terminal fragments obtained contained at least one of these possible metal binding residues. This suggested that cisplatin likely coordinates to all these binding sites probably through multiple coordination modes.

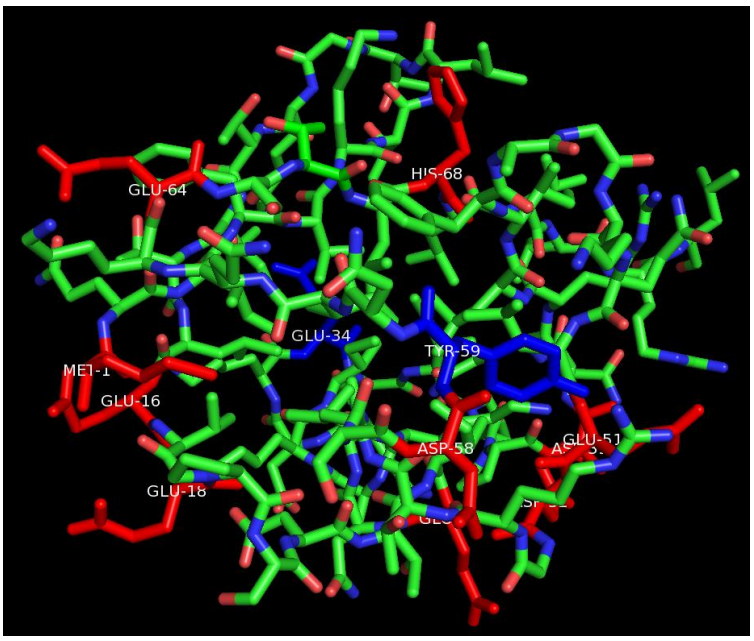

MQIFVKTLTGKTITLEVEPSDTIENVKAKIQDKEGIPPDQQRLIFAGKQLEDGRTLSDYNIQKESTLHLVLRLRGG

Figure 5.5 Most likely binding sites of metals on bovine ubiquitin. Crystal structure of bovine ubiquitin is above its full amino acid sequence bottom. Predicted accessible binding residues are labeled red, and inaccessible binding residues are labelled blue.

We were then interested in knowing whether there was a preference in binding of Pt to specific sites in the ubiquitin sequence. For this, we tried to analyze the abundance of all metallated fragments ions obtained from CID/HCD of cisplatin-ubiquitin metallated adducts. For all fragments obtained with a good similarity, we sub-categorized them into N-terminal fragments from residue 1-39 abbreviated L, C-terminal fragments from residue 1-37 abbreviated R, and all other fragments abbreviated M (Figure 5.6).

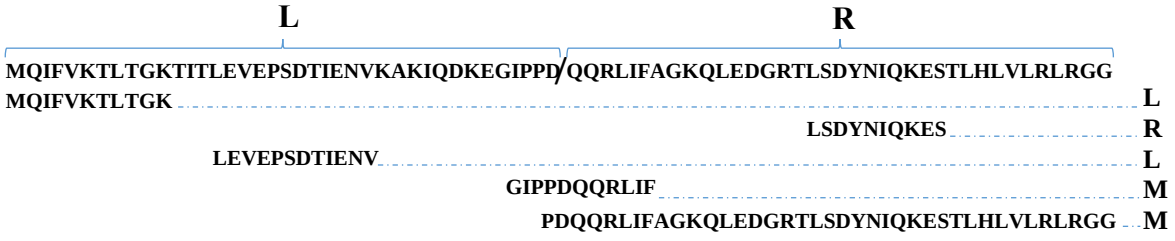

Figure 5.6 Classification of L, R, M fragments. Full sequence of ubiquitin given above with examples of different fragments and their classifications given below. N-terminal fragments from residue 1-39 abbreviated L, C-terminal fragments from residue 1-37 abbreviated R, and all other fragments abbreviated M.

Initially, we analyzed the distribution of M, L and R fragments obtained from MS/MS fragmentation of plain ubiquitin via CID (Figure 5.7) and HCD (Figure 5.8) to observe the distribution of daughter ions produced from the different fragmentation methods and the

reliability of the data for subsequent analysis of metallated adducts. In this case, we required a fragmentation method should produce an equal distribution of R to L fragments which would allow us to see if metalation modified this distribution. Both HCD and CID fragmentation of different charge states of ubiquitin gave very reproducible results. In CID, there was a very even distribution between L and R fragments (Figure 5.7), however for HCD, there was a bias towards L fragments with a L:R ratio of around 6:4 (Figure 5.8). Thus, we selected CID fragmentation for analysis of metallated adducts.

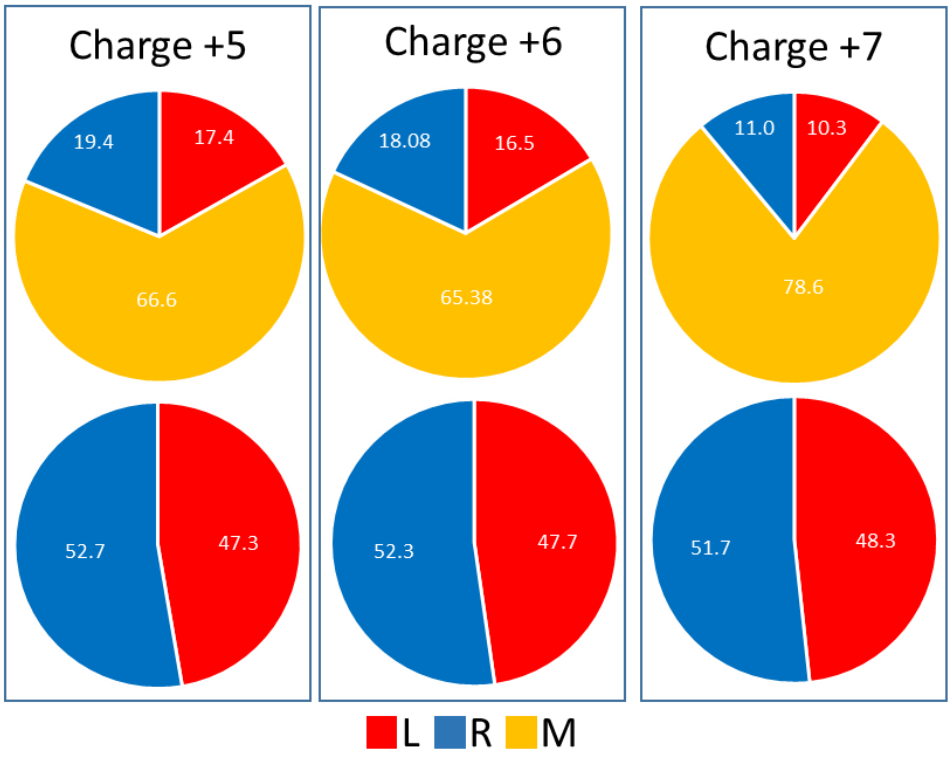

Figure 5.7 Percentage abundance of L, R and M metallated daughter ions from CID fragmentation of ubiquitin. Parents ions [5H+ Ubiquitin]$^{5+}$, [6H+ Ubiquitin]$^{6+}$ and [7H+ Ubiquitin]$^{7+}$ were chosen for fragmentation. Criteria for L, R, M fragments are in Figure 5.6.

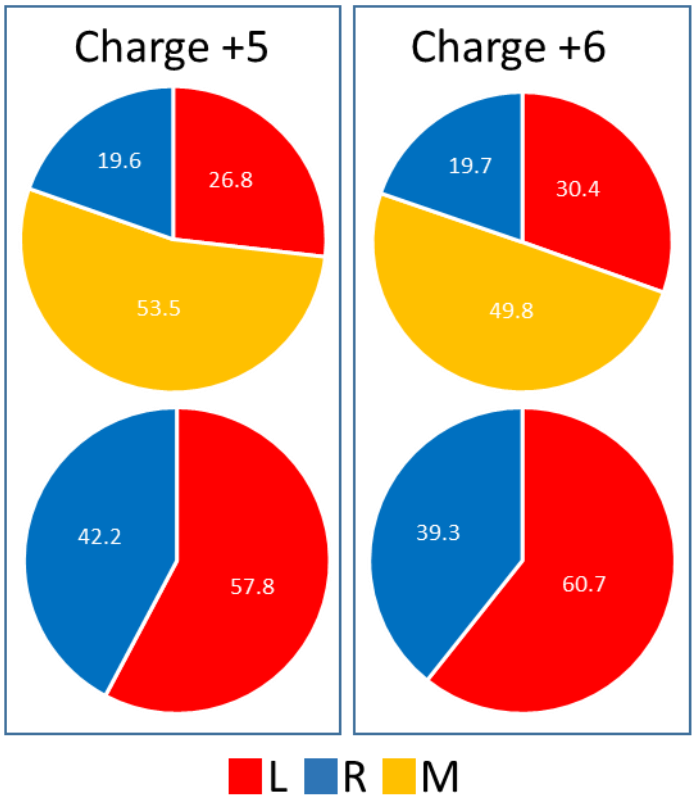

Figure 5.8 Percentage abundance of L, R and M metallated daughter ions from HCD fragmentation of ubiquitin. Parents ions [5H+ Ubiquitin]$^{5+}$ and [6H+ Ubiquitin]$^{6+}$ were chosen for fragmentation. Criteria for L, R, M fragments are in Figure 5.6.

From CID fragmentation of cisplatin-ubiquitin adducts with charge states of +9, +10, and +11, we saw a higher abundance of L type adducts where there was a 2:1 ratio of L:R metallated adducts observed (Figure 5.9). This showed that there was a preference of binding of Pt to residues corresponding to L residues in ubiquitin. Considering this, we compared the polarity of both halves of the protein and found that L sequence had an isoelectric point (PI) of 4.62 and the R sequence had a PI of 9.34. Since cisplatin is aquated with loss of Cl ligands forming a cationic species in water, it was thus likely that the binding preference for L portion of ubiquitin was due to the relative negative polarity of this portion.

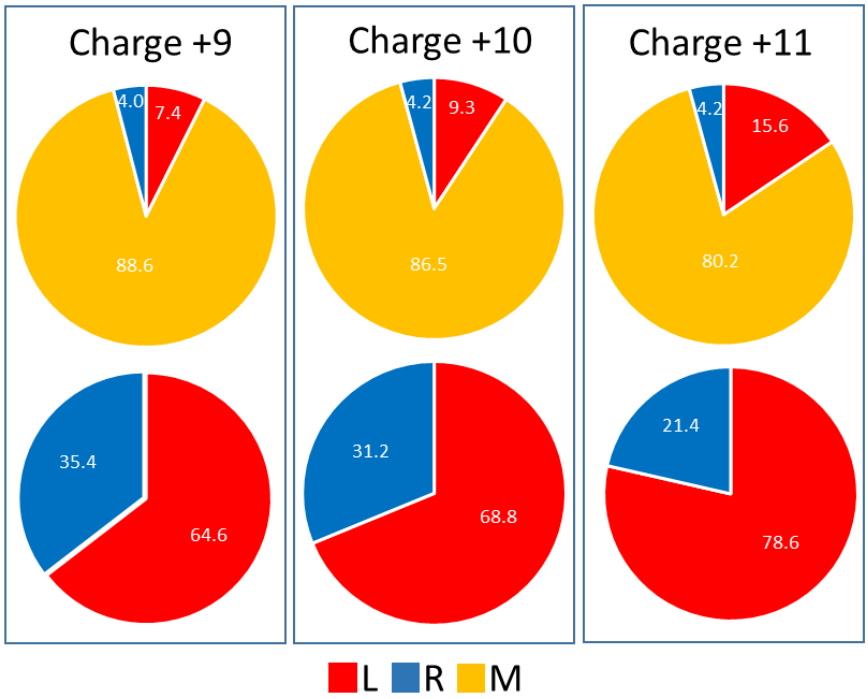

Figure 5.9 Percentage abundance of L, R and M metallated daughter ions from CID fragmentation of ubiquitin incubated with cisplatin. Parents ions $[7H+ \text{Ubiquitin} + PtN_2H_6]^{9+}$, $[8H+ \text{Ubiquitin} + PtN_2H_8O]^{10+}$ and $[9H+ \text{Ubiquitin} + PtN_2H_6]^{11+}$ were chosen for fragmentation. Criteria for L, R and M fragments are in Figure 5.6.

We also observed an increase in the percentage of M fragments from an average of 70% in platin ubiquitin to 85% in platinated ubiquitin (Figures 5.7 & 5.8). When analyzed as a distribution of the number of amino acid residues per fragment, we saw that the number of amino acid residues from platinated M fragments was higher than that of M fragments from ubiquitin (Figure 5.10). This observation could be explained by the binding of Pt stabilizing the protein against fragmentation. Alternatively, the collision energy from CID could be absorbed by the Pt center or spent on fragmentation of cisplatin bound ligands thus reducing its availability for breaking peptide bonds resulting formation of larger fragments.

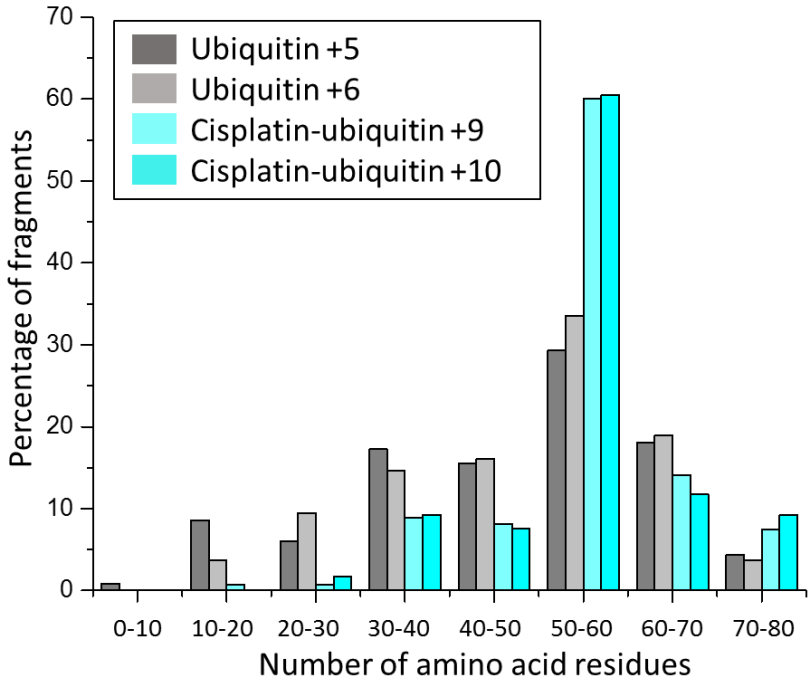

Figure 5.10 Percentage abundance of M metallated daughter ions classified into different amino acid lengths from CID fragmentation of ubiquitin incubated with cisplatin. Parents ions [7H+ Ubiquitin + PtN_2H_6]$^{9+}$, [8H+ Ubiquitin + PtN_2H_8O]$^{10+}$ and [9H+ Ubiquitin + PtN_2H_6]$^{11+}$ were chosen for fragmentation. Criteria for L, R, M fragments are in Figure 5.6.

Next, we proceeded to study the binding of RAPTA-T to ubiquitin. For incubations of 1:5 (protein:drug) ratio of ubiquitin with RAPTA-T, the metallated adducts [8H+ Ubiquitin + RuC_7H_8]^{10} and [9H+ Ubiquitin + RuC_7H_8]$^{11+}$ were subjected to MS/MS fragmentation via CID, HCD, ETD (Figure 5.11). We observed very similar metallated fragments covering nearly the full protein sequence showing the complexity of Ru binding to ubiquitin where the metal can potentially bind to multiple binding sites (up to 11 residues) on ubiquitin. The only possible binding residue where we did not see a metallated fragment was Glu16. We observed a similar trend with cisplatin, where ruthenated ubiquitin fragments obtained upon CID fragmentation consisted of mostly L type fragments with a L:R ratio of approximately 2:1 (Figure 5.12). This could be explained by a similar activation mechanism of RAPTA-T forming a cationic species thus preferring the more negatively charged L region in ubiquitin. There was a decrease in the number of M fragments from CID found in ruthenated ubiquitin, from an average of 70% in plain ubiquitin (Figure 5.7) to 50% in ruthenated ubiquitin (Figure 5.12). However, the distribution of the number of amino acid residues per fragment still showed a shift towards larger M fragments from CID on ruthenated ubiquitin (Figure 5.13).

[8H+ Ubiquitin + RuC_7H_8]$^{10+}$

CID

MQIFVKTLTGKTITLEVEPSDTIENVKAKIQDKEGIPPDQQRLIFAGKQLEDGRTLSDYNIQKESTLHLVLRLRGG (b11, 66%)
MQIFVKTLTGKTITLEVEPSDTIENVKAKIQDKEGIPPDQQRLIFAGKQLEDGRTLSDYNIQKESTLHLVLRLRGG (b73y21, 88%)
MQIFVKTLTGKTITLEVEPSDTIENVKAKIQDKEGIPPDQQRLIFAGKQLEDGRTLSDYNIQKESTLHLVLRLRGG (b18y75, 86%)
MQIFVKTLTGKTITLEVEPSDTIENVKAKIQDKEGIPPDQQRLIFAGKQLEDGRTLSDYNIQKESTLHLVLRLRGG (a57y37, 77%)
MQIFVKTLTGKTITLEVEPSDTIENVKAKIQDKEGIPPDQQRLIFAGKQLEDGRTLSDYNIQKESTLHLVLRLRGG (b57y35, 72%)

HCD

MQIFVKTLTGKTITLEVEPSDTIENVKAKIQDKEGIPPDQQRLIFAGKQLEDGRTLSDYNIQKESTLHLVLRLRGG (b11, 66%)
MQIFVKTLTGKTITLEVEPSDTIENVKAKIQDKEGIPPDQQRLIFAGKQLEDGRTLSDYNIQKESTLHLVLRLRGG (a37y54, 90%)
MQIFVKTLTGKTITLEVEPSDTIENVKAKIQDKEGIPPDQQRLIFAGKQLEDGRTLSDYNIQKESTLHLVLRLRGG (b73y21, 88%)
MQIFVKTLTGKTITLEVEPSDTIENVKAKIQDKEGIPPDQQRLIFAGKQLEDGRTLSDYNIQKESTLHLVLRLRGG (a44y49, 87%)
MQIFVKTLTGKTITLEVEPSDTIENVKAKIQDKEGIPPDQQRLIFAGKQLEDGRTLSDYNIQKESTLHLVLRLRGG (a37y49, 85%)
MQIFVKTLTGKTITLEVEPSDTIENVKAKIQDKEGIPPDQQRLIFAGKQLEDGRTLSDYNIQKESTLHLVLRLRGG (b34y50, 77%)
MQIFVKTLTGKTITLEVEPSDTIENVKAKIQDKEGIPPDQQRLIFAGKQLEDGRTLSDYNIQKESTLHLVLRLRGG (b48y42, 76%)
MQIFVKTLTGKTITLEVEPSDTIENVKAKIQDKEGIPPDQQRLIFAGKQLEDGRTLSDYNIQKESTLHLVLRLRGG (b37y53, 74%)
MQIFVKTLTGKTITLEVEPSDTIENVKAKIQDKEGIPPDQQRLIFAGKQLEDGRTLSDYNIQKESTLHLVLRLRGG (b31y54, 70%)
MQIFVKTLTGKTITLEVEPSDTIENVKAKIQDKEGIPPDQQRLIFAGKQLEDGRTLSDYNIQKESTLHLVLRLRGG (b57y35, 66%)
MQIFVKTLTGKTITLEVEPSDTIENVKAKIQDKEGIPPDQQRLIFAGKQLEDGRTLSDYNIQKESTLHLVLRLRGG (a42y50, 66%)

ETD

MQIFVKTLTGKTITLEVEPSDTIENVKAKIQDKEGIPPDQQRLIFAGKQLEDGRTLSDYNIQKESTLHLVLRLRGG (c10, 66%)
MQIFVKTLTGKTITLEVEPSDTIENVKAKIQDKEGIPPDQQRLIFAGKQLEDGRTLSDYNIQKESTLHLVLRLRGG (z17, 87%)

[9H+ Ubiquitin + RuC_7H_8]$^{11+}$

CID

MQIFVKTLTGKTITLEVEPSDTIENVKAKIQDKEGIPPDQQRLIFAGKQLEDGRTLSDYNIQKESTLHLVLRLRGG (b11, 70%)
MQIFVKTLTGKTITLEVEPSDTIENVKAKIQDKEGIPPDQQRLIFAGKQLEDGRTLSDYNIQKESTLHLVLRLRGG (a73y19, 88%)
MQIFVKTLTGKTITLEVEPSDTIENVKAKIQDKEGIPPDQQRLIFAGKQLEDGRTLSDYNIQKESTLHLVLRLRGG (a44y49, 87%)
MQIFVKTLTGKTITLEVEPSDTIENVKAKIQDKEGIPPDQQRLIFAGKQLEDGRTLSDYNIQKESTLHLVLRLRGG (a36y58, 75%)
MQIFVKTLTGKTITLEVEPSDTIENVKAKIQDKEGIPPDQQRLIFAGKQLEDGRTLSDYNIQKESTLHLVLRLRGG (b57y35, 67%)
MQIFVKTLTGKTITLEVEPSDTIENVKAKIQDKEGIPPDQQRLIFAGKQLEDGRTLSDYNIQKESTLHLVLRLRGG (b42y51, 67%)

HCD

MQIFVKTLTGKTITLEVEPSDTIENVKAKIQDKEGIPPDQQRLIFAGKQLEDGRTLSDYNIQKESTLHLVLRLRGG (b11, 65%)
MQIFVKTLTGKTITLEVEPSDTIENVKAKIQDKEGIPPDQQRLIFAGKQLEDGRTLSDYNIQKESTLHLVLRLRGG (a73y19, 89%)
MQIFVKTLTGKTITLEVEPSDTIENVKAKIQDKEGIPPDQQRLIFAGKQLEDGRTLSDYNIQKESTLHLVLRLRGG (a37y54, 86%)
MQIFVKTLTGKTITLEVEPSDTIENVKAKIQDKEGIPPDQQRLIFAGKQLEDGRTLSDYNIQKESTLHLVLRLRGG (a44y49, 80%)
MQIFVKTLTGKTITLEVEPSDTIENVKAKIQDKEGIPPDQQRLIFAGKQLEDGRTLSDYNIQKESTLHLVLRLRGG (a48y39, 66%)
MQIFVKTLTGKTITLEVEPSDTIENVKAKIQDKEGIPPDQQRLIFAGKQLEDGRTLSDYNIQKESTLHLVLRLRGG (a49y44, 65%)

ETD

MQIFVKTLTGKTITLEVEPSDTIENVKAKIQDKEGIPPDQQRLIFAGKQLEDGRTLSDYNIQKESTLHLVLRLRGG (c10, 72%)
MQIFVKTLTGKTITLEVEPSDTIENVKAKIQDKEGIPPDQQRLIFAGKQLEDGRTLSDYNIQKESTLHLVLRLRGG (y10, 61%)

Figure 5.11 Top down MS/MS results from CID, HCD and ETD fragmentation of [8H+ Ubiquitin + RuC_7H_8]$^{10+}$ and [9H+ Ubiquitin + RuC_7H_8]$^{11+}$. In each row, the full ubiquitin sequence is shown and metallated fragments found are highlighted in red.

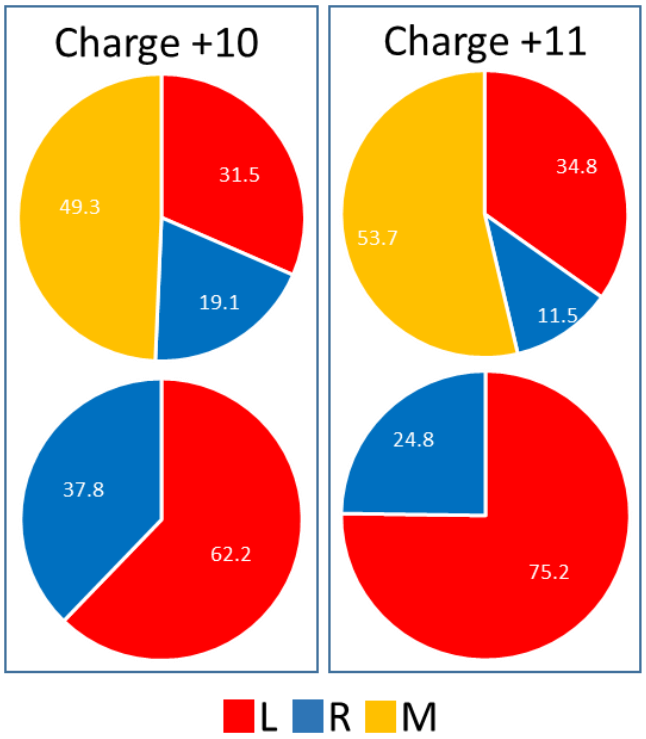

Figure 5.12 Percentage abundance of L, R and M metallated daughter ions from CID fragmentation of ubiquitin incubated with RAPTA-T. Parents ions [8H+ Ubiquitin + $RuC_7H_8]^{10+}$ and [9H+ Ubiquitin + $RuC_7H_8]^{11+}$ were chosen for fragmentation. Criteria for L, R, M fragments are in Figure 5.6.

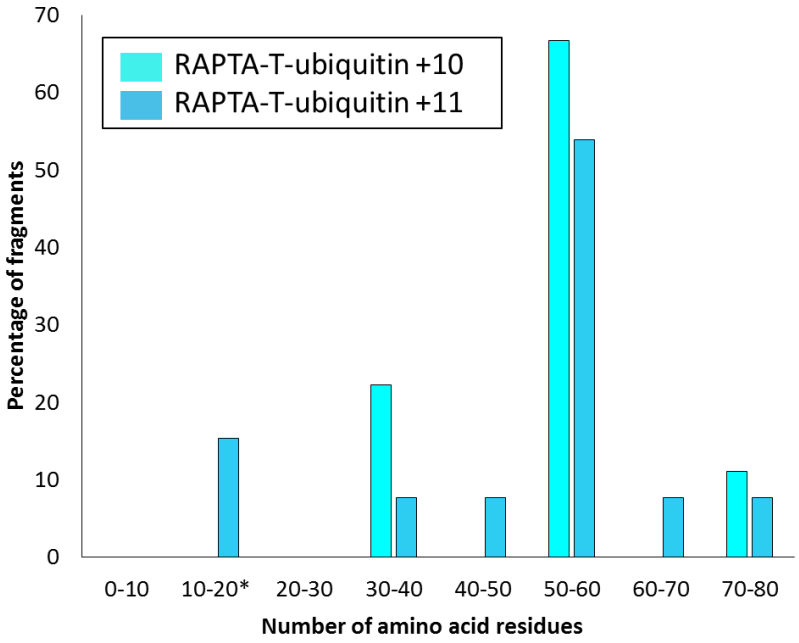

Figure 5.13 Percentage abundance of M metallated daughter ions classified into different amino acid lengths from CID fragmentation of ubiquitin incubated with RAPTA-T. Parents ions [8H+ Ubiquitin + $RuC_7H_8]^{10+}$ and [9H+ Ubiquitin + $RuC_7H_8]^{11+}$ were chosen for fragmentation. Criteria for L, R, M fragments are in Figure 5.6.

5.2.3 Analysis of bottom up MS/MS of metallodrug-ubiquitin incubations

To validate the bottom up analysis option in the MSAPM tool we digested both cisplatin and RAPTA-T incubated ubiquitin samples with LysylC and GluC which cleaves peptide bonds at the C-terminal to Lys and Glu residues respectively. In full scans of ubiquitin digested with LysylC and GluC, we obtained digested fragments covering the full protein sequence of the protein with no miscleavage sites (data not shown). For analysis of metal-protein digests, the tool enabled matching of multiple metal-protein adduct species with high similarities enabling us to easily map metallated digested fragments along the protein sequence. The tool also simplified selection of parent ions for MS/MS fragmentation and subsequent interpretation of these results for narrowing down metal binding residues. In cisplatin-ubiquitin incubations digested with LysylC, we detected a large number of metallated digest fragments spanning the full protein sequence (Figure 5.14). Similarly LysylC digested samples of ubiquitin incubated with RAPTA-T revealed metallated digested fragments covering the full protein sequence (Figure 5.15) but for GluC digests metallated fragments covered 85% of the protein sequence (Figure 5.16). These results validated the proteolytic enzyme function implemented in the tool and also confirmed our top down findings of multiple possible metal binding sites on ubiquitin.

A ^{1}MQIFVKTLTGKTITLEVEPSDTIENVKAKIQDKEGIPPDQQRLIFAGKQLEDGRTLSDYNIQKESTLHLVLRLRGG^{76}

B

^{1}MQIFV^{6}

^{7}KTLTGKTITLEVEPSDTIENVKAK^{29}

^{7}KTLTGKTITLEVEPSDTIENVKAKIQDK^{33}

^{12}TITLEVEPSDTIENVK^{27}

^{12}TITLEVEPSDTIENVKAK^{29}

^{28}AKIQDK^{33}

^{30}IQDK^{33}

^{30}IQDKEGIPPDQQRLIFAGK^{48}

^{30}IQDKEGIPPDQQRLIFAGKQLEDGRTLSDYNIQKESTLHLVLRLRGG^{76}

^{34}EGIPPDQQRLIFAGK^{48}

^{34}EGIPPDQQRLIFAGKQLEDGRTLSDYNIQK^{63}

^{49}KQLEDGRTLSDYNIQK^{63}

C

Metal adduct	Type	Theoretical mass	Experimental mass	Similarity (%)	Charge (+)
PtNH3	D1>6	976.4168	488.2079	86.46	2
Pt	D1>6	959.3903	479.6946	80.94	2
Pt	D7>29	2681.313	1340.656	77.73	2
Pt	D7>33	3165.577	1582.788	72.62	2
PtN2H6	D12>27	2015.938	1007.968	90.23	2
PtN2H6	D12>27	2016.946	672.3147	76.52	3
PtN2H6	D12>29	2216.078	738.6921	81.56	3
PtN2H6	D12>29	2215.07	1107.534	80.46	2
PtN2H6	D28>33	930.4251	465.212	82.82	2
PtN2H6	D30>33	731.293	365.646	88.59	2
PtNH3	D30>33	714.2665	357.1327	83.9	2
PtN2H6	D30>48	2382.19	794.0627	94.48	3
PtN2H6	D30>48	2381.182	1190.59	76.87	2
PtN2H6	D30>48	2383.198	595.7988	71.48	4
PtNH3	D30>76	5557.864	1852.621	72.15	3
PtN2H6	D34>48	1897.925	632.6412	91.44	3
PtN2H6	D34>48	1897.917	948.4581	90.55	2
PtN2H6	D34>63	3658.795	1219.598	76.23	3
PtN2H6	D34>63	3693.763	1846.881	71.64	2
PtN2H6	D49>63	2008.906	669.6347	94.65	3
PtN2H6	D49>63	2007.898	1003.948	92.55	2
PtNH3	D49>63	1991.879	663.9591	77.48	3
PtNH3	D49>63	1990.871	995.4351	76.55	2

Figure 5.14 MS full scans of bottom up digestion of Cisplatin:Ubiquitin incubations with LysylC. **A**: Full length ubiquitin sequence with predicted binding sites in red and inaccessible binding sites in blue. **B**: List of metallated digested fragments detected by the tool (similarly labelled as **A**) **C**: List of metallated digested adducts (different digest fragments highlighted in different colors).

A ^{1}MQIFVKTLTGKTITLEVEPSDTIENVKAKIQDKEGIPPDQQRLIFAGKQLEDGRTLSDYNIQKESTLHLVLRLRGG^{76}

B

^{1}MQIFV^{6}

^{7}KTLTGKTITLEVEPSDTIENVK^{27}

^{28}AKIQDKEGIPPDQQRLIFAGKQLEDGRTLSDYNIQK^{63}

^{30}IQDKEGIPPDQQRLIFAGK^{48}

^{34}EGIPPDQQRLIFAGK^{48}

^{49}QLEDGRTLSDYNIQKESTLHLVLRLRGG^{76}

^{64}ESTLHLVLRLRGG^{76}

C

Metal adduct	Type	Theoretical mass	Experimental mass	Similarity (%)	Charge (+)
C7H8Ru	D1>6	958.3924	479.1957	97.03	2
C13H2ON3PRu	D1>6	959.4003	319.7995	97.01	3
C7H8Ru	D1>6	866.3298	433.1644	96.42	2
Ru	D1>6	1023.407	511.7028	87.83	2
C13H2ON3PRu	D1>6	1116.477	372.1585	83	3
C7H8Ru	D1>6	1024.415	341.471	79.25	3
Ru	D7>27	2547.205	849.0678	69.38	3
C6H12N3PRu	D28>63	4307.14	1435.713	81.42	3
C13H2ON3PRu	D28>63	4308.148	1077.036	79.64	4
C13H2ON3PRu	D28>63	4309.156	861.8306	74.21	5
C13H2ON3PRu	D28>63	4344.125	1086.031	71.26	4
C7H8Ru	D30>48	2505.224	626.3053	76.62	4
C7H8Ru	D34>48	2019.951	673.3165	97.03	3
C6H12N3PRu	D34>48	2018.943	1009.471	83.61	2
C13H2OClN3PRu	D49>76	3598.739	1199.579	75.56	3
C13H2ON3PRu	D49>76	3562.763	1187.587	60.1	3
C13H2ON3PRu	D64>76	1644.816	548.2716	90.64	3
C13H2OClN3PRu	D64>76	1801.893	600.6305	85.74	3
C7H8Ru	D64>76	1838.878	459.7189	78.09	4
C13H2ON3PRu	D64>76	1802.901	450.7247	71.37	4
C13H2ON3PRu	D64>76	1837.87	612.6228	68.71	3
C7H8ClRu	D64>76	1552.754	517.584	64.6	3

Figure 5.15 MS full scans of bottom up digestion of RAPTA-T: Ubiquitin incubations with LysylC. **A**: Full length ubiquitin sequence with predicted binding sites in red and inaccessible binding sites in blue. **B**: List of metallated digested fragments detected by the tool (similarly labelled as **A**) **C**: List of metallated digested adducts (different digest fragments highlighted in different colors).

A ^{1}MQIFVKTLTGKTITLEVEPSDTIENVKAKIQDKEGIPPDQQRLIFAGKQLEDGRTLSDYNIQKESTLHLVLRLRGG^{76}

B ^{1}MQIFVKTLTGKTITLE^{16}

^{22}TIENVKAKIQD^{32}

^{40}QQRLIFAGKQLED^{52}

^{52}DGRTLSDYNIQKESTLHLVLRLRGG^{76}

^{65}STLHLVLRLRGG^{76}

C

Metal adduct	Type	Theoretical mass	Experimental mass	Similarity (%)	Charge (+)
C7H8Ru	D1>16	2017.002	672.3335	98.68	3
C7H8Ru	D1>16	2015.994	1007.997	98.57	2
C13H20ClN3PRu	D1>16	2082.016	694.0049	93.35	3
C13H20ClN3PRu	D1>16	2018.01	504.502	90.37	4
C6H12N3PRu	D1>16	1923.932	961.9653	78.15	2
C13H20N3PRu	D1>16	2100.027	700.0085	69.95	3
C7H8Ru	D22>32	1643.706	1643.705	69.44	1
Ru	D40>52	1773.767	1773.766	67.54	1
Ru	D52>76	3194.593	638.9181	70.81	5
Ru	D65>76	1707.82	853.9092	95.01	2
C6H12N3PRu	D65>76	1708.827	569.6086	94.91	3
C13H20N3PRu	D65>76	1672.851	557.6163	92.24	3

Figure 5.16 MS full scans of bottom up digestion of RAPTA-T: Ubiquitin incubations with GluC. **A**: Full length ubiquitin sequence with predicted binding sites in red and inaccessible binding sites in blue. **B**: List of metallated digested fragments detected by the tool (similarly labelled as **A**) **C**: List of metallated digested adducts (different digest fragments highlighted in different colors).

We then proceeded to perform MS/MS experiments on selected digested metal fragments to show the applicability of the tool to facilitate narrowing down of metal binding sites on digested proteins. For cisplatin-ubiquitin incubated samples digested with LysylC, we selected the parent ions $[PtNH_3$ + Met1-Lys6$]^{2+}$, $[PtN_2H_6$ + Thr-Lys27$]^{2+}$, $[PtN_2H_6$ + Ile30-Lys48$]^{3+}$, and $[PtN_2H_6$ + Glu49-Lys63$]^{3+}$ for MS/MS fragmentation via CID, HCD or ETD (Figure 5.17). We analyzed the smallest terminal N and C metallated adducts and internal fragments to narrow down metal binding sites. CID fragmentation of $[PtNH_3$ + Met1-Lys6$]^{2+}$ revealed a single metallated a_5 fragment. Since this ion did not contain any other potential metal binding sites, we assigned the metal binding site to the terminal Met residue. For the ion $[PtN_2H_6$ + Thr12-Lys27$]^{2+}$ CID fragmentation revealed a single y_{15} fragment, which did not allow precise assignment of a specific residue considering this ion contained 4 possible metal binding residues. Fragmentation of $[PtN_2H_6$ + Ile30-Lys48$]^{3+}$ via HCD revealed a y_{15} terminal and $b_{13}y_{18}$ internal metallated fragment. CID fragmentation of the same ion revealed an N-terminal a10, C-terminal y11 and internal a18y18 metallated fragment. Combined results allowed us to unequivocally assign the cisplatin binding site on this ion to Asp39. The $[PtN_2H_6$ + Glu49-Lys63$]^{3+}$ ion was fragmented by CID, HCD, and ETD fragmentation. We found a b11y10 metallated internal fragment from CID, a13 N-terminal and b11y12 internal metallated fragments from HCD together with a c10 N-terminal and z9 C-terminal metallated fragments from ETD. Combined results allowed us to assign the binding site on this ion to Asp58.

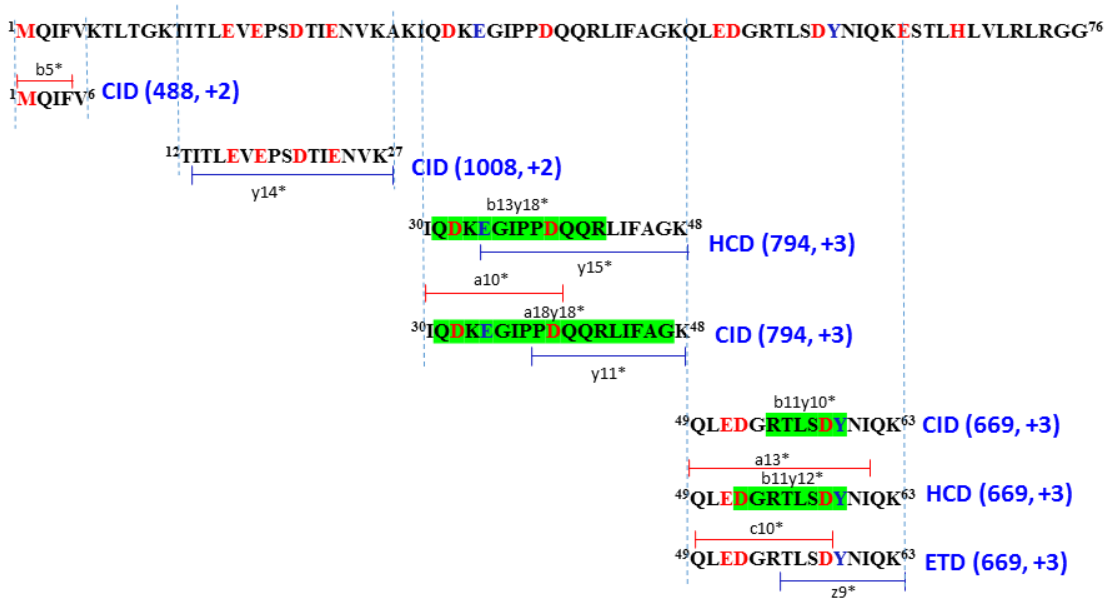

Figure 5.17 MS/MS of metallated fragments of Cisplatin: Ubiquitin incubations digested with LysylC. Full length ubiquitin sequence with probable binding sites in red and inaccessible binding sites in blue is shown above. Each metallated digest parent ion chosen for MS/MS is displayed with fragmentation type, mass and charge state. Relevant metallated MS/MS daughter ions obtained are displayed as N-terminal ions top, C-terminal ions bottom and internal ions highlighted green on the parent ion sequence.

For RAPTA-T:Ubiquitin incubations digested with LysylC, we fragmented the ions $[C_{13}H_{20}N_3PRu + Met1\text{-}Lys6]^{2+}$, $[C_{13}H_{20}N_3PRu + Ala28\text{-}Lys63]^{4+}$, $[C_7H_8Ru + Glu34\text{-}Lys48]^{3+}$, $[C_{13}H_{20}N_3PRu + Gln49\text{-}Gly76]^{3+}$ (Figure 5.18). With CID fragmentation of $[C_{13}H_{20}N_3PRu + Met1\text{-}Lys6]^{2+}$ we found a single metallated a5 fragment allowing us to assign Met1 as a binding site of RAPTA-T. CID & HCD fragmentation of $[C_{13}H_{20}N_3PRu + Ala28\text{-}Lys63]^{4+}$ revealed two metallated internal fragments $b_{16}y_{35}$ and $b_{35}y_{19}$ showing there were at least two metal binding sites in this 35 amino acid peptide digest. This combined with HCD fragmentation of $[C_7H_8Ru + Glu34\text{-}Lys48]^{3+}$ which had a11 N-terminal, y11 c-terminal and a b11y9 internal metallated fragment allowed us to assign Asp39 as a RAPTA-T binding site. Though CID fragmentation of the $[C_{13}H_{20}N_3PRu + Gln49\text{-}Gly76]^{3+}$ we obtained a26, y23 and b24y16 metallated fragments. HCD fragmentation of the same ion revealed an additional b23y17 internal metallated fragment allowing us to narrow down binding of RAPTA-T to either Glu64 or His68.

Figure 5.18 MS/MS of metallated fragments of RAPTA-T: Ubiquitin incubations digested with LysylC. Full length ubiquitin sequence with probable binding sites in red and inaccessible binding sites in blue is shown above. Each metallated digest parent ion chosen for MS/MS is displayed with fragmentation type, mass and charge state. Relevant metallated MS/MS daughter ions obtained are displayed as N-terminal ions top, C-terminal ions bottom and internal ions highlighted green on the parent ion sequence.

For GluC digests, we chose two terminal metallated digested ions $[C_{13}H_{20}ClN_3PRu$ + Met1-Glu16$]^{3+}$ and $[C_{13}H_{20}N_3PRu$ + Ser65-Gly76$]^{3+}$ (Figure 5.19). CID and HCD fragmentation of revealed terminal a7 and y8 metallated fragments confirming Met1 as a binding site and allowing us to assign Glu16 as an additional binding residue of RAPTA-T. Though fragmenting the $[C_{13}H_{20}N_3PRu$ + Ser65-Gly76$]^{3+}$ ion via HCD and CID we observed a10, y9 and y10 metallated fragments allowing us to assign His68 as a RAPTA-T binding site.

Figure 5.19 MS/MS of metallated fragments of RAPTA-T: Ubiquitin incubations digested with GluC. Full length ubiquitin sequence with probable binding sites in red and inaccessible binding sites in blue is shown above. Each metallated digest parent ion chosen for MS/MS is displayed with fragmentation type, mass and charge state. Relevant metallated MS/MS daughter ions obtained are displayed as N-terminal ions top, C-terminal ions bottom and internal ions highlighted green on the parent ion sequence.

5.3 Conclusions

Here we developed and optimized a web-based tool for automated analysis of complex mass spectra of proteins with modifications. The tool enables a comprehensive match of all possible combinations of user defined protein modifications and is especially useful for top down and bottom up MS experiments on metal-protein adducts. Using ubiquitin as a model protein, we studied its interaction with the metallodrugs cisplatin and RAPTA-T. Our results revealed the complexity of the interactions of these metallodrugs with ubiquitin, where the metal can potentially bind more than 10 different sites on ubiquitin. Through analysis of abundance of different metallated fragments obtained, we show a preference of metal binding at more negatively charged regions on the proteins, and reason that this is due to the cationic nature of the metallodrug upon activation. Taken together our results suggest that design of metallodrugs that target a specific protein site can be a challenging due to the promiscuity of metal binding to proteins. Careful tuning of ligands in terms of sterics and kinetics would be essential to achieve such selectivity.

5.4 Experimental

Tool development was performed by Dr. Luc Patiny. MS data acquisition was performed with aid from Dr's. Laure Menin and Daniel Ortiz from the EPFL mass spectrometry centre.

5.4.1 Materials

Ubiquitin from bovine erythrocytes was purchased from Sigma Aldrich, cisplatin was purchased from Tokyo Chemical Industries, RAPTA-T was synthesized according literature methods.[116] . MS grade LysylC and GluC endoproteinase was purchased from Thermo Fisher Scientific, USA.

5.4.2 Sample preparation

100 µM ubiquitin was incubated with metal complexes (RAPTA-T or cisplatin) at a 1:1 and 1:5 protein: drug ratio at 37° C for 0.5 to 18 hours. All incubations were performed in sterile MiliQ water. Excess drug was removed with three rounds of centrifugation using 3kDa-cutoff Amicon Ultra centrifugal filters according to manufacturers instructions. Incubated proteins were snap frozen in liquid N_2 and stored at -20 ° C prior to top down analysis. For bottom up sample preparation, metallodrug-protin inccubations were digested with MS grade LysylC or GluC according to manufacturer's instructions.

5.4.3 Mass spectrometry analysis

CID, HCD and ETD fragmentation studies were performed on an ETDenabled hybrid linear ion trap (LTQ) Orbitrap Elite mass spectrometer (Thermo Scientific, Bremen, Germany) coupled to a Triversa Nanomate (Advion) chip-based electrospray system. The samples were diluted at a final concentration of 10 µM in a solution of $CH_3CN/H_2O/HCOOH$ (50:49.9:0.1) or directly infused in water using a spray voltage of 1.6 kV. The automatic gain control (AGC) target was set to 1×10^6 for full scans in the Orbitrap mass analyzer. ETD experiments used fluoranthene as the reagent anion and the target for fluoranthene anions was set to 5×10^5. Precursor ions for MS/MS were detected in the Orbitrap mass analyzer at a resolving power of 30,000 (at 400 m/z) with an isolation width of 8, and product ions were transferred to the FTMS operated with an AGC of 5×10^4 over a m/z range of 200-3000. The reaction time with the fluoranthene radical anions into the LTQ was set from 50 to 100 ms. For CID and HCD fragmentation normalized collision energies of 20-35% were used. A total of 100 scans were averaged for each fragmentation spectra. The Orbitrap FTMS was calibrated for the high mass range, keeping a mass accuracy in the 1-3 ppm level.

5.4.4 Tool development and layout

The MSAPM tool was developed based on http://www.chemcalc.org.[180] General layout of the tool is described in Figure 5.15, and the parameter input window is described in Figure 5.21.

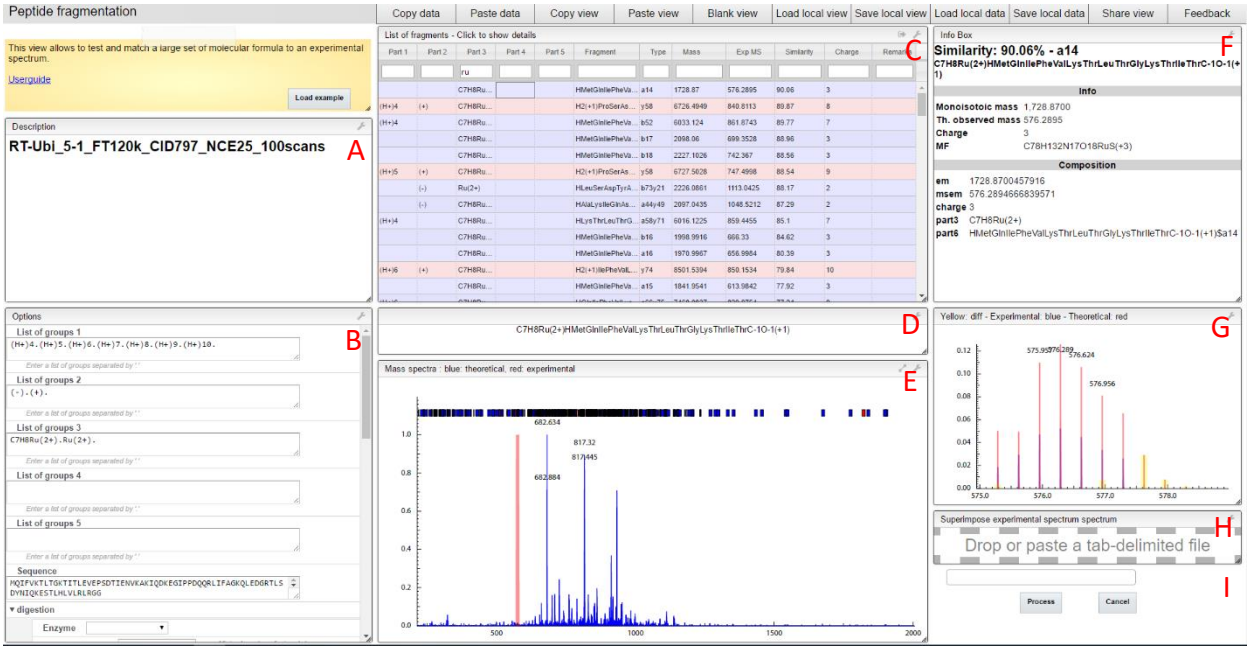

Figure 5.20 Cheminfo tool graphical user interface. Various modules are labelled A to J corresponding to A) experimental description, B) parameter input (detailed description in figure 5.21) C) fragment list with modifying groups (part 1-5), fragment sequence, fragment type, theoretical mass, experimental/observed mass, percentage similarity and charge D) enlarged window for fragment sequence E) experimental MS spectra (blue), with theoretical match of selected fragment (red) selection carried out by left clicking fragment of interest in module C F) fragment details G) matching of theoretical to experimental spectra window (with comparison zone specified in module B) H) drag and drop spectra (accepts.txt files) I) process and cancel commands.

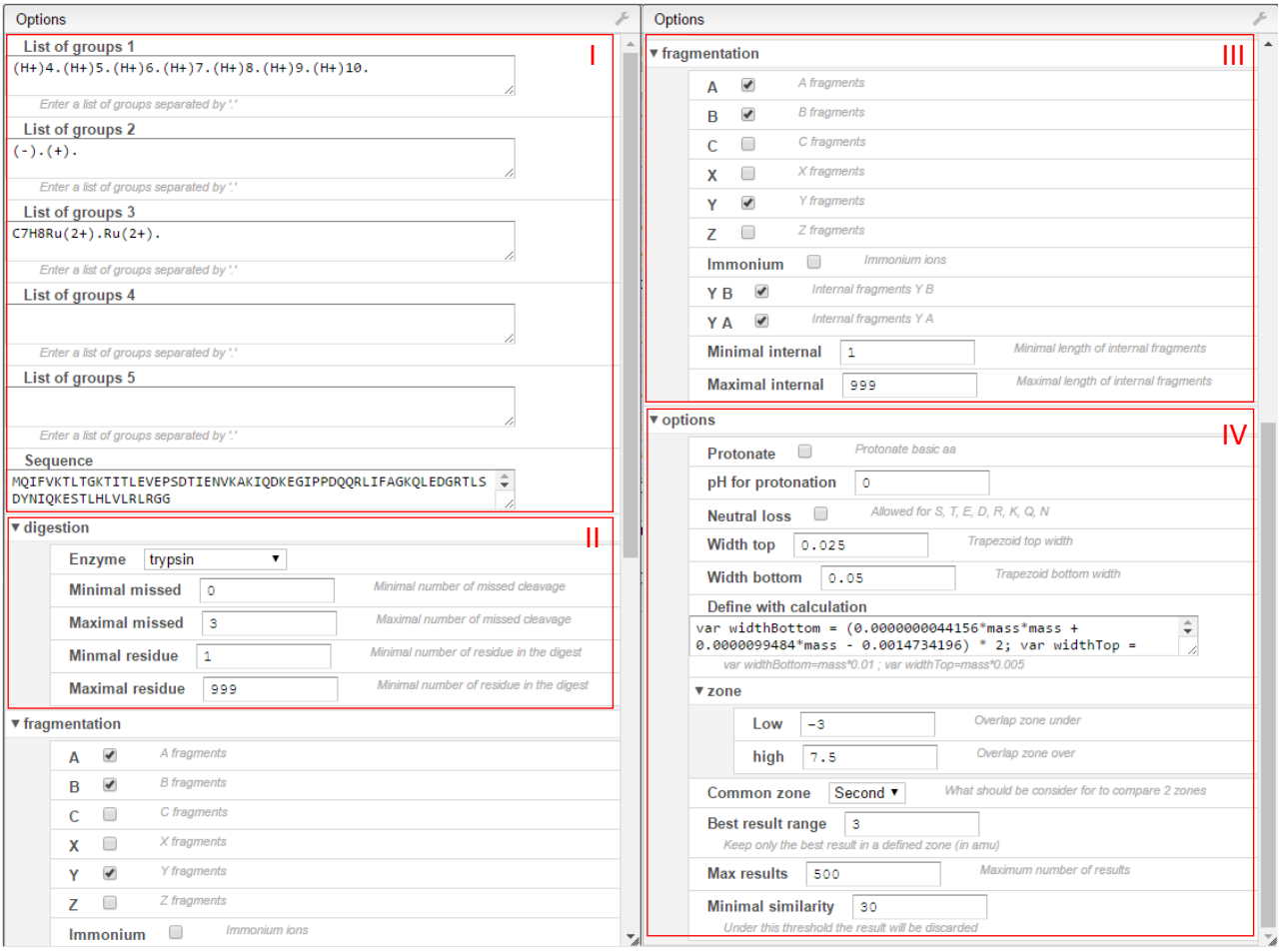

Figure 5.21 Cheminfo script parameter input module, labelled I to IV. I) List of modifiable groups applied onto the protein sequence specified in the sequence box II) Enzymatic digest parameters for bottom up experiments III) MS/MS experiment parameters including fragment types, internal fragments and length of internal fragments IV) Other option including protonation of basic amino acids, neutral losses, bottom and top widths for of trapezoid for matching theoretical to experimental spectra (inputting a formula overwrites the fixed value specified), zone which specifies the mass range in Da/charge where theoretical spectra is overlapped with experimental spectra to calculate similarities (low and high specifies mass range in Da/charge before and after the monoisotopic mass of the peak of interest respectively), common zone (which specifies how similarity matching between theoretical and experimental spectra is performed), best result range which keeps only the best defined number of results within the scanned zone, max results number and minimal similarity score displayed.

5.4.5 Input parameters and data interpretation

General

Pre-processing of all MS/MS spectra obtained was done in ThermoFisher Excalibur, and files were exported as .txt files before input into the Cheminfo tool. Hydrogens, modifiable charge and metal adduct types were introduced in the various boxes (Figure 2, I). In the options section (Figure 2, IV), protonation of basic amino acids was left unchecked. Neutral loss was scanned for MS/MS spectra of selected shorter peptides in bottom up experiments. Trapezoid widths were calculated via polynomial fitting of widths (FWHM) across the m/z range of each spectra (calculated in ThermoFisher Excalibur), and inputted as a general formula:

$$var\ widthbottom = [\text{a(mass)(mass)} + \text{b (mass)} + \text{c}].2; \text{var widthtop} = \frac{\text{Width Bottom}}{4}$$

Zone widths were selected based on complexity of the expected isotopic pattern (typically applied values, -3 to 7.5 for ruthenium and -2 to 6.5 for platinum) and the common zone parameter "second" was used for all processing. Best result range was set at 3, max results at 500 and minimal similarity at 30%.

Enzymatic digests

Enzyme used was selected from the dropdown menu (in our case LysC, and GluC), maximal missed cleavage sites were set at 3, and min/max residue numbers were set at 1 and 999 respectively.

MS/MS spectra

Selection of fragment ions were based on fragmentation type. a, b and y ions including y-b and y-a internal fragments were chosen for CID and HCD fragmentation and c, y and z ions were chosen for ETD spectra.

Data interpretation

Though the tool provides percentage similarity scores, a general cutoff of 65% was used. In cases of ambiguity, spectral peaks were compared manually in the spectral window (Figure 5.20, G & E), before selection.

Chapter 6
Application of the MSAPM tool to aid determination of protein-metallodrug binding sites on the breast cancer susceptibility protein type-1 (BRCA1) zinc binding domain.

6.1 Introduction

Zinc finger (ZF) proteins participate in protein/nucleic acid and protein/protein interactions in many groups of proteins. They play a diverse role in many cellular processes, including transcription, DNA repair, cellular signaling and apoptosis. They are classified into several groups based on the structural properties in the region of the zinc-binding site.[183] The Really Interesting New Gene (RING) finger protein is a one of them. The structure of RING finger domain is characterized by two zinc ions coordinated to eight amino acids, typically cysteine and histidine ($Cys_3His_1Cys_4$) residues. The coordinated zinc maintains the functional tertiary structure[184] and its substitution by another metal ion causes a loss of tertiary structure leading to loss of protein function.[185–187] Currently, ZF proteins have been investigated as therapeutic targets for treatment of diverse conditions including cancer, HIV, and bacterial infection. Most ZF protein inhibitors act by coordinating to the active-site metal ion or interacting with residues around the active site, leading to distortion of tertiary structure, displacement of zinc ions and loss of protein conformation and function.[185,188–193]

Breast cancer is also the most common cause of cancer death among women (522,000 deaths in 2012) and the most frequently diagnosed cancer among women in 140 countries worldwide, accounting for one in four of all cancers in women.[194] The breast cancer susceptibility gene 1 (BRCA1) is responsible for a hereditary predisposition to breast cancer. BRCA1 is essential for maintaining genomic stability and is associated with a number of cellular processes, including DNA repair, cell cycle checkpoint, transcriptional regulation and protein ubiquitination.[194,195]BRCA1 contains three major domains, including the Zn^{2+} finger RING domain (BRCA1 RING domain) at the *N*-terminus, the nuclear localization signal domain (NLS), and the BRCA1 C-terminal domain (BRCT domain).[196] The RING domain is characterized by a conserved pattern of one histidine and seven cysteine residues arranged in an interleaved fashion forming two distinct Zn^{2+}-binding sites in which two pairs of cysteines (Cys^{24}, Cys^{27} and Cys^{44}, Cys^{47}) form site I and a cysteine and histidine pair together with another pair of cysteines (Cys^{39}, His^{41} and Cys^{61}, Cys^{64}) form site II.[196] The BRCA1 RING domain preferentially forms a heterodimer with another RING domain (BRCA1-associated RING domain 1, BARD1).[196,197] The structure of the BRCA1/BARD1 RING dimer comprises a four helix bundle forming the binding interface. Heterodimerization stabilizes the proper conformation of the BRCA1 RING domain to allow E3 ubiquitin ligase activity.[198,199] This activity is subsequently lost on chelation of Zn^{2+} in the BRCA1 RING domain, suggesting the

activity is regulated by the Zn^{2+} ion concentration.[199] Many cancer-predisposing substitution mutations, such as C24R, T37R, C39Y, C61G,and C64Y, which potentially impair Zn^{2+} coordination and BRCA1 RING structural integrity have been identified.[196,200] In addition, these mutations have been shown to affect ubiquitin ligase function and, in turn, many cellular processes, including cell-cycle progression, cell differentiation, apoptosis, response to DNA damage, DNA repair and transcription.[201] Other mutations, for example L52F and L63F, are located in proximity to site II and may exert an indirect effect on Zn^{2+} coordination and, in turn, ubiquitination.[201] The D67Y BRCA1 mutation has been identified in eight European patients. At the same site D67E has been observed.[202] This amino acid resitdue is located in the vicinity of Zn^{2+}-binding site II (defined by residues 58-68), and forms a recognition interface with a ubiquitin-conjugating enzyme.[201] The consequences of the mutations have yet to be elucidated.

Several preclinical and clinical studies have identified the possibility of using BRCA1 inactivation as a target for breast and ovarian cancer treatment.[203–207] There is evidence to suggest that mutations in the BRCA1 RING domain result in a loss of the E3 ubiquitin ligase activity and conferred hypersensitivity of cancer cells to DNA-damaging chemotherapy and γ-irradiation.[200,208–210] In addition, cisplatin has recently been reported to affect the conformation of the apo-form of the BRCA1 RING finger domain forming intra- and intermolecular Pt-BRCA1 adducts.[211] A preferential Pt(II)-binding site was found at His-117,[211] that led to inactivation of the BRCA1-mediated ubiquitin ligase activity of both wild-type and variant BRCA1 proteins.[26,30] These studies suggest that the ZF motif of the BRCA1 protein could be a target for metal-based drugs.

RAPTA complexes, $Ru(\eta^6\text{-arene})(PTA)Cl_2$ (PTA = 1,3,5-triaza-7-phosphaadamantane), have been shown to exhibit promising antitumor properties.[212] The mechanism of action of these complexes has been partially elucidated and is profoundly different to the biochemical mode of action of classical platinum anticancer drugs.[213–217] For example, whereas cisplatin targets DNA, the RAPTA complexes form strong interactions with proteins.[55,213] Studies indicate that the RAPTA complexes have high affinities for cysteine residues, possibly targeting cysteine-rich proteins such as those involved in DNA regulation and thereby mediating their therapeutic effect via epigenetic pathways.[55]

To the best of our knowledge, the interactions of RAPTA compounds with the BRCA1 protein have not been reported and, hence, we describe an investigation of the interactions of

ZF domain RING of BRCA1 proteins, both wild-type and variants D67Y and D67E, with RAPTA-C and RAPTA-EA in comparison with cisplatin.

6.2 Results and discussion

Adducts formed following incubation of the complexes with BRCA1 were initially investigated by gel shift assays (Figure 6.1), showing that the RAPTA complexes induce intermolecular crosslinks, resulting in dimers or larger aggregates. The binding affinity of each complex to the proteins was further investigated using ICP-MS. RAPTA-EA was found to exhibit a similar binding affinity to the BRCA1 RING domain (both wild-type and variants), which was ca. 5-fold higher than RAPTA-C and RAPTA-T. However, the binding affinity of each complex was not significantly different for the mutations compared to the wild-type (Figure 6.2).

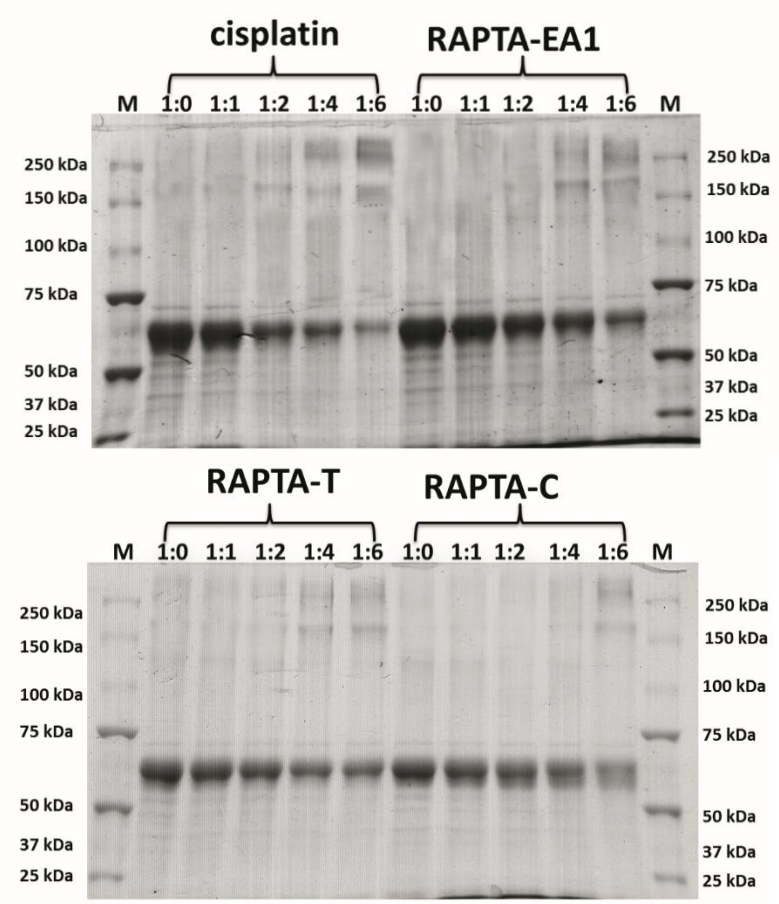

Figure 6.1 Intermolecular cross-linking of the metal-BRCA1 adducts. Ten µM of BRCA1 protein was pre-incubated with 30 µM of $ZnCl_2$ at 4 °C for 8 h. Holo-BRCA1 were incubated with cisplatin or RAPTA complexes at various molar ratios (protein: drug) of 1:0, 1:1, 1:2, 1:4, and 1:6, at 4 °C for 24 h, and electrophoresed on 8 % SDS/PAGE. The bands of protein were detected by silver staining. Lane M corresponds to the electrophoretic mobility of standard protein markers indicated in kDa.

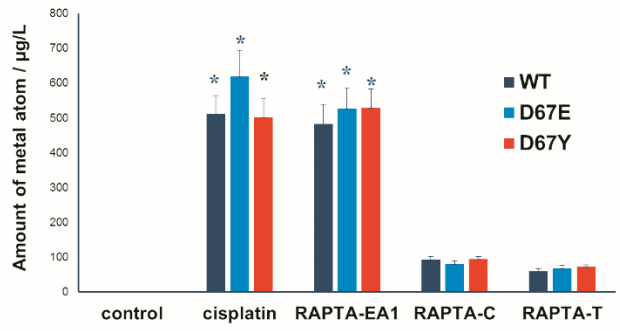

Figure 6.2 The binding affinity of cisplatin and the RAPTA complexes to the BRCA1 proteins evaluated by ICP-MS analysis. RAPTA-EA1 and cisplatin have a ca. 5-fold high binding affinity compared to RAPTA-C and RAPTA-T. Statistically significance differences from the untreated control are indicated by ***p*<0.01. The binding affinity is not significantly affected by the amino acid substitutions.

Cancer therapies include inducing DNA damage and disrupting DNA repair pathways. Among the different types of DNA damage, DNA double-strand breaks (DSB) are one of the most deleterious and harmful. Cells mount a coordinated response to these lesions, the failure of which can lead to genomic instability and cell death.[78,218–223] Hence, blocking this response during chemo- or radiotherapy could potentiate the therapy. As the BRCA1 protein is involved in the DSB repair process and, as RAPTA complexes have been shown to be inhibitors of this protein, they may prove to be useful in combination therapies. Many studies of BRCA1 functions have shown that it is involved in genomic stability maintenance. The malfunction of this protein reportedly results from mutations at the *N*-terminus of Zn^{2+} finger RING domain gene. In particular, cancer-predisposing site II substitutions at positions 39, 61, and 64 potentially impair Zn^{2+} ion coordination and have been shown to disrupt the RING integrity and protein function.[196,201] As shown in Figure 6.1, RAPTA compounds form intermolecular metal-BRCA1 crosslinks.

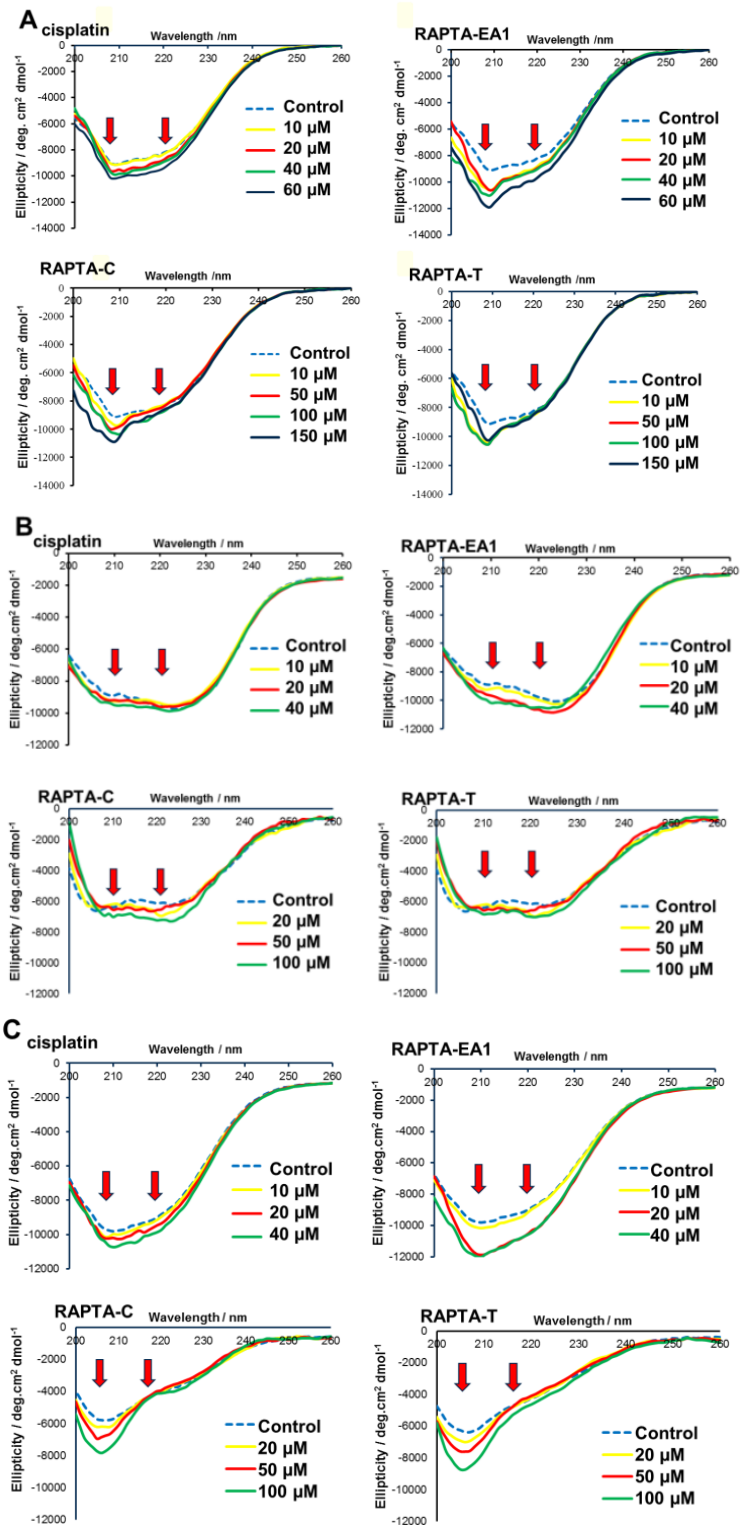

Figure 6.3 The CD spectra of the complexes induced secondary structure change of holo-form of the BRCA1 RING domain (residues 1-304), both wild-type and variant (D67Y and D67E) at a number of concentration. Ten μM of BRCA1 protein was pre-incubated with 30 μM of $ZnCl_2$ for 8 h. Samples were incubated with complexes in the dark at 4 °C for 24 h before CD measurement at 25 ºC with the scanning rate of 50 nm/min. The mean residues ellipticity and wavelength ranging from 200 to 260 nm were plotted. A) wild-type protein. B) D67E protein. C) D67Y protein.

Circular dichroism (CD) was used to verify whether the RAPTA complexes alter the conformation of the *N*-terminal BRCA1 RING domain proteins (Figure 6.3). CD spectra of both wild-type and variant BRCA1 RING domain proteins change upon RAPTA binding in a concentration dependent manner, characterized by a large increase in negative elipticity at 208 and 220 nm. Using the CONTIN program, the content of the secondary structure of both wild-type and variant BRCA1 RING proteins were predicted (Figure 6.4A-C). The complexes disrupt the secondary structure of the BRCA1 RING proteins leading to an increase in α-helical content and a decrease in β-sheets forms. The binding constant (K) and free energy (ΔG) of the RAPTA-BRCA1 complexes (1:5; protein to metal) were predicted[224] (Table 6.1). RAPTA-EA1 has a higher binding constant and gave rise to a lower free energy than other complexes. In addition, the RAPTA complexes and cisplatin have higher binding constants and lower free energies in the D67Y protein than in the D67E or wild-type proteins. This suggests that RAPTA-EA1 interacts with the Zn^{2+} binding sites and other residues rather than the Zn^{2+} binding sites of the protein alone, and affects the overall conformation of BRCA1. The differences in the binding constants and free energies may be attributed to the differences in the structure of the metal complexes (preferential binding sites of the complexes were determined by mass spectrometry – see below). Moreover, it is notable that the structure of the D67Y protein is more susceptible towards binding the RAPTA complexes than the D67E or wild-type proteins, consistent with previous studies which showed that cisplatin perturbs the secondary structure of BRCA1 RING domain protein.[211,213]

Complexes	**Wild-type**		**D67E**		**D67Y**	
	Binding constant (K) M^{-1}	Free energy (ΔG) cal mol^{-1}	Binding constant (K) M^{-1}	Free energy (ΔG) cal mol^{-1}	Binding constant (K) M^{-1}	Free energy (ΔG) cal mol^{-1}
cisplatin	$4.85 \pm 0.23 \times 10^4$	1792.64	$6.11 \pm 0.44 \times 10^5$	291.46	$6.46 \pm 0.46 \times 10^5$	285.97
RAPTA-EA1	$2.72 \pm 0.65 \times 10^6$	-594.32	$8.85 \pm 0.68 \times 10^5$	72.44	$2.99 \pm 0.02 \times 10^6$	-650.81
RAPTA-C	$2.03 \pm 0.02 \times 10^5$	945.44	$2.99 \pm 0.04 \times 10^5$	714.81	$3.69 \pm 0.02 \times 10^5$	589.68
RAPTA-T	$2.13 \pm 0.07 \times 10^5$	916.47	$2.89 \pm 0.03 \times 10^5$	735.57	$3.73 \pm 0.07 \times 10^5$	582.65

Table 6.1 Binding constant and free energy predicted by the CONTIN program on the binding of RAPTA complexes to the BRCA1 proteins. ±SD of three independent experiments.

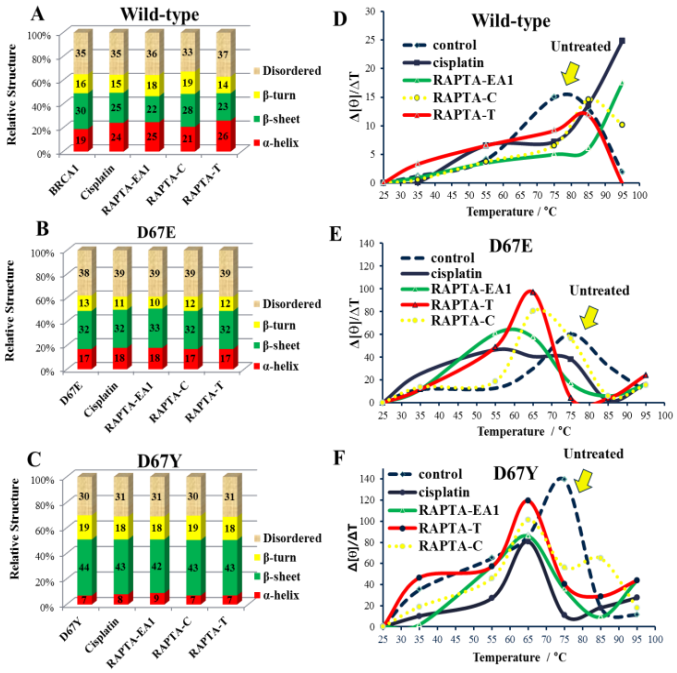

Figure 6.4 Secondary structure and thermal alteration of the treated BRCA1 RING domain proteins, both wild-type and variants (D67Y and D67E). The effect of the complexes on the secondary structure of proteins were predicted using the CONTIN program. (A-C) The relative secondary structure of treated BRCA1 proteins with 20, 50, and 50 µM of the complexes. (D-F) Thermal denaturation curves of the metalated BRCA1 adducts. The denaturation curves of the metal-BRCA1 adducts are plotted in terms of $\Delta[\Theta]208\ nm/\Delta T$.

The thermal stability of the BRCA1 RING proteins induced by the complexes was also determined by CD. The thermal denaturation curves were plotted and analyzed (Figure 6.4, D-F and Table 6.2). The RAPTA complexes stabilize the wild-type protein structure with an associated increase in melting temperatures (*Tm*). In contrast, the *Tm* in both the D67Y and D67E proteins decreased as a result RAPTA binding. The results are consistent with previous studies which show that the ZF domain forms the thermostable structure.[225] The *Tm* of the BRCA1 RING domains are high (in the range 74-79°C), however, the interactions between surface residues and solvent appear to be altered as the variant proteins were slightly less thermostable compared to the wild-type protein.[226] This difference may also reflect an altered microenvironment around the mutation site.

	Control *Tm* (°C)	cisplatin *Tm* (°C)	RAPTA-EA1 *Tm* (°C)	RAPTA-C *Tm* (°C)	RAPTA-T *Tm* (°C)
WT	78.9 ± 0.2	>95	>95	83.1 ± 0.4	85.2 ± 0.2
D67E	75.2 ± 0.3	63.8 ± 0.5	60.1 ± 0.2	64.2 ± 0.2	66.8 ± 0.4
D67Y	74.9 ± 0.4	65.0 ± 0.2	64.2 ± 0.3	65.3 ± 0.2	65.1 ± 0.1

Table 6.2 Thermal stability of the wild-type and variant (D67E and D67Y) BRCA1 RING protein treated with the complexes and characterized by CD. The melting temperatures (*Tm*) were analyzed by $\Delta[\theta]/\Delta T$. ±SD of three independent experiments.

The zinc ejection assay was used ascertain whether the complexes disrupt the conformation of the BRCA1 RING domain protein sufficiently to dislodge the zinc ion from its binding sites (Figures 6.5 and 6.6). The results show that the binding of RAPTA complexes and cisplatin to all three BRCA1 proteins releases the Zn^{2+} ion in a dose dependent manner (Figure 6.6). In addition, the rate of zinc ion ejection by RAPTA-EA1 is markedly higher than that induced by the other compounds (Figure 6.5). Targeting the ZF motif of the BCA2 protein by metalation was shown to result in the release of the zinc ion and led to a reduction in E3 ligase activity.[189] Similarly, platinum complexes have been reported to interact with the C-terminus of the HIV nucleocapsid NCp7 zinc finger domain and leading to the ejection of Zn^{2+} ions.[185]

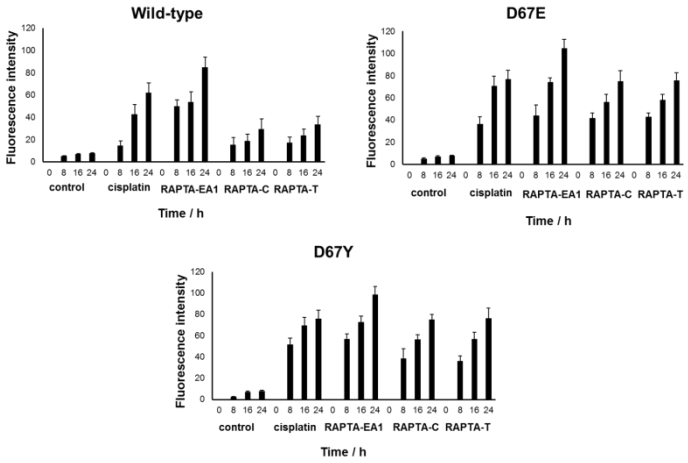

Figure 6.5 Time-dependent zinc ejection assay on BRCA1 RING domain, both wild-type and variant (D67E and D67Y) proteins were treated with the complexes. Reactions were performed in zinc ejection buffer (10% glycerol, 50 mM Tris-HCl buffer, pH 7.6). The ejection of zinc ions from the protein was monitored by the change in fluorescence of the zinc-selective fluorophore TSQ (6-Methoxy-8-*p*-Toluenesulfonamido-Quinoline) using a spectrofluorometer (excitation filter, 360 nm; emission filter, 490 nm).

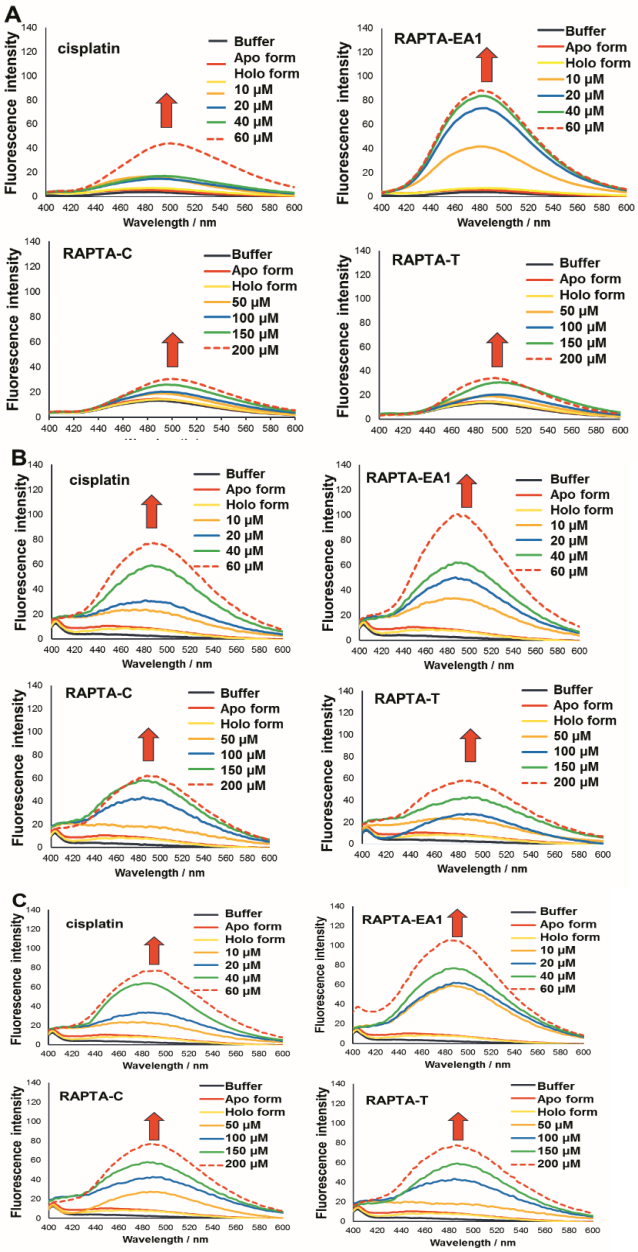

Figure 6.6 Concentration-dependent zinc ejection assay on the BRCA1 RING domain. Both wild-type and variant proteins were treated with the complexes. (A) wild-type protein, (B) D67E protein and (C) D67Y protein.

The effect of the RAPTA complexes on BRCA1 E3 ubiquitin ligase activity was investigated (Figure 6.7). The BRCA1/BARD1 RING complex in the presence of ATP exhibits an E3 ubiquitin ligase activity that promotes the formation of high molecular weight polyubiquitin species, which are not observed in the absence of ATP. The *N*-terminal BRCA1 RING domain proteins, both wild-type and variants (D67E and D67Y) were incubated with various concentrations of the complexes at 4 ^{o}C for 24 hours, and then assaying for E3 ligase activity; E3 ligase activity decreases in a dose-dependent manner in all cases (Figure 6.8). The IC_{50} value for inactivation of E3 ubiquitin ligase activity by RAPTA-EA1 is markedly greater

than the corresponding values for RAPTA-C, RAPTA-T and cisplatin (Table 6.3). The inactivation of BRCA1 E3 ligase activity induced by RAPTA-EA1 is similar to that induced by other complexes.[227] Surprisingly, the D67E and D67Y variant proteins showed hypersensitivity to the RAPTA complexes, especially the D67Y variant (Figure 6.8), consistent with previous study showing that platination of the wild-type BRCA1 protein hardly affects the native structure and function of the protein whereas platination of the D67E BRCA1 results in distinct changes on structure and function.[208]

	WT (μM)	**D67E (μM)**	**D67Y (μM)**
RAPTA-EA1	55.4 ± 0.3	5.6 ± 0.8	2.8 ± 0.5
RAPTA-C	167.8 ± 0.5	148.3 ± 0.4	126.5 ± 0.6
RAPTA-T	95.3 ± 0.2	78.9 ± 0.3	74.6 ± 0.1
Cisplatin*	60*	60*	32*

Table 6.3 Half inhibition of BRCA1/BARD1 E3 ligase activity inactivated by the complexes. ±SD of three independent experiments.

* A. Atipairin, A. Ratanaphan, *Breast Cancer: Basic and Clinical Research*, **2011**, 5, 201-208.

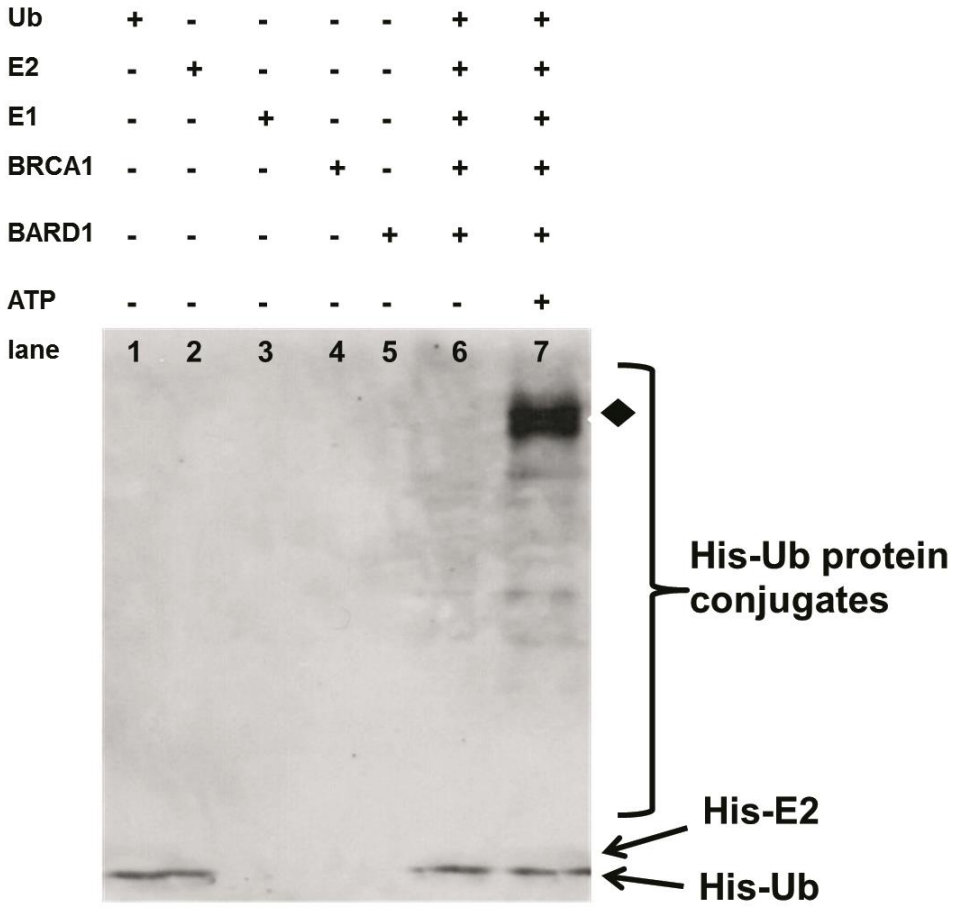

Figure 6.7 In vitro E3 ubiquitin ligase activity metallated-BRCA1 RING domain. The E3 ligase reaction in the presence or absence of E3 ligase component was evaluated. Complete reaction mixtures, containing 20 µM Ub, 300 nM E1, 5 µM UbcH5c, 3 µg BRCA1 (residues1-304), and 3 µg BARD1 (residues 26-327), were incubated at 37°C for 3 h. Lack of ATP components in the reactions were carried out under the same conditions. Samples were then resolved on 8% SDS-PAGE and then performed by western blotting with anti-6-His –HRP conjugated antibody. An apparent ubiquitinated product was indicated by filled diamond.

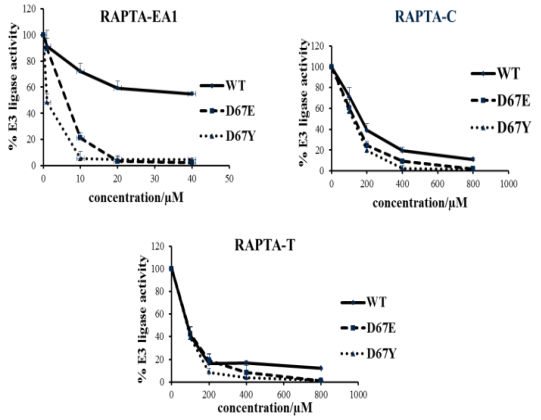

Figure 6.8 The effect of the RAPTA-treated BRCA1 RING domain proteins on E3 ubiquitin ligase activity. The apparent ubiquitinated products (indicated by filled diamonds) in the gels shown in Figure S3 were quantified with a Bio-Rad GS-700 Imaging Densitometer. The relative E3 ligase activity of the BRCA1 adducts (%) is plotted as a function of the concentration of the RAPTA complexes.

The effect of the complexes on cell viability was determined on MCF-7, HCC1937 and MDA-MB-231 breast cancer cell lines (Table 6.4). The HCC1937 cell line was selected as it contains a BRCA1 mutation, 5382insC.[228] RAPTA-C and RAPTA-T are inactive (IC_{50} > 1000 µM), whereas RAPTA-EA1 is considerable more cytotoxic than cisplatin in this cell line. Real-time monitoring of the proliferation of these breast cancer cells was probed in situ using a xCEELigence system, showing that RAPTA-EA1 and cisplatin inhibit the proliferation of all three cancer cell lines within a few hours, indicative of a direct cytotoxic response. A continuous reduction in the cell index (CI) was observed at a high concentration of the complexes (Figure 6.9).

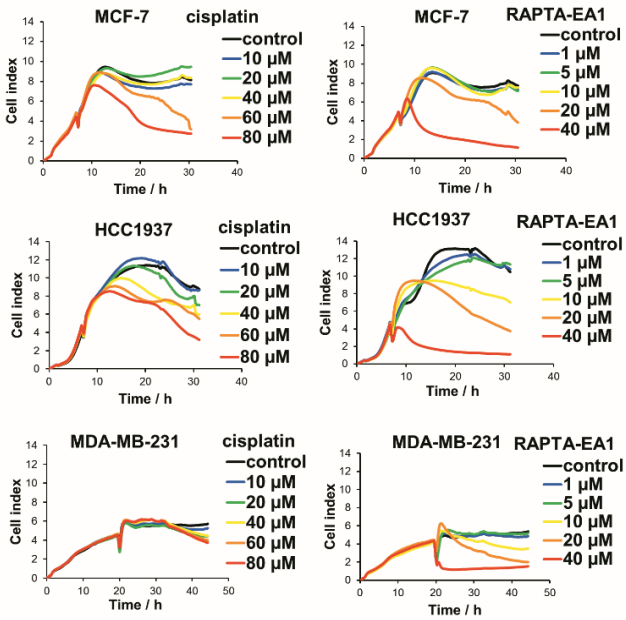

Figure 6.9 Real-time monitoring of the affect of the complexes on human breast cancer cells using the *xCEE*Ligence system. Cells were seeded onto an E-plate and allowed to grow prior to the introduction of the complexes at various concentrations. After addition of the complexes the cells were allowed to grow for a further 24 h. The cell index (CI) was recorded every 15 min. Each concentration was performed in triplicates.

	MCF-7	**MDA-MB-231**	**HCC1937**
Cisplatin	19±1	>150	23±1
RAPTA-EA1	54±1	15.5±0.5	11.2±0.3
RAPTA-C	>1000	>1000	>1000
RAPTA-T	>1000	>1000	>1000

Table 6.4 IC_{50} values (µM) for the complexes on MCF-7, MDA-MB-231 and HCC1937 cells after 24 h (data reflect the mean and SD of results from three separate experiments, each performed in triplicates).

The IC_{50} values of cells treated with RAPTA-EA1 (40 μM) decrease rapidly in the HCC1937 and MDA-MB-231 cell lines. RAPTA-EA1 appears to be more active against the BRCA1-defective HCC1937 cells than the BRCA1-competent MCF-7 or MDA-MB-231 cells, consistent with the observation that RAPTA-EA1 more strongly affects variant BRCA1 compared to the wild-type protein. Combined, these studies imply that an increased sensitivity in BRCA1-mutated breast cancer cells might be related to a dysfunctional BRCA1 unable to repair DNA damage induced by treatment with the complex, ultimately leading to cell death.[227] In addition, it has been reported that overexpression of BRCA1 in human BRCA1-competent breast cancer MCF-7 cells results in an increased resistance to cisplatin.[229] In contrast, BRCA1-defective HCC1937 cells are significantly more sensitive to cisplatin,[230] consistent with this study.

To determine the preferential binding sites of the RAPTA complexes on the BRCA1 ZF region, Electron Transfer Dissociation (ETD) fragmentation mass spectrometry was performed on a 50 amino acid synthetic peptide mimicking the ZF region of BRCA1 incubated with RAPTA-EA1 and RAPTA-C. ETD fragmentation is a well-established technique used to probe the localization of post-translational modifications[231] (such as glycosylation and phosphorylation) and drug metalation sites on peptides[232] and proteins. ETD causes fragmentation of the N-C_α bonds of the peptide backbone generating C and Z type peptide fragments which can be used to identify modified amino acid residues on a peptide.

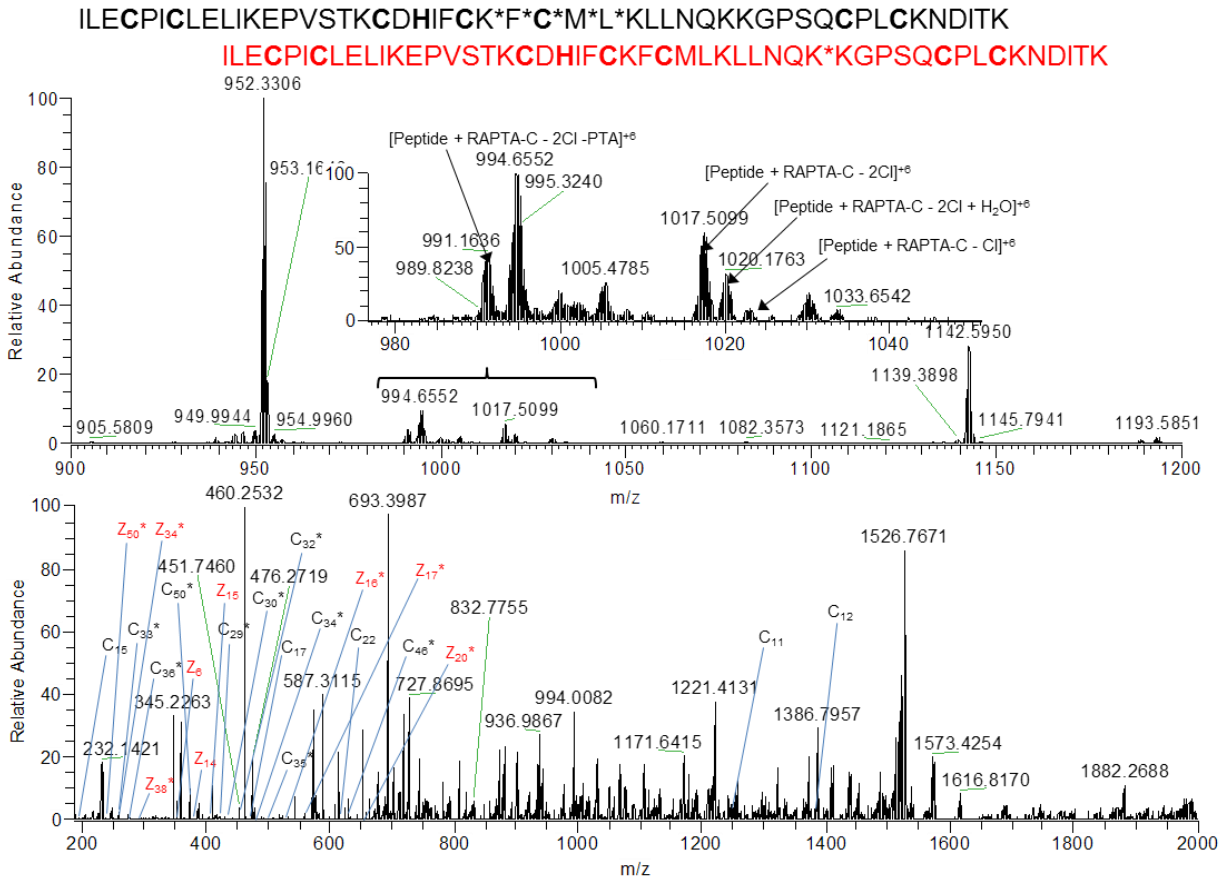

Figure 6.10 LTQ Orbitrap FTMS of RAPTA-C after incubation with the BRCA1 peptide. Top spectra: full scan 900-1200 m/z mass spectra of the 1:5 peptide:complex ratio showing the formation single adduct peaks with different ligand states (shown in more detail in the inset). The ion at m/z 953.3306 (+6) corresponds to the native BRCA1 peptide. Bottom specrtra: ETD spectra of the [BRCA1 +7H + RAPTA-C -2Cl]$^{9+}$ adduct after a 100 ms interaction period with the fluoroanthene radical anions showing metallation at the peptide fragment Lys^{25}Phe^{26}Cys^{27}Met^{28}Leu^{29} (corresponding sequence in black) and Lys^{35} (corresponding sequence in red). Residues labelled with * correspond to a metallated fragment. Residues in bold correspond to zinc binding residues on the peptide.

Initially full scans mass spectra of the 1:5 peptide:complex incubations were analyzed and showed adducts with a 1:1 stoichiometry for RAPTA-C, and up to 1:3 adducts with RAPTA-EA1 (Figures 6.10 and 6.11). Adducts corresponding to RAPTA species that are consistent with previous MS studies were observed.[182] Further ETD fragmentation was performed on suitable drug peptide adducts; for RAPTA-C the most intense adducts [Peptide + RAPTA-C -2Cl] at +7 and +9 charge states and for RAPTA-EA [Peptide + RAPTA-EA -3Cl +2OH] at +8 and +9 charge states were selected for ETD fragmentation. Analysis of C-type ETD fragments (fragments from the amino terminus) of RAPTA-C peptide adduct showed an absence of any metallated fragments before residue Cys^{24} (C^{24}) and the first metallated fragment at residue Leu^{29} (C^{29}) indicating that binding takes place along a short peptide stretch, Lys^{25}Phe^{26}Cys^{27}Met^{28}Leu^{29} (residues 45-49 on full length BRCA1). Analysis of Z fragments

(fragments from the carboxyl terminus) showed no metallated fragments until Lys^{34} (Z^{15}), with a first metallated fragment at Lys^{35} (Z^{16}), narrowing down to a binding site on Lys^{35} corresponding to residue 55 on full length BRCA1 (Figure 6.10 and Appendix C Table C.1). For RAPTA-EA, similar analysis of C-type fragments showed the absence of metallated fragments until Phe^{23} (C^{23}), and the first metallated fragment at Met^{28} (C^{28}), narrowing down the binding site to a short peptide stretch Cys^{24}Lys^{25}Phe^{26}Cys^{27}Met^{28} (residues 44-48 on full length BRCA1). Z fragment analysis showed that similarly, RAPTA- EA binds at Lys^{35} (Figure 6.11 and Appendix C Table C.2). The binding sites of the RAPTA complexes on the BRCA1 RING domain are different to those reported for cisplatin, where binding was found at the His^{117} residue.[211]

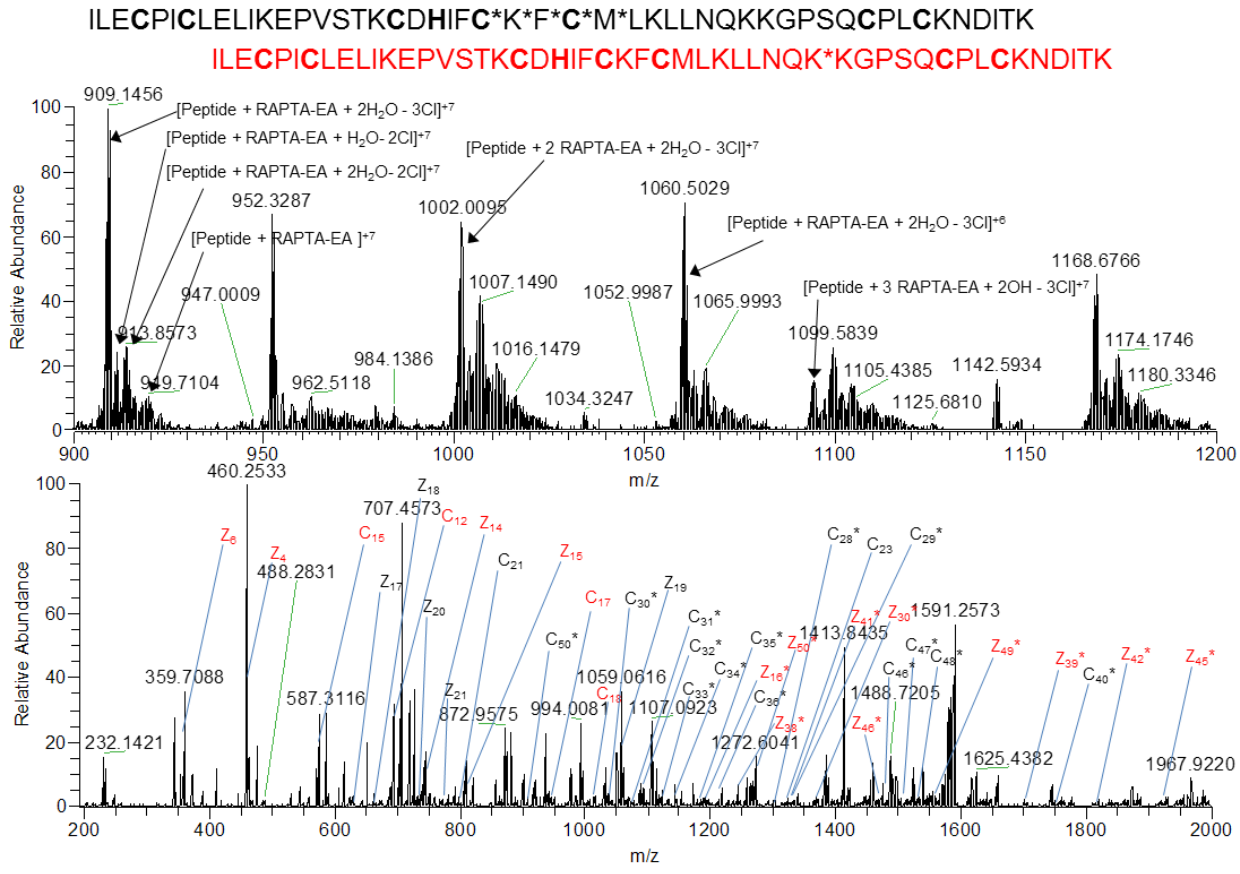

Figure 6.11 LTQ Orbitrap FTMS of RAPTA-EA after incubation with the BRCA1 peptide. Top: full scan 900-1200 m/z mass spectra of the 1:5 peptide:complex ratio showing the formation up to 3 adduct peaks with different ligand states. The ion at m/z 909.1456 (+7) corresponds to the native BRCA1 peptide. Bottom: ETD spectra of the [BRCA1peptide + RAPTA-EA -3Cl +2OH] $^{9+}$ adduct after a 100 ms interaction period with the fluoroanthene radical anions showing metallation at the peptide fragment Cys^{24}Lys^{25}Phe^{26}Cys^{27}Met^{28} (corresponding sequence in black) and Lys^{35}(corresponding sequence in red). Fragments labelled with * correspond to a metallated fragment. Residues in bold correspond to zinc binding residues on the peptide.

The similar binding sites observed for both RAPTA complexes suggest that the different arene ligands have little impact on the localization of binding, although it does significantly affect stoichiometry and kinetics. As mentioned above, RAPTA binding leads to zinc ion displacement, which is not surprising based on the close proximity of the binding regions to site I of the RING domain of BRCA1 (Cys^{24}, Cys^{27} and Cys^{44}, Cys^{47}), which would also leads to conformational changes on this region and loss of protein function.

Taken together the results from this study allow us to construct a functional model of RAPTA effects on the BRCA1 protein (Figure 6.12), where uptake and binding of RAPTA complexes to the ZF domain of the RING domain of BRCA1 results in zinc displacement, disrupting the secondary structure of the protein. As a consequence of this ruthenation process the RING heterodimer BRCA1/BARD1-mediated E3 ubiquitin ligase activity is inactivated resulting in a loss of protein function.

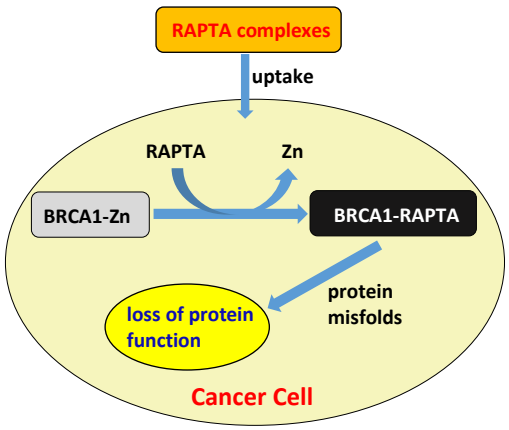

Figure 6.12 Functional model of the effect of RAPTA complexes on BRCA1 protein.

6.3 Conclusions

In summary, RAPTA-EA1 binds to the ZF domain of the BRCA1 RING protein, especially in the variant protein, disrupting the secondary structure of the protein and resulting in ejection of the zinc ion from the binding site. This process results in a loss of protein function. These results indicate that the ZF motif of dysfunctional BRCA1 proteins could be a molecular target for ruthenium-based drugs in breast cancer chemotherapy and that RAPTA-EA1 in particular has potential in the treatment of breast cancers, especially if used in combination with DNA damaging agents.

6.4 Experimental

For clarity and contextual understanding, the full body of results are presented here. MS top down experiments were performed in the EPFL. All other biochemistry experiments were conducted in the lab of Professor Adisorn Ratanaphan, Prince Songkla University, Songkhla, Thailand.

6.4.1 Materials

RAPTA-T, RAPTA-C[116] and RAPTA-EA1[120] were prepared as previously described. Cisplatin was purchased from Tokyo Chemical Industry Pte. Ltd, Tokyo, Japan. The synthetic peptide of the ZF region of BRCA1, from the N-terminus, amino acid sequence ILECPICLEL IKEPVSTKCD HIFCKFCMLK LLNQKKGPSQ CPLCKNDITK, was purchased from CASLO ApS, Lynby, Denmark.

6.4.2 Protein expression and purification

The *N*-terminal BRCA1 RING domain proteins, both wild-type and variants (D67E and D67Y) containing 304 amino acid residues, were produced as previously described.[26] The purified protein was identified on 8% Coomassie blue-stained SDS-PAGE and subsequently confirmed by sequencing the tryptic digested peptides.

6.4.3 Gel shift assay

The interaction of complexes with the BRCA1 variants was investigated using a gel shift assay. The complexes were prepared as stock solutions in deionized water. The BRCA1 protein (10 μM) was pre-incubated with 30 μM of $ZnCl_2$ at 4 °C for 8 h. The holo-BRCA1 protein was then incubated with the complexes at various molar ratios of protein: drug at 4 °C for 24 h, and electrophoresed on 8% SDS/PAGE. The bands of protein were detected by silver staining.

6.4.4 ICP-MS analysis

The *N*-terminal BRCA1 (1-304) proteins, both wild-type and variant (D67E and D67Y), were prepared in deionized water. $ZnCl_2$ was prepared as a 1 mM stock solution in deionized water. The holo-BRCA1 was pre-incubated with $ZnCl_2$ at the molar ratio of 1:3 (BRCA1:$ZnCl_2$) at 4 °C for 8 h, and any unbound $ZnCl_2$ was removed by dialysis in deionized water. 10 μM of holo-BRCA1 proteins were treated with the complexes (50 μM) for 24 h at 4 °C. Unbound complex in the samples was removed by dialysis in deionized water. The amount of protein was then

determined by the Bradford assay, using BSA as a standard. Three microgram of metallated-protein was used to determination complex binding. The extent of metalation was determined by inductively coupled plasma-mass spectrometry (ICP-MS) (Agilent Technologies, USA).

6.4.5 Circular dichroism

The *N*-terminal BRCA1 (1-304) proteins (10 μM), both wild-type and variant (D67E and D67Y), were pre-incubated with 3 mol. equiv. of $ZnCl_2$ at 4 °C for 8 h. The holo-BRCA1 protein was treated with the complexes at various concentrations at 4 °C for 24 h. Metal-dependent folding of the protein was monitored by acquiring CD spectra over the range 200-260 nm using a Jasco J720 spectropolarimeter (Japan Spectroscopic Co. Ltd., Japan). Binding measurements were carried out at 20 °C using a 0.1 cm quartz cuvette. Five spectra were averaged with a step size of 0.1 nm, a 2 s response time and a 1 nm bandwidth. Data were baseline-corrected by the subtraction of each metal complex concentration. The secondary structures of proteins were predicted using the CONTIN program.[233] The binding constant was determined as described previously.[224] CD experiments, involving thermal denaturation, were performed in three separate scans in the range from 25 to 95 °C at 208 nm with a heating rate of 1 °C min^{-1}. Thermal renaturation (20 °C after heating at 95 °C) was also observed after the same length of time as for denaturation.

6.4.6 Zinc ejection assay

The holo-BRCA1 protein was incubated with the complexes as described in the section on ICP-MS analysis. Briefly, 10 μM of purified holo-BRCA1 protein was incubated with the complexes at various molar ratios of protein to drug in a zinc ejection assay buffer (10% glycerol, 50 mM Tris-HCl buffer, pH 7.6). The reaction mixtures were incubated in the dark for 8, 16, or 24 h at 4 °C. The ejection of zinc from the protein was monitored by the change in fluorescence of the zinc-selective fluorophore TSQ (6-Methoxy-8-*p*-Toluenesulfonamido-Quinoline) in the assay buffer. The zinc ejection assay was initiated by the addition of 20 μM (final concentration) TSQ in mixtures at room temperature. Immediately after reaction initiation the TSQ fluorescence was monitored at each concentration or time (excitation filter, 360 nm; emission filter, 490 nm) using a spectrofluorometer (FP 2600 Jasco Corporation). A zinc chloride standard curve was generated under the same conditions in the absence of BRCA1 protein (Figure 6.13). To control for fluorescence changes in the assay not due to the effect of the complexes binding to TSQ,

the results from above experiments were subtracted with fluorescence intensity of each compound in the presence of TSQ.

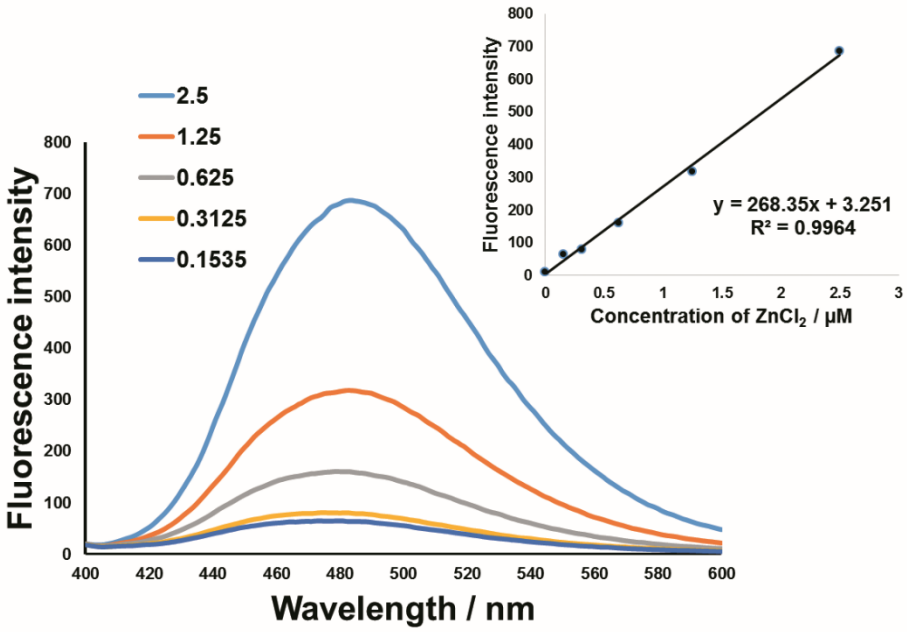

Figure 6.13 A standard curve of $ZnCl_2$ monitored by fluorescence spectrophotometry. Zinc chloride was dissolved in zinc ejection buffer (10% glycerol, 50 mM Tris-HCl buffer, pH 7.6) at various concentrations (µM; color lines). Fluorescence intensity was initiated by the addition of 20 µM (final concentration) TSQ in each concentration of zinc chloride at room temperature, and plotted against emission wavelength at 490 nm (excitation wavelength at 360 nm) using a spectrofluorometer (FP 2600 Jasco Corporation).

6.4.7 In vitro ubiquitination assay and western blotting

The in vitro ubiquitination assay was performed as previously described.[30] Briefly, the holo-BRCA1 protein was pre-incubated with $ZnCl_2$ at the molar ratio of 1:3 (BRCA1: $ZnCl_2$) at 4 °C for 8 h, and any unbound $ZnCl_2$ was removed by dialysis against deionized water. The holo-BRCA1 protein was then treated with thecomplexes at various concentrations for 24 h at 4 °C. Unbound complexes in the samples were removed by dialysis against deionized water. The amount of protein was then determined by the Bradford assay using BSA as a standard .The ubiquitin ligase reactions (20 µl) contained 20 µM Ub, 300 nM E1, 5 µM UbcH5c, 3 µg BRCA1 or a metallated-BRCA1 adduct, and 3 µg BARD1 in a buffer [50 mM Tris (pH 7.5), 0.5 mM DTT, 5 mM ATP, 2.5 mM $MgCl_2$ and 5 µM $ZnCl_2$]. Two separate reactions were incubated at 37 °C for 3 h, and then terminated by adding an equal volume of SDS-loading dye before electrophoresis on 8% SDS-PAGE. The separated protein was then transferred to the PVDF membrane and immunodetected with anti-His6 HRP (Horseradish Peroxidase) conjugated (chemiluminescent method, QIAGEN) at a dilution of 1:2000 and performed according to the

manufacturer's protocol. The blot was detected by chemiluminescence (SuperSignal TM, Pierce) on X-ray film. The relative E3 ligase activity of the metallated-BRCA1 adduct was quantified by normalizing the density of an apparent band of the ubiquitinated-protein conjugates to that of the parental BRCA1 as the control, using a Bio-Rad GS-700 Imaging Densitometer. The experiment was performed in duplicate.

6.4.8 Real-time monitoring of cell growth profiling

Real time growth kinetics of MCF-7, MDA-MB-231 and HCC1937 cells towards complexes treatments were examined using the Real-Time Cellular Analyzer (RTCA) (*xCEL*Ligence System, Roche Applied Science, Mannheim, Germany). RTCA utilizes E-plate which contains interdigitated micro-electrodes integrated on the bottom of the E-plate. The cell number, viability, morphology and degree of adherence of cells in contact with the electrodes will affect the local ionic environment leading to an increase in the electrode impedance, represented as the Cell Index (CI). For each experiment, briefly, 100 µl of medium were added in 96-wells E-plate and background readings were recorded. Cell suspension (100 µl) at cell density of $5x10^4$ cells/well was added to each well of the E-plate. The attachment, spreading and proliferation of the cells were monitored every 15 min over the following 7 hours for MCF-7 cells and HCC1937 cells and 18 hours for MDA-MB-231 cells (allowing cell attachment, spreading and cell entered logarithmic growth phase). When the cells entered logarithmic phase, the plate was removed from the RTCA machine. The cells were washed once with PBS to remove any cell debris and either fresh medium containing a various concentration of complexes or fresh medium (control) was added to each well. The plate was reinserted into the RTCA machine and proliferation of the cells was further assessed every 15 for the next 24 hours.

6.4.9 Statistical analysis

Values are shown as the standard error of the mean unless indicated otherwise. Data were analyzed and, where appropriate, the significance of the differences between the mean values was determined using one-way *ANOVA*. A probability of 0.01 was deemed statistically significant. The following notation was used throughout: * $p < 0.01$, relative to control.

6.4.10 Mass spectrometry studies with model peptide

The BRCA1 peptide (10 µM) was incubated with RAPTA-C or RAPTA-EA) at a 1:1 and 1:5 protein:complex ratios at 4° C for 24 h. All incubations were performed in sterile MilliQ water. Incubated proteins were stored at -20 °C until analysis. Electron-Transfer Dissociation (ETD)

peptide fragmentation studies were performed on an ETD enabled hybrid linear ion trap (LTQ) Orbitrap Elite mass spectrometer (Thermo Scientific, Bremen, Germany) coupled to a Triversa Nanomate (Advion) chip-based electrospray system. The samples were infused using a spray voltage of 1.6 kV. The automatic gain control (AGC) target was set to $1x10^6$ for full scans in the Orbitrap mass analyzer. ETD experiments used fluoranthene as the reagent anion and the target for fluoranthene anions was set to $5x10^5$. Precursor ions for MS/MS were detected in the Orbitrap mass analyzer at a resolving power of 120,000 (at 400 m/z) with an isolation width of 3, and product ions were transferred to the FTMS operated with an AGC of $5x10^4$ over a *m/z* range of 200-2000. The reaction time with the fluoranthene radical anions into the LTQ was set from 50 to 100 ms. A minimum of 100 scans were averaged for each ETD fragmentation spectra. The Orbitrap FTMS was calibrated for the normal mass range keeping a mass accuracy in the 1-3 ppm level. Data were analyzed using the tool available at http://www.cheminfo.org.[180]

Chapter 7
Conclusions and perspectives

The MS strategies developed and applied in this thesis represent a range of novel approaches to study the mechanism of action of metallodrugs. The methods used in this work were chosen and adapted to the unique chemical nature of metallodrugs, which oftentimes are prodrugs with labile ligands and have a variety of biological targets. We chose to focus on three aspects of metallodrug action, namely their intracellular distribution and ligand state, their biological protein targets, and finally the nature of their binding to proteins.

With respect to the imaging ruthenium and platinum metallodrugs, we developed a NanoSIMS imaging MS approach to visualize both the distribution and ligand state of these compounds with isotopic labelling. We showed that for cisplatin, ovarian cancer cells resistant to the drug exhibit markedly reduced cellular accumulation and in drug sensitive cells, we found accumulation in the mitochondria and authophagosome. For RAPTA-T, we observed partial loss of the arene and possibly the phosphine ligand which could be involved in drug activation. RAPTA-T's distribution pattern was markedly different between ovarian and breast cancer cells, and we observed a larger extent of membrane association of the drug in invasive cancer cell lines, which could partly explain how RAPTA-T exerts its anti-metastatic activity.

For determining protein targets of metallodrugs, we applied a protein expression profiling approach FITExP, which applies biological controls and statistical correlations to overcome limitations of simple protein expression studies in finding *bone fide* protein targets of drugs. Through FITExP analysis, the main targets obtained for cisplatin were DNA repair related, which were in line with the main mechanism of cisplatin on nuclear DNA. For RAPTA-EA, the protein targets obtained were related to regulation of oxidative stress response and is thought to be conferred mainly by the ethacrynic acid moiety in the drug. This is in great contrast to the simple RAPTA-type complex RAPTA-T, which seemed to have a broad mechanism of action targeting proteins involved in both metastasis and tumorigenicity. We then cross validated the top two targets obtained from FITExP analysis of RAPTA-T namely MAT2A, which catalyzes the formation of S-adenosylmethionine a cellular methyl donor and PLD3 which catalyzes the hydrolysis of membrane phospholipids. We found RAPTA-T to be an uncompetitive inhibitor of MAT2A at an IC_{50} of ~75 μM, which suggests it could be useful for cancers where MAT2A is upregulated such as liver and colorectal cancers.

For studying the binding nature of metallodrugs to proteins, we realized a large bottleneck to the application of MS for these studies is the lack of tools for automated matching

of complex MS spectra from modified proteins. Thus, a major focus was on the development and optimization of such a tool, which we named the MSAPM tool. This tool was then applied to study the interaction of metallodrugs with two biologically relevant proteins, ubiquitin and BRCA1. With the aid of the tool, we revealed the complexity of the interactions of cisplatin and RAPTA-T with ubiquitin, where the metallodrug was potentially bound to more than 10 different sites. Through analysis of abundance of different metallated fragments obtained, we showed a preference of metal binding at more negatively charged regions on ubiquitin, and reason that this is due to the cationic nature of the metallodrug upon activation. For the zinc finger protein BRCA1, studying the interaction of RAPTA-C and RAPTA-EA on a 50 amino acid peptide mimicking the zinc finger region of the protein revealed that metallodrug binding occurred in close proximity to zinc binding sites which helped explain zinc displacement induced by these drugs. Overall, the tool greatly facilitated the use of MS in depth studies of metallodrug bound proteins.

Looking ahead, the work presented in this dissertation opened up some new avenues which can be explored further. For visualization of metal drugs via NanoSIMS, the methods we developed can be further applied to study biologically relevant problems for a myriad of different metallodrugs. Fundamental improvements in NanoSIMS methods such as improvement of cell sample integrity for analysis, increasing sensitivity for transition metals, improving spatial resolution and increasing analytical throughput should be pursued.

For elucidating biological targets of metallodrugs, approaches that identify protein targets based on perturbation of protein stability (briefly discussed in Chapter 1) could be explored as these possess all the advantages of the FITExP for metallodrugs but do not rely on the assumption of exceptional regulation during late apoptosis making it more generalizable. Much work remains on the validation of the RAPTA-T target MAT2A, as binding assays should be carried out and cell/tissue level enzyme inhibition of RAPTA-T should be performed. For PLD3 validation, owing to the lack of activity of the expressed protein, alternate methods must be found to study the effects of RAPTA-T on PLD3, such as performing activity assays in whole cells. The use of structural methods such as NMR or protein crystallography as well as computational methods could also be explored to validate these targets.

For the MSAPM tool, a major challenge remains with the processing of MS spectra of very large proteins as the theoretical possibilities of protein modifications increase

exponentially with size which would need to be solved by improving the processing algorithm used. Implementation of additional functions such as identifying c-z and c-y internal fragments for ETD fragmentation, additional enzyme digest options and matching polynucleotide modifications should also be explored. In addition, integration of this tool to a protein/peptide database such as MASCOT could facilitate the use of this tool in identification of metallated proteins in large protein mixtures, which is currently a major challenge.

Studying the mechanism of action of metallodrugs is an imposing challenge mainly due to the lack of good methods to perform these studies. The MS methods developed in this dissertation can be used to solve part of the puzzle, but should be complemented with other analytical, biophysical and biochemical methods to obtain the full picture of metallodrug action. We sincerely hope that the developments described here can be applied and further improved upon to create robust and reliable methods in elucidating the mechanism of action of metal based anti-cancer drugs

Appendix A
Tables of associated proteins obtained from FITExP analysis

Protein	Acronym	P-value	Regulation
Interstitial collagenase	MMP1	1.33E-06	Up
Pentraxin-related protein PTX3	PTX3	7.77E-06	Up
Protein-methionine sulfoxide oxidase MICAL2	MICAL2	1.87E-04	Down
Membrane-associated tyrosine- and threonine-specific cdc2-inhibitory kinase	I3L1V2	2.41E-04	Down
Transforming growth factor beta-1-induced transcript 1 protein	TGFB1I1	3.35E-04	Down
Tubulin beta-2A chain	TUBB2A	4.81E-04	Up
Stathmin	STMN1	7.28E-04	Down
Tubulin beta-6 chain	TUBB6	9.47E-04	Up
Cysteine-rich motor neuron 1 protein	CRIM1	1.70E-03	Down
Transforming acidic coiled-coil-containing protein 1	G8JLK4	1.84E-03	Down
Protein Niban	NIBAN	4.30E-03	Down
Ubiquitin-conjugating enzyme E2 C	UBE2C	4.93E-03	Down
MAP7 domain-containing protein 1	MAP7D1	5.36E-03	Up
Nucleolar complex protein 3 homolog	A6NJZ9	6.27E-03	Down
Rac GTPase-activating protein 1	RACGAP1	6.83E-03	Down
Calmodulin-regulated spectrin-associated protein 3	CAMSAP3	1.00E-02	Up
Microtubule-associated protein RP/EB family member 2	G5E9I6	1.31E-02	Up
Anterior gradient protein 2 homolog	B5MC07	1.31E-02	Up
Insulin-like growth factor-binding protein 7	IGFBP7	1.43E-02	Up
Protein kinase C and casein kinase substrate in neurons protein 3	PACSIN3	1.81E-02	Down
Protein GREB1	GREB1	1.88E-02	Up
Discoidin, CUB and LCCL domain-containing protein 2	DCBLD2	1.93E-02	Down
Cyclin-dependent kinase 1	CDK1	1.96E-02	Down
Monocarboxylate transporter 4	MCT4	2.09E-02	Down
KN motif and ankyrin repeat domain-containing protein 2	KANK2	2.16E-02	Down
Cysteine and glycine-rich protein 2	F8VW96	2.32E-02	Up
Tubulin beta-3 chain	TUBB3	3.43E-02	Up
Unconventional myosin-Vc	MYO5C	3.86E-02	Down
Tubulin alpha-4A chain	A8MUB1	3.97E-02	Up
Lysine-rich nucleolar protein 1	KNOP1	4.24E-02	Down
EPH receptor B4, isoform CRA_b	Q96L35	4.89E-02	Up

Table A.1 Associated protein list for Paclitaxel obtained from FITExP analysis.

Protein	Acronym	P-value	Regulation
Growth/differentiation factor 15	GDF15	4.01E-11	Up
Heat shock 70 kDa protein 6	HSPA6	1.54E-09	Down
Threonylcarbamoyladenosine tRNA methylthiotransferase	CDKAL1	3.22E-07	Down
Interstitial collagenase	MMP1	1.13E-06	Up
Methylated-DNA--protein-cysteine methyltransferase	MGMT	3.06E-05	Down
Brain-specific angiogenesis inhibitor 1-associated protein 2-like protein 1	BAIAP2L1	9.67E-05	Up
Desmocollin-2	DSC2	1.14E-04	Up
Protein GREB1	GREB1	1.39E-04	Down
Ladinin-1	LAD1	1.58E-04	Up
60S ribosomal protein L7-like 1	RPL7L1	2.30E-04	Down
Protein S100-P	S100P	3.00E-04	Up
Receptor tyrosine-protein kinase erbB-2	ERBB2	3.84E-04	Up
Insulin-like growth factor-binding protein 7	IGFBP7	4.70E-04	Down
Protein LLP homolog	LLPH	7.96E-04	Down
F-box/WD repeat-containing protein 7	B7Z2C8	1.03E-03	Down
Integrin alpha-6 heavy chain (Fragment)	C9JK10	1.14E-03	Down
Tubulin beta-2A chain	TUBB2A	1.29E-03	Up
Ubiquitin-like protein ISG15	ISG15	1.58E-03	Up
Probable dimethyladenosine transferase	DIMT1	1.61E-03	Down
DNA damage-binding protein 2	DDB2	1.77E-03	Up
Syntaxin-8	STX8	2.06E-03	Down
Alpha-2-HS-glycoprotein	FETUA	2.56E-03	Up
Epidermal growth factor receptor kinase substrate 8-like protein 1	Eps8l1	2.97E-03	Up
Pumilio domain-containing protein KIAA0020	KIAA0020	4.15E-03	Down
Cyclin-dependent kinase inhibitor 1B	CDKN1B	4.33E-03	Up
U3 small nucleolar RNA-associated protein 14 homolog A	E9PEL7	4.41E-03	Down
HEAT repeat-containing protein 6	K7EIX2	5.01E-03	Down
Beta-1-syntrophin	SNTB1	6.63E-03	Down
60S ribosomal protein L7	RPL7	7.47E-03	Down
DNA polymerase	A6NMQ1	7.58E-03	Down
Anthrax toxin receptor 2	J3KPY9	8.06E-03	Down
LIM and calponin homology domains-containing protein 1 (Fragment)	H0Y8P3	9.98E-03	Down
Ferritin light chain	FTL	1.04E-02	Up
C-terminal 80 kDa form (Fragment)	H0YDM2	1.11E-02	Down
cAMP-dependent protein kinase inhibitor beta	Q5T0Z6	1.32E-02	Down
Taperin	TPRN	1.33E-02	Up
Epiplakin	EPIPL	1.42E-02	Up
NADPH:adrenodoxin oxidoreductase, mitochondrial	E7EQC1	1.53E-02	Up
Trans-acting T-cell-specific transcription factor GATA-3	GATA3	1.53E-02	Down
HLA class II histocompatibility antigen gamma chain	E7ESL3	1.61E-02	Up
MARCKS-related protein	MRP	1.86E-02	Up
Retrotransposon-derived protein PEG10	PEG10	2.05E-02	Up

Kinesin-like protein KIF20A	B4DL79	2.08E-02	Up
39S ribosomal protein L17, mitochondrial	MRPL17	2.34E-02	Up
EPH receptor B4, isoform CRA_b	Q96L35	2.69E-02	Up
Rho guanine nucleotide exchange factor 5	ARHGEF5	2.96E-02	Up
Tubulin beta-3 chain	TUBB3	3.00E-02	Up
Epiplakin	E9PPU0	3.48E-02	Up
Protein HEXIM1	HEXIM1	3.70E-02	Up
RNA-binding protein with multiple-splicing	F5H357	3.85E-02	Down
Claspin	CLSPN	3.91E-02	Up
60S ribosomal protein L36	RPL36	4.17E-02	Down
Nuclear factor NF-kappa-B p100 subunit	NFKB2	4.43E-02	Up
Tetratricopeptide repeat protein 38	E7ES35	4.48E-02	Down
Protein KTI12 homolog	KTI12	4.54E-02	Up
Molybdopterin molybdenumtransferase	G3V582	4.69E-02	Down

Table A.2 Associated protein list for Cisplatin obtained from FITExP analysis

Protein	Acronym	P-value	Regulation
Heme oxygenase 1	HMOX1	1.64E-08	Up
Heat shock 70 kDa protein 1A/1B	HSP71	5.85E-07	Up
ATP-binding cassette sub-family B member 6, mitochondrial (Fragment)	H7BXK9	7.04E-07	Up
All-trans-retinol 13,14-reductase (Fragment)	H7C3J0	2.31E-06	Down
TRAF-type zinc finger domain-containing protein 1	TRAFD1	3.74E-06	Up
Sequestosome-1	SQSTM1	4.18E-05	Up
Probable ATP-dependent RNA helicase DDX58	F5H5W6	5.36E-05	Down
Actin filament-associated protein 1-like 2	F5GZE1	6.72E-05	Down
Protein POF1B	POF1B	8.45E-05	Down
Torsin-4A	TOR4A	1.03E-04	Down
Sulfiredoxin-1	SRXN1	1.95E-04	Up
Chloride intracellular channel protein 6	CLIC6	2.31E-04	Up
DNA polymerase subunit gamma-1	POLG	2.57E-04	Down
Gasdermin-D (Fragment)	E9PIB2	5.60E-04	Down
DnaJ homolog subfamily B member 4	DNAJB4	7.26E-04	Up
NAD(P)H dehydrogenase [quinone] 1	B4DLR8	1.29E-03	Up
Transforming growth factor beta-1-induced transcript 1 protein	TGFB1I1	1.35E-03	Down
Thioredoxin reductase 1, cytoplasmic	E7ESI6	1.89E-03	Up
Plasminogen activator inhibitor 1	PAI1	2.05E-03	Up
Glutamate--cysteine ligase regulatory subunit	GCLM	2.97E-03	Up
Cytochrome c oxidase copper chaperone	C9J8T6	3.55E-03	Down
Heat shock 70 kDa protein 4L	E7ES43	4.25E-03	Up
Lamina-associated polypeptide 2, isoform alpha	TMPO	4.60E-03	Down
General transcription factor 3C polypeptide 5	H7BY84	4.80E-03	Down
Cysteine and histidine-rich domain-containing protein 1	E9PPQ5	5.29E-03	Up
HAUS augmin-like complex subunit 8	C9JBZ4	5.90E-03	Down
Heat shock protein 105 kDa	HSPH1	6.08E-03	Up

Tubulin beta-4A chain	TUBB4A	6.10E-03	Down
Poly(A) RNA polymerase, mitochondrial	PAPD1	6.91E-03	Down
UDP-glucose 6-dehydrogenase	UGDH	7.60E-03	Up
BRCA1-associated ATM activator 1	BRAT1	7.87E-03	Down
Flavin reductase (NADPH)	BLVRB	8.63E-03	Up
DnaJ homolog subfamily B member 1	DNAJB1	9.58E-03	Up
Sorting nexin-18	SNX18	9.73E-03	Down
5'-nucleotidase domain-containing protein 2	E9PAL9	1.02E-02	Down
Tripeptidyl-peptidase 1	TPP1	1.49E-02	Up
Sterol O-acyltransferase 1 (Fragment)	B1APM4	1.55E-02	Up
Interferon-induced protein with tetratricopeptide repeats 3	IFIT3	1.56E-02	Down
SAGA-associated factor 29 homolog	SGF29	1.81E-02	Down
Cadherin EGF LAG seven-pass G-type receptor 2	CELSR2	1.82E-02	Down
Kinesin-like protein KIF20A	B4DL79	1.85E-02	Down
TBC1 domain family member 15 (Fragment)	C9JA93	1.86E-02	Up
Annexin A6	ANXA6	2.21E-02	Down
Protein FAM83B	FAM83B	2.60E-02	Down
Trans-acting T-cell-specific transcription factor GATA-3	GATA3	3.22E-02	Down
NADP-dependent malic enzyme	ME1	3.25E-02	Up
Mitochondrial genome maintenance exonuclease 1	MGME1	3.72E-02	Down
Threonine--tRNA ligase, mitochondrial	TARS2	3.90E-02	Down
Protein S100-A4	S100A4	4.13E-02	Down
Coiled-coil-helix-coiled-coil-helix domain-containing protein 1	CHCHD1	4.31E-02	Down
Glucose-6-phosphate 1-dehydrogenase	G6PD	4.39E-02	Up
Insulin-like growth factor-binding protein 4	B4E351	4.49E-02	Down
Ly6/PLAUR domain-containing protein 3	LYPD3	4.84E-02	Up
Heat shock protein HSP 90-alpha	HSP90AA1	4.84E-02	Up

Table A.3 Associated protein list for RAPTA-EA obtained from FITExP analysis

Protein	Acronym	P-value	Regulation
EGF-like repeat and discoidin I-like domain-containing protein 3	EDIL3	3.22E-09	Up
N-terminal Xaa-Pro-Lys N-methyltransferase 1	NTM1A	1.26E-07	Down
Squalene monooxygenase	ERG1	2.66E-06	Down
All-trans-retinol 13,14-reductase (Fragment)	H7C3J0	7.80E-06	Down
Histone-lysine N-methyltransferase SETD7	SETD7	1.45E-05	Down
S-adenosylmethionine synthase isoform type-2	MAT2A	1.46E-05	Up
Protein GREB1	GREB1	3.09E-05	Down
Ribosomal RNA small subunit methyltransferase NEP1	EMG1	3.23E-05	Down
Metallothionein-2	MT2	1.02E-04	Up
Chromosome transmission fidelity protein 8 homolog isoform 2	CHTF8	1.02E-04	Up
Ubiquitin-conjugating enzyme E2 T	UBE2T	1.89E-04	Down
Alpha-2-HS-glycoprotein	FETUA	2.58E-04	Up
Programmed cell death protein 4	PDCD4	2.62E-04	Up

Chromatin target of PRMT1 protein	CHTOP	2.84E-04	Up
BolA-like protein 1	BOLA1	4.21E-04	Up
Torsin-4A	TOR4A	6.35E-04	Up
Claspin	CLSPN	6.41E-04	Down
Ribonucleoside-diphosphate reductase subunit M2	RRM2B	7.75E-04	Down
Retrotransposon-derived protein PEG10	PEG10	1.08E-03	Down
Laminin subunit beta-3	LAMB3	1.08E-03	Down
Heat shock protein beta-8	HSPB8	1.39E-03	Down
Sperm-associated antigen 5	SPAG5	1.71E-03	Down
Importin subunit alpha-2	KPNA2	1.74E-03	Down
Phospholipase D3	PLD3	1.88E-03	Up
40S ribosomal protein S4, Y isoform 1 (Fragment)	C9JEH7	1.97E-03	Down
G2 and S phase-expressed protein 1	GTSE1	3.08E-03	Down
RNA-binding protein 47	RBM47	3.65E-03	Up
Zinc finger HIT domain-containing protein 2	ZNHIT2	1.25E-02	Up
Biogenesis of lysosome-related organelles complex 1 subunit 3	BLOC1S3	1.28E-02	Up
DnaJ homolog subfamily A member 4	F5H170	1.71E-02	Down
Proteasome subunit beta type-10 (Fragment)	J3QQN1	1.82E-02	Up
[Pyruvate dehydrogenase [acetyl-transferring]]-phosphatase 1, mitochondrial	PDP1	2.30E-02	Up
BAG family molecular chaperone regulator 1	J3QTA2	2.39E-02	Up
Hydroxymethylglutaryl-CoA synthase, cytoplasmic	HMGCS1	2.53E-02	Down
Myeloid leukemia factor 2	MLF2	2.67E-02	Down
Neuropilin-1	Q5T7F1	2.78E-02	Up
Desmocollin-2	DSC2	3.27E-02	Down
DnaJ homolog subfamily A member 1	DNAJA1	3.30E-02	Down
Nitric oxide synthase-interacting protein (Fragment)	NOSIP	3.58E-02	Down
Hepatocyte nuclear factor 3-alpha	B7ZAP5	3.67E-02	Up
E3 ubiquitin-protein ligase AMFR	AMFR	4.70E-02	Down
Phosphoserine aminotransferase	PSAT1	4.70E-02	Up

Table A.4 Associated protein list for RAPTA-T obtained from FITExP analysis

Appendix B
Tables of metallated fragment from MS/MS experiments of metallodrugs on ubiquitin

Metallated adduct	Similarity	Abundance	Type	Theoretical mass	Experimental mass	PPM Error
[3H + PtN2H8O + b74y36]5+	87.2	2.76	R	4243.2670	4243.2642	-0.65
[H + PtN2H6 + a57y36]3+	83.9	2.17	R	2116.0869	2116.0853	-0.78
[H + PtNH3 + a55y38]3+	83.9	2.54	R	2142.0298	2142.0282	-0.77
[PtN2H8O + b74y25]4+	81.9	5.65	R	2956.5085	2956.5063	-0.74
[PtN2H8O + b74y16]2+	76.1	2.98	R	1935.0620	1935.0609	-0.57
[3H + PtN2H6 + a71y56]7+	70.9	2.40	R	5991.1186	5991.1147	-0.64
[Pt + b18]3+	97.3	17.73	L	2228.1005	2228.0988	-0.74
[PtNH3 + b16]3+	92.9	3.48	L	2017.0160	2017.0144	-0.82
[PtN2H6 + a28y67]2+	91.7	3.36	L	2227.0938	2227.0927	-0.49
[PtNH3 + a22y71]2+	90.4	5.21	L	1998.9716	1998.9705	-0.55
[PtNH3 + a17]3+	88.5	2.13	L	2088.0895	2088.0879	-0.79
[Pt + b33y58]3+	88.5	3.49	L	1862.8616	1862.8600	-0.88
[PtN2H6 + a23y70]3+	82.8	2.14	L	2000.9872	2000.9856	-0.82
[Pt + a17]3+	79.6	4.47	L	2071.0630	2071.0613	-0.79
[H + Pt + a21y72]3+	79.5	2.13	L	1980.9736	1980.9719	-0.83
[2H + Pt + a30y74]4+	75.2	2.70	L	3238.7307	3238.7285	-0.68
[PtN2H6 + b28y66]2+	75.1	3.93	L	2198.0673	2198.0662	-0.50
[H + PtN2H8O + a29y65]3+	72.6	1.56	L	2189.0907	2189.0891	-0.75
[PtN2H8O + a29y65]2+	72.5	3.33	L	2188.0829	2188.0818	-0.50
[H + PtN2H6 + b29y65]3+	70.6	9.61	L	2199.0751	2199.0734	-0.75
[PtN2H6 + a30y63]2+	70.1	2.57	L	2069.0247	2069.0236	-0.53
[5H + PtN2H6 + y58]8+	98.3	84.47	M	6762.5537	6762.5493	-0.65
[6H + PtNH3 + y58]9+	96.2	9.92	M	6746.5350	6746.5300	-0.73
[4H + PtNH3 + b52]7+	95.9	12.85	M	6051.1484	6051.1446	-0.63
[7H + Pt + y74]10+	95.6	5.81	M	8503.5450	8503.5396	-0.65
[5H + PtNH3 + y58]8+	95.2	39.73	M	6745.5272	6745.5228	-0.65
[6H + PtN2H6 + y58]9+	94.9	21.39	M	6763.5615	6763.5566	-0.73
[7H + PtN2H6 + y74]10+	94.8	6.50	M	8537.5981	8537.5927	-0.64
[5H + Pt + y58]8+	94.2	30.32	M	6728.5006	6728.4962	-0.65
[5H + PtN2H8O + b64y71]8+	94.1	9.65	M	6873.5732	6873.5688	-0.64
[4H + Pt + b52]7+	92.2	6.80	M	6034.1219	6034.1180	-0.64
[6H + Pt + y58]9+	91.6	7.22	M	6729.5084	6729.5035	-0.73
[3H + Pt + a63y72]7+	91.4	5.08	M	6761.5248	6761.5209	-0.57
[6H + PtNH3 + b64y71]8+	91.3	5.72	M	6839.5439	6839.5395	-0.64
[6H + Pt + b71y64]8+	90.7	5.56	M	6856.5381	6856.5337	-0.64
[6H + PtN2H8O + b64y71]9+	90.6	3.79	M	6874.5810	6874.5760	-0.72
[4H + PtNH3 + y58]7+	89.9	2.80	M	6744.5193	6744.5155	-0.57
[6H + Pt + b61y73]8+	89.7	2.16	M	6683.4580	6683.4536	-0.66

[4H + PtN2H6 + b52]7+	88.2	4.49	M	6068.1750	6068.1711	-0.63
[6H + PtNH3 + y74]10+	85.7	6.40	M	8519.5638	8519.5583	-0.64
[4H + Pt + a64y72]8+	84.6	2.02	M	6891.5752	6891.5708	-0.64
[6H + PtN2H8O + b63y73]8+	83.6	2.33	M	6991.6752	6991.6708	-0.63
[2H + PtN2H6 + a70y44]5+	83.6	3.08	M	4522.3174	4522.3147	-0.61
[4H + PtN2H6 + a72y61]8+	83.5	2.61	M	6689.4659	6689.4615	-0.66
[6H + PtN2H6 + b60y74]8+	82.4	4.61	M	6717.5111	6717.5067	-0.65
[6H + PtN2H6 + b73y60]8+	82.1	4.51	M	6703.5179	6703.5135	-0.65
[4H + Pt + y58]7+	81.5	2.79	M	6727.4928	6727.4889	-0.57
[6H + Pt + y75]10+	81.3	2.67	M	8630.5958	8630.5903	-0.64
[7H + PtNH3 + b63y71]9+	79.6	1.15	M	6711.5091	6711.5042	-0.74
[7H + PtN2H6 + b64y72]9+	79.6	3.23	M	6956.6467	6956.6417	-0.71
[H + PtN2H8O + a54y40]3+	78.6	15.91	M	2270.1248	2270.1231	-0.72
[6H + PtNH3 + y60]8+	78.2	1.58	M	6974.6460	6974.6416	-0.63
[3H + PtN2H6 + b52y62]5+	78.0	2.83	M	4505.2770	4505.2742	-0.61
[PtN2H8O + b56y44]4+	77.3	1.20	M	2938.4867	2938.4845	-0.75
[5H + Pt + y60]8+	76.1	1.39	M	6956.6116	6956.6072	-0.63
[3H + PtN2H6 + b50y75]6+	76.0	1.62	M	5692.0571	5692.0538	-0.58
[5H + Pt + y59]9+	75.9	1.32	M	6857.5432	6857.5383	-0.72
[7H + PtN2H8O + b64y72]9+	74.7	1.58	M	6974.6572	6974.6523	-0.71
[6H + PtN2H8O + a71y62]8+	73.9	2.50	M	6666.4751	6666.4707	-0.66
[5H + PtN2H8O + a68y67]9+	73.1	1.81	M	6840.5265	6840.5216	-0.72
[6H + PtN2H6 + a65y69]8+	72.4	2.61	M	6686.4649	6686.4605	-0.66
[6H + PtN2H8O + a61y73]9+	71.3	1.56	M	6707.5268	6707.5218	-0.74
[3H + Pt + a52]7+	71.3	0.81	M	6005.1191	6005.1153	-0.64
[5H + PtNH3 + a61y73]8+	71.1	2.25	M	6671.4818	6671.4774	-0.66
[7H + PtNH3 + b61y73]9+	70.8	0.25	M	6701.4924	6701.4875	-0.74
[5H + PtN2H8O + b61y66]7+	70.2	5.72	M	5988.0812	5988.0773	-0.64
[8H + PtN2H6 + b74]10+	70.2	4.49	M	8665.6515	8665.6460	-0.63

Table B.1 Most important metallated fragments obtained by CID fragmentation of the adduct [9H+ Ubiquitin + $PtN_2H_8O]^{11+}$ (m/z 801.4281) after incubation of ubiquitin with cisplatin (1:1, protein:drug ratio). Similarities are expressed as percentages, abundances are expressed as percentage of the most abundant peak in the spectra, and type is classified based on criteria in Figure 5.6.

Metallated adduct	Similarity	Abundance	Type	Theoretical mass	Experimental mass	PPM Error
[H + PtN2H6 + y24]4+	96.3	5.04	R	2956.5323	2956.5301	-0.74
[H + PtNH3 + y24]4+	96.2	2.07	R	2939.5057	2939.5035	-0.75
[Pt + b74y19]3+	93.5	0.82	R	2275.1315	2275.1299	-0.72
[H + PtNH3 + b74y25]4+	93.1	1.44	R	2922.4792	2922.4770	-0.75
[3H + PtN2H6 + y37]6+	92.9	0.95	R	4485.3685	4485.3652	-0.73
[H + Pt + a57y37]3+	91.6	1.42	R	2210.0924	2210.0908	-0.74
[Pt + b57y35]2+	91.1	1.35	R	1980.9623	1980.9612	-0.55
[PtN2H6 + y18]3+	89.1	0.59	R	2326.2112	2326.2095	-0.71
[H + PtN2H6 + a62y34]3+	88.8	0.37	R	2465.2031	2465.2014	-0.67

[Pt + a57y37]2+	88.6	0.90	R	2209.0846	2209.0835	-0.50
[PtN2H6 + b62y24]2+	88.3	0.34	R	1377.5879	1377.5868	-0.80
[H + Pt + a73y21]3+	87.3	0.79	R	2292.1594	2292.1578	-0.72
[H + PtN2H6 + a59y36]3+	85.8	0.39	R	2394.1772	2394.1755	-0.69
[2H + PtN2H6 + y37]5+	85.8	0.86	R	4484.3606	4484.3579	-0.61
[H + PtNH3 + y26]3+	74.3	0.39	R	3183.5753	3183.5736	-0.52
PtNH3 + b18]3+	97.1	3.10	L	2245.1270	2245.1254	-0.73
[PtN2H6 + a28y67]2+	96.7	4.60	L	2227.0938	2227.0927	-0.49
[Pt + b18]3+	96.7	9.95	L	2228.1005	2228.0988	-0.74
[PtNH3 + a17]3+	95.5	1.45	L	2088.0895	2088.0879	-0.79
[Pt + a17]3+	94.4	2.56	L	2071.0630	2071.0613	-0.79
[PtNH3 + b16]3+	94.4	2.09	L	2017.0160	2017.0144	-0.82
[PtNH3 + b17]3+	93.0	1.35	L	2116.0844	2116.0828	-0.78
[Pt + b36]3+	91.9	0.49	L	4194.1376	4194.1359	-0.39
[Pt + b16]3+	91.2	1.26	L	1999.9895	1999.9878	-0.82
[2H + PtNH3 + b33]5+	90.7	0.62	L	3914.0317	3914.0289	-0.70
[PtNH3 + b21]3+	88.6	1.36	L	2544.2388	2544.2371	-0.65
[Pt + b33y58]3+	86.0	0.72	L	1862.8616	1862.8600	-0.88
[PtN2H8O + b21y68]2+	85.9	1.03	L	1618.7292	1618.7281	-0.68
[Pt + b32]3+	82.3	0.26	L	3766.8945	3766.8929	-0.44
[Pt + a20]3+	82.0	0.56	L	2384.1903	2384.1887	-0.69
[Pt + b39]4+	82.0	1.51	L	4503.2701	4503.2679	-0.49
[PtNH3 + b36]3+	81.7	0.36	L	4211.1641	4211.1625	-0.39
[PtNH3 + a20]3+	80.3	0.40	L	2401.2169	2401.2152	-0.69
[H + Pt + b32]4+	79.9	1.43	L	3767.9023	3767.9001	-0.58
[Pt + a33y58]3+	79.1	0.26	L	1834.8667	1834.8651	-0.90
[PtN2H6 + b18]3+	78.5	0.37	L	2262.1536	2262.1519	-0.73
[PtNH3 + a24y72]2+	77.6	0.30	L	2340.1666	2340.1655	-0.47
[Pt + a18]3+	77.5	1.78	L	2200.1056	2200.1039	-0.75
[PtNH3 + a35y54]2+	75.3	0.33	L	1637.7979	1637.7968	-0.67
[Pt + a15]3+	71.4	0.27	L	1842.9520	1842.9503	-0.89
[Pt + b11]2+	71.1	0.66	L	1442.6834	1442.6823	-0.76
[5H + PtN2H8O + b63y71]7+	98.4	32.43	M	6744.5306	6744.5267	-0.57
[3H + PtNH3 + b52]6+	98.1	4.84	M	6050.1406	6050.1373	-0.54
[4H + Pt + y58]7+	97.9	35.57	M	6727.4928	6727.4889	-0.57
[3H + PtN2H6 + b52]6+	97.9	7.03	M	6067.1672	6067.1639	-0.54
[5H + PtN2H6 + y58]8+	97.5	15.39	M	6762.5537	6762.5493	-0.65
[5H + Pt + y58]8+	97.2	10.98	M	6728.5006	6728.4962	-0.65
[5H + PtNH3 + y58]8+	96.9	10.27	M	6745.5272	6745.5228	-0.65
[6H + PtN2H6 + b64y71]8+	96.6	1.99	M	6856.5704	6856.5660	-0.64
[4H + PtN2H6 + y58]7+	96.1	49.31	M	6761.5459	6761.5420	-0.57
[5H + PtN2H8O + b64y71]8+	96.0	3.12	M	6873.5732	6873.5688	-0.64
[4H + PtN2H8O + b63y71]6+	96.0	1.40	M	6743.5227	6743.5194	-0.49
[3H + Pt + b52]6+	95.7	8.46	M	6033.1141	6033.1108	-0.55
[6H + Pt + y74]9+	95.4	5.92	M	8502.5372	8502.5323	-0.58
[6H + PtNH3 + b64y7]8+	95.4	2.35	M	6839.5439	6839.5395	-0.64

[4H + Pt + y60]7+	95.1	3.38	M	6955.6038	6955.5999	-0.55
[4H + Pt + y62]7+	94.3	0.62	M	7197.7304	7197.7266	-0.53
[3H + Pt + y58]6+	94.1	1.23	M	6726.4850	6726.4817	-0.49
[5H + PtNH3 + b64y71]7+	93.6	3.35	M	6838.5360	6838.5322	-0.56
[5H + Pt + b71y64]7+	93.3	5.29	M	6855.5302	6855.5264	-0.56
[3H + PtN2H8O + a61y67]6+	92.8	2.19	M	6015.0921	6015.0888	-0.55
[3H + PtN2H8O + b68y70]7+	92.7	0.57	M	7181.6852	7181.6814	-0.53
[2H + PtN2H8O + b69y42]4+	92.6	1.68	M	4212.1169	4212.1147	-0.52
[3H + PtNH3 + y61]7+	92.5	1.65	M	7100.6651	7100.6613	-0.54
[4H + PtNH3 + y60]7+	92.3	2.74	M	6972.6303	6972.6265	-0.55
[5H + PtNH3 + y62]7+	91.9	0.45	M	7215.7648	7215.7610	-0.53
[6H + PtN2H6 + y74]9+	91.6	5.48	M	8536.5903	8536.5854	-0.58
[H + PtN2H6 + a70y44]4+	91.6	0.41	M	4521.3096	4521.3074	-0.49
[5H + PtNH3 + b63y71]7+	91.4	8.14	M	6709.4935	6709.4896	-0.57
[4H + PtN2H6 + y60]7+	91.3	6.07	M	6989.6569	6989.6530	-0.55
[2H + Pt + b63y58]5+	91.2	0.58	M	5275.6355	5275.6328	-0.52
[6H + Pt + y73]9+	91.1	2.27	M	8389.4532	8389.4482	-0.59
[6H + PtNH3 + y74]9+	91.1	5.92	M	8519.5638	8519.5588	-0.58
[3H + PtN2H6 + b52y62]5+	90.5	0.88	M	4505.2770	4505.2742	-0.61
[3H + PtN2H6 + y58]6+	90.2	1.84	M	6760.5381	6760.5348	-0.49
[4H + Pt + y63]7+	90.1	0.57	M	7298.7781	7298.7743	-0.53
[4H + PtNH3 + b64y70]6+	90.0	0.34	M	6709.4333	6709.4300	-0.49
[H + PtN2H6 + b55y68]5+	89.2	0.59	M	5418.7751	5418.7724	-0.51
[2H + PtN2H8O + a57y58]4+	89.2	1.86	M	4538.3335	4538.3313	-0.48
[5H + Pt + a63]8+	89.0	1.96	M	7282.7919	7282.7876	-0.60
[3H + PtNH3 + y40]6+	88.9	0.26	M	4777.4744	4777.4711	-0.69
[2H + PtN2H8O + a48y61]4+	88.8	10.78	M	3895.9886	3895.9864	-0.56
[4H + PtN2H6 + y59]7+	88.8	5.41	M	6890.5885	6890.5846	-0.56
[5H + PtN2H6 + a60y72]7+	88.3	0.66	M	6428.3559	6428.3521	-0.60
[5H + Pt + b69y66]7+	88.2	4.33	M	6872.5204	6872.5166	-0.56
[4H + Pt + y44]7+	88.1	0.31	M	5188.6987	5188.6949	-0.74
[5H + PtNH3 + b58]7+	87.8	2.95	M	6681.4695	6681.4657	-0.57
[4H + Pt + y61]7+	87.6	2.34	M	7084.6464	7084.6425	-0.54
[6H + PtNH3 + a63y73]8+	86.4	0.37	M	6928.6432	6928.6388	-0.63
[3H + PtN2H6 + a63y66]7+	86.2	0.35	M	6196.2136	6196.2097	-0.62
[5H + PtN2H6 + y62]7+	86.0	0.56	M	7232.7914	7232.7875	-0.53
[5H + Pt + y62]8+	85.9	0.52	M	7198.7383	7198.7339	-0.61
[4H + PtNH3 + b63y73]6+	84.8	0.17	M	6954.6225	6954.6192	-0.47
[3H + PtNH3 + b62y74]7+	84.7	1.21	M	6938.6037	6938.5999	-0.55
[5H + Pt + y60]8+	84.3	0.75	M	6956.6116	6956.6072	-0.63
[4H + Pt + y65]8+	84.3	0.75	M	7512.9099	7512.9055	-0.58
[6H + Pt + b63y73]8+	83.8	0.84	M	6939.6116	6939.6072	-0.63
[2H + Pt + b46]5+	83.7	0.55	M	5361.7776	5361.7749	-0.51
[6H + PtN2H8O + a70y63]8+	83.6	0.45	M	6654.4387	6654.4343	-0.66
[PtN2H8O + a44y71]4+	83.6	0.36	M	4547.4052	4547.4031	-0.48
[2H + PtNH3 + b48]5+	83.5	0.50	M	5563.9206	5563.9179	-0.49

[4H + PtNH3 + a59y75]8+	83.0	1.02	M	6684.4896	6684.4853	-0.66
[4H + Pt + b64y71]8+	82.9	1.37	M	6820.5017	6820.4973	-0.64
[5H + PtN2H8O + a69]8+	82.9	0.66	M	8015.2049	8015.2006	-0.55
[5H + PtNH3 + b58]8+	82.3	0.71	M	6681.4695	6681.4652	-0.66
[5H + PtNH3 + a69y67]7+	82.2	0.51	M	6918.5735	6918.5697	-0.56
[7H + Pt + b74y74]9+	82.2	1.38	M	8371.4915	8371.4866	-0.59
[3H + PtN2H8O + b42y72]6+	82.1	0.39	M	4451.3239	4451.3206	-0.74
[5H + PtN2H6 + b73y60]8+	82.1	0.86	M	6702.5101	6702.5057	-0.65
[5H + PtN2H6 + b58]7+	81.7	2.39	M	6698.4961	6698.4923	-0.57
[3H + PtN2H8O + a75y57]7+	80.9	1.06	M	6578.4689	6578.4651	-0.58
[5H + Pt + b74y58]8+	80.7	0.37	M	6596.4471	6596.4427	-0.67
[4H + PtNH3 + a61y73]8+	79.7	0.86	M	6670.4740	6670.4696	-0.66
[5H + PtN2H6 + b68y71]8+	79.6	0.38	M	7293.7853	7293.7809	-0.60
[3H + Pt + b62y7]7+	79.4	0.98	M	7049.6358	7049.6319	-0.54
[2H + PtN2H6 + b43y56]4+	79.3	0.37	M	2848.4285	2848.4263	-0.77
[2H + Pt + b44y67]4+	79.2	0.98	M	4082.0778	4082.0756	-0.54
[7H + PtN2H6 + b74]9+	79.0	1.29	M	8664.6437	8664.6388	-0.57
[4H + PtN2H6 + b73y60]7+	78.9	2.39	M	6701.5023	6701.4984	-0.57
[H + Pt + y44]5+	78.3	0.45	M	5185.6753	5185.6725	-0.53
[3H + Pt + b62y74]7+	78.3	0.58	M	6921.5772	6921.5733	-0.55
[4H + PtNH3 + a63]8+	78.1	0.85	M	7298.8107	7298.8063	-0.60
[6H + Pt + a70y68]8+	77.9	1.39	M	7102.6709	7102.6665	-0.62
[4H + PtN2H6 + b58y73]6+	77.7	0.45	M	6325.3051	6325.3019	-0.52
[3H + PtNH3 + b62y75]7+	77.5	1.71	M	7066.6623	7066.6585	-0.54
[8H + PtN2H8O + b74]10+	77.4	0.23	M	8683.6621	8683.6566	-0.63
[2H + PtN2H8O + a59y43]4+	77.4	0.15	M	3149.5347	3149.5326	-0.70
[6H + Pt + y75]10+	77.4	0.98	M	8630.5958	8630.5903	-0.64
[5H + PtN2H8O + b74y74]9+	76.8	11.94	M	8421.5396	8421.5346	-0.59
[5H + PtN2H6 + y59]8+	76.7	0.70	M	6891.5963	6891.5919	-0.64
[Pt + b52y58]3+	76.3	0.21	M	3997.9627	3997.9611	-0.41
[5H + Pt + a72y57]7+	75.9	0.89	M	6202.2143	6202.2104	-0.62
[6H + PtN2H6 + b58]8+	75.8	0.86	M	6699.5039	6699.4995	-0.66
[7H + Pt + y74]10+	75.6	0.64	M	8503.5450	8503.5396	-0.65
[6H + Pt + y72]9+	75.3	0.43	M	8242.3847	8242.3798	-0.60
[4H + PtN2H8O + a61y69]7+	75.3	1.37	M	6230.2316	6230.2278	-0.62
[5H + PtNH3 + a74y75]9+	75.1	3.69	M	8486.5661	8486.5612	-0.58
[4H + PtNH3 + y56]7+	75.0	1.22	M	6560.4345	6560.4307	-0.59
[4H + Pt + y61]8+	74.8	0.38	M	7084.6464	7084.6420	-0.62
[6H + PtN2H6 + a68y67]8+	74.8	0.66	M	6823.5238	6823.5194	-0.64
[5H + Pt + b74y64]7+	74.8	0.46	M	7280.8165	7280.8127	-0.53
[4H + Pt + y54]7+	74.6	0.57	M	6327.3334	6327.3295	-0.61
[4H + PtNH3 + a61y75]7+	74.4	0.50	M	6911.6166	6911.6128	-0.56
[4H + PtN2H8O + a68y66]7+	74.3	0.68	M	6782.4973	6782.4934	-0.57
[2H + PtN2H8O + a63y66]6+	74.2	0.57	M	6213.2163	6213.2130	-0.53
[2H + PtNH3 + a70y50]6+	73.9	1.05	M	5188.6875	5188.6842	-0.63
[2H + PtN2H6 + a63y48]4+	73.5	0.33	M	4227.1642	4227.1620	-0.52

[4H + PtN2H8O + b71y62]7+	73.5	2.51	M	6692.4543	6692.4505	-0.57
[4H + Pt + a62y73]8+	73.0	0.45	M	6781.5060	6781.5016	-0.65
[6H + PtNH3 + a69y64]8+	73.0	0.21	M	6633.4172	6633.4128	-0.66
[4H + PtNH3 + b75y59]7+	72.9	0.97	M	6798.5299	6798.5261	-0.56
[5H + Pt + b64y73]8+	72.4	0.36	M	7067.6463	7067.6419	-0.62
[4H + PtN2H6 + b57y67]6+	72.4	1.24	M	5520.8670	5520.8637	-0.60
[3H + PtN2H8O + a62y72]7+	72.2	2.95	M	6685.4935	6685.4896	-0.57
[5H + Pt + b64y74]8+	71.8	0.74	M	7180.7304	7180.7260	-0.61
[3H + PtN2H8O + b74y58]7+	71.2	12.17	M	6646.4951	6646.4913	-0.58
[2H + PtNH3 + b52y75]6+	71.0	0.39	M	5918.0923	5918.0890	-0.56
[4H + PtN2H6 + a72y61]8+	70.9	1.02	M	6689.4659	6689.4615	-0.66
[5H + Pt + a63y71]8+	70.5	0.69	M	6664.4720	6664.4676	-0.66
[4H + Pt + b54]7+	87.4	4.85	M	6247.2445	6247.2406	-0.61

Table B.2 Most important metallated fragments obtained by CID fragmentation of the adduct [8H+ Ubiquitin + $PtN_2H_8O]^{10+}$ (m/z 881.4702) after incubation of ubiquitin with cisplatin (1:1, protein:drug ratio). Similarities are expressed as percentages, abundances are expressed as percentage of the most abundant peak in the spectra, and type is classified based on criteria in Figure 5.6.

Metallated adduct	Similarity	Theoretical mass	Experimental mass	PPM Error
[PtN2H6 + a30y75]3+	85.2	3398.8267	3398.8251	-0.47
[PtN2H8O + b27y72]2+	84.7	2744.4050	2744.4038	-0.44
[PtNH3 + b46y71]4+	83.3	4758.4686	4758.4664	-0.46
[PtN2H8O + y39]4+	83.1	4712.4353	4712.4332	-0.45
[PtN2H8O + a33y67]3+	81.7	2857.4639	2857.4622	-0.59
[4H + Pt + y58]7+	80.8	6727.4928	6727.4886	-0.62
[PtNH3 + a67y23]2+	78.7	1833.8463	1833.8452	-0.60
[Pt + a73y43]4+	76.5	4740.4230	4740.4208	-0.46
[PtN2H6 + a30y67]3+	76.0	2468.2728	2468.2713	-0.61
[PtN2H8O + a33y67]2+	75.3	2857.4639	2857.4628	-0.38
[PtNH3 + b45y52]3+	74.8	2631.3375	2631.3357	-0.68
[PtN2H6 + b44y53]2+	74.5	2630.3382	2630.3372	-0.38
[PtN2H6 + a46y72]4+	71.9	4846.5686	4846.5664	-0.45
[PtN2H8O + b50y67]4+	70.2	4776.4904	4776.4880	-0.50
[PtN2H8O + a47y52]2+	70.2	2766.4383	2766.4372	-0.40
[PtN2H6 + b31y57]2+	70.0	1556.7400	1556.7390	-0.64
[PtN2H6 + b27y74]2+	69.0	2986.5469	2986.5458	-0.37
[PtNH3 + a44y56]2+	67.5	2914.4754	2914.4744	-0.34
[PtN2H6 + b27y74]3+	66.3	2986.5469	2986.5453	-0.54
[4H + PtN2H8O + b55y66]6+	64.8	5281.7400	5281.7370	-0.57

Table B.3 Most important metallated fragments obtained by HCD fragmentation of the adduct [8H+ Ubiquitin + $PtN_2H_8O]^{10+}$ (m/z 881.4702) after incubation of ubiquitin with cisplatin (1:1, protein:drug ratio).

Metallated adduct	Similarity	Theoretical mass	Experimental mass	PPM Error
[5H + Pt + z66]2+	95.4	7624.9861	7624.9850	-0.14
[7H + PtN2H8O + c37]2+	94.7	4367.3353	4367.3342	-0.25
[4H + PtNH3 + y67]2+	93.6	7715.0528	7715.0518	-0.13
[7H + PtN2H8O + z53]2+	93.2	6252.3099	6252.3088	-0.18
[5H + Pt + z62]2+	92.7	7181.7117	7181.7106	-0.15
[3H + PtN2H6 + y62]2+	92.3	7230.7757	7230.7746	-0.15
[H + Pt + c38]2+	92.3	4406.2775	4406.2764	-0.25
[4H + PtN2H6 + z65]2+	92.2	7529.9364	7529.9354	-0.13
[9H + PtN2H8O + c18]1+	91.7	2306.2611	2306.2606	-0.22
[4H + PtNH3 + y62]2+	91.7	7214.7570	7214.7558	-0.17
[2H + PtNH3 + c75]3+	91.6	8716.6260	8716.6245	-0.17
[H + PtNH3 + c59]2+	91.3	6857.5281	6857.5270	-0.16
[5H + PtNH3 + z65]2+	91.1	7513.9177	7513.9166	-0.15
[3H + PtN2H6 + z55]2+	90.9	6444.3998	6444.3986	-0.19
[6H + Pt + z59]2+	90.9	6841.5245	6841.5234	-0.16
[3H + PtNH3 + y45]2+	90.7	5319.7444	5319.7434	-0.19
[H + PtN2H6 + c38]2+	90.4	4440.3306	4440.3294	-0.27
[H + PtN2H6 + c59]2+	90.2	6874.5547	6874.5536	-0.16
[5H + PtNH3 + y74]3+	89.7	8518.5559	8518.5543	-0.19
[2H + Pt + c44]2+	89.6	5160.6987	5160.6976	-0.21
[7H + PtN2H8O + c65]2+	89.4	7597.9673	7597.9662	-0.14
[5H + PtN2H6 + z66]3+	89.2	7659.0392	7659.0375	-0.22
[7H + PtNH3 + z29]2+	89.2	3541.8333	3541.8322	-0.31
[5H + Pt + z66]3+	89.0	7624.9861	7624.9845	-0.21
[6H + Pt + z73]3+	88.6	8372.4266	8372.4249	-0.20
[PtN2H6 + c31]2+	88.2	3702.9472	3702.9462	-0.27
[PtNH3 + y17]1+	88.2	2146.1213	2146.1207	-0.28
[7H + PtN2H6 + c65]2+	88.1	7579.9568	7579.9556	-0.16
[9H + PtN2H8O + c74]4+	88.1	8701.6965	8701.6944	-0.24
[5H + PtN2H6 + z50]2+	88.0	5890.1297	5890.1286	-0.19
[PtN2H6 + c64]2+	88.0	7485.8700	7485.8688	-0.16
[2H + PtN2H8O + y36]2+	88.0	4374.3126	4374.3116	-0.23
[5H + PtNH3 + z73]3+	87.9	8388.4453	8388.4437	-0.19
[2H + Pt + c59]3+	87.8	6841.5094	6841.5078	-0.23
[6H + Pt + z70]3+	87.6	7998.1948	7998.1932	-0.20
[5H + Pt + y75]3+	87.5	8629.5880	8629.5864	-0.19
[7H + Pt + y31]2+	87.3	3669.8919	3669.8908	-0.30
[4H + PtNH3 + y75]3+	87.2	8645.6067	8645.6049	-0.21
[H + PtN2H6 + c75]3+	87.2	8732.6448	8732.6430	-0.21
[3H + Pt + c75]3+	87.1	8700.6073	8700.6057	-0.18
[4H + PtN2H8O + y50]2+	87.0	5924.1590	5924.1580	-0.17
[5H + PtNH3 + y65]3+	86.7	7530.9442	7530.9426	-0.21
[4H + PtN2H6 + y70]3+	86.7	8047.2588	8047.2573	-0.19
[H + PtNH3 + c44]2+	86.6	5176.7174	5176.7162	-0.23

[PtN2H6 + c41]2+	86.4	4810.4669	4810.4658	-0.23
[4H + Pt + y66]2+	86.2	7641.0048	7641.0038	-0.13
[5H + PtN2H8O + y50]3+	86.2	5925.1669	5925.1653	-0.27
[4H + PtN2H6 + z70]3+	86.1	8030.2323	8030.2305	-0.22
[5H + PtN2H6 + z73]3+	86.0	8405.4719	8405.4702	-0.20
[H + Pt + c28]2+	85.5	3300.6643	3300.6632	-0.33
[8H + PtNH3 + z28]1+	85.4	3414.7461	3414.7456	-0.15
[2H + Pt + c62]2+	85.3	7196.6950	7196.6938	-0.17
[Pt + c24]2+	85.1	2887.4131	2887.4120	-0.38
[PtN2H6 + c30]2+	85.0	3574.8886	3574.8876	-0.28
[PtN2H6 + y25]2+	84.6	3070.5514	3070.5504	-0.33
[6H + PtN2H6 + z59]3+	84.5	6875.5776	6875.5758	-0.26
[2H + Pt + y52]2+	84.5	6083.1911	6083.1900	-0.18
[1H + PtNH3 + c38]2+	84.5	4423.3040	4423.3030	-0.23
[6H + Pt + y42]2+	84.4	4933.5768	4933.5758	-0.20
[5H + PtNH3 + y52]2+	84.0	6103.2411	6103.2400	-0.18
[4H + PtN2H8O + z50]2+	83.9	5907.1325	5907.1314	-0.19
[H + PtN2H6 + c42]2+	83.9	4967.5758	4967.5746	-0.24
[5H + PtN2H8O + y73]3+	83.8	8440.5090	8440.5072	-0.21
[4H + PtN2H8O + z27]2+	83.4	3317.6934	3317.6922	-0.36
[PtNH3 + c73]3+	83.4	8501.4878	8501.4861	-0.20
[4H + PtNH3 + y66]2+	83.2	7658.0314	7658.0302	-0.16
[H + PtN2H8O + y53]2+	83.1	6263.2895	6263.2884	-0.18
[PtN2H6 + c27]2+	83.1	3262.6725	3262.6714	-0.34
[9H + PtN2H8O + y36]2+	83.1	4381.3674	4381.3664	-0.23
[2H + Pt + c64]2+	82.7	7453.8325	7453.8314	-0.15
[Pt + y24]2+	82.7	2921.4714	2921.4702	-0.41
[3H + PtNH3 + y37]2+	82.7	4468.3419	4468.3408	-0.25
[4H + PtN2H8O + y23]1+	82.5	2920.5449	2920.5443	-0.21
[7H + Pt + z58]2+	82.4	6713.4897	6713.4886	-0.16
[6H + PtNH3 + c32]1+	82.4	3806.9946	3806.9940	-0.16
[5H + PtNH3 + z65]3+	82.0	7513.9177	7513.9161	-0.21
[2H + PtN2H6 + z45]3+	81.9	5318.7366	5318.7348	-0.34
[H + PtNH3 + y22]2+	81.9	2726.3832	2726.3820	-0.44
[PtN2H6 + c44]2+	81.7	5192.7361	5192.7350	-0.21
[PtN2H6 + z17]2+	81.4	2146.1213	2146.1202	-0.51
[5H + Pt + y70]3+	81.4	8014.2135	8014.2120	-0.19
[7H + PtN2H8O + z53]3+	80.7	6252.3099	6252.3081	-0.29
[9H + PtN2H6 + c65]3+	80.6	7581.9724	7581.9708	-0.21
[1H + PtN2H6 + c40]2+	80.5	4683.4161	4683.4150	-0.23
[5H + Pt + z75]3+	80.4	8612.5614	8612.5599	-0.17
[5H + PtNH3 + z29]1+	80.4	3539.8176	3539.8171	-0.14
[3H + PtN2H8O + y27]2+	80.3	3333.7121	3333.7110	-0.33
[H + PtN2H6 + z36]2+	80.2	4338.2677	4338.2666	-0.25
[H + PtN2H6 + c31]1+	79.6	3703.9550	3703.9545	-0.13

[PtN2H6 + y30]2+	79.5	3625.8531	3625.8520	-0.30
[PtNH3 + c74]3+	79.2	8657.5889	8657.5872	-0.20
[5H + PtNH3 + y50]3+	79.1	5890.1297	5890.1280	-0.29
[7H + PtN2H8O + c65]3+	79.1	7597.9673	7597.9656	-0.22
[8H + PtN2H6 + y29]1+	79.0	3576.8942	3576.8937	-0.14
[6H + PtNH3 + z45]2+	78.7	5305.7413	5305.7402	-0.21
[9H + Pt + z28]1+	78.6	3398.7274	3398.7269	-0.15
[4H + PtNH3 + z62]3+	78.6	7197.7304	7197.7287	-0.24
[5H + PtN2H6 + y67]2+	78.4	7733.0872	7733.0862	-0.13
[1H + Pt + c39]2+	78.3	4521.3044	4521.3034	-0.22
[PtN2H6 + c74]3+	78.2	8674.6155	8674.6137	-0.21
[7H + PtN2H6 + z29]2+	78.2	3558.8598	3558.8588	-0.28
[3H + PtN2H6 + c54]2+	78.1	6297.3163	6297.3152	-0.17
[7H + Pt + z62]3+	78.1	7183.7274	7183.7256	-0.25
[9H + Pt + z70]3+	77.9	8001.2183	8001.2166	-0.21
[9H + PtN2H8O + c18]2+	77.6	2306.2611	2306.2600	-0.48
[4H + Pt + z65]2+	77.6	7495.8833	7495.8822	-0.15
[4H + PtN2H6 + y62]3+	77.5	7231.7835	7231.7820	-0.21
[PtN2H6 + c39]2+	77.5	4554.3497	4554.3486	-0.24
[H + PtN2H6 + z25]2+	76.8	3054.5327	3054.5316	-0.36
[H + Pt + c41]2+	76.7	4777.4216	4777.4204	-0.25
[6H + Pt + c75]3+	76.5	8703.6308	8703.6291	-0.20
[1H + PtNH3 + c59]3+	76.5	6857.5281	6857.5266	-0.22
[8H + PtN2H8O + y65]3+	76.4	7569.0048	7569.0033	-0.20
[PtN2H6 + c75]4+	76.3	8731.6369	8731.6348	-0.24
[2H + Pt + c51]2+	75.9	5934.1058	5934.1048	-0.17
[3H + PtN2H8O + y27]1+	75.6	3333.7121	3333.7116	-0.15
[2H + PtN2H6 + z66]3+	75.4	7656.0157	7656.0141	-0.21
[2H + PtN2H6 + y75]3+	75.2	8660.6176	8660.6160	-0.18
[2H + PtNH3 + c64]3+	74.9	7470.8591	7470.8574	-0.23
[3H + PtN2H6 + z59]3+	74.9	6872.5541	6872.5524	-0.25
[H + PtN2H6 + z75]3+	74.8	8642.5832	8642.5815	-0.20
[Pt + c29]2+	74.6	3427.7515	3427.7504	-0.32
[8H + PtN2H6 + z74]3+	74.4	8521.5794	8521.5777	-0.20
[7H + Pt + y31]1+	73.6	3669.8919	3669.8913	-0.16
[9H + Pt + z23]1+	73.4	2856.4938	2856.4932	-0.21
[9H + Pt + z36]2+	73.3	4312.2772	4312.2760	-0.28
[PtN2H8O + c75]3+	73.0	8749.6475	8749.6458	-0.19
[9H + PtN2H8O + y75]3+	72.8	8685.6829	8685.6813	-0.18
[4H + PtNH3 + y67]3+	72.7	7715.0528	7715.0511	-0.22
[7H + PtNH3 + z33]1+	72.7	3930.0443	3930.0438	-0.13
[2H + PtN2H6 + z74]3+	72.6	8515.5325	8515.5309	-0.19
[9H + Pt + z30]1+	72.4	3583.8438	3583.8433	-0.14
[5H + PtNH3 + y74]4+	72.1	8518.5559	8518.5536	-0.27
[5H + PtN2H8O + y24]1+	72.1	2978.5741	2978.5736	-0.17

[1H + PtN2H6 + c33]2+	72.0	3947.0769	3947.0758	-0.28
[3H + Pt + c58]2+	71.9	6679.4539	6679.4528	-0.16
[3H + Pt + z38]2+	71.9	4549.3158	4549.3146	-0.26
[9H + PtN2H8O + z20]1+	71.8	2538.3246	2538.3240	-0.24
[4H + PtN2H6 + z69]2+	71.7	7929.1846	7929.1834	-0.15
[3H + Pt + z52]2+	71.7	6067.1723	6067.1712	-0.18
[9H + PtNH3 + z53]2+	71.5	6219.2884	6219.2874	-0.16
[4H + PtN2H6 + c75]3+	71.4	8735.6682	8735.6667	-0.17
[8H + Pt + c75]4+	71.3	8705.6464	8705.6444	-0.23
[7H + PtN2H8O + y50]2+	70.9	5927.1825	5927.1814	-0.19
[1H + Pt + y66]2+	70.8	7637.9814	7637.9802	-0.16
[8H + PtNH3 + z59]2+	70.8	6860.5667	6860.5656	-0.16
[8H + PtNH3 + y50]2+	70.8	5893.1532	5893.1522	-0.17
[8H + Pt + z62]2+	70.6	7184.7352	7184.7340	-0.17
[9H + PtN2H8O + y23]1+	70.4	2925.5840	2925.5834	-0.21
[H + PtN2H6 + c33]1+	70.3	3947.0769	3947.0764	-0.13
[8H + PtN2H8O + y73]3+	70.2	8443.5325	8443.5309	-0.19
[2H + PtN2H6 + z46]2+	70.2	5446.7952	5446.7940	-0.22

Table B.4 Most important metallated fragments obtained by ETD fragmentation of the adduct [8H+ Ubiquitin + $PtN_2H_8O]^{10+}$ (m/z 881.4702) after incubation of ubiquitin with cisplatin (1:1, protein:drug ratio). Similarities are expressed as percentages, abundances are expressed as percentage of the most abundant peak in the spectra, and type is classified based on criteria in Figure 5.6.

Metallated adduct	Similarity	Abundance	Type	Theoretical mass	Experimental mass	PPM Error
[PtNH3 + b74y19]3+	95.9	1.88	R	2292.1581	2292.1564	-0.72
[PtNH3 + a70y37]3+	95.6	2.68	R	3766.8997	3766.8980	-0.44
[PtN2H6 + y18]3+	94.0	1.49	R	2326.2112	2326.2095	-0.71
[PtN2H6 + b62y24]2+	93.5	0.71	R	1377.5879	1377.5868	-0.80
[H + PtN2H6 + y24]4+	92.2	1.02	R	2956.5323	2956.5301	-0.74
[Pt + b74y19]3+	91.7	0.98	R	2275.1315	2275.1299	-0.72
[Pt + a70y37]3+	87.0	0.80	R	3749.8731	3749.8715	-0.44
[2H + Pt + y37]5+	86.8	4.40	R	4450.3075	4450.3048	-0.62
[H + Pt + y24]4+	86.6	0.58	R	2922.4792	2922.4770	-0.75
[H + PtNH3 + a71y35]4+	82.3	0.98	R	3624.8744	3624.8722	-0.61
[PtN2H6 + a59y36]3+	78.6	0.36	R	2393.1694	2393.1677	-0.69
[2H + Pt + a70y37]4+	76.8	0.82	R	3751.8888	3751.8866	-0.58
[H + PtN2H6 + a62y34]3+	76.5	0.64	R	2465.2031	2465.2014	-0.67
[Pt + b63y36]2+	74.8	0.76	R	2870.3917	2870.3906	-0.38
[Pt + b73y33]4+	73.7	2.96	R	3634.8350	3634.8328	-0.60
[PtNH3 + a73y21]3+	72.1	1.54	R	2308.1781	2308.1765	-0.71
[2H + PtN2H6 + y37]5+	95.0	3.58	R	4484.3606	4484.3579	-0.61
[Pt + b36]3+	96.0	2.94	L	4194.1376	4194.1359	-0.39
[PtNH3 + b32y74]4+	95.8	1.79	L	3524.8220	3524.8198	-0.62

[H + PtN2H6 + a28y67]3+	94.0	1.23	L	2228.1016	2228.1000	-0.74
[PtN2H6 + b31y70]4+	93.7	0.72	L	2939.5057	2939.5035	-0.75
[H + PtNH3 + a36y61]3+	93.3	1.80	L	2509.2028	2509.2012	-0.66
[H + PtNH3 + a36y53]2+	92.9	2.21	L	1637.7979	1637.7968	-0.67
[H + PtN2H6 + b39]4+	92.1	5.76	L	4538.3310	4538.3288	-0.48
[H + Pt + b32]4+	90.9	3.35	L	3767.9023	3767.9001	-0.58
[PtN2H6 + a28y67]2+	90.3	10.01	L	2227.0938	2227.0927	-0.49
[Pt + b16y73]2+	90.2	1.37	L	1627.8063	1627.8052	-0.67
[PtNH3 + b36]3+	88.4	1.27	L	4211.1641	4211.1625	-0.39
[PtNH3 + a32y73]4+	88.3	0.67	L	3383.7430	3383.7408	-0.65
[H + PtN2H6 + b36]4+	84.9	2.96	L	4229.1985	4229.1963	-0.52
[H + Pt + b30]3+	83.2	2.04	L	3524.8168	3524.8152	-0.47
[Pt + b33]3+	83.1	0.78	L	3894.9895	3894.9878	-0.42
[Pt + b22]2+	76.8	1.13	L	2628.2599	2628.2588	-0.42
[Pt + b21]2+	76.2	1.39	L	2527.2122	2527.2111	-0.43
[PtN2H6 + b38y58]3+	76.1	0.60	L	2390.1684	2390.1667	-0.69
[PtNH3 + b21]2+	75.3	0.45	L	2544.2388	2544.2377	-0.43
[PtNH3 + b16]3+	75.2	0.47	L	2017.0160	2017.0144	-0.82
[H + PtNH3 + b32y73]4+	75.0	1.21	L	3412.7458	3412.7436	-0.64
[Pt + b11]2+	73.6	3.52	L	1442.6834	1442.6823	-0.76
[3H + PtNH3 + y58]6+	96.7	26.16	M	6743.5115	6743.5082	-0.49
[3H + Pt + y60]6+	96.4	7.06	M	6954.5960	6954.5927	-0.47
[3H + Pt + b54]6+	95.8	28.53	M	6246.2366	6246.2333	-0.53
[4H + Pt + y58]7+	95.7	26.37	M	6727.4928	6727.4889	-0.57
[3H + Pt + y58]6+	95.6	36.51	M	6726.4850	6726.4817	-0.49
[4H + Pt + y62]7+	95.5	7.44	M	7197.7304	7197.7266	-0.53
[5H + Pt + y74]8+	95.2	9.87	M	8501.5294	8501.5250	-0.52
[4H + PtN2H6 + y63]7+	94.9	10.05	M	7332.8312	7332.8274	-0.52
[4H + Pt + b64y73]7+	94.9	7.82	M	7066.6385	7066.6347	-0.54
[2H + Pt + b52]5+	94.8	4.64	M	6032.1062	6032.1035	-0.45
[3H + Pt + y61]6+	94.7	6.16	M	7083.6386	7083.6353	-0.46
[4H + Pt + y60]7+	94.6	9.44	M	6955.6038	6955.5999	-0.55
[2H + PtNH3 + b51y70]6+	94.3	2.41	M	5187.6909	5187.6876	-0.63
[5H + PtNH3 + y73]8+	94.1	4.99	M	8405.4719	8405.4675	-0.52
[5H + PtN2H6 + y73]8+	94.0	4.07	M	8422.4984	8422.4940	-0.52
[4H + Pt + y61]7+	93.8	11.56	M	7084.6464	7084.6425	-0.54
[4H + PtN2H6 + a63y66]7+	93.8	1.62	M	6197.2214	6197.2176	-0.62
[3H + Pt + y62]6+	93.7	1.98	M	7196.7226	7196.7193	-0.46
[4H + PtNH3 + y65]7+	93.4	3.31	M	7529.9364	7529.9326	-0.51
[2H + PtN2H6 + b52]5+	93.4	3.11	M	6066.1593	6066.1566	-0.45
[3H + Pt + y59]6+	92.7	8.51	M	6855.5275	6855.5243	-0.48
[3H + PtNH3 + y60]6+	92.5	5.97	M	6971.6225	6971.6192	-0.47
[4H + PtN2H6 + y62]7+	92.5	7.85	M	7231.7835	7231.7797	-0.53
[5H + PtN2H6 + y74]8+	92.1	8.53	M	8535.5825	8535.5781	-0.51
[H + Pt + y40]4+	92.1	2.32	M	4758.4322	4758.4300	-0.46

[4H + PtNH3 + y58]7+	91.9	14.14	M	6744.5193	6744.5155	-0.57
[4H + Pt + a63]7+	91.5	8.35	M	7281.7841	7281.7803	-0.53
[4H + PtNH3 + b71y64]6+	91.5	3.68	M	6871.5490	6871.5457	-0.48
[4H + PtNH3 + y61]7+	91.3	8.58	M	7101.6729	7101.6691	-0.54
[3H + PtN2H6 + b71y65]6+	91.1	1.75	M	6988.6154	6988.6121	-0.47
[4H + PtNH3 + y52]7+	91.0	0.62	M	6102.2333	6102.2294	-0.63
[5H + PtNH3 + y71]8+	90.5	2.20	M	8159.3350	8159.3307	-0.54
[H + PtNH3 + y40]4+	90.5	2.89	M	4775.4587	4775.4565	-0.46
[4H + PtNH3 + a70y68]6+	90.4	1.58	M	7117.6818	7117.6785	-0.46
[5H + PtNH3 + b63y71]7+	90.2	9.04	M	6709.4935	6709.4896	-0.57
[2H + PtN2H6 + a59y71]5+	90.0	0.88	M	6212.2211	6212.2183	-0.44
[4H + Pt + y59]7+	90.0	4.96	M	6856.5354	6856.5315	-0.56
[3H + Pt + y53]6+	89.7	6.35	M	6213.2415	6213.2382	-0.53
[2H + PtNH3 + b52]5+	89.6	2.14	M	6049.1328	6049.1300	-0.45
[4H + PtNH3 + b64y71]6+	89.2	5.08	M	6837.5282	6837.5249	-0.48
[4H + Pt + b63]7+	89.1	4.53	M	7309.7790	7309.7752	-0.53
[4H + PtNH3 + a71y62]6+	89.0	2.56	M	6629.4223	6629.4190	-0.50
[6H + Pt + y74]9+	88.9	2.44	M	8502.5372	8502.5323	-0.58
[4H + PtNH3 + a73y58]7+	88.8	2.16	M	6428.3698	6428.3660	-0.60
[2H + Pt + y58]5+	88.7	1.55	M	6725.4771	6725.4744	-0.41
[2H + PtNH3 + y61]6+	88.7	3.26	M	7099.6573	7099.6540	-0.46
[4H + PtNH3 + b63y71]6+	88.5	9.45	M	6708.4856	6708.4823	-0.49
[3H + Pt + a71y62]6+	88.4	1.11	M	6611.3879	6611.3846	-0.50
[3H + Pt + b62]7+	88.2	3.06	M	7180.6762	7180.6724	-0.53
[4H + Pt + y52]7+	88.1	1.50	M	6085.2067	6085.2029	-0.63
[4H + Pt + y63]7+	87.8	8.24	M	7298.7781	7298.7743	-0.53
[5H + PtNH3 + y60]7+	87.6	5.94	M	6973.6382	6973.6343	-0.55
[PtN2H6 + b51y38]2+	87.6	1.40	M	1756.8462	1756.8451	-0.62
[5H + Pt + a70y69]7+	87.5	5.85	M	7214.7471	7214.7433	-0.53
[3H + PtN2H6 + b58]6+	87.5	6.77	M	6696.4804	6696.4772	-0.49
[2H + Pt + b60]6+	87.4	3.79	M	6938.5258	6938.5225	-0.47
[4H + PtN2H6 + a59y71]7+	87.4	1.83	M	6214.2367	6214.2329	-0.62
[5H + PtNH3 + b64y71]7+	86.5	2.82	M	6838.5360	6838.5322	-0.56
[4H + PtNH3 + y70]7+	86.0	0.48	M	8030.2323	8030.2284	-0.48
[5H + PtN2H6 + y72]8+	85.9	1.51	M	8275.4300	8275.4256	-0.53
[4H + PtNH3 + y64]7+	85.8	2.49	M	7428.8887	7428.8849	-0.52
[H + PtN2H6 + a56y58]5+	85.8	0.87	M	4432.2831	4432.2803	-0.62
[4H + Pt + b74y56]7+	85.5	0.89	M	6411.3545	6411.3507	-0.60
[2H + PtNH3 + y53]6+	85.5	7.24	M	6229.2602	6229.2569	-0.53
[2H + PtN2H6 + b52y62]4+	85.4	8.93	M	4504.2691	4504.2670	-0.49
[5H + Pt + b72y69]7+	85.1	4.16	M	7511.9272	7511.9234	-0.51
[2H + Pt + a63y72]6+	84.8	12.08	M	6760.5169	6760.5136	-0.49
[H + PtN2H6 + a47y65]3+	84.7	0.98	M	4177.1387	4177.1370	-0.39
[4H + Pt + a70y70]6+	84.7	1.38	M	7314.7870	7314.7837	-0.45
[2H + PtNH3 + y40]5+	84.6	4.91	M	4776.4666	4776.4638	-0.57

[5H + Pt + y72]8+	84.1	2.69	M	8241.3769	8241.3725	-0.53
[3H + PtN2H6 + b64y74]6+	83.9	1.19	M	7212.7678	7212.7645	-0.46
[5H + Pt + y64]7+	83.9	5.25	M	7412.8700	7412.8662	-0.52
[4H + PtNH3 + y63]7+	83.7	9.75	M	7315.8047	7315.8008	-0.52
[4H + Pt + b64y73]6+	83.5	3.56	M	7066.6385	7066.6352	-0.47
[6H + PtNH3 + y74]8+	83.3	9.57	M	8519.5638	8519.5594	-0.52
[6H + Pt + y70]8+	83.1	2.19	M	8015.2214	8015.2170	-0.55
[3H + PtN2H6 + y63]6+	83.0	1.13	M	7331.8234	7331.8201	-0.45
[H + PtN2H6 + b62y47]3+	83.0	1.21	M	3997.9614	3997.9597	-0.41
[2H + Pt + y50]5+	82.8	1.06	M	5870.0797	5870.0770	-0.47
[3H + Pt + a72y60]6+	82.4	0.94	M	6525.3624	6525.3591	-0.50
[3H + Pt + y42]5+	82.2	0.76	M	4930.5534	4930.5506	-0.56
[2H + PtNH3 + a69y54]6+	82.1	1.04	M	5544.8571	5544.8538	-0.59
[5H + PtNH3 + b58]7+	82.0	2.04	M	6681.4695	6681.4657	-0.57
[PtN2H6 + a47y52]2+	81.8	1.71	M	2748.4277	2748.4266	-0.40
[4H + Pt + b62y75]7+	81.7	2.93	M	7050.6436	7050.6397	-0.54
[2H + PtN2H6 + a65y71]6+	81.7	0.64	M	6911.5762	6911.5729	-0.48
[5H + Pt + b73y68]8+	81.4	1.09	M	7511.9272	7511.9228	-0.58
[4H + Pt + b63y71]7+	81.3	2.71	M	6691.4591	6691.4552	-0.57
[2H + Pt + y52]6+	81.0	3.45	M	6083.1911	6083.1878	-0.54
[5H + Pt + y73]8+	80.6	6.93	M	8388.4453	8388.4409	-0.52
[6H + PtNH3 + a68y73]8+	80.4	2.12	M	7495.9085	7495.9041	-0.59
[3H + PtN2H6 + b52]6+	80.4	1.32	M	6067.1672	6067.1639	-0.54
[6H + Pt + b75]9+	80.3	2.21	M	8686.6042	8686.5993	-0.57
[5H + PtN2H6 + b68y72]7+	80.2	1.20	M	7392.8537	7392.8499	-0.52
[2H + PtNH3 + b65y71]6+	80.2	1.50	M	6922.5446	6922.5413	-0.48
[H + Pt + b54y62]4+	78.7	0.53	M	4682.3308	4682.3286	-0.47
[Pt + b52y65]4+	78.4	1.18	M	4783.3798	4783.3776	-0.46
[4H + Pt + a72y60]7+	78.2	1.14	M	6526.3702	6526.3664	-0.59
[H + PtN2H6 + a66y50]5+	77.7	1.14	M	4742.4108	4742.4080	-0.58
[5H + PtNH3 + a63y66]7+	77.6	0.47	M	6181.2027	6181.1988	-0.62
[5H + PtNH3 + b58y73]7+	77.6	0.74	M	6309.2864	6309.2826	-0.61
[3H + Pt + a50]6+	77.3	1.42	M	5761.0496	5761.0463	-0.57
[4H + PtNH3 + a62y74]7+	77.3	1.85	M	6911.6166	6911.6128	-0.56
[3H + Pt + a64y73]7+	77.0	1.23	M	7037.6358	7037.6319	-0.55
[6H + PtNH3 + y75]8+	76.8	1.95	M	8647.6223	8647.6180	-0.51
[5H + PtN2H6 + y65]7+	76.8	8.86	M	7547.9708	7547.9669	-0.51
[3H + Pt + b60]7+	76.6	2.68	M	6939.5336	6939.5298	-0.55
[4H + PtN2H6 + b68y66]6+	76.4	0.81	M	6792.4816	6792.4783	-0.48
[3H + PtNH3 + a61y69]6+	76.3	3.25	M	6194.1867	6194.1834	-0.53
[4H + Pt + b63y71]6+	75.9	3.95	M	6691.4591	6691.4558	-0.49
[4H + Pt + a65y69]7+	75.1	1.15	M	6650.3961	6650.3923	-0.58
[3H + Pt + y70]7+	75.1	0.80	M	8012.1979	8012.1940	-0.48
[4H + Pt + b61]6+	74.2	2.04	M	7053.6255	7053.6222	-0.47
[2H + PtN2H6 + a68y67]6+	74.0	2.96	M	6819.4925	6819.4892	-0.48

[4H + PtNH3 + a74y75]8+	73.5	4.87	M	8485.5583	8485.5539	-0.52
[3H + PtNH3 + b65y71]7+	73.3	1.49	M	6923.5524	6923.5486	-0.55
[4H + PtN2H6 + b69y68]6+	73.0	2.97	M	7063.6348	7063.6315	-0.47
[H + Pt + y43]4+	72.9	0.63	M	5057.5803	5057.5781	-0.43
[3H + PtNH3 + b63y71]5+	71.9	0.45	M	6707.4778	6707.4751	-0.41
[3H + Pt + b73y62]6+	71.6	0.64	M	6908.5680	6908.5647	-0.48
[3H + PtN2H6 + a63y70]6+	71.6	0.48	M	6568.4145	6568.4112	-0.50
[4H + PtNH3 + y56]6+	71.5	1.17	M	6560.4345	6560.4312	-0.50
[2H + Pt + b60]5+	71.2	0.58	M	6938.5258	6938.5230	-0.40
[H + PtNH3 + b56y55]3+	70.8	0.40	M	4144.1397	4144.1380	-0.40
[5H + Pt + a61y72]7+	70.8	0.59	M	6507.3869	6507.3830	-0.59
[3H + PtNH3 + b75y53]7+	70.7	0.84	M	6155.2360	6155.2322	-0.62
[4H + PtNH3 + b63y59]6+	70.6	0.52	M	5423.7203	5423.7170	-0.61
[2H + Pt + a61y69]6+	70.4	1.65	M	6176.1523	6176.1490	-0.53
[2H + PtNH3 + y58]5+	92.1	0.76	M	6742.5037	6742.5009	-0.41
[3H + Pt + b74y58]6+	86.8	1.56	M	6594.4315	6594.4282	-0.50
[H + Pt + b54y59]4+	84.9	0.90	M	4341.1357	4341.1335	-0.51
[3H + PtNH3 + a72y60]6+	80.0	4.40	M	6542.3889	6542.3856	-0.50
[4H + PtNH3 + b71y55]6+	74.3	0.95	M	5888.0678	5888.0645	-0.56
[H + PtNH3 + y42]4+	73.6	0.62	M	4945.5643	4945.5621	-0.44
[4H + PtNH3 + b65y73]7+	72.5	0.94	M	7170.6971	7170.6932	-0.54
[3H + PtN2H6 + b52]7+	72.4	0.65	M	6067.1672	6067.1633	-0.63
[H + Pt + y44]5+	79.3	3.69	M	5185.6753	5185.6725	-0.53

Table B.5 Most important metallated fragments obtained by CID fragmentation of the adduct [7H+ Ubiquitin + $PtN_2H_6]^{9+}$ (m/z 977.2928) after incubation of ubiquitin with cisplatin (1:1, protein:drug ratio). Similarities are expressed as percentages, abundances are expressed as percentage of the most abundant peak in the spectra, and type is classified based on criteria in Figure 5.6.

Metallated adduct	Similarity	Theoretical mass	Experimental mass	PPM Error
[Pt + a49y63]4+	95.4	4184.0996	4184.0972	-0.57
[4H + Pt + y58]7+	92.0	6727.4928	6727.4886	-0.62
[4H + PtN2H6 + b64y70]6+	91.3	6726.4598	6726.4566	-0.48
[Pt + a54y40]3+	90.8	2217.0533	2217.0516	-0.77
[4H + PtNH3 + b63y71]6+	90.7	6708.4856	6708.4824	-0.48
[PtN2H6 + b62y24]2+	90.3	1377.5879	1377.5868	-0.80
[PtN2H6 + a62y24]2+	90.1	1349.5930	1349.5918	-0.89
[PtN2H6 + b71y44]4+	89.9	4661.3808	4661.3784	-0.51
[Pt + a73y43]4+	88.5	4740.4230	4740.4208	-0.46
[Pt + b57y35]2+	87.8	1980.9623	1980.9612	-0.56
[Pt + y42]4+	87.8	4927.5299	4927.5276	-0.47
[4H + PtNH3 + b64y71]6+	87.3	6837.5282	6837.5250	-0.47
[Pt + a54y58]3+	87.2	4183.0904	4183.0887	-0.41
[PtN2H6 + b62y29]2+	86.5	1990.8950	1990.8940	-0.50
[4H + PtNH3 + a61y69]6+	86.1	6195.1945	6195.1914	-0.50
[Pt + a50y56]3+	85.5	3541.8135	3541.8117	-0.51
[Pt + y43]4+	85.0	5056.5725	5056.5704	-0.42
[4H + Pt + y53]6+	85.0	6214.2493	6214.2462	-0.50
[4H + Pt + b63y71]6+	84.7	6691.4591	6691.4556	-0.52
[5H + PtNH3 + b63y71]7+	84.5	6709.4935	6709.4895	-0.60
[PtN2H6 + a24y75]3+	84.5	2745.4042	2745.4026	-0.58
[Pt + b54y31]2+	84.2	1150.4609	1150.4598	-0.96
[4H + PtNH3 + a71y62]6+	84.2	6629.4223	6629.4192	-0.47
[Pt + b74y19]3+	83.5	2275.1315	2275.1298	-0.75
[Pt + b32y58]2+	83.5	1734.7667	1734.7656	-0.63
[PtNH3 + a22y72]2+	83.1	2098.0400	2098.0388	-0.57
[PtN2H6 + a73y32]2+	82.9	3527.8091	3527.8080	-0.31
[Pt + y40]4+	82.1	4757.4244	4757.4220	-0.50
[Pt + a51y61]4+	81.9	4212.0945	4212.0924	-0.50
[PtNH3 + a44y56]2+	81.7	2914.4754	2914.4744	-0.34
[Pt + b51y70]4+	81.7	5168.6487	5168.6464	-0.44
[4H + Pt + b60y74]6+	81.4	6681.4424	6681.4392	-0.48
[4H + Pt + y59]6+	81.2	6856.5354	6856.5318	-0.53
[Pt + a74y40]4+	81.2	4597.3760	4597.3736	-0.52
[PtNH3 + a67y23]2+	81.0	1833.8463	1833.8452	-0.60
[PtNH3 + b50y48]2+	80.7	2716.3903	2716.3892	-0.40
[PtN2H6 + b46y71]4+	80.6	4775.4951	4775.4928	-0.48
[PtN2H6 + b62y30]2+	80.5	2047.9165	2047.9154	-0.54
[4H + PtNH3 + y58]6+	78.8	6744.5193	6744.5160	-0.49
[4H + PtNH3 + b63y73]6+	78.8	6954.6225	6954.6192	-0.47
[4H + Pt + a71y62]6+	78.3	6612.3957	6612.3924	-0.50
[PtNH3 + a48y52]3+	78.0	2859.4961	2859.4944	-0.59
[PtNH3 + a30y70]2+	78.0	2766.4257	2766.4246	-0.40
[PtN2H6 + a31y74]3+	77.3	3398.8267	3398.8251	-0.47

[PtN2H6 + b43y54]2+	77.2	2630.3382	2630.3372	-0.38
[Pt + a75y42]3+	77.1	4824.5029	4824.5013	-0.33
[Pt + b75y30]3+	77.1	3516.7679	3516.7662	-0.48
[Pt + a74y41]3+	76.8	4710.4600	4710.4584	-0.34
[4H + Pt + a61y69]6+	76.3	6178.1680	6178.1646	-0.55
[Pt + b38y72]4+	76.1	3868.9916	3868.9892	-0.62
[Pt + b74y40]4+	75.5	4625.3709	4625.3688	-0.45
[PtN2H6 + a35y55]2+	75.4	1755.8721	1755.8710	-0.63
[4H + PtN2H6 + b58y73]6+	75.3	6325.3051	6325.3020	-0.49
[PtN2H6 + a36y75]3+	75.3	4069.1553	4069.1535	-0.44
[4H + Pt + a67y66]6+	75.2	6593.3747	6593.3712	-0.53
[Pt + b21]3+	74.8	2527.2122	2527.2105	-0.67
[PtN2H6 + a46y72]4+	74.8	4846.5686	4846.5664	-0.45
[Pt + a54y53]3+	74.8	3669.8469	3669.8454	-0.41
[PtNH3 + b59y52]4+	74.7	4165.0798	4165.0776	-0.53
[PtN2H6 + a70y35]3+	74.7	3527.8091	3527.8074	-0.48
[Pt + b31y58]2+	74.5	1619.7397	1619.7386	-0.68
[5H + Pt + b63y71]7+	74.4	6692.4669	6692.4634	-0.52
[PtN2H6 + a30y67]3+	74.0	2468.2728	2468.2713	-0.61
[PtN2H6 + b52y66]4+	73.9	4945.5279	4945.5256	-0.47
[PtN2H6 + a24y75]2+	73.4	2745.4042	2745.4032	-0.36
[PtNH3 + b31y70]3+	73.4	2922.4792	2922.4776	-0.55
[PtN2H6 + a33y70]3+	73.3	3154.6327	3154.6311	-0.51
[4H + PtN2H6 + b70y67]6+	73.1	7061.6555	7061.6520	-0.50
[PtNH3 + b50y52]2+	73.0	3128.6337	3128.6326	-0.35
[4H + PtN2H6 + b66y66]6+	72.8	6542.3386	6542.3352	-0.52
[PtNH3 + a66y51]4+	72.7	4823.4448	4823.4428	-0.41
[Pt + b54y58]3+	72.3	4211.0853	4211.0838	-0.36
[Pt + b50y70]4+	72.2	5039.6061	5039.6040	-0.42
[PtNH3 + a30y71]3+	72.2	2894.5207	2894.5191	-0.55
[PtNH3 + a32y65]3+	72.1	2509.2154	2509.2138	-0.64
[PtN2H6 + b70y46]4+	72.1	4791.3822	4791.3800	-0.46
[PtN2H6 + b27y74]2+	71.6	2986.5469	2986.5458	-0.37
[4H + PtNH3 + a60y72]6+	71.4	6410.3215	6410.3184	-0.48
[PtN2H6 + a38y74]3+	71.2	4135.2022	4135.2006	-0.39
[Pt + b72y40]3+	70.9	4356.1857	4356.1839	-0.41
[4H + Pt + a72y60]6+	70.3	6526.3702	6526.3668	-0.52
[Pt + a45y56]2+	70.2	3044.5173	3044.5162	-0.36
[4H + PtN2H6 + b64y71]7+	70.0	6854.5548	6854.5512	-0.53
[PtNH3 + b73y24]2+	69.4	2650.3433	2650.3422	-0.42
[Pt + b48y59]3+	68.6	3641.7931	3641.7915	-0.44
[5H + PtNH3 + b62y72]7+	68.5	6680.4669	6680.4633	-0.54
[4H + PtNH3 + b68y65]6+	68.2	6647.3601	6647.3568	-0.50
[5H + Pt + y71]8+	68.1	8142.3085	8142.3040	-0.55
[PtNH3 + a20y70]2+	68.0	1654.8020	1654.8008	-0.73

[4H + PtNH3 + y58]7+	67.8	6744.5193	6744.5154	-0.58
[Pt + b31y70]3+	67.7	2905.4526	2905.4511	-0.52
[Pt + a73y21]3+	67.6	2291.1516	2291.1498	-0.79
[PtNH3 + b59y53]4+	67.3	4294.1224	4294.1204	-0.47
[PtNH3 + y43]4+	67.2	5073.5990	5073.5968	-0.43
[PtNH3 + a36y61]2+	67.1	2508.1950	2508.1938	-0.48
[Pt + a74y17]2+	67.0	1969.0463	1969.0452	-0.56
[Pt + b60y58]3+	67.0	4904.3823	4904.3805	-0.37
[PtNH3 + b44y70]3+	66.3	4412.2681	4412.2665	-0.36
[PtN2H6 + b43y54]3+	66.1	2630.3382	2630.3367	-0.57
[4H + PtNH3 + b74y60]7+	66.1	6840.5768	6840.5729	-0.57
[PtN2H6 + b63y31]3+	65.7	2247.0486	2247.0468	-0.80
[PtN2H6 + b58y33]2+	65.6	1860.8572	1860.8562	-0.54
[Pt + a50y69]4+	65.3	4910.5635	4910.5612	-0.47
[4H + Pt + b72y57]6+	65.0	6229.2013	6229.1982	-0.50

Table B.6 Most important metallated fragments obtained by HCD fragmentation of the adduct [7H+ Ubiquitin + $PtN_2H_6]^{9+}$ (m/z 977.2928) after incubation of ubiquitin with cisplatin (1:1, protein:drug ratio).

Metallated adduct	Similarity	Theoretical mass	Experimental mass	PPM Error
[4H + PtN2H6 + z70]3+	95.9	8030.2323	8030.2305	-0.22
[4H + PtN2H6 + z66]3+	95.1	7658.0314	7658.0298	-0.21
[4H + PtNH3 + y65]2+	94.2	7529.9364	7529.9354	-0.13
[9H + PtN2H6 + c69]3+	94.1	8046.2471	8046.2454	-0.21
[4H + PtN2H6 + z74]3+	94.0	8517.5481	8517.5466	-0.18
[4H + Pt + z66]2+	93.5	7623.9783	7623.9772	-0.14
[4H + PtN2H6 + z65]3+	93.4	7529.9364	7529.9349	-0.20
[Pt + c38]2+	93.2	4406.2775	4406.2764	-0.25
[4H + PtNH3 + z66]2+	93.0	7641.0048	7641.0038	-0.13
[H + PtN2H6 + c59]2+	92.6	6874.5547	6874.5536	-0.16
[6H + Pt + z58]2+	92.3	6712.4819	6712.4808	-0.16
[PtN2H6 + c42]2+	92.2	4967.5758	4967.5746	-0.24
[4H + PtN2H6 + z66]2+	91.9	7658.0314	7658.0302	-0.16
[2H + PtN2H6 + c75]4+	91.8	8733.6526	8733.6504	-0.25
[PtN2H6 + c64]2+	91.5	7485.8700	7485.8688	-0.16
[9H + Pt + z37]2+	91.4	4440.3358	4440.3346	-0.27
[2H + PtNH3 + c62]2+	91.1	7213.7215	7213.7204	-0.15
[5H + Pt + c74]3+	91.1	8645.6015	8645.5998	-0.20
[4H + Pt + y65]2+	91.0	7512.9099	7512.9088	-0.15

[5H + Pt + z65]2+	90.8	7496.8911	7496.8900	-0.15
[4H + Pt + z66]3+	90.0	7623.9783	7623.9765	-0.24
[PtN2H6 + c75]3+	89.9	8732.6448	8732.6430	-0.21
[Pt + c59]2+	89.8	6840.5016	6840.5004	-0.18
[5H + PtNH3 + z75]3+	89.3	8629.5880	8629.5864	-0.19
[4H + PtNH3 + y67]2+	89.2	7715.0528	7715.0518	-0.13
[8H + Pt + z62]2+	89.2	7184.7352	7184.7340	-0.17
[6H + PtN2H6 + c65]2+	89.0	7578.9490	7578.9478	-0.16
[6H + PtN2H6 + z75]4+	88.9	8647.6223	8647.6200	-0.27
[5H + PtN2H6 + z73]3+	88.8	8405.4719	8405.4702	-0.20
[PtNH3 + c75]3+	88.6	8715.6182	8715.6165	-0.20
[7H + PtN2H6 + y53]2+	88.2	6251.3259	6251.3248	-0.18
[4H + PtN2H6 + z62]3+	87.9	7214.7570	7214.7552	-0.25
[2H + Pt + c59]3+	87.8	6841.5094	6841.5078	-0.23
[6H + PtN2H6 + y31]2+	87.5	3702.9371	3702.9360	-0.30
[2H + PtN2H6 + c54]2+	87.0	6296.3085	6296.3074	-0.17
[6H + Pt + z70]3+	86.8	7998.1948	7998.1932	-0.20
[5H + PtNH3 + c32]1+	86.5	3805.9867	3805.9862	-0.13
[6H + PtN2H6 + y29]2+	86.1	3574.8786	3574.8774	-0.34
[PtN2H6 + c62]2+	85.7	7229.7402	7229.7392	-0.14
[PtNH3 + c59]2+	85.3	6856.5203	6856.5192	-0.16
[5H + PtNH3 + z29]1+	85.3	3539.8176	3539.8171	-0.14
[8H + Pt + y24]2+	85.2	2929.5340	2929.5328	-0.41
[2H + Pt + c62]2+	85.2	7196.6950	7196.6938	-0.17
[5H + PtNH3 + z74]3+	85.0	8501.5294	8501.5278	-0.19
[3H + PtN2H6 + y62]3+	84.8	7230.7757	7230.7740	-0.24
[4H + Pt + y70]3+	84.7	8013.2057	8013.2040	-0.21
[7H + PtN2H6 + y24]1+	83.7	2962.5792	2962.5787	-0.17
[3H + Pt + c75]3+	83.4	8700.6073	8700.6057	-0.18
[5H + Pt + z75]3+	83.1	8612.5614	8612.5599	-0.17
[5H + PtN2H6 + z59]3+	83.0	6874.5697	6874.5681	-0.23
[7H + PtN2H6 + y33]1+	83.0	3964.0974	3964.0969	-0.13
[9H + Pt + z37]3+	82.5	4440.3358	4440.3342	-0.36
[PtN2H6 + c28]1+	82.2	3333.7096	3333.7091	-0.15
[PtN2H6 + y66]2+	81.2	7671.0266	7671.0256	-0.13
[2H + PtN2H6 + c58]3+	81.0	6712.4992	6712.4976	-0.24
[3H + PtNH3 + y52]2+	80.8	6101.2254	6101.2244	-0.16
[3H + PtN2H6 + z46]2+	80.8	5447.8030	5447.8018	-0.22
[PtN2H6 + c28]2+	80.1	3333.7096	3333.7086	-0.30
[7H + PtN2H6 + z36]2+	79.9	4344.3146	4344.3136	-0.23
[8H + Pt + z38]2+	79.8	4554.3549	4554.3538	-0.24
[Pt + y24]2+	79.7	2921.4714	2921.4702	-0.41
[7H + Pt + c61]2+	79.6	7073.6755	7073.6744	-0.16
[3H + Pt + c58]2+	79.2	6679.4539	6679.4528	-0.16
[4H + PtN2H6 + z68]2+	79.2	7816.1005	7816.0994	-0.14

[4H + Pt + c61]2+	79.1	7070.6520	7070.6510	-0.14
[PtN2H6 + c31]1+	78.9	3702.9472	3702.9467	-0.14
[7H + PtNH3 + y33]1+	78.8	3947.0709	3947.0703	-0.15
[8H + Pt + y28]1+	78.5	3414.7461	3414.7456	-0.15
[PtN2H6 + c30]1+	78.3	3574.8886	3574.8881	-0.14
[4H + Pt + y65]3+	78.2	7512.9099	7512.9081	-0.24
[2H + PtNH3 + y73]3+	77.6	8402.4484	8402.4468	-0.19
[2H + Pt + c74]3+	77.6	8642.5780	8642.5764	-0.19
[6H + Pt + z32]1+	77.6	3798.9259	3798.9253	-0.16
[4H + Pt + c75]4+	77.2	8701.6151	8701.6128	-0.26
[6H + Pt + c75]3+	77.1	8703.6308	8703.6291	-0.20
[Pt + c42]2+	76.9	4933.5227	4933.5216	-0.22
[2H + PtNH3 + y55]2+	76.4	6443.3919	6443.3908	-0.17
[PtN2H6 + y75]3+	76.2	8659.6098	8659.6080	-0.21
[3H + PtNH3 + y45]2+	76.2	5319.7444	5319.7434	-0.19
[8H + PtNH3 + z33]1+	75.7	3931.0522	3931.0516	-0.15
[4H + PtN2H6 + y67]2+	75.7	7732.0794	7732.0782	-0.16
[PtN2H6 + c27]2+	75.6	3262.6725	3262.6714	-0.34
[PtN2H6 + c74]3+	75.3	8674.6155	8674.6137	-0.21
[PtNH3 + y17]1+	75.2	2147.1291	2147.1286	-0.23
[5H + Pt + z62]2+	75.1	7181.7117	7181.7106	-0.15
[5H + Pt + y66]3+	74.7	7642.0127	7642.0110	-0.22
[PtN2H6 + c35]2+	74.6	4133.1410	4133.1398	-0.29
[3H + PtN2H6 + c68]3+	74.5	7927.1161	7927.1145	-0.20
[PtNH3 + c64]2+	74.4	7468.8434	7468.8424	-0.13
[9H + Pt + z70]3+	74.2	8001.2183	8001.2166	-0.21
[4H + PtNH3 + c75]3+	73.7	8718.6417	8718.6402	-0.17
[PtNH3 + y36]2+	73.2	4338.2677	4338.2666	-0.25
[8H + Pt + z59]2+	73.2	6843.5401	6843.5390	-0.16
[2H + Pt + y75]3+	72.7	8626.5645	8626.5627	-0.21
[8H + PtN2H6 + c65]3+	72.2	7580.9646	7580.9631	-0.20
[5H + PtNH3 + z62]3+	72.2	7198.7383	7198.7367	-0.22
[5H + PtN2H6 + z50]2+	71.8	5890.1297	5890.1286	-0.19
[PtN2H6 + c64]3+	71.3	7485.8700	7485.8682	-0.24
[7H + PtNH3 + y74]3+	71.3	8520.5716	8520.5700	-0.19
[5H + PtN2H6 + c17]1+	71.0	2155.1766	2155.1761	-0.23
[PtN2H6 + c52]2+	70.8	6081.1702	6081.1692	-0.16
[8H + PtNH3 + z44]2+	70.5	5192.7300	5192.7290	-0.19
[4H + PtN2H6 + c75]3+	70.5	8735.6682	8735.6667	-0.17
[5H + PtNH3 + z69]2+	70.4	7913.1659	7913.1648	-0.14

Table B.7 Most important metallated fragments obtained by ETD fragmentation of the adduct [7H+ Ubiquitin + $PtN_2H_6]^{9+}$ (m/z 977.2928) after incubation of ubiquitin with cisplatin (1:1, protein:drug ratio).

Metallated adduct	Similarity	Abundance	Type	Theoretical mass	Experimental mass	PPM Error
[Ru + b73y21]2+	88.2	7.54	R	2226.0861	2226.0850	-0.49
[C7H8Ru + b57y35]2+	67.0	1.21	R	1979.9645	1979.9634	-0.56
[C7H8Ru + a54y37]2+	62.3	1.25	R	1906.9230	1906.9218	-0.63
[C7H8Ru + a14]3+	90.1	1.53	L	1728.8700	1728.8685	-0.87
[C7H8Ru + b17]3+	89.0	4.49	L	2098.0600	2098.0584	-0.76
[C7H8Ru + b18]3+	88.6	7.91	L	2227.1026	2227.1010	-0.72
[C7H8Ru + b16]3+	84.6	2.96	L	1998.9916	1998.9900	-0.80
[C7H8Ru + a16]3+	80.4	1.17	L	1970.9967	1970.9952	-0.76
[C7H8Ru + a15]3+	77.9	1.01	L	1841.9541	1841.9526	-0.81
[C7H8Ru + a36y58]2+	75.1	1.38	L	2133.0170	2133.0158	-0.56
[C7H8Ru + a17]3+	73.6	1.39	L	2070.0651	2070.0636	-0.72
[C7H8Ru + b14]2+	71.6	2.34	L	1756.8650	1756.8638	-0.68
[C7H8Ru + b11]2+	70.6	2.65	L	1441.6855	1441.6844	-0.76
[C7H8Ru + a18]3+	67.3	1.42	L	2199.1077	2199.1062	-0.68
[C7H8Ru + a21y72]3+	60.0	2.08	L	1978.9679	1978.9662	-0.86
[4H + C7H8Ru + y58]8+	89.9	6.03	M	6726.4949	6726.4904	-0.67
[4H + C7H8Ru + b52]7+	89.8	19.59	M	6033.1240	6033.1201	-0.65
[5H + C7H8Ru + y58]9+	88.5	1.96	M	6727.5028	6727.4982	-0.68
[C7H8Ru + a44y49]2+	87.3	3.41	M	2097.0435	2097.0424	-0.52
[4H + C7H8Ru + a58y7]7+	85.1	3.17	M	6016.1225	6016.1185	-0.66
[6H + C7H8Ru + y74]10+	79.8	1.65	M	8501.5394	8501.5340	-0.64
[6H + C7H8Ru + a66y75]9+	77.2	1.94	M	7468.8837	7468.8786	-0.68
[6H + C7H8Ru + y60]9+	75.4	1.76	M	6956.6216	6956.6166	-0.72
[7H + C7H8Ru + b64y73]9+	71.3	0.85	M	7068.6641	7068.6594	-0.66
[C7H8Ru + a46y71]4+	70.1	1.53	M	4712.4493	4712.4472	-0.45
[C7H8Ru + b42y51]2+	66.6	1.38	M	2126.0336	2126.0326	-0.47
[5H + C7H8Ru + b60]8+	64.3	1.14	M	6940.5514	6940.5472	-0.61
[4H + C7H8Ru + b51y73]6+	60.5	2.36	M	5545.9140	5545.9104	-0.65

Table B.8 Most important metallated fragments obtained by CID fragmentation of the adduct [9H+ Ubiquitin + RuC_7H_8]]$^{11+}$ (m/z 796.6043) after incubation of ubiquitin with RAPTA-T (1:5, protein:drug ratio). Similarities are expressed as percentages, abundances are expressed as percentage of the most abundant peak in the spectra, and type is classified based on criteria in Figure 5.6.

Metallated adduct	Similarity	Theoretical mass	Experimental mass	PPM Error
[Ru + a73y19]2+	88.8	1997.9751	1997.9740	-0.55
[Ru + a37y54]2+	86.0	1737.8477	1737.8466	-0.63
[C7H8Ru + a15]3+	81.2	1841.9541	1841.9526	-0.81
[C7H8Ru + a46y71]4+	80.8	4712.4493	4712.4472	-0.45
[C7H8Ru + a44y49]2+	79.5	2097.0435	2097.0424	-0.52
[C7H8Ru + b16]3+	76.9	1998.9916	1998.9900	-0.80
[C7H8Ru + a16]3+	71.5	1970.9967	1970.9952	-0.76
[C7H8Ru + b13]2+	68.6	1655.8173	1655.8162	-0.66
[C7H8Ru + b14]2+	67.3	1756.8650	1756.8638	-0.68
[Ru + a48y39]2+	66.1	1328.6053	1328.6042	-0.83
[C7H8Ru + a14]3+	66.0	1728.8700	1728.8685	-0.87
[C7H8Ru + a46y71]3+	65.7	4712.4493	4712.4477	-0.34
[C7H8Ru + b17]3+	65.5	2098.0600	2098.0584	-0.76
[C7H8Ru + b11]2+	65.5	1441.6855	1441.6844	-0.76
[Ru + a49y44]2+	65.2	1980.9597	1980.9586	-0.56
[C7H8Ru + a75y42]4+	61.7	4823.5051	4823.5028	-0.48
[Ru + b73y21]3+	60.3	2226.0861	2226.0843	-0.81

Table B.9 Most important metallated fragments obtained by HCD fragmentation of the adduct [9H+ Ubiquitin + RuC_7H_8]]$^{11+}$ (m/z 796.6043) after incubation of ubiquitin with RAPTA-T (1:5, protein:drug ratio).

Metallated adduct	Similarity	Theoretical mass	Experimental mass	PPM Error
[3H + C7H8Ru + c75]3+	96.7	8699.6095	8699.6079	-0.18
[3H + C7H8Ru + c59]2+	96.2	6841.5194	6841.5182	-0.18
[3H + C7H8Ru + c75]4+	93.6	8699.6095	8699.6072	-0.26
[C7H8Ru + c24]3+	93.5	2886.4152	2886.4137	-0.52
[C7H8Ru + c24]2+	93.2	2886.4152	2886.4142	-0.35
[7H + C7H8Ru + y31]2+	92.3	3668.8940	3668.8930	-0.27
[2H + C7H8Ru + c42]3+	92.1	4933.5327	4933.5309	-0.36
[C7H8Ru + c29]2+	92.0	3426.7536	3426.7526	-0.29
[7H + C7H8Ru + y29]3+	92.0	3540.8354	3540.8337	-0.48
[C7H8Ru + c28]2+	91.6	3298.6587	3298.6576	-0.33
[8H + C7H8Ru + y45]2+	91.6	5306.7591	5306.7580	-0.21
[3H + C7H8Ru + y75]3+	91.5	8626.5745	8626.5729	-0.19
[C7H8Ru + c74]3+	91.0	8640.5724	8640.5706	-0.21
[C7H8Ru + c28]3+	90.9	3299.6665	3299.6649	-0.48
[C7H8Ru + c40]2+	90.5	4648.3652	4648.3640	-0.26
[3H + C7H8Ru + c59]3+	90.5	6841.5194	6841.5177	-0.25
[C7H8Ru + c38]2+	90.2	4405.2796	4405.2786	-0.23
[6H + Ru + c75]3+	90.0	8610.5704	8610.5688	-0.19
[C7H8Ru + c39]2+	89.8	4520.3066	4520.3054	-0.27

[2H + C7H8Ru + c38]3+	89.6	4406.2875	4406.2857	-0.41
[C7H8Ru + c27]2+	89.5	3227.6215	3227.6204	-0.34
[C7H8Ru + c30]2+	89.5	3539.8377	3539.8366	-0.31
[7H + C7H8Ru + y31]3+	89.4	3668.8940	3668.8923	-0.46
[C7H8Ru + c32]2+	89.3	3782.9232	3782.9222	-0.26
[C7H8Ru + c25]2+	88.6	3000.4582	3000.4570	-0.40
[3H + C7H8Ru + z17]2+	88.5	2114.0938	2114.0928	-0.47
[Ru + y41]2+	88.4	4777.4480	4777.4468	-0.25
[C7H8Ru + c23]2+	88.1	2757.3727	2757.3716	-0.40
[3H + C7H8Ru + z17]1+	86.8	2114.0938	2114.0933	-0.24
[2H + C7H8Ru + c44]2+	86.4	5159.7008	5159.6998	-0.19
[C7H8Ru + c27]3+	85.7	3228.6294	3228.6276	-0.56
[C7H8Ru + c24]1+	85.4	2886.4152	2886.4147	-0.17
[2H + C7H8Ru + c54]2+	85.0	6261.2575	6261.2564	-0.18
[C7H8Ru + c35]2+	84.8	4098.0901	4098.0890	-0.27
[4H + C7H8Ru + y27]2+	84.8	3281.6584	3281.6574	-0.30
[2H + Ru + z40]3+	84.4	4649.3530	4649.3514	-0.34
[8H + Ru + c65]3+	84.4	7453.8511	7453.8495	-0.21
[2H + C7H8Ru + c44]3+	83.9	5159.7008	5159.6991	-0.33
[C7H8Ru + c42]2+	83.5	4932.5249	4932.5238	-0.22
[C7H8Ru + c21]1+	83.4	2543.2409	2543.2404	-0.20
[C7H8Ru + c14]2+	82.9	1773.8915	1773.8904	-0.62
[C7H8Ru + c39]3+	82.8	4520.3066	4520.3049	-0.38
[8H + C7H8Ru + z33]2+	82.5	3913.0278	3913.0266	-0.31
[8H + C7H8Ru + y36]2+	82.0	4327.2981	4327.2970	-0.25
[C7H8Ru + c20]2+	82.0	2428.2140	2428.2128	-0.49
[C7H8Ru + c41]3+	80.4	4776.4237	4776.4221	-0.33
[8H + C7H8Ru + z29]2+	80.1	3524.8167	3524.8156	-0.31
[C7H8Ru + y75]3+	80.0	8623.5510	8623.5495	-0.17
[4H + C7H8Ru + c59]4+	79.7	6842.5272	6842.5252	-0.29
[3H + C7H8Ru + c51]3+	79.2	5934.1158	5934.1143	-0.25
[9H + C7H8Ru + y60]2+	79.1	6959.6451	6959.6440	-0.16
[9H + Ru + y37]2+	78.9	4364.3019	4364.3008	-0.25
[C7H8Ru + c16]1+	78.8	2016.0182	2016.0176	-0.30
[4H + C7H8Ru + c74]4+	78.3	8643.5958	8643.5936	-0.25
[4H + C7H8Ru + c74]3+	78.0	8643.5958	8643.5943	-0.17
[7H + C7H8Ru + z75]3+	77.4	8613.5792	8613.5775	-0.20
[C7H8Ru + c16]2+	77.2	2016.0182	2016.0170	-0.60
[C7H8Ru + c13]2+	77.2	1672.8438	1672.8428	-0.60
[C7H8Ru + c21]2+	77.1	2543.2409	2543.2398	-0.43
[C7H8Ru + c75]3+	76.7	8696.5860	8696.5845	-0.17
[2H + C7H8Ru + c53]3+	76.4	6105.1564	6105.1548	-0.26
[C7H8Ru + c28]1+	75.6	3298.6587	3298.6581	-0.18
[3H + Ru + c75]3+	75.2	8607.5469	8607.5451	-0.21
[C7H8Ru + c75]4+	75.1	8696.5860	8696.5840	-0.23

[6H + C7H8Ru + y75]3+	75.0	8629.5980	8629.5963	-0.20
[C7H8Ru + c13]1+	74.9	1672.8438	1672.8433	-0.30
[C7H8Ru + c34]2+	74.1	4040.0608	4040.0596	-0.30
[9H + C7H8Ru + z44]2+	73.9	5175.7135	5175.7124	-0.21
[6H + C7H8Ru + c75]4+	73.8	8702.6330	8702.6308	-0.25
[9H + C7H8Ru + z36]2+	73.7	4311.2793	4311.2782	-0.26
[4H + C7H8Ru + y37]2+	73.7	4451.3253	4451.3242	-0.25
[2H + Ru + z23]1+	73.7	2756.3786	2756.3780	-0.22
[5H + Ru + c20]2+	73.3	2341.1905	2341.1894	-0.47
[C7H8Ru + c27]1+	72.8	3227.6215	3227.6210	-0.15
[C7H8Ru + c11]1+	72.8	1458.7121	1458.7115	-0.41
[3H + C7H8Ru + c51]2+	72.6	5934.1158	5934.1148	-0.17
[C7H8Ru + c17]3+	72.5	2115.0866	2115.0849	-0.80
[9H + C7H8Ru + y64]3+	72.3	7415.9035	7415.9019	-0.22
[C7H8Ru + c10]2+	72.2	1330.6171	1330.6160	-0.83
[C7H8Ru + c74]4+	72.1	8640.5724	8640.5700	-0.28
[C7H8Ru + c22]2+	71.1	2644.2886	2644.2874	-0.45
[7H + C7H8Ru + z33]3+	70.6	3912.0199	3912.0183	-0.41
[7H + C7H8Ru + y28]1+	69.6	3412.7405	3412.7399	-0.18
[C7H8Ru + c9]2+	69.1	1273.5957	1273.5946	-0.86
[9H + C7H8Ru + y60]3+	69.1	6959.6451	6959.6433	-0.26
[4H + Ru + y15]1+	69.0	1812.9386	1812.9381	-0.28
[6H + C7H8Ru + c75]3+	68.6	8702.6330	8702.6313	-0.20
[C7H8Ru + c23]3+	68.4	2757.3727	2757.3711	-0.58
[7H + C7H8Ru + c59]4+	68.4	6845.5507	6845.5484	-0.34
[C7H8Ru + c11]2+	68.0	1458.7121	1458.7110	-0.75
[5H + C7H8Ru + c43]2+	67.6	5049.6402	5049.6392	-0.20
[C7H8Ru + c14]1+	67.0	1773.8915	1773.8910	-0.28
[C7H8Ru + c8]2+	66.7	1172.5480	1172.5468	-1.02
[9H + C7H8Ru + c74]3+	66.7	8648.6350	8648.6334	-0.19
[3H + C7H8Ru + c28]2+	66.7	3301.6821	3301.6810	-0.33
[9H + C7H8Ru + y44]2+	66.3	5192.7400	5192.7390	-0.19
[Ru + c75]3+	66.1	8604.5234	8604.5217	-0.20
[3H + C7H8Ru + y50]2+	65.9	5870.0897	5870.0886	-0.19
[C7H8Ru + c59]2+	65.8	6838.4959	6838.4948	-0.16
[3H + C7H8Ru + y40]2+	65.4	4759.4500	4759.4488	-0.25
[9H + Ru + z18]1+	64.8	2191.1415	2191.1410	-0.23
[6H + Ru + y37]2+	64.2	4361.2784	4361.2772	-0.28
[4H + C7H8Ru + c38]2+	64.2	4408.3031	4408.3020	-0.25
[3H + C7H8Ru + c58]2+	64.1	6678.4561	6678.4550	-0.16
[2H + Ru + y41]3+	63.9	4779.4636	4779.4620	-0.33
[6H + C7H8Ru + c59]2+	63.7	6844.5429	6844.5418	-0.16
[5H + C7H8Ru + y57]2+	63.4	6630.4500	6630.4490	-0.15
[9H + C7H8Ru + y75]3+	63.1	8632.6214	8632.6197	-0.20
[6H + C7H8Ru + c59]3+	63.0	6844.5429	6844.5411	-0.26

[C7H8Ru + c26]3+	63.0	3099.5266	3099.5250	-0.52
[6H + C7H8Ru + c64]3+	62.8	7456.8660	7456.8642	-0.24
[5H + C7H8Ru + c54]2+	62.7	6264.2810	6264.2798	-0.19
[C7H8Ru + c45]3+	62.6	5305.7614	5305.7598	-0.30
[C7H8Ru + c7]2+	61.9	1059.4639	1059.4628	-1.04
[5H + Ru + z37]2+	61.4	4343.2440	4343.2430	-0.23
[9H + C7H8Ru + y29]2+	61.2	3542.8511	3542.8500	-0.31
[4H + Ru + y38]2+	61.1	4474.2897	4474.2886	-0.25
[3H + Ru + z64]4+	61.1	7300.7674	7300.7652	-0.30
[4H + C7H8Ru + z59]3+	61.1	6838.5110	6838.5093	-0.25
[9H + C7H8Ru + y42]2+	61.1	4935.6025	4935.6014	-0.22
[9H + C7H8Ru + z24]1+	60.9	2912.5174	2912.5168	-0.21
[9H + Ru + y18]1+	60.8	2208.1681	2208.1675	-0.27
[9H + C7H8Ru + z75]4+	60.7	8615.5949	8615.5928	-0.24
[6H + Ru + y10]1+	60.7	1241.6784	1241.6779	-0.40
[9H + Ru + c44]2+	60.6	5074.6930	5074.6918	-0.24
[9H + C7H8Ru + z60]3+	60.5	6942.6185	6942.6168	-0.24
[5H + C7H8Ru + c45]2+	60.4	5309.7927	5309.7916	-0.21
[2H + Ru + z53]3+	60.3	6102.1467	6102.1449	-0.29
[9H + C7H8Ru + y70]3+	60.3	8017.2470	8017.2453	-0.21
[5H + C7H8Ru + c44]2+	60.2	5162.7243	5162.7232	-0.21

Table B.10 Most important metallated fragments obtained by ETD fragmentation of the adduct [9H+ Ubiquitin + RuC_7H_8]]$^{11+}$ (m/z 796.6043) after incubation of ubiquitin with RAPTA-T (1:5, protein:drug ratio).

Metallated adduct	Similarity	Abundance	Type	Theoretical mass	Experimental mass	PPM Error
[Ru + b73y21]2+	87.3	5.62	R	2226.0861	2226.0850	-0.49
[C7H8Ru + a57y37]3+	76.8	1.40	R	2208.0867	2208.0852	-0.68
[C7H8Ru + b57y35]2+	71.9	0.74	R	1979.9645	1979.9634	-0.56
[C7H8Ru + a54y37]2+	61.7	0.45	R	1906.9230	1906.9218	-0.63
[C7H8Ru + b18]3+	87.4	3.73	L	2227.1026	2227.1010	-0.72
[C7H8Ru + b18y75]2+	85.8	1.94	L	2096.0621	2096.0610	-0.52
[C7H8Ru + b17]3+	78.9	2.22	L	2098.0600	2098.0584	-0.76
[C7H8Ru + a17]3+	78.1	0.72	L	2070.0651	2070.0636	-0.72
[C7H8Ru + a14]3+	77.0	1.02	L	1728.8700	1728.8685	-0.87
[C7H8Ru + a18]3+	75.6	0.69	L	2199.1077	2199.1062	-0.68
[C7H8Ru + b16]3+	75.2	1.65	L	1998.9916	1998.9900	-0.80
[C7H8Ru + b11]2+	69.5	1.07	L	1441.6855	1441.6844	-0.76
[C7H8Ru + a16]3+	62.3	0.48	L	1970.9967	1970.9952	-0.76
[4H + C7H8Ru + y58]8+	89.4	2.18	M	6726.4949	6726.4904	-0.67
[5H + C7H8Ru + b74y59]7+	88.9	4.58	M	6724.4919	6724.4877	-0.62
[7H + C7H8Ru + b74y75]9+	87.1	2.12	M	8498.5523	8498.5470	-0.62
[6H + Ru + b69y67]8+	71.6	0.98	M	6837.4892	6837.4848	-0.64
[C7H8Ru + a46y71]4+	70.1	1.32	M	4712.4493	4712.4472	-0.45
[5H + Ru + b69y67]7+	67.1	0.58	M	6836.4814	6836.4779	-0.51
[H + C7H8Ru + a50y62]4+	66.8	1.94	M	4195.1381	4195.1360	-0.50
[4H + C7H8Ru + b52]6+	66.4	2.85	M	6033.1240	6033.1206	-0.56
[5H + C7H8Ru + y58]7+	66.3	4.58	M	6727.5028	6727.4991	-0.55

Table B.11 Most important metallated fragments obtained by CID fragmentation of the adduct [8H+ Ubiquitin + $RuC_7H_8]^{10+}$ (m/z 876.1640) after incubation of ubiquitin with RAPTA-T (1:5, protein:drug ratio. Similarities are expressed as percentages, abundances are expressed as percentage of the most abundant peak in the spectra, and type is classified based on criteria in Figure 5.6.

Metallated adduct	Similarity	Theoretical mass	Experimental mass	PPM Error
[C7H8Ru + b16]3+	91.4	1998.9916	1998.9900	-0.80
[Ru + a37y54]2+	89.5	1737.8477	1737.8466	-0.63
[C7H8Ru + a15]3+	88.4	1841.9541	1841.9526	-0.81
[Ru + b73y21]2+	87.8	2226.0861	2226.0850	-0.49
[C7H8Ru + b17]3+	87.5	2098.0600	2098.0584	-0.76
[C7H8Ru + a44y49]2+	86.8	2097.0435	2097.0424	-0.52
[C7H8Ru + b15]3+	86.7	1869.9490	1869.9474	-0.86
[C7H8Ru + a16]3+	86.5	1970.9967	1970.9952	-0.76
[Ru + a37y49]2+	84.5	1154.5148	1154.5136	-1.04
[C7H8Ru + b18]3+	83.8	2227.1026	2227.1010	-0.72
[C7H8Ru + b14]3+	80.7	1756.8650	1756.8633	-0.97
[Ru + a49y44]2+	79.8	1980.9597	1980.9586	-0.56
[C7H8Ru + a17]3+	79.3	2070.0651	2070.0636	-0.72
[C7H8Ru + b34y50]2+	77.0	1135.5090	1135.5078	-1.06
[Ru + b48y42]2+	76.3	1623.7585	1623.7574	-0.68
[C7H8Ru + a75y42]4+	76.3	4823.5051	4823.5028	-0.48
[C7H8Ru + b49y68]3+	76.1	4711.3925	4711.3908	-0.36
[Ru + b37y53]2+	74.4	1652.7586	1652.7574	-0.73
[C7H8Ru + b13]2+	73.9	1655.8173	1655.8162	-0.66
[Ru + b37y55]3+	73.7	1866.8903	1866.8886	-0.91
[Ru + a37y54]3+	73.5	1737.8477	1737.8460	-0.98
[C7H8Ru + a50y67]4+	71.9	4695.4340	4695.4316	-0.51
[Ru + a48y39]2+	70.2	1328.6053	1328.6042	-0.83
[C7H8Ru + a74y40]3+	69.5	4596.3781	4596.3765	-0.35
[Ru + b31y54]2+	69.5	1126.5199	1126.5188	-0.98
[C7H8Ru + b14]2+	69.0	1756.8650	1756.8638	-0.68
[C7H8Ru + b11]2+	68.1	1441.6855	1441.6844	-0.76
[C7H8Ru + b57y35]3+	66.3	1979.9645	1979.9628	-0.86
[C7H8Ru + a75y42]3+	66.2	4823.5051	4823.5035	-0.33
[Ru + a42y50]2+	65.6	1906.9077	1906.9066	-0.58
[C7H8Ru + b18y65]2+	64.7	980.3919	980.3908	-1.12
[Ru + a41y51]3+	63.0	1849.8750	1849.8735	-0.81
[Ru + b37y52]3+	61.9	1523.7160	1523.7144	-1.05
[C7H8Ru + a45y69]3+	60.6	4412.2695	4412.2680	-0.34
[C7H8Ru + a38y72]3+	60.3	3839.9988	3839.9973	-0.39

Table B.12 Most important metallated fragments obtained by HCD fragmentation of the adduct [8H+ Ubiquitin + RuC_7H_8]$^{10+}$ (m/z 876.1640) after incubation of ubiquitin with RAPTA-T (1:5, protein:drug ratio.

Metallated adduct	Similarity	Theoretical mass	Experimental mass	PPM Error
[2H + C7H8Ru + c75]4+	91.0	8698.6017	8698.5996	-0.24
[9H + Ru + y37]2+	84.2	4364.3019	4364.3008	-0.25
[C7H8Ru + c31]2+	84.2	3667.8963	3667.8952	-0.30
[2H + C7H8Ru + c74]4+	83.6	8641.5802	8641.5780	-0.25
[C7H8Ru + c30]2+	83.3	3539.8377	3539.8366	-0.31
[H + C7H8Ru + c38]2+	82.7	4405.2796	4405.2786	-0.23
[6H + C7H8Ru + z59]3+	81.6	6840.5266	6840.5250	-0.23
[C7H8Ru + c24]2+	79.2	2886.4152	2886.4142	-0.35
[C7H8Ru + c28]2+	79.1	3298.6587	3298.6576	-0.33
[H + C7H8Ru + c38]3+	78.1	4405.2796	4405.2780	-0.36
[2H + C7H8Ru + z17]2+	77.0	2113.0860	2113.0850	-0.47
[C7H8Ru + c42]3+	75.4	4931.5170	4931.5155	-0.30
[7H + C7H8Ru + y29]3+	72.6	3540.8354	3540.8337	-0.48
[C7H8Ru + c14]2+	71.4	1773.8915	1773.8904	-0.62
[C7H8Ru + c31]3+	70.8	3667.8963	3667.8945	-0.49
[C7H8Ru + c9]2+	69.6	1273.5957	1273.5946	-0.86
[C7H8Ru + c10]2+	66.1	1330.6171	1330.6160	-0.83
[H + C7H8Ru + c28]3+	66.0	3299.6665	3299.6649	-0.48
[C7H8Ru + c75]5+	65.3	8696.5860	8696.5835	-0.29
[5H + C7H8Ru + c75]4+	65.2	8701.6251	8701.6228	-0.26
[C7H8Ru + c24]3+	61.0	2886.4152	2886.4137	-0.52
[5H + C7H8Ru + c74]4+	60.6	8644.6037	8644.6016	-0.24

Table B.13 Most important metallated fragments obtained by ETD fragmentation of the adduct [8H+ Ubiquitin + $RuC_7H_8]^{10+}$ (m/z 876.1640) after incubation of ubiquitin with RAPTA-T (1:5, protein:drug ratio.

Appendix C
Tables of metallated fragment from MS/MS experiments of metallodrugs on BRCA1 peptide

Ion Type (Fragment from ETD)	Theoretical m/z	Experimental m/z	Mass Error (ppm)
C_{12}^{+}	1385.78949	1385.79004	-0.40
$[C_{15} + H]^{2+}$	855.98027	855.98082	-0.64
$[C_{24} + H]^{2+}$	1373.69987	1373.700415	-0.40
$[C_{29}$ + RAPTA-C -2Cl $]^{3+}$	1253.59048	1253.591027	-0.44
$[C_{30}$ + RAPTA-C -2Cl $]^{3+}$	1296.2888	1296.289347	-0.42
$[C_{32}$ + RAPTA-C -2Cl $]^{3+}$	1371.67817	1371.678723	-0.40
$[C_{33}$ + H + RAPTA-C -2Cl $]^{4+}$	1057.52118	1057.52173	-0.52
$[C_{34}$ + RAPTA-C -2Cl $]^{3+}$	1452.37868	1452.379223	-0.37
$[C_{36}$ + RAPTA-C -2Cl $]^{3+}$	1537.77532	1537.775867	-0.36
$[C_{39}$ + H + RAPTA-C -2Cl $]^{3+}$	1618.48001	1618.48056	-0.34
$[C_{45}$ + H + RAPTA-C -2Cl $]^{3+}$	1842.58292	1842.583473	-0.30
$[C_{48}$ + H + RAPTA-C -2Cl $]^{4+}$	1467.22358	1467.224133	-0.38
$[Z_6 + H]^{+}$	702.39066	702.3912	-0.77
$[Z_{14} + H]^{2+}$	744.35898	744.35953	-0.74
$[Z_{15} + H]^{2+}$	808.40646	808.40701	-0.68
$[Z_{16}$ + RAPTA-C -2Cl $]^{2+}$	1067.99151	1067.99206	-0.51
$[Z_{17}$ + RAPTA-C -2Cl $]^{2+}$	1132.0208	1132.02135	-0.49
$[Z_{18}$ + RAPTA-C -2Cl $]^{3+}$	792.69466	792.69521	-0.69
$[Z_{20}$ + RAPTA-C -2Cl $]^{2+}$	1302.12633	1302.126875	-0.42
$[Z_{26}$ + H + RAPTA-C -2Cl $]^{3+}$	1118.55067	1118.551217	-0.49
$[Z_{30}$ + H + RAPTA-C -2Cl $]^{3+}$	1285.29086	1285.29141	-0.43
$[Z_{38}$ + 2H + RAPTA-C -2Cl $]^{4+}$	1179.06361	1179.064155	-0.46
$[Z_{45}$ + H + RAPTA-C -2Cl $]^{4+}$	1381.9324	1381.932948	-0.40
$[Z_{49}$ + RAPTA-C -2Cl $]^{4+}$	1492.22759	1492.228143	-0.37
$[Z_{50}$ + 2H + RAPTA-C -2Cl $]^{5+}$	1217.00347	1217.004022	-0.45

Table C.1 Most important C and Z fragments obtained by ETD fragmentation of the adduct [BRCA1 +5H + RAPTA-C -2Cl]$^{7+}$ (m/z 871.8649) after incubation of BRCA1 peptide with RAPTA-C (1:5, protein:drug ratio)

Ion Type (Fragment from ETD)	Theoretical m/z	Experimental m/z	Mass Error (ppm)
C_{12}^{+}	1385.78949	1385.79004	-0.40
$[C_{15} + H]^{2+}$	855.98027	855.98082	-0.64
$[C_{18} + H]^{2+}$	1014.0676	1014.068155	-0.55
$[C_{20} + H]^{2+}$	1123.08567	1123.086215	-0.49
$[C_{29} + 3H + RAPTA\text{-}EA + 2OH - 3Cl]^{3+}$	1339.93206	1339.93261	-0.41
$[C_{31} + 2H + RAPTA\text{-}EA + 2OH - 3Cl]^{3+}$	1419.98913	1419.989677	-0.39
$[C_{32} + H + RAPTA\text{-}EA + 2OH - 3Cl]^{3+}$	1457.34787	1457.348423	-0.38
$[C_{34} + 2H + RAPTA\text{-}EA + 2OH - 3Cl]^{4+}$	1153.7881	1153.78865	-0.48
$[C_{36} + H + RAPTA\text{-}EA + 2OH - 3Cl]^{4+}$	1217.58363	1217.584175	-0.45
$[C_{39} + H + RAPTA\text{-}EA + 2OH - 3Cl]^{3+}$	1703.81377	1703.81432	-0.32
$[C_{46} + 2H + RAPTA\text{-}EA + 2OH - 3Cl]^{4+}$	1474.70006	1474.700613	-0.37
$[C_{47} + H + RAPTA\text{-}EA + 2OH - 3Cl]^{4+}$	1503.20484	1503.20539	-0.37
$[C_{50} + 5H + RAPTA\text{-}EA + 2OH - 3Cl]^{5+}$	1271.81537	1271.815914	-0.43
Z_{14}^{2+}	743.35116	743.351705	-0.73
Z_{15}^{2+}	807.39864	807.399185	-0.68
$[Z_{16} + H + RAPTA\text{-}EA + 2OH - 3Cl]^{2+}$	1196.49606	1196.49661	-0.46
$[Z_{16} + 2H + RAPTA\text{-}EA + 2OH - 3Cl]^{3+}$	797.9998	798.00035	-0.69
$[Z_{18} + RAPTA\text{-}EA + 2OH - 3Cl]^{2+}$	1317.0429	1317.04345	-0.42
$[Z_{20} + 2H + RAPTA\text{-}EA + 2OH - 3Cl]^{3+}$	954.08968	954.0902267	-0.57
$[Z_{38} + 3H + RAPTA\text{-}EA + 2OH - 3Cl]^{3+}$	1657.75469	1657.75524	-0.33
$[Z_{38} + 3H + RAPTA\text{-}EA + 2OH - 3Cl]^{4+}$	1243.31588	1243.31643	-0.44
$[Z_{41} + 4H + RAPTA\text{-}EA + 2OH - 3Cl]^{4+}$	1332.13361	1332.13416	-0.41
$[Z_{45} + 2H + RAPTA\text{-}EA + 2OH - 3Cl]^{3+}$	1928.24642	1928.246963	-0.28
$[Z_{5} + H]^{+}$	574.29569	574.29624	-0.96
$[Z_{50} + 3H + RAPTA\text{-}EA + 2OH - 3Cl]^{4+}$	1585.50675	1585.507303	-0.35

Table C.2 Most important C and Z fragments obtained by ETD fragmentation of the adduct [BRCA1 +7H + RAPTA-EA +2OH -3Cl]$^{8+}$ (*m/z* 795.1339) after incubation of BRCA1 peptide with RAPTA-EA (1:5, protein:drug ratio).

References

1. What Is Cancer? *National Cancer Institute* Available at: http://www.cancer.gov/about-cancer/what-is-cancer. (Accessed: 21st April 2016)
2. WHO | Cancer. *WHO* Available at: http://www.who.int/mediacentre/factsheets/fs297/en/. (Accessed: 21st April 2016)
3. Investing in Cancer Prevention and Control to Reduce Global Economic Burden. *ASCO Annual Meeting* (2015). Available at: http://am.asco.org/investing-cancer-prevention-and-control-reduce-global-economic-burden. (Accessed: 21st April 2016)
4. Mukherjee, S. *The emperor of all maladies: a biography of cancer*. (Scribner, 2010).
5. Robinson, D. H. & Toledo, A. H. Historical development of modern anesthesia. *J. Investig. Surg. Off. J. Acad. Surg. Res.* **25,** 141–149 (2012).
6. Evolution of cancer treatments: Surgery | American Cancer Society. Available at: http://www.cancer.org/cancer/cancerbasics/thehistoryofcancer/the-history-of-cancer-cancer-treatment-surgery. (Accessed: 17th June 2016)
7. Paget, S. The distribution of secondary growths in cancer of the breast. 1889. *Cancer Metastasis Rev.* **8,** 98–101 (1989).
8. Beatson, G. On The Treatment of Inoperable Cases of Carcinoma Of The Mamma: Suggestions for a New Method of Treatment, With Illustrative Cases. *The Lancet* **148,** 162–165 (1896).
9. Röntgen, W. C. On a New Kind of Rays. *Science* **3,** 227–231 (1896).
10. Fenn, J. E. & Udelsman, R. First Use of Intravenous Chemotherapy Cancer Treatment: Rectifying the Record. *J. Am. Coll. Surg.* **212,** 413–417 (2011).
11. Meyer, L. M., Miller, F. R., Rowen, M. J., Bock, G. & Rutzky, J. Treatment of Acute Leukemia with Amethopterin (4-amino, 10-methyl pteroyl glutamic acid). *Acta Haematol.* **4,** 157–167 (1950).
12. Hutchinson, E. Efficient delivery. *Nat. Rev. Cancer* **5,** 759–759 (2005).
13. Sudhakar, A. History of Cancer, Ancient and Modern Treatment Methods. *J. Cancer Sci. Ther.* **1,** 1–4 (2009).
14. Scott, A. M., Allison, J. P. & Wolchok, J. D. Monoclonal antibodies in cancer therapy. *Cancer Immun.* **12,** (2012).
15. Anassi, E. & Ndefo, U. A. Sipuleucel-T (Provenge) Injection. *Pharm. Ther.* **36,** 197–202 (2011).

16. Vanneman, M. & Dranoff, G. Combining immunotherapy and targeted therapies in cancer treatment. *Nat. Rev. Cancer* **12,** 237–251 (2012).
17. Capdeville, R., Buchdunger, E., Zimmermann, J. & Matter, A. Glivec (STI571, imatinib), a rationally developed, targeted anticancer drug. *Nat. Rev. Drug Discov.* **1,** 493–502 (2002).
18. SJ, H., 15, et al M. 2015;64:237-242 A. & 2015. Two-thirds of patients with invasive cancer likely to survive 5 years. Available at: http://www.healio.com/hematology-oncology/breast-cancer/news/online/%7B68c032a9-a6a3-459e-8034-3088827269e6%7D/two-thirds-of-patients-with-invasive-cancer-likely-to-survive-5-years. (Accessed: 19th June 2016)
19. Baldo, B. A. & Pham, N. H. Adverse reactions to targeted and non-targeted chemotherapeutic drugs with emphasis on hypersensitivity responses and the invasive metastatic switch. *Cancer Metastasis Rev.* **32,** 723–761 (2013).
20. Overview of Targeted Therapies for Cancer - My Cancer Genome. Available at: https://www.mycancergenome.org/content/molecular-medicine/overview-of-targeted-therapies-for-cancer/. (Accessed: 21st April 2016)
21. Holohan, C., Van Schaeybroeck, S., Longley, D. B. & Johnston, P. G. Cancer drug resistance: an evolving paradigm. *Nat. Rev. Cancer* **13,** 714–726 (2013).
22. Chabner, B. A. & Roberts, T. G. Chemotherapy and the war on cancer. *Nat. Rev. Cancer* **5,** 65–72 (2005).
23. PR Tufts CSDD 2014 Cost Study | Tufts Center for the Study of Drug Development. Available at: http://csdd.tufts.edu/news/complete_story/pr_tufts_csdd_2014_cost_study. (Accessed: 19th June 2016)
24. The Drug Approval Process. *Medscape* Available at: http://www.medscape.com/viewarticle/405869. (Accessed: 19th June 2016)
25. Rosenberg, B., Van Camp, L. & Krigas, T. Inhibition of Cell Division in Escherichia coli by Electrolysis Products from a Platinum Electrode. *Nature* **205,** 698–699 (1965).
26. Use of Cisplatin for Cancer Treatment. *National Cancer Institute* Available at: http://www.cancer.gov/research/progress/discovery/cisplatin. (Accessed: 17th June 2016)
27. Einhorn, L. H. Treatment of testicular cancer: a new and improved model. *J. Clin. Oncol. Off. J. Am. Soc. Clin. Oncol.* **8,** 1777–1781 (1990).
28. National Comprehensive Cancer Network Guidelines for Treatment of Cancer by Site. (2013).

29. Dorcier, A. *et al.* In Vitro Evaluation of Rhodium and Osmium RAPTA Analogues: The Case for Organometallic Anticancer Drugs Not Based on Ruthenium. *Organometallics* **25,** 4090–4096 (2006).
30. New-Generation Platinum Agents for Solid Tumors. *Medscape* Available at: http://www.medscape.com/viewarticle/589012. (Accessed: 17th June 2016)
31. Hargrave-Thomas, E., Yu, B. & Reynisson, J. Serendipity in anticancer drug discovery. *World J. Clin. Oncol.* **3,** 1–6 (2012).
32. Groessl, M., Zava, O. & Dyson, P. J. Cellular uptake and subcellular distribution of ruthenium-based metallodrugs under clinical investigation versus cisplatin. *Metallomics* **3,** 591–599 (2011).
33. Gasser, G., Ott, I. & Metzler-Nolte, N. Organometallic Anticancer Compounds. *J. Med. Chem.* **54,** 3–25 (2011).
34. Griffiths, J. A Brief History of Mass Spectrometry. *Anal. Chem.* **80,** 5678–5683 (2008).
35. Overview of Mass Spectrometry. Available at: https://www.thermofisher.com/ch/en/home/life-science/protein-biology/protein-biology-learning-center/protein-biology-resource-library/pierce-protein-methods/overview-mass-spectrometry.html.html. (Accessed: 7th July 2016)
36. Legin, A. A. *et al.* NanoSIMS combined with fluorescence microscopy as a tool for subcellular imaging of isotopically labeled platinum-based anticancer drugs. *Chem. Sci.* (2014). doi:10.1039/C3SC53426J
37. Wedlock, L. E. *et al.* Visualising gold inside tumour cells following treatment with an antitumour gold(I) complex. *Met. Integr. Biometal Sci.* **3,** 917–925 (2011).
38. Florea, A.-M. & Büsselberg, D. Cisplatin as an Anti-Tumor Drug: Cellular Mechanisms of Activity, Drug Resistance and Induced Side Effects. *Cancers* **3,** 1351–1371 (2011).
39. Chandra, S. in *Mass Spectrometry Imaging* (eds. Rubakhin, S. S. & Sweedler, J. V.) 113–130 (Humana Press, 2010).
40. Wedlock, L. E. *et al.* NanoSIMS multi-element imaging reveals internalisation and nucleolar targeting for a highly-charged polynuclear platinum compound. *Chem. Commun.* **49,** 6944 (2013).
41. Gulin, A. A., Pavlyukov, M. S., Gularyan, S. K. & Nadtochenko, V. A. Visualization of the spatial distribution of Pt+ ions in cisplatin-treated glioblastoma cells by time-of-flight secondary ion mass spectrometry. *Biochem. Mosc. Suppl. Ser. Membr. Cell Biol.* **9,** 202–209 (2015).

42. Duan, X., He, C., Kron, S. J. & Lin, W. Nanoparticle formulations of cisplatin for cancer therapy. *Wiley Interdiscip. Rev. Nanomed. Nanobiotechnol.* n/a-n/a (2016). doi:10.1002/wnan.1390
43. Proetto, M. T. *et al.* Cellular Delivery of Nanoparticles Revealed with Combined Optical and Isotopic Nanoscopy. *ACS Nano* **10,** 4046–4054 (2016).
44. Legin, A. A. *et al.* Multi-scale imaging of anticancer platinum(IV) compounds in murine tumor and kidney. *Chem. Sci.* (2016). doi:10.1039/C5SC04383B
45. Ott, I. On the medicinal chemistry of gold complexes as anticancer drugs. *Coord. Chem. Rev.* **253,** 1670–1681 (2009).
46. van Rijt, S. H. & Sadler, P. J. Current applications and future potential for bioinorganic chemistry in the development of anticancer drugs. *Drug Discov. Today* **14,** 1089–1097 (2009).
47. Bindoli, A. *et al.* Thioredoxin reductase: A target for gold compounds acting as potential anticancer drugs. *Coord. Chem. Rev.* **253,** 1692–1707 (2009).
48. Becker, J. S. *et al.* Bioimaging of metals by laser ablation inductively coupled plasma mass spectrometry (LA-ICP-MS). *Mass Spectrom. Rev.* **29,** 156–175 (2010).
49. Wang, H. A. O. *et al.* Fast chemical imaging at high spatial resolution by laser ablation inductively coupled plasma mass spectrometry. *Anal. Chem.* **85,** 10107–10116 (2013).
50. Drescher, D. *et al.* Quantitative Imaging of Gold and Silver Nanoparticles in Single Eukaryotic Cells by Laser Ablation ICP-MS. *Anal. Chem.* **84,** 9684–9688 (2012).
51. Theiner, S. *et al.* LA-ICP-MS imaging in multicellular tumor spheroids - a novel tool in the preclinical development of metal-based anticancer drugs. *Met. Integr. Biometal Sci.* **8,** 398–402 (2016).
52. Mehta, G., Hsiao, A. Y., Ingram, M., Luker, G. D. & Takayama, S. Opportunities and challenges for use of tumor spheroids as models to test drug delivery and efficacy. *J. Control. Release Off. J. Control. Release Soc.* **164,** 192–204 (2012).
53. Schreiber-Brynzak, E. *et al.* Behavior of platinum(iv) complexes in models of tumor hypoxia: cytotoxicity, compound distribution and accumulation. *Met. Integr. Biometal Sci.* **8,** 422–433 (2016).
54. Rix, U. & Superti-Furga, G. Target profiling of small molecules by chemical proteomics. *Nat. Chem. Biol.* **5,** 616–624 (2009).
55. Babak, M. V. *et al.* Target profiling of an antimetastatic RAPTA agent by chemical proteomics: relevance to the mode of action. *Chem. Sci.* **6,** 2449–2456 (2015).

56. Wolters, D. A., Stefanopoulou, M., Dyson, P. J. & Groessl, M. Combination of metallomics and proteomics to study the effects of the metallodrug RAPTA-T on human cancer cells. *Metallomics* **4,** 1185 (2012).
57. Guidi, F. *et al.* The molecular mechanisms of antimetastatic ruthenium compounds explored through DIGE proteomics. *J. Inorg. Biochem.* **118,** 94–99 (2013).
58. Zhang, G. *et al.* Cisplatin treatment leads to changes in nuclear protein and microRNA expression. *Mutat. Res. Toxicol. Environ. Mutagen.* **746,** 66–77 (2012).
59. Liu, H. *et al.* Identification of Cervical Cancer Proteins Associated With Treatment With Paclitaxel and Cisplatin in Patients: *Int. J. Gynecol. Cancer* **21,** 1452–1457 (2011).
60. Le Moguen, K. *et al.* A proteomic kinetic analysis of IGROV1 ovarian carcinoma cell line response to cisplatin treatment. *PROTEOMICS* **7,** 4090–4101 (2007).
61. Yim, E.-K., Lee, K.-H., Kim, C.-J. & Park, J.-S. Analysis of differential protein expression by cisplatin treatment in cervical carcinoma cells. *Int. J. Gynecol. Cancer* **16,** 690–697 (2006).
62. Li, Z., Zhao, X., Yang, J. & Wei, Y. Proteomics profile changes in cisplatin-treated human ovarian cancer cell strain. *Sci. China C Life Sci.* **48,** 648–657 (2005).
63. Alexey Chernobrovkin, C. M.-V. Functional Identification of Target by Expression Proteomics (FITExP) reveals protein targets and highlights mechanisms of action of small molecule drugs. *Sci. Rep.* **5,** (2015).
64. Lomenick, B. *et al.* Target identification using drug affinity responsive target stability (DARTS). *Proc. Natl. Acad. Sci.* **106,** 21984–21989 (2009).
65. Savitski, M. M. *et al.* Tracking cancer drugs in living cells by thermal profiling of the proteome. *Science* **346,** 1255784 (2014).
66. Zhang, Y., Fonslow, B. R., Shan, B., Baek, M.-C. & Yates, J. R. Protein Analysis by Shotgun/Bottom-up Proteomics. *Chem. Rev.* **113,** 2343–2394 (2013).
67. Catherman, A. D., Skinner, O. S. & Kelleher, N. L. Top Down proteomics: Facts and perspectives. *Biochem. Biophys. Res. Commun.* **445,** 683–693 (2014).
68. Garcia, B. A. What Does the Future Hold for Top Down Mass Spectrometry? *J. Am. Soc. Mass Spectrom.* **21,** 193–202 (2010).
69. Lanucara, F., Holman, S. W., Gray, C. J. & Eyers, C. E. The power of ion mobility-mass spectrometry for structural characterization and the study of conformational dynamics. *Nat. Chem.* **6,** 281–294 (2014).

70. Chalmers, M. J., Busby, S. A., Pascal, B. D., West, G. M. & Griffin, P. R. Differential hydrogen/deuterium exchange mass spectrometry analysis of protein–ligand interactions. *Expert Rev. Proteomics* **8,** 43–59 (2011).
71. Li, H. *et al.* Use of Top-down and Bottom-up Fourier Transform Ion Cyclotron Resonance Mass Spectrometry for Mapping Calmodulin Sites modified by Platinum Anticancer Drugs. *Anal. Chem.* **83,** 9507–9515 (2011).
72. Li, H. *et al.* Mass Spectrometric Strategies to Improve the Identification of Pt(II)-Modification Sites on Peptides and Proteins. *J. Am. Soc. Mass Spectrom.* **25,** 1217–1227 (2014).
73. Khalaila, I., Allardyce, C. S., Verma, C. S. & Dyson, P. J. A mass spectrometric and molecular modelling study of cisplatin binding to transferrin. *Chembiochem Eur. J. Chem. Biol.* **6,** 1788–1795 (2005).
74. Sze, C. M. *et al.* Interaction of cisplatin and analogue Pt(en)Cl2 with the copper metallo-chaperone Atox1. *Metallomics* **5,** 946–954 (2013).
75. Moreno-Gordaliza, E., Cañas, B., Palacios, M. A. & Gómez-Gómez, M. M. Novel insights into the bottom-up mass spectrometry proteomics approach for the characterization of Pt-binding proteins: The insulin-cisplatin case study. *The Analyst* **135,** 1288–1298 (2010).
76. Moreno-Gordaliza, E., Cañas, B., Palacios, M. A. & Gómez-Gómez, M. M. Top-Down Mass Spectrometric Approach for the Full Characterization of Insulin−Cisplatin Adducts. *Anal. Chem.* **81,** 3507–3516 (2009).
77. Hartinger, C. G., Tsybin, Y. O., Fuchser, J. & Dyson, P. J. Characterization of platinum anticancer drug protein-binding sites using a top-down mass spectrometric approach. *Inorg. Chem.* **47,** 17–19 (2008).
78. Casini, A. *et al.* Exploring metallodrug–protein interactions by mass spectrometry: comparisons between platinum coordination complexes and an organometallic ruthenium compound. *JBIC J. Biol. Inorg. Chem.* **14,** 761–770 (2009).
79. Murray, B. S., Menin, L., Scopelliti, R. & Dyson, P. J. Conformational control of anticancer activity: the application of arene-linked dinuclear ruthenium(II) organometallics. *Chem. Sci.* **5,** 2536–2545 (2014).
80. Wedlock, L. E. & Berners-Price, S. J. Recent Advances in Mapping the Sub-cellular Distribution of Metal-Based Anticancer Drugs. *Aust. J. Chem.* **64,** 692–704 (2011).
81. Legin, A. A. *et al.* NanoSIMS combined with fluorescence microscopy as a tool for subcellular imaging of isotopically labeled platinum-based anticancer drugs. *Chem. Sci.* **5,** 3135–3143 (2014).

82. Antonarakis, E. S. & Emadi, A. Ruthenium-based chemotherapeutics: are they ready for prime time? *Cancer Chemother. Pharmacol.* **66,** 1–9 (2010).
83. Hoppe, P., Cohen, S. & Meibom, A. NanoSIMS: Technical Aspects and Applications in Cosmochemistry and Biological Geochemistry. *Geostand. Geoanalytical Res.* **37,** 111–154 (2013).
84. Moore, K. L., Lombi, E., Zhao, F.-J. & Grovenor, C. R. M. Elemental imaging at the nanoscale: NanoSIMS and complementary techniques for element localisation in plants. *Anal. Bioanal. Chem.* **402,** 3263–3273 (2012).
85. Groessl, M., Zava, O. & Dyson, P. J. Cellular uptake and subcellular distribution of ruthenium-based metallodrugs under clinical investigation versus cisplatin. *Met. Integr. Biometal Sci.* **3,** 591–599 (2011).
86. Kopf, S. H. *et al.* Heavy water and (15) N labelling with NanoSIMS analysis reveals growth rate-dependent metabolic heterogeneity in chemostats. *Environ. Microbiol.* **17,** 2542–2556 (2015).
87. Dorcier, A. *et al.* Binding of Organometallic Ruthenium(II) and Osmium(II) Complexes to an Oligonucleotide: A Combined Mass Spectrometric and Theoretical Study†. *Organometallics* **24,** 2114–2123 (2005).
88. Assessment, U. E. N. C. for E. IRIS Toxicological Review and Summary Documents for Toluene (External Review Draft). Available at: http://cfpub.epa.gov/ncea/cfm/recordisplay.cfm?deid=54498. (Accessed: 2nd September 2015)
89. Bergamo, A., Masi, A., Dyson, P. J. & Sava, G. Modulation of the metastatic progression of breast cancer with an organometallic ruthenium compound. *Int. J. Oncol.* 1281–1289 (2008). doi:10.3892/ijo_00000119
90. Nowak-Sliwinska, P. *et al.* Organometallic Ruthenium(II) Arene Compounds with Antiangiogenic Activity. *J. Med. Chem.* **54,** 3895–3902 (2011).
91. Adhireksan, Z. *et al.* Ligand substitutions between ruthenium–cymene compounds can control protein versus DNA targeting and anticancer activity. *Nat. Commun.* **5,** (2014).
92. Wu, B. *et al.* A Ruthenium Antimetastasis Agent Forms Specific Histone Protein Adducts in the Nucleosome Core. *Chem. – Eur. J.* **17,** 3562–3566 (2011).
93. Wolters, D. A., Stefanopoulou, M., Dyson, P. J. & Groessl, M. Combination of metallomics and proteomics to study the effects of the metallodrug RAPTA-T on human cancer cells. *Metallomics* **4,** 1185 (2012).

94. Timerbaev, A. R. Recent progress of ICP-MS in the development of metal-based drugs and diagnostic agents. *J. Anal. At. Spectrom.* **29,** 1058–1072 (2014).
95. Zayed, A. *et al.* Determination of Pt–DNA adducts and the sub-cellular distribution of Pt in human cancer cell lines and the leukocytes of cancer patients, following mono- or combination treatments, by inductively-coupled plasma mass spectrometry. *Int. J. Mass Spectrom.* **307,** 70–78 (2011).
96. Bergamo, A., Masi, A., Dyson, P. J. & Sava, G. Modulation of the metastatic progression of breast cancer with an organometallic ruthenium compound. *Int. J. Oncol.* **33,** 1281–1289 (2008).
97. Shen, D.-W., Pouliot, L. M., Hall, M. D. & Gottesman, M. M. Cisplatin Resistance: A Cellular Self-Defense Mechanism Resulting from Multiple Epigenetic and Genetic Changes. *Pharmacol. Rev.* **64,** 706–721 (2012).
98. Chaffey, N. Hayat MA. 2000. Principles and techniques of electron microscopy: biological applications. 4th edn. 543pp. Cambridge: Cambridge University Press. £65 (hardback). *Ann. Bot.* **87,** 546–548 (2001).
99. Liang, X.-J. *et al.* Trafficking and localization of platinum complexes in cisplatin-resistant cell lines monitored by fluorescence-labeled platinum. *J. Cell. Physiol.* **202,** 635–641 (2005).
100. Chen, K. G. *et al.* Melanosomal sequestration of cytotoxic drugs contributes to the intractability of malignant melanomas. *Proc. Natl. Acad. Sci.* **103,** 9903–9907 (2006).
101. Siddik, Z. H. Cisplatin: mode of cytotoxic action and molecular basis of resistance. *Oncogene* **22,** 7265–7279 (2003).
102. Eskelinen, E.-L. & Saftig, P. Autophagy: a lysosomal degradation pathway with a central role in health and disease. *Biochim. Biophys. Acta* **1793,** 664–673 (2009).
103. Bao, L. *et al.* Induction of autophagy contributes to cisplatin resistance in human ovarian cancer cells. *Mol. Med. Rep.* **11,** 91–98 (2015).
104. Podratz, J. L. *et al.* Cisplatin induced Mitochondrial DNA Damage In Dorsal Root Ganglion Neurons. *Neurobiol. Dis.* **41,** 661–668 (2011).
105. Yang, Z. *et al.* Cisplatin preferentially binds mitochondrial DNA and voltage-dependent anion channel protein in the mitochondrial membrane of head and neck squamous cell carcinoma: possible role in apoptosis. *Clin. Cancer Res. Off. J. Am. Assoc. Cancer Res.* **12,** 5817–5825 (2006).

106. Marullo, R. *et al.* Cisplatin Induces a Mitochondrial-ROS Response That Contributes to Cytotoxicity Depending on Mitochondrial Redox Status and Bioenergetic Functions. *PLoS ONE* **8,** (2013).
107. Lacroix, M. & Leclercq, G. Relevance of Breast Cancer Cell Lines as Models for Breast Tumours: An Update. *Breast Cancer Res. Treat.* **83,** 249–289
108. Neve, R. M. *et al.* A collection of breast cancer cell lines for the study of functionally distinct cancer subtypes. *Cancer Cell* **10,** 515–527 (2006).
109. Rouault, T. A. Biogenesis of iron-sulfur clusters in mammalian cells: new insights and relevance to human disease. *Dis. Model. Mech.* **5,** 155–164 (2012).
110. Shaw, T. J., Senterman, M. K., Dawson, K., Crane, C. A. & Vanderhyden, B. C. Characterization of Intraperitoneal, Orthotopic, and Metastatic Xenograft Models of Human Ovarian Cancer. *Mol. Ther.* **10,** 1032–1042 (2004).
111. Dhara, S. C. A rapid method for the synthesis of cis-[Pt(NH3)2Cl2]. *Indian Journal of Chemistry* 193–194 (1970).
112. Eller, K., Henkes, E., Rossbacher, R. & Höke, H. in *Ullmann's Encyclopedia of Industrial Chemistry* (Wiley-VCH Verlag GmbH & Co. KGaA, 2000).
113. Daigle, D. J., Pepperman, A. B. & Vail, S. L. Synthesis of a monophosphorus analog of hexamethylenetetramine. *J. Heterocycl. Chem.* **11,** 407–408 (1974).
114. Scolaro, C. *et al.* In Vitro and in Vivo Evaluation of Ruthenium(II)−Arene PTA Complexes. *J. Med. Chem.* **48,** 4161–4171 (2005).
115. McDonald, K. L. & Webb, R. I. Freeze substitution in 3 hours or less. *J. Microsc.* **243,** 227–233 (2011).
116. Scolaro, C. *et al.* In vitro and in vivo evaluation of ruthenium(II)-arene PTA complexes. *J. Med. Chem.* **48,** 4161–4171 (2005).
117. Nowak-Sliwinska, P. *et al.* Organometallic ruthenium(II) arene compounds with antiangiogenic activity. *J. Med. Chem.* **54,** 3895–3902 (2011).
118. Wills, R. H. *et al.* Insights into the binding sites of organometallic ruthenium anticancer compounds on peptides using ultra-high resolution mass spectrometry. *J. Am. Soc. Mass Spectrom.* **25,** 662–672 (2014).
119. Wolters, D. A., Stefanopoulou, M., Dyson, P. J. & Groessl, M. Combination of metallomics and proteomics to study the effects of the metallodrug RAPTA-T on human cancer cells. *Met. Integr. Biometal Sci.* **4,** 1185–1196 (2012).
120. Ang, W. H. *et al.* Rational Design of an Organometallic Glutathione Transferase Inhibitor. *Angew. Chem. Int. Ed.* **48,** 3854–3857 (2009).

121. Weaver, B. A. How Taxol/paclitaxel kills cancer cells. *Mol. Biol. Cell* **25,** 2677–2681 (2014).
122. Jensen, L. J. *et al.* STRING 8—a global view on proteins and their functional interactions in 630 organisms. *Nucleic Acids Res.* **37,** D412–D416 (2009).
123. Ross, J. S. & Fletcher, J. A. The HER-2/neu Oncogene in Breast Cancer: Prognostic Factor, Predictive Factor, and Target for Therapy. *STEM CELLS* **16,** 413–428 (1998).
124. Pegram, M. D. & Slamon, D. J. Combination therapy with trastuzumab (Herceptin) and cisplatin for chemoresistant metastatic breast cancer: evidence for receptor-enhanced chemosensitivity. *Semin. Oncol.* **26,** 89–95 (1999).
125. Li, J. *et al.* DNA damage binding protein component DDB1 participates in nucleotide excision repair through DDB2 DNA-binding and cullin 4A ubiquitin ligase activity. *Cancer Res.* **66,** 8590–8597 (2006).
126. Welsh, C. *et al.* Reduced levels of XPA, ERCC1 and XPF DNA repair proteins in testis tumor cell lines. *Int. J. Cancer* **110,** 352–361 (2004).
127. Köberle, B., Masters, J. R. W., Hartley, J. A. & Wood, R. D. Defective repair of cisplatin-induced DNA damage caused by reduced XPA protein in testicular germ cell tumours. *Curr. Biol.* **9,** 273–278 (1999).
128. Martin, L. P., Hamilton, T. C. & Schilder, R. J. Platinum Resistance: The Role of DNA Repair Pathways. *Am. Assoc. Cancer Res.* **14,** 1291–1295 (2008).
129. Chu, G. Cellular responses to cisplatin. The roles of DNA-binding proteins and DNA repair. *J. Biol. Chem.* **269,** 787–790 (1994).
130. Nikolay, R., van den Bruck, D., Achenbach, J. & Nierhaus, K. H. in *eLS* (John Wiley & Sons, Ltd, 2001).
131. Smith, L. *et al.* The proteomic analysis of cisplatin resistance in breast cancer cells. *Oncol. Res.* **16,** 497–506 (2007).
132. Parker, A. R. *et al.* BNP7787-Mediated Modulation of Paclitaxel- and Cisplatin-Induced Aberrant Microtubule Protein Polymerization In vitro. *Am. Assoc. Cancer Res.* **9,** 2558–2567 (2010).
133. Hayes, J. D., Flanagan, J. U. & Jowsey, I. R. Glutathione transferases. *Annu. Rev. Pharmacol. Toxicol.* **45,** 51–88 (2005).
134. Townsend, D. M., Findlay, V. L. & Tew, K. D. Glutathione S-transferases as regulators of kinase pathways and anticancer drug targets. *Methods Enzymol.* **401,** 287–307 (2005).
135. Whitley, D., Goldberg, S. P. & Jordan, W. D. Heat shock proteins: A review of the molecular chaperones. *J. Vasc. Surg.* **29,** 748–751 (1999).

136. UniProt: a hub for protein information. Available at: http://nar.oxfordjournals.org/content/43/D1/D204. (Accessed: 22nd June 2016)
137. Pruitt, K. D. *et al.* RefSeq: an update on mammalian reference sequences. *Nucleic Acids Res.* **42,** D756-763 (2014).
138. Chatterjee, S., Biondi, I., Dyson, P. J. & Bhattacharyya, A. A bifunctional organometallic ruthenium drug with multiple modes of inducing apoptosis. *JBIC J. Biol. Inorg. Chem.* **16,** 715–724 (2011).
139. Yachie, A. *et al.* Oxidative stress causes enhanced endothelial cell injury in human heme oxygenase-1 deficiency. *J. Clin. Invest.* **103,** 129–135 (1999).
140. Rizzardini, M., Lupi, M., Bernasconi, S., Mangolini, A. & Cantoni, L. Mitochondrial dysfunction and death in motor neurons exposed to the glutathione-depleting agent ethacrynic acid. *J. Neurol. Sci.* **207,** 51–58 (2003).
141. Pozzesi, N. *et al.* Maesopsin 4-O-β-D-Glucoside, a Natural Compound Isolated from the Leaves of Artocarpus tonkinensis, Inhibits Proliferation and Up-Regulates HMOX1, SRXN1 and BCAS3 in Acute Myeloid Leukemia. *J. Chemother.* **23,** 150–157 (2011).
142. Veal, E. A., Toone, W. M., Jones, N. & Morgan, B. A. Distinct Roles for Glutathione S-Transferases in the Oxidative Stress Response in Schizosaccharomyces pombe. *J. Biol. Chem.* **277,** 35523–35531 (2002).
143. Takechi, R. *et al.* Role of the tumor necrosis factor receptor-associated factor-type zinc finger domain containing protein 1 (TRAFD1) from the hard tick Haemaphysalis longicornis in immunity against bacterial infection. *Ticks Tick-Borne Dis.* **7,** 36–45 (2016).
144. Su, W., Chen, Q. & Frohman, M. A. Targeting phospholipase D with small-molecule inhibitors as a potential therapeutic approach for cancer metastasis. *Future Oncol.* **5,** 1477–1486 (2009).
145. Scott, S. A. *et al.* Design of isoform-selective phospholipase D inhibitors that modulate cancer cell invasiveness. *Nat. Chem. Biol.* **5,** 108–117 (2009).
146. Zhang, T. *et al.* Overexpression of methionine adenosyltransferase II alpha (MAT2A) in gastric cancer and induction of cell cycle arrest and apoptosis in SGC-7901 cells by shRNA-mediated silencing of MAT2A gene. *Acta Histochem.* **115,** 48–55 (2013).
147. Wang, Q. *et al.* Inhibition of hepatocelluar carcinoma MAT2A and MAT2beta gene expressions by single and dual small interfering RNA. *J. Exp. Clin. Cancer Res.* **27,** 72 (2008).

148. Zhang, W. *et al.* Fluorinated N,N-Dialkylaminostilbenes Repress Colon Cancer by Targeting Methionine S-Adenosyltransferase 2A. *ACS Chem. Biol.* **8,** 796–803 (2013).
149. Theocharis, S. E., Margeli, A. P., Klijanienko, J. T. & Kouraklis, G. P. Metallothionein expression in human neoplasia. *Histopathology* **45,** 103–118 (2004).
150. Casini, A. *et al.* Reactivity of an antimetastatic organometallic ruthenium compound with metallothionein-2: relevance to the mechanism of action. *Metallomics* **1,** 434–441 (2009).
151. He, F. *et al.* Solution structure of the zinc finger HIT domain in protein FON. *Protein Sci. Publ. Protein Soc.* **16,** 1577–1587 (2007).
152. Lunde, B. M., Moore, C. & Varani, G. RNA-binding proteins: modular design for efficient function. *Nat. Rev. Mol. Cell Biol.* **8,** 479–490 (2007).
153. Vanharanta, S. *et al.* Loss of the multifunctional RNA-binding protein RBM47 as a source of selectable metastatic traits in breast cancer. *eLife* **3,** (2014).
154. Sakurai, T. *et al.* RNA-binding motif protein 47 inhibits Nrf2 activity to suppress tumor growth in lung adenocarcinoma. *Oncogene* (2016). doi:10.1038/onc.2016.35
155. Fan, J. *et al.* Tyr-phosphorylation of PDP1 toggles recruitment between ACAT1 and SIRT3 to regulate pyruvate dehydrogenase complex. *Mol. Cell* **53,** 534–548 (2014).
156. van Dijk, T. B. *et al.* Friend of Prmt1, a novel chromatin target of protein arginine methyltransferases. *Mol. Cell. Biol.* **30,** 260–272 (2010).
157. Takai, H. *et al.* 5-Hydroxymethylcytosine plays a critical role in glioblastomagenesis by recruiting the CHTOP-methylosome complex. *Cell Rep.* **9,** 48–60 (2014).
158. Lu, D. *et al.* Ethacrynic Acid Exhibits Selective Toxicity to Chronic Lymphocytic Leukemia Cells by Inhibition of the Wnt/β-Catenin Pathway. *PLoS ONE* **4,** (2009).
159. Liu, B. *et al.* Ethacrynic acid improves the antitumor effects of irreversible epidermal growth factor receptor tyrosine kinase inhibitors in breast cancer. *Oncotarget* (2014). doi:10.18632/oncotarget.10846
160. Brody, J. P., Williams, B. A., Wold, B. J. & Quake, S. R. Significance and statistical errors in the analysis of DNA microarray data. *Proc. Natl. Acad. Sci. U. S. A.* **99,** 12975–12978 (2002).
161. Breitling, R., Armengaud, P., Amtmann, A. & Herzyk, P. Rank products: a simple, yet powerful, new method to detect differentially regulated genes in replicated microarray experiments. *FEBS Lett.* **573,** 83–92 (2004).
162. Schwämmle, V., León, I. R. & Jensen, O. N. Assessment and Improvement of Statistical Tools for Comparative Proteomics Analysis of Sparse Data Sets with Few Experimental Replicates. *J. Proteome Res.* **12,** 3874–3883 (2013).

163. Franceschini, A. *et al.* STRING v9.1: protein-protein interaction networks, with increased coverage and integration. *Nucleic Acids Res.* **41,** D808-815 (2013).
164. Munck, A., Böhm, C., Seibel, N. M., Hashemol Hosseini, Z. & Hampe, W. Hu-K4 is a ubiquitously expressed type 2 transmembrane protein associated with the endoplasmic reticulum. *FEBS J.* **272,** 1718–1726 (2005).
165. Kolesnikov, Y. S. *et al.* Molecular structure of phospholipase D and regulatory mechanisms of its activity in plant and animal cells. *Biochem. Biokhimiia* **77,** 1–14 (2012).
166. Bottiglieri, T. S-Adenosyl-l-methionine (SAMe): from the bench to the bedside—molecular basis of a pleiotrophic molecule. *Am. J. Clin. Nutr.* **76,** 1151S–1157S (2002).
167. Addgene: MAT2AA-c001. Available at: http://www.addgene.org/53648/. (Accessed: 15th August 2016)
168. Rilak, A., Puchta, R. & Bugarčić, Ž. D. Mechanism of the reactions of ruthenium(II) polypyridyl complexes with thiourea, sulfur-containing amino acids and nitrogen-containing heterocycles. *Polyhedron* **91,** 73–83 (2015).
169. Scolaro, C., Hartinger, C. G., Allardyce, C. S., Keppler, B. K. & Dyson, P. J. Hydrolysis study of the bifunctional antitumour compound RAPTA-C, [Ru(η6-p-cymene)Cl2(pta)]. *J. Inorg. Biochem.* **102,** 1743–1748 (2008).
170. Strelow, J. *et al.* in *Assay Guidance Manual* (eds. Sittampalam, G. S. et al.) (Eli Lilly & Company and the National Center for Advancing Translational Sciences, 2004).
171. Gibson, D. G. *et al.* Enzymatic assembly of DNA molecules up to several hundred kilobases. *Nat. Methods* **6,** 343–345 (2009).
172. Muller, N., Girard, P., Hacker, D. L., Jordan, M. & Wurm, F. M. Orbital shaker technology for the cultivation of mammalian cells in suspension. *Biotechnol. Bioeng.* **89,** 400–406 (2005).
173. Backliwal, G., Hildinger, M., Hasija, V. & Wurm, F. M. High-density transfection with HEK-293 cells allows doubling of transient titers and removes need for a priori DNA complex formation with PEI. *Biotechnol. Bioeng.* **99,** 721–727 (2008).
174. Backliwal, G. *et al.* Valproic acid: a viable alternative to sodium butyrate for enhancing protein expression in mammalian cell cultures. *Biotechnol. Bioeng.* **101,** 182–189 (2008).
175. Zhao, T. & King, F. L. Mass-spectrometric characterization of cisplatin binding sites on native and denatured ubiquitin. *JBIC J. Biol. Inorg. Chem.* **16,** 633–639 (2011).
176. Casini, A., Temperini, C., Gabbiani, C., Supuran, C. T. & Messori, L. The X-ray Structure of the Adduct between NAMI-A and Carbonic Anhydrase Provides Insights into the Reactivity of this Metallodrug with Proteins. *ChemMedChem* **5,** 1989–1994 (2010).

177. Hartinger, C. G. *et al.* Mass spectrometric analysis of ubiquitin–platinum interactions of leading anticancer drugs: MALDI versus ESI. *J. Anal. At. Spectrom.* **22,** 960–967 (2007).
178. Mandal, R. & Li, X.-F. Top-down characterization of proteins and drug-protein complexes using nanoelectrospray tandem mass spectrometry. *Rapid Commun. Mass Spectrom. RCM* **20,** 48–52 (2006).
179. Yin, S. & Loo, J. A. Top-down mass spectrometry of supercharged native protein–ligand complexes. *Int. J. Mass Spectrom.* **300,** 118–122 (2011).
180. Patiny, L. & Borel, A. ChemCalc: A Building Block for Tomorrow's Chemical Infrastructure. *J. Chem. Inf. Model.* **53,** 1223–1228 (2013).
181. Gibson, D. & Costello, C. A mass spectral study of the binding of the anticancer drug cisplatin to ubiquitin. *Eur. J. Mass Spectrom.* **5,** 501 (1999).
182. Meier, S. M., Tsybin, Y. O., Dyson, P. J., Keppler, B. K. & Hartinger, C. G. Fragmentation methods on the balance: unambiguous top-down mass spectrometric characterization of oxaliplatin-ubiquitin binding sites. *Anal. Bioanal. Chem.* **402,** 2655–2662 (2012).
183. Krishna, S. S., Majumdar, I. & Grishin, N. V. Structural classification of zinc fingers: survey and summary. *Nucleic Acids Res.* **31,** 532–550 (2003).
184. Kuwahara, J. & Coleman, J. E. Role of the zinc(II) ions in the structure of the three-finger DNA binding domain of the Sp1 transcription factor. *Biochemistry (Mosc.)* **29,** 8627–8631 (1990).
185. Anzellotti, A. I., Liu, Q., Bloemink, M. J., Scarsdale, J. N. & Farrell, N. Targeting retroviral Zn finger-DNA interactions: a small-molecule approach using the electrophilic nature of trans-platinum-nucleobase compounds. *Chem. Biol.* **13,** 539–548 (2006).
186. Quintal, S. M., dePaula, Q. A. & Farrell, N. P. Zinc finger proteins as templates for metal ion exchange and ligand reactivity. Chemical and biological consequences. *Met. Integr. Biometal Sci.* **3,** 121–139 (2011).
187. Klug, A. The Discovery of Zinc Fingers and Their Applications in Gene Regulation and Genome Manipulation. *Annu. Rev. Biochem.* **79,** 213–231 (2010).
188. Anzellotti, A. I. & Farrell, N. P. Zinc metalloproteins as medicinal targets. *Chem. Soc. Rev.* **37,** 1629–1651 (2008).
189. Brahemi, G. *et al.* Exploring the Structural Requirements for Inhibition of the Ubiquitin E3 Ligase Breast Cancer Associated Protein 2 (BCA2) as a Treatment for Breast Cancer. *J. Med. Chem.* **53,** 2757–2765 (2010).

190. de Paula, Q. A., Mangrum, J. B. & Farrell, N. P. Zinc finger proteins as templates for metal ion exchange: Substitution effects on the C-finger of HIV nucleocapsid NCp7 using M(chelate) species (M=Pt, Pd, Au). *J. Inorg. Biochem.* **103,** 1347–1354 (2009).
191. Mendes, F. *et al.* Metal-based inhibition of poly(ADP-ribose) polymerase--the guardian angel of DNA. *J. Med. Chem.* **54,** 2196–2206 (2011).
192. Quintal, S., Viegas, A., Erhardt, S., Cabrita, E. J. & Farrell, N. P. Platinated DNA affects zinc finger conformation. Interaction of a platinated single-stranded oligonucleotide and the C-terminal zinc finger of nucleocapsid protein HIVNCp7. *Biochemistry (Mosc.)* **51,** 1752–1761 (2012).
193. Wang, L. H. *et al.* Disruption of estrogen receptor DNA-binding domain and related intramolecular communication restores tamoxifen sensitivity in resistant breast cancer. *Cancer Cell* **10,** 487–499 (2006).
194. Huen, M. S. Y., Sy, S. M. H. & Chen, J. BRCA1 and its toolbox for the maintenance of genome integrity. *Nat. Rev. Mol. Cell Biol.* **11,** 138–148 (2010).
195. O'Donovan, P. J. & Livingston, D. M. BRCA1 and BRCA2: breast/ovarian cancer susceptibility gene products and participants in DNA double-strand break repair. *Carcinogenesis* **31,** 961–967 (2010).
196. Brzovic, P. S., Rajagopal, P., Hoyt, D. W., King, M. C. & Klevit, R. E. Structure of a BRCA1-BARD1 heterodimeric RING-RING complex. *Nat. Struct. Biol.* **8,** 833–837 (2001).
197. Wu, L. C. *et al.* Identification of a RING protein that can interact in vivo with the BRCA1 gene product. *Nat. Genet.* **14,** 430–440 (1996).
198. Hashizume, R. *et al.* The RING heterodimer BRCA1-BARD1 is a ubiquitin ligase inactivated by a breast cancer-derived mutation. *J. Biol. Chem.* **276,** 14537–14540 (2001).
199. Lorick, K. L. *et al.* RING fingers mediate ubiquitin-conjugating enzyme (E2)-dependent ubiquitination. *Proc. Natl. Acad. Sci. U. S. A.* **96,** 11364–11369 (1999).
200. Ruffner, H., Joazeiro, C. A., Hemmati, D., Hunter, T. & Verma, I. M. Cancer-predisposing mutations within the RING domain of BRCA1: loss of ubiquitin protein ligase activity and protection from radiation hypersensitivity. *Proc. Natl. Acad. Sci. U. S. A.* **98,** 5134–5139 (2001).
201. Brzovic, P. S. *et al.* Binding and recognition in the assembly of an active BRCA1/BARD1 ubiquitin-ligase complex. *Proc. Natl. Acad. Sci. U. S. A.* **100,** 5646–5651 (2003).

202. Patmasiriwat, P. *et al.* Analysis of breast cancer susceptibility genes BRCA1 and BRCA2 in Thai familial and isolated early-onset breast and ovarian cancer. *Hum. Mutat.* **20,** 230 (2002).
203. Farmer, H. *et al.* Targeting the DNA repair defect in BRCA mutant cells as a therapeutic strategy. *Nature* **434,** 917–921 (2005).
204. Kennedy, R. D., Quinn, J. E., Mullan, P. B., Johnston, P. G. & Harkin, D. P. The role of BRCA1 in the cellular response to chemotherapy. *J. Natl. Cancer Inst.* **96,** 1659–1668 (2004).
205. Byrski, T. *et al.* Pathologic complete response rates in young women with BRCA1-positive breast cancers after neoadjuvant chemotherapy. *J. Clin. Oncol. Off. J. Am. Soc. Clin. Oncol.* **28,** 375–379 (2010).
206. Price, M. & Monteiro, A. N. A. Fine tuning chemotherapy to match BRCA1 status. *Biochem. Pharmacol.* **80,** 647–653 (2010).
207. Tassone, P. *et al.* Loss of BRCA1 function increases the antitumor activity of cisplatin against human breast cancer xenografts in vivo. *Cancer Biol. Ther.* **8,** 648–653 (2009).
208. Atipairin, A. & Ratanaphan, A. In Vitro Enhanced Sensitivity to Cisplatin in D67Y BRCA1 RING Domain Protein. *Breast Cancer Basic Clin. Res.* **5,** 201–208 (2011).
209. Ransburgh, D. J. R., Chiba, N., Ishioka, C., Toland, A. E. & Parvin, J. D. Identification of breast tumor mutations in BRCA1 that abolish its function in homologous DNA recombination. *Cancer Res.* **70,** 988–995 (2010).
210. Wei, L. *et al.* Rapid recruitment of BRCA1 to DNA double-strand breaks is dependent on its association with Ku80. *Mol. Cell. Biol.* **28,** 7380–7393 (2008).
211. Atipairin, A., Canyuk, B. & Ratanaphan, A. Cisplatin affects the conformation of apo form, not holo form, of BRCA1 RING finger domain and confers thermal stability. *Chem. Biodivers.* **7,** 1949–1967 (2010).
212. Weiss, A. *et al.* In vivo anti-tumor activity of the organometallic ruthenium(II)-arene complex [Ru(η6-p-cymene)Cl2(pta)] (RAPTA-C) in human ovarian and colorectal carcinomas. *Chem. Sci.* **5,** 4742–4748 (2014).
213. Atipairin, A., Canyuk, B. & Ratanaphan, A. Substitution of aspartic acid with glutamic acid at position 67 of the BRCA1 RING domain retains ubiquitin ligase activity and zinc(II) binding with a reduced transition temperature. *J. Biol. Inorg. Chem. JBIC Publ. Soc. Biol. Inorg. Chem.* **16,** 217–226 (2011).

214. Ang, W. H., Casini, A., Sava, G. & Dyson, P. J. Organometallic ruthenium-based antitumor compounds with novel modes of action. *J. Organomet. Chem.* **696,** 989–998 (2011).
215. Adhireksan, Z. *et al.* Ligand substitutions between ruthenium–cymene compounds can control protein versus DNA targeting and anticancer activity. *Nat. Commun.* **5,** 3462 (2014).
216. Chakree, K., Ovatlarnporn, C., Dyson, P. J. & Ratanaphan, A. Altered DNA Binding and Amplification of Human Breast Cancer Suppressor Gene BRCA1 Induced by a Novel Antitumor Compound, [Ru(η6-p-phenylethacrynate)Cl2(pta)]. *Int. J. Mol. Sci.* **13,** 13183–13202 (2012).
217. Ratanaphan, A., Temboot, P. & Dyson, P. J. In vitro ruthenation of human breast cancer suppressor gene 1 (BRCA1) by the antimetastasis compound RAPTA-C and its analogue CarboRAPTA-C. *Chem. Biodivers.* **7,** 1290–1302 (2010).
218. Amir, E., Seruga, B., Serrano, R. & Ocana, A. Targeting DNA repair in breast cancer: a clinical and translational update. *Cancer Treat. Rev.* **36,** 557–565 (2010).
219. Helleday, T., Petermann, E., Lundin, C., Hodgson, B. & Sharma, R. A. DNA repair pathways as targets for cancer therapy. *Nat. Rev. Cancer* **8,** 193–204 (2008).
220. Lieberman, H. B. DNA damage repair and response proteins as targets for cancer therapy. *Curr. Med. Chem.* **15,** 360–367 (2008).
221. Powell, S. N. & Bindra, R. S. Targeting the DNA damage response for cancer therapy. *DNA Repair* **8,** 1153–1165 (2009).
222. Ratanaphan, A. A DNA repair BRCA1 estrogen receptor and targeted therapy in breast cancer. *Int. J. Mol. Sci.* **13,** 14898–14916 (2012).
223. Zhu, Y., Hu, J., Hu, Y. & Liu, W. Targeting DNA repair pathways: a novel approach to reduce cancer therapeutic resistance. *Cancer Treat. Rev.* **35,** 590–596 (2009).
224. Engel, G. Estimation of binding parameters of enzyme-ligand complex from fluorometric data by a curve fitting procedure: seryl-tRNA synthetase-tRNA Ser complex. *Anal. Biochem.* **61,** 184–191 (1974).
225. Matthews, J. M. *et al.* A class of zinc fingers involved in protein-protein interactions biophysical characterization of CCHC fingers from fog and U-shaped. *Eur. J. Biochem. FEBS* **267,** 1030–1038 (2000).
226. Pjura, P. & Matthews, B. W. Structures of randomly generated mutants of T4 lysozyme show that protein stability can be enhanced by relaxation of strain and by improved hydrogen bonding via bound solvent. *Protein Sci. Publ. Protein Soc.* **2,** 2226–2232 (1993).

227. Nhukeaw, T., Temboot, P., Hansongnern, K. & Ratanaphan, A. Cellular responses of BRCA1-defective and triple-negative breast cancer cells and in vitro BRCA1 interactions induced by metallo-intercalator ruthenium(II) complexes containing chloro-substituted phenylazopyridine. *BMC Cancer* **14,** 73 (2014).
228. Tomlinson, G. E. *et al.* Characterization of a breast cancer cell line derived from a germ-line BRCA1 mutation carrier. *Cancer Res.* **58,** 3237–3242 (1998).
229. Husain, A., He, G., Venkatraman, E. S. & Spriggs, D. R. BRCA1 up-regulation is associated with repair-mediated resistance to cis-diamminedichloroplatinum(II). *Cancer Res.* **58,** 1120–1123 (1998).
230. Quinn, J. E., Carser, J. E., James, C. R., Kennedy, R. D. & Harkin, D. P. BRCA1 and implications for response to chemotherapy in ovarian cancer. *Gynecol. Oncol.* **113,** 134–142 (2009).
231. Zhurov, K. O., Fornelli, L., Wodrich, M. D., Laskay, Ü. A. & Tsybin, Y. O. Principles of electron capture and transfer dissociation mass spectrometry applied to peptide and protein structure analysis. *Chem. Soc. Rev.* **42,** 5014–5030 (2013).
232. Williams, J. P., Brown, J. M., Campuzano, I. & Sadler, P. J. Identifying drug metallation sites on peptides using electron transfer dissociation (ETD), collision induced dissociation (CID) and ion mobility-mass spectrometry (IM-MS). *Chem. Commun. Camb. Engl.* **46,** 5458–5460 (2010).
233. Provencher, S. W. & Glöckner, J. Estimation of globular protein secondary structure from circular dichroism. *Biochemistry (Mosc.)* **20,** 33–37 (1981).